



저작자표시-비영리-변경금지 2.0 대한민국

이용자는 아래의 조건을 따르는 경우에 한하여 자유롭게

- 이 저작물을 복제, 배포, 전송, 전시, 공연 및 방송할 수 있습니다.

다음과 같은 조건을 따라야 합니다:



저작자표시. 귀하는 원저작자를 표시하여야 합니다.



비영리. 귀하는 이 저작물을 영리 목적으로 이용할 수 없습니다.



변경금지. 귀하는 이 저작물을 개작, 변형 또는 가공할 수 없습니다.

- 귀하는, 이 저작물의 재이용이나 배포의 경우, 이 저작물에 적용된 이용허락조건을 명확하게 나타내어야 합니다.
- 저작권자로부터 별도의 허가를 받으면 이러한 조건들은 적용되지 않습니다.

저작권법에 따른 이용자의 권리는 위의 내용에 의하여 영향을 받지 않습니다.

이것은 [이용허락규약\(Legal Code\)](#)을 이해하기 쉽게 요약한 것입니다.

[Disclaimer](#)

**Ph.D. Dissertation of Engineering**

**Preservation and Rehabilitation of  
Historical Unreinforced Masonry  
Structures**

**무보강 조적식 역사 구조물의 보존과 복구**

**August 2021**

**Graduate School of Engineering  
Seoul National University  
Architecture and Architectural Engineering  
Fahimeh Yavartanoo**

# **Preservation and Rehabilitation of Historical Unreinforced Masonry Structures**

**Advisor: Thomas Kang**

**Submitting a Ph.D. Dissertation of Architecture  
and Architectural Engineering**

**August 2021**

**Graduate School of Engineering  
Seoul National University  
Architecture and Architectural Engineering**

**Fahimeh Yavartanoo**

**Confirming the Ph.D. Dissertation written by  
Fahimeh Yavartanoo**

**August 2021**

Chair	<u>Sung-Gul Hong</u>
Vice Chair	<u>Thomas Kang</u>
Examiner	<u>Cheol-Ho Lee</u>
Examiner	<u>Hong-Gun Park</u>
Examiner	<u>Mehrdad Hejazi</u>

## **Abstract**

# **Preservation and Rehabilitation of Historical Unreinforced Masonry Structures**

Fahimeh Yavartanoo

Department of Architecture and Architectural Engineering

College of Engineering

Seoul National University

Historical structures constitute the most significant part of the cultural, architectural, and historical values of past peoples, which play an important role in transmitting these values to future generations. Many of these cultural heritage buildings have been severely damaged by past earthquakes or other natural disasters. In terms of structural property, the main defects are related to high specific mass, low tensile strength, low to moderate shear strength, and low ductility. The seismic behavior of masonry buildings highly depends on the material properties, geometry, configuration, arrangements of units, connections, foundation strength, etc. These features may cause them to be vulnerable to a sudden movement which can be terminated by the partial or entire collapse of the structure. Therefore, preservation and protection of this type of structure is an interesting topic and of great concern for the engineering community. This dissertation deals with a detailed architectural

and structural characterization of different types of unreinforced masonry (URM) walls as the most important structural element and explains their typical damage caused by seismic loads. Then, several retrofitting methods including their advantages and shortcomings were investigated to choose an appropriate method for analytical studies. Among all types of URM walls, the dry-stack stone masonry wall was selected and its behavior under monotonic and cyclic loads was evaluated using finite element method (FEM). To validate the results of numerical analysis, all FEM models were calibrated with a set of experimental investigations that have been conducted by other researchers. Then, some parametric studies were conducted for different arrangements and scales of units and walls. Regarding the results of numerical analysis and failure modes observed in the models, an appropriate retrofitting method was determined. Given the existing limitations on retrofitting historical structures, inserting rebars into the wall was considered as one of the most efficient and practical retrofit techniques. Finally, a parametric study has been done for materials and arrangements of inserted rebars with a hope to achieve the most efficient case. The results obtained by this study led to a deeper understanding of the seismic behavior of URM walls and how it can be enhanced by a proper retrofit technique.

**Keywords:** Preservation, historical structures, masonry wall, dry-stack stone wall, seismic behavior, damage, FEM analysis, calibration, failure mechanisms, retrofitting methods.

**Student Number:** 2016-38382

## Contents

<b>Abstract .....</b>	<b>i</b>
<b>Contents.....</b>	<b>iii</b>
<b>List of Tables .....</b>	<b>ix</b>
<b>List of Figures .....</b>	<b>xii</b>
<b>List of Symbols .....</b>	<b>xxvi</b>
<b>Chapter 1. Introduction .....</b>	<b>1</b>
1.1 History and Motivation.....	2
1.2 Scope and Methodology .....	10
1.3 Organization .....	13
<b>Chapter 2. Technical Investigation of HURM Structures.....</b>	<b>15</b>
2.1 General Description.....	16
2.2 Architectural Characterization.....	17
2.2.1 Material classification .....	18
2.2.2 Geometry .....	24
2.3 Structural Characterization .....	26
2.3.1 Structural components.....	27
2.3.2 Masonry components .....	34

2.4 Wall Behavior.....	37
2.4.1 Wall behavior under compressive load.....	39
2.4.2 Wall behavior under tensile load.....	41
2.4.3 Wall behavior under shear load.....	43
2.5 Summary.....	44
<b>Chapter 3. Typical Seismic Damage in HURM Buildings.....</b>	<b>45</b>
3.1 Typical Damage of HURM Structures.....	46
3.2 Damage in Non-Structural Elements.....	48
3.3 Damage in Structural Elements.....	49
3.3.1 Connection failure.....	50
3.3.2 Wall failure.....	53
3.3.3 Diaphragm failure.....	61
3.3.4 Foundation failure.....	61
3.4 Impact of Erosion on the Performance of HURM Buildings.....	63
3.4.1 Wind.....	65
3.4.2 Temperature.....	66
3.4.3 Rain and humidity.....	66
3.4.4 Biological damage.....	67
3.4.5 Human intervention.....	68
3.5 Summary.....	68
<b>Chapter 4. Technical Issues and Methods of Preservation for HURM Structures.....</b>	<b>69</b>

4.1 Preservation Techniques for HURM .....	70
4.2 Improving Structural Integrity .....	73
4.2.1 Confinements .....	73
4.2.2 Transversal anchorage .....	78
4.2.3 Strengthening of junction .....	78
4.2.4 Textile reinforced mortar and steel reinforced grout .....	79
4.2.5 Mortar joint treatment .....	81
4.2.6 Strengthening of roof diaphragm .....	86
4.3 Reducing Seismic Demands .....	87
4.3.1 Base isolation .....	87
4.3.2 Seismic damper .....	89
4.4 Upgrading Structural Components .....	89
4.4.1 Reinforced concrete wall .....	90
4.4.2 Moment and braced frames .....	91
4.4.3 Surface treatment .....	92
4.4.4 External reinforcements .....	96
4.4.5 Post-tensioning .....	106
4.4.6 Mesh reinforcement .....	109
4.4.7 Reticulatus system .....	113
4.5 Technical Comparison .....	116
4.6 Summary .....	120

<b>Chapter 5. Experimental and Numerical Methods for HURM Structures.....</b>	<b>121</b>
5.1 General Description.....	122
5.2 Experimental Method .....	123
5.2.1 Material test.....	124
5.2.2 Structural test .....	133
5.3 Numerical Analysis Methods .....	137
5.3.1 Concept of macro and micro approaches .....	140
5.3.2 Kinematic method .....	146
5.3.3 Finite element method.....	149
5.3.4 Discrete element method.....	153
5.4 Analysis Types .....	155
5.4.1 Linear static analysis (LSA).....	159
5.4.2 Linear dynamic analysis (LDA).....	161
5.4.3 Nonlinear static analysis (NSA).....	164
5.4.4 Nonlinear dynamic analysis (NDA).....	167
5.5 Material and Joint Behavior .....	168
5.6 Summary.....	174
<b>Chapter 6. Numerical Modeling of Stone Wall .....</b>	<b>175</b>
6.1 General Descriptions .....	176
6.2 Experimental Research Program .....	178
6.3 ABAQUS Software .....	187

6.4 Numerical Model.....	191
6.5 Calibration and Validation of Numerical Models .....	198
6.6 Sensitivity Analysis .....	207
6.6.1 Penalty stiffness sensitivity analysis .....	207
6.6.2 Mesh size sensitivity analysis .....	210
6.6.3 Friction coefficient sensitivity analysis.....	214
6.6.4 Comparison of 2D and 3D analyses.....	218
6.6.5 Comparison of pushover and cyclic analysis .....	224
6.7 Parametric Study.....	232
6.8 Summary.....	245
<b>Chapter 7. FEM Analysis of Stone Masonry Walls Retrofitted by Rebars.....</b>	<b>247</b>
7.1 Proposed Retrofit Technique .....	248
7.2 Material Properties .....	251
7.3 Numerical Modeling Assumptions.....	254
7.4 Retrofitting Program.....	256
7.4.1 Horizontal rebar models.....	256
7.4.2 Vertical rebar models .....	262
7.4.3 Diagonal rebar models .....	282
7.5 Comparative Studies.....	302
7.6 Cyclic Analysis.....	306
7.7 Summary.....	318

<b>Chapter 8. Summary and Conclusion .....</b>	<b>319</b>
8.1 Summary.....	320
8.2 Conclusion.....	322
8.3 Future Work.....	328
<b>References.....</b>	<b>329</b>
<b>Acknowledgment.....</b>	<b>359</b>
<b>Abstract in Korean.....</b>	<b>360</b>

## List of Tables

<b>Table 4-1</b> Advantages of URM retrofitting methods .....	118
<b>Table 4-2</b> Disadvantages of URM retrofitting methods.....	119
<b>Table 6-1</b> Mean values of modulus of elasticity ( $E$ ) of granite stone .....	184
<b>Table 6-2</b> Influence of $E_S$ on mechanical properties of wall ( $\mu = 0.4, \sigma = 0.2 \text{ N/mm}^2$ ) .....	204
<b>Table 6-3</b> Influence of $E_S$ on mechanical properties of wall ( $\mu = 0.4, \sigma = 0.5 \text{ N/mm}^2$ ) .....	205
<b>Table 6-4</b> Influence of $E_S$ on mechanical properties of wall ( $\mu = 0.4, \sigma = 0.875 \text{ N/mm}^2$ ) .....	205
<b>Table 6-5</b> Influence of $E_S$ on mechanical properties of wall ( $\mu = 0.4, \sigma = 1.25 \text{ N/mm}^2$ ) .....	205
<b>Table 6-6</b> Effect of $F_f$ on mechanical properties of calibrated model ( $\sigma = 0.2 \text{ MPa}$ ) .....	209
<b>Table 6-7</b> Effect of $F_f$ on mechanical properties of calibrated model ( $\sigma = 0.5 \text{ MPa}$ ) .....	209
<b>Table 6-8</b> Effect of $F_f$ on mechanical properties of calibrated model ( $\sigma = 0.875 \text{ MPa}$ ) .....	209
<b>Table 6-9</b> Effect of $F_f$ on mechanical properties of calibrated model ( $\sigma = 1.25 \text{ MPa}$ ) .....	210
<b>Table 6-10</b> Effect of mesh size on mechanical properties ( $\sigma = 0.2 \text{ MPa}$ ).....	213
<b>Table 6-11</b> Effect of mesh size on mechanical properties ( $\sigma = 0.5 \text{ MPa}$ ) .....	213
<b>Table 6-12</b> Effect of mesh size on mechanical properties ( $\sigma = 0.875 \text{ MPa}$ ).....	213

<b>Table 6-13</b> Effect of mesh size on mechanical properties ( $\sigma = 1.25$ MPa).....	214
<b>Table 6-14</b> Effect of friction coefficient on mechanical properties of calibrated model ( $\sigma = 0.2$ MPa) .....	216
<b>Table 6-15</b> Effect of friction coefficient on mechanical properties of calibrated model ( $\sigma = 0.5$ MPa) .....	217
<b>Table 6-16</b> Effect of friction coefficient on mechanical properties of calibrated model ( $\sigma = 0.875$ MPa) .....	217
<b>Table 6-17</b> Effect of friction coefficient on mechanical properties of calibrated model ( $\sigma = 1.25$ MPa) .....	218
<b>Table 6-18</b> Cyclic dissipated energy of walls (kN-mm) .....	231
<b>Table 7-1</b> Material property of rebars ( $d = 6$ mm) for retrofitting stone wall.....	253
<b>Table 7-2</b> Details of finite element models strengthen with horizontal rebars .....	258
<b>Table 7-3</b> Details of finite element models strengthen with vertical rebars .....	264
<b>Table 7-4</b> The strength of retrofitted wall with vertical rebars ( $F_{ur} / F_{uURM}$ ) .....	270
<b>Table 7-5</b> Ductility, hardening stiffness, and strength of retrofitted walls with vertical rebars, $\sigma = 0.2$ MPa .....	273
<b>Table 7-6</b> Ductility, hardening stiffness, and strength of retrofitted walls with vertical rebars, $\sigma = 0.5$ MPa .....	273
<b>Table 7-7</b> Ductility, hardening stiffness, and strength of retrofitted walls with vertical rebars, $\sigma = 0.875$ MPa .....	274
<b>Table 7-8</b> Ductility, hardening stiffness, and strength of retrofitted walls with vertical rebars, $\sigma = 1.25$ MPa .....	274
<b>Table 7-9</b> Details of finite element models strengthened with diagonal rebars.....	284
<b>Table 7-10</b> The strength of retrofitted wall with diagonal rebars ( $F_{ur} / F_{uURM}$ ) .....	290

<b>Table 7-11</b> Ductility, hardening stiffness, and strength of retrofitted walls with diagonal rebars, $\sigma = 0.2$ MPa.....	293
<b>Table 7-12</b> Ductility, hardening stiffness, and strength of retrofitted walls with diagonal rebars, $\sigma = 0.5$ MPa.....	293
<b>Table 7-13</b> Ductility, hardening stiffness, and strength of retrofitted walls with diagonal rebars, $\sigma = 0.875$ MPa.....	294
<b>Table 7-14</b> Ductility, hardening stiffness, and strength of retrofitted walls with diagonal rebars, $\sigma = 1.25$ MPa.....	294
<b>Table 7-15</b> Normalized value of cyclic dissipated energy of retrofitted walls .....	317

## List of Figures

<b>Figure 1-1</b> Different types of masonry structures.....	2
<b>Figure 1-2</b> Selected masonry structure for this study.....	3
<b>Figure 1-3</b> Ancient stone masonry buildings.....	4
<b>Figure 1-4</b> Out-of-plane behavior of the walls of masonry buildings with rigid floors (Redrawn based on Tomažević, 1999) .....	7
<b>Figure 1-5</b> Out-of-plane failure of old URM building (Adapted from Novelli and D’Ayala, 2019).....	8
<b>Figure 1-6</b> In-plane failure of old URM building: a) Shear failure of spandrels with shallow masonry arches; b) Flexural failure of spandrels (Adapted from Dazio and Beyer, 2010) .....	8
<b>Figure 1-7</b> Scope and methodology of the study.....	12
<b>Figure 2-1</b> Masonry wall types: a) Traditional masonry wall (Redrawn based on Wood and Burns, 2019); b) Modern masonry wall (Redrawn based on IMI, 2011) .....	17
<b>Figure 2-2</b> Preparation and use of clay brick (Adapted from Dalkılıç and Nabikoğlu, 2017) .....	20
<b>Figure 2-3</b> Brick masonry walls with various bond types (Redrawn based on Lat, 2020) .....	21
<b>Figure 2-4</b> Segment of stone heritage: a) Pyramids of Cairo in Egypt; b) Inca wall in Peru (Adapted from Quiroz, 2011).....	23
<b>Figure 2-5</b> Types of arrangements of historical masonry constructions: a) Regular masonry; b) Irregular masonry; c) Three-layer masonry.....	25

---

<b>Figure 2-6</b> Foundations types of historical structures (Adapted from Przewłócki <i>et al.</i> , 2005) .....	29
<b>Figure 2-7</b> Historical masonry walls: a) Sawn dry-stack wall without bonding mortar; b) Regular stone wall with bonding mortar; c) Irregular stone wall with bonding mortar; d) Rubble wall with irregular bonding mortar thickness .....	31
<b>Figure 2-8</b> Curved structural components: a) Arch; b) Vault; c) Dome .....	32
<b>Figure 2-9</b> Buttresses: a) Adding a thick wall behind the arch; b) Adding partial arches on the side of the main arch .....	33
<b>Figure 2-10</b> Seismic performance of URM buildings: a) Local damage mechanisms; b) Global response (Redrawn based on Simões, 2018).....	39
<b>Figure 2-11</b> Failure modes due to high vertical loading: a) Transversal tension; b) Crushing; c) Separation due to weak plane (Redrawn based on Meli, 1998) .	41
<b>Figure 2-12</b> Failure mechanism of masonry under tensile loading: a) Masonry wall under tension; b) Failure of the bond; c) Failure of the units; d) Cohesion failure (Redrawn based on Meli, 1998) .....	42
<b>Figure 2-13</b> Failure of wall under diagonal tension (shear): a) Wall with mortar; b) Wall without mortar (dry-stack) (Redrawn based on Meli, 1998) .....	43
<b>Figure 3-1</b> Damage in non-structural elements: a) Severe damage of RC cornice; b) Poorly connected balcony; c) Timber joists attacked by termites (Adapted from Jiménez <i>et al.</i> , 2018) .....	49
<b>Figure 3-2</b> In-plane and out-of-plane failure mechanism of URM walls (Redrawn based on Zamani Ahari, 2013) .....	53
<b>Figure 3-3</b> Typical in-plane and out-of-plane failure of URM buildings (Adapted from Malena <i>et al.</i> , 2019).....	54
<b>Figure 3-4</b> Principal in-plane failure modes of HURM walls .....	57

**Figure 3-5** Typical hysteresis loops of URM walls: a) Stepped cracking; b) Diagonal cracking; c) Horizontal cracking and crushing (Redrawn based on Mistler, 2006) .....60

**Figure 3-6** Leaning Tower of Pisa, Italy (Adapted from Quiroz, 2011).....62

**Figure 4-1** Confining of masonry wall: a) Tie column; b) Tie beam; c) Combination of tie column and beam ..... 75

**Figure 4-2** Tie bars retrofit method: a) Section; b) Plan; c) Details of the tie bars constraint against seismic actions (Redrawn based on Spina *et al.*, 2004) .....77

**Figure 4-3** Transversal anchorage system in multi-layer masonry walls (Adapted from Meireles and Bento, 2013) ..... 78

**Figure 4-4** L-shaped steel bars: a) Reinforcing masonry junctions; b) and c) Failure patterns observed retrofitted walls at the corner with L-shaped steel bars (Adapted from Dutta *et al.*, 2013) ..... 79

**Figure 4-5** Steel reinforced grout (SRG) system: a) Ultra-high tensile strength steel cord; b) Steel cord embedded in the mortar (Adapted from De Santis, 2017) 80

**Figure 4-6** Compatibility and performance criteria (Adapted from Apostolopoulou *et al.*, 2017) .....83

**Figure 4-7** Criteria set from the methodological approach for the selection of the restoration mortar (Adapted from Apostolopoulou *et al.*, 2017).....84

**Figure 4-8** Detail of grout injection technique: a) 3D view; b) Elevation (Redrawn based on Schuller *et al.*, 1994) .....85

**Figure 4-9** Application of roof diaphragm system (Adapted from Meireles and Bento, 2013) (Unit: cm; Conversion: 1 cm = 0.394 in.).....87

**Figure 4-10** Base isolation technique for masonry walls .....88

**Figure 4-11** Concrete wall (Adapted from Branco and Guerreiro, 2011) .....90

<b>Figure 4-12</b> Application of: a) Concrete moment frame; b) Eccentric bracing in walkway; c) Eccentric bracing core (Adapted from Meireles and Bento, 2013) .....	92
<b>Figure 4-13</b> Application of shotcrete to URM wall (Adapted from El Gawady <i>et al.</i> , 2006) .....	94
<b>Figure 4-14</b> Ferro-cement retrofitting method (Adapted from ACI, 2018).....	95
<b>Figure 4-15</b> Bamboo reinforced wall: a) External horizontal and vertical bamboo; b) Connection of ring beam, wall, and bamboo; c) Connection of external horizontal bamboo at the corner (Adapted from Dowling <i>et al.</i> , 2005).....	98
<b>Figure 4-16</b> Application of FRP in retrofitting of historical structures: a) FRP strips in Siro Pumping Station, St. Benedetto Po, Italy; b) FRP Tendons in the Church of Panaghia Faneromeni, Greece (Adapted from Abdulsalam and Ali, 2014) .....	100
<b>Figure 4-17</b> Retrofitting of URM wall using GFRP (Adapted from Bhattacharya <i>et al.</i> , 2014) .....	101
<b>Figure 4-18</b> Implementation of NSM CFRP retrofit: a) 1886 birdcage tavern (New Zealand); b) Rear chimney; c) Campbell free kindergarten (CFK) (Adapted from Dizhur <i>et al.</i> , 2014).....	104
<b>Figure 4-19</b> Process of implementation FRP-NSM in stone masonry building ...	105
<b>Figure 4-20</b> Proposed NSM-FRP method for retrofitting historical buildings such as Mireuksaji stone pagoda (Iksan, South Koea, 1915).....	106
<b>Figure 4-21</b> Post-tensioning technique: a) Post-tensioning reinforcement (Adapted from Amiraslanzadeh <i>et al.</i> , 2012); b) Post-tensioning strap (Adapted from Turer <i>et al.</i> , 2007).....	108
<b>Figure 4-22</b> Polymer mesh reinforcement: a) Geogrid; b) Soft fence mesh (Adapted from Blondet <i>et al.</i> , 2006) .....	110
<b>Figure 4-23</b> Application of polymer grids combined with fiber lime–cement mortar in stone masonry structures (Adapted from Juhásová <i>et al.</i> , 2008).....	111

**Figure 4-24** Application of PP packaging strip mesh: a) Non-retrofitted; b) Retrofitted wall panel (Adapted from Macabuag *et al.*, 2012)..... 113

**Figure 4-25** Application of Reticulatus system: a) Detail of a through connector; b) Detail of a not-through connector (Adapted from Corradi *et al.*, 2016) ..... 114

**Figure 4-26** Reticulatus system: a) Strut-and-tie model for a reinforced portion of a wall subjected to an in-plane load; b) Reinforcement layout (Redrawn based on Corradi *et al.*, 2016) ..... 116

**Figure 5-1** Different methods for evaluating structural behavior of HURM buildings ..... 122

**Figure 5-2** Possible bond strength tests: a) Direct tensile bond strength test; b) Flexural bond strength test (Redrawn based on Oliveira, 2003)..... 126

**Figure 5-3** Shear-compression loading test: a) Couplet test; b) Triplet test; c) Test set-up developed by van der Pluijm (1993) (Redrawn based on Oliveira, 2003) ..... 128

**Figure 5-4** Examples of standard protocols for cyclic test ..... 136

**Figure 5-5** Numerical methods for analyzing the behavior of HURM structures 139

**Figure 5-6** General definition of macro-and micro-modeling ..... 141

**Figure 5-7** Micro- and macro-modeling approaches for masonry structures ..... 142

**Figure 5-8** Formation of a kinematic chain for in-plane behavior (Redrawn based on Pappas, 2012) ..... 147

**Figure 6-1** Modeling procedure dealt with in this chapter ..... 178

**Figure 6-2** Details of experimental test specimens: a) Dry stack sawn masonry; b) Irregular masonry with bonding mortar joints; c) Rubble masonry wall (Redrawn based on Vasconcelos, 2005) ..... 183

**Figure 6-3** Experiment test set-up: a) Front view; b) Side view (Adapted from Vasconcelos, 2005)..... 185

---

<b>Figure 6-4</b> Results of monotonic test for walls with dry-stack joints: a) Force-displacement curves; b) Failure mechanism (Adapted from Vasconcelos, 2005) .....	186
<b>Figure 6-5</b> Modeling framework in ABAQUS .....	188
<b>Figure 6-6</b> Main modules in ABAQUS/CAE .....	189
<b>Figure 6-7</b> Main components of the numerical model .....	192
<b>Figure 6-8</b> Components of friction model (Adapted from ABAQUS, 2020) .....	194
<b>Figure 6-9</b> 2D finite element model .....	198
<b>Figure 6-10</b> Calibration and validation procedure .....	202
<b>Figure 6-11</b> Failure mechanism .....	203
<b>Figure 6-12</b> Influence of $E_S$ on force-displacement curves under different levels of pre-compression load ( $\sigma$ ) and $\mu = 0.4$ .....	204
<b>Figure 6-13</b> Comparison of mechanical properties of the wall obtained by experiment and calibrated model .....	206
<b>Figure 6-14</b> Influence of $F_f$ on force-displacement curves of the calibrated model under different levels of pre-compression load ( $\sigma$ ) .....	208
<b>Figure 6-15</b> Mesh pattern .....	211
<b>Figure 6-16</b> Influence of mesh size on force-displacement curves of the calibrated model under different levels of pre-compression load ( $\sigma$ ) .....	212
<b>Figure 6-17</b> Influence of friction coefficient on force-displacement curves of the calibrated model under different levels of pre-compression load ( $\sigma$ ) .....	215
<b>Figure 6-18</b> a) Restrained mid-surface of components for out-of-plane motion; b) 3D mesh .....	219
<b>Figure 6-19</b> Comparison of force-displacement curves of 2D and 3D models under different levels of pre-compression load ( $\sigma$ ) .....	220

**Figure 6-20** von Mises stress distribution (MPa) under gravity load .....221

**Figure 6-21** von Mises stress distribution (MPa) under different levels of pre-compression load ( $\sigma$ ) .....222

**Figure 6-22** von Mises stress distribution (MPa) at maximum lateral load under different levels of pre-compression load ( $\sigma$ ) .....223

**Figure 6-23** Loading protocol for conducting cyclic test (Adapted from Vasconcelos, 2005) .....225

**Figure 6-24** Cyclic behavior of walls with dry-stack joints (Adapted from Vasconcelos, 2005).....225

**Figure 6-25** Cyclic force-displacement curves under different levels of pre-compression load ( $\sigma$ ) and friction coefficient ( $\mu$ ).....227

**Figure 6-26** Comparison of experimental and numerical cyclic analysis of walls with dry-stack joints .....228

**Figure 6-27** Comparison of failure mechanism by pushover and cyclic analysis under different levels of pre-compression load ( $\sigma$ ) .....229

**Figure 6-28** Comparison of pushover and cyclic force-displacement curves under different levels of pre-compression load ( $\sigma$ ) .....230

**Figure 6-29** Different size of stone unit in the masonry wall .....233

**Figure 6-30** Stress distribution and failure mechanism based on stone unit size under different levels of pre-compression load ( $\sigma = 0.2$  and  $0.5$  MPa).....234

**Figure 6-31** Stress distribution and failure mechanism based on stone unit size under different levels of pre-compression load ( $\sigma = 0.875$  and  $1.25$  MPa).....235

**Figure 6-32** Force-displacement curves for different size of stone unit under different levels of pre-compression load ( $\sigma$ ) .....236

**Figure 6-33** Walls with different aspect ratios for parametric study .....238

**Figure 6-34** Stress distribution (MPa) and failure mechanism of walls with  $H = 1.2$  (m) and variable  $L$  under different levels of pre-compression load ( $\sigma$ ).....239

**Figure 6-35** Stress distribution (MPa) and failure mechanism of walls with  $H = 2.4$  (m) and variable  $L$  under different levels of pre-compression load ( $\sigma$ ).....240

**Figure 6-36** Stress distribution (MPa) and failure mechanism of walls with  $H = 3.6$  (m) and variable  $L$  under different levels of pre-compression load ( $\sigma$ ).....241

**Figure 6-37** The effect of height on the behavior of walls under different levels of pre-compression load ( $\sigma$ ).....243

**Figure 6-38** The effect of width on the behavior of walls under different levels of pre-compression load ( $\sigma$ ).....244

**Figure 6-39** The effect of wall-size on the behavior of walls under different levels of pre-compression load ( $\sigma$ ) .....245

**Figure 7-1** Different shapes of traditional anchorage used for HURM buildings (Adapted from Redgwick, 2017).....249

**Figure 7-2** Traditional anchorage used for HURM buildings (Adapted from Palmer, 2017) .....250

**Figure 7-3** Detail of embedding system .....250

**Figure 7-4** Stress-strain diagrams for different materials (Redrawn based on Islam, 2008) .....254

**Figure 7-5** Horizontal arrangement of rebars in the stone masonry wall .....257

**Figure 7-6** Force-displacement curve of walls with horizontal stainless steel rebars under different levels of pre-compression load ( $\sigma$ ) .....259

**Figure 7-7** Failure mechanism of walls with horizontal stainless steel rebars,  $\sigma = 0.2$  MPa .....260

**Figure 7-8** Failure mechanism of walls with Horizontal stainless steel rebars,  $\sigma = 1.25$  MPa .....261

<b>Figure 7-9</b> Vertical arrangement of rebars in the stone masonry wall .....	263
<b>Figure 7-10</b> Force-displacement curve of walls with vertical stainless steel rebars under different levels of pre-compression load ( $\sigma$ ) .....	265
<b>Figure 7-11</b> Failure mechanism of walls with vertical stainless steel rebars, $\sigma = 0.2$ MPa .....	266
<b>Figure 7-12</b> Failure mechanism of walls with vertical stainless steel rebars, $\sigma = 0.5$ MPa .....	267
<b>Figure 7-13</b> Failure mechanism of walls with vertical stainless steel rebars, $\sigma = 0.875$ MPa .....	267
<b>Figure 7-14</b> Failure mechanism of walls with vertical stainless steel rebars, $\sigma = 1.25$ MPa .....	267
<b>Figure 7-15</b> Force-displacement curve of walls with vertical titanium rebars under different levels of pre-compression load ( $\sigma$ ) .....	268
<b>Figure 7-16</b> Failure mechanism of walls with vertical titanium rebars, $\sigma = 0.2$ MPa .....	268
<b>Figure 7-17</b> Failure mechanism of walls with vertical titanium rebars, $\sigma = 0.5$ MPa .....	269
<b>Figure 7-18</b> Failure mechanism of walls with vertical titanium rebars, $\sigma = 0.875$ MPa .....	269
<b>Figure 7-19</b> Failure mechanism of walls with vertical titanium rebars, $\sigma = 1.25$ MPa .....	269
<b>Figure 7-20</b> Force-displacement curve of walls with vertical FRP rebars, $\sigma = 0.2$ MPa .....	272
<b>Figure 7-21</b> Force-displacement curve of walls with vertical FRP rebars, $\sigma = 0.5$ MPa .....	272

---

<b>Figure 7-22</b> Force-displacement curve of walls with vertical FRP rebars, $\sigma = 0.875$ MPa .....	272
<b>Figure 7-23</b> Force-displacement curve of walls with vertical FRP rebars, $\sigma = 1.25$ MPa .....	273
<b>Figure 7-24</b> Failure mechanism of walls with vertical CFRP1 rebars, $\sigma = 0.2$ MPa .....	275
<b>Figure 7-25</b> Failure mechanism of walls with vertical CFRP1 rebars, $\sigma = 0.5$ MPa .....	275
<b>Figure 7-26</b> Failure mechanism of walls with vertical CFRP1 rebars, $\sigma = 0.875$ MPa .....	276
<b>Figure 7-27</b> Failure mechanism of walls with vertical CFRP1 rebars, $\sigma = 1.25$ MPa .....	276
<b>Figure 7-28</b> Failure mechanism of walls with vertical CFRP2 rebars, $\sigma = 0.2$ MPa .....	276
<b>Figure 7-29</b> Failure mechanism of walls with vertical CFRP2 rebars, $\sigma = 0.5$ MPa .....	277
<b>Figure 7-30</b> Failure mechanism of walls with vertical CFRP2 rebars, $\sigma = 0.875$ MPa .....	277
<b>Figure 7-31</b> Failure mechanism of walls with vertical CFRP2 rebars, $\sigma = 1.25$ MPa .....	277
<b>Figure 7-32</b> Failure mechanism of walls with vertical EGFRP rebars, $\sigma = 0.2$ MPa .....	278
<b>Figure 7-33</b> Failure mechanism of walls with vertical EGFRP rebars, $\sigma = 0.5$ MPa .....	278
<b>Figure 7-34</b> Failure mechanism of walls with vertical EGFRP rebars, $\sigma = 0.875$ MPa .....	278

**Figure 7-35** Failure mechanism of walls with vertical EGFRP rebars,  $\sigma = 1.25$  MPa .....279

**Figure 7-36** Failure mechanism of walls with vertical SGFRP rebars,  $\sigma = 0.2$  MPa .....279

**Figure 7-37** Failure mechanism of walls with vertical SGFRP rebars,  $\sigma = 0.5$  MPa .....279

**Figure 7-38** Failure mechanism of walls with vertical SGFRP rebars,  $\sigma = 0.875$  MPa .....280

**Figure 7-39** Failure mechanism of walls with vertical SGFRP rebars,  $\sigma = 1.25$  MPa .....280

**Figure 7-40** Failure mechanism of walls with vertical AFRP rebars,  $\sigma = 0.2$  MPa .....280

**Figure 7-41** Failure mechanism of walls with vertical AFRP rebars,  $\sigma = 0.5$  MPa .....281

**Figure 7-42** Failure mechanism of walls with vertical AFRP rebars,  $\sigma = 0.875$  MPa .....281

**Figure 7-43** Failure mechanism of walls with vertical AFRP rebars,  $\sigma = 1.25$  MPa .....281

**Figure 7-44** Diagonal arrangement of rebars in the stone masonry wall.....283

**Figure 7-45** Force-displacement curve of walls with diagonal stainless steel rebars under different levels of pre-compression load ( $\sigma$ ) .....285

**Figure 7-46** Failure mechanism of walls with diagonal stainless steel rebars,  $\sigma = 0.2$  MPa .....286

**Figure 7-47** Failure mechanism of walls with diagonal stainless steel rebars,  $\sigma = 0.5$  MPa .....287

---

<b>Figure 7-48</b> Failure mechanism of walls with diagonal stainless steel rebars, $\sigma = 0.875$ MPa .....	287
<b>Figure 7-49</b> Failure mechanism of walls with diagonal stainless steel rebars, $\sigma = 1.25$ MPa .....	287
<b>Figure 7-50</b> Force-displacement curve of walls with diagonal titanium rebars under different levels of pre-compression load ( $\sigma$ ) .....	288
<b>Figure 7-51</b> Failure mechanism of walls with diagonal titanium rebars, $\sigma = 0.2$ MPa .....	288
<b>Figure 7-52</b> Failure mechanism of walls with diagonal titanium rebars, $\sigma = 0.5$ MPa .....	289
<b>Figure 7-53</b> Failure mechanism of walls with diagonal titanium rebars, $\sigma = 0.875$ MPa .....	289
<b>Figure 7-54</b> Failure mechanism of walls with diagonal titanium rebars, $\sigma = 1.25$ MPa .....	289
<b>Figure 7-55</b> Force-displacement curve of walls with diagonal FRP rebars, $\sigma = 0.2$ MPa .....	292
<b>Figure 7-56</b> Force-displacement curve of walls with diagonal FRP rebars, $\sigma = 0.5$ MPa .....	292
<b>Figure 7-57</b> Force-displacement curve of walls with diagonal FRP rebars, $\sigma = 0.875$ MPa .....	292
<b>Figure 7-58</b> Force-displacement curve of walls with diagonal FRP rebars, $\sigma = 1.25$ MPa .....	293
<b>Figure 7-59</b> Failure mechanism of walls with diagonal CFRP1 rebars, $\sigma = 0.2$ MPa .....	295
<b>Figure 7-60</b> Failure mechanism of walls with diagonal CFRP1 rebars, $\sigma = 0.5$ MPa .....	295

**Figure 7-61** Failure mechanism of walls with diagonal CFRP1 rebars,  $\sigma = 0.875$  MPa .....296

**Figure 7-62** Failure mechanism of walls with diagonal CFRP1 rebars,  $\sigma = 1.25$  MPa .....296

**Figure 7-63** Failure mechanism of walls with diagonal CFRP2 rebars,  $\sigma = 0.2$  MPa .....296

**Figure 7-64** Failure mechanism of walls with diagonal CFRP2 rebars,  $\sigma = 0.5$  MPa .....297

**Figure 7-65** Failure mechanism of walls with diagonal CFRP2 rebars,  $\sigma = 0.875$  MPa .....297

**Figure 7-66** Failure mechanism of walls with diagonal CFRP2 rebars,  $\sigma = 1.25$  MPa .....297

**Figure 7-67** Failure mechanism of walls with diagonal EGFRP rebars,  $\sigma = 0.2$  MPa .....298

**Figure 7-68** Failure mechanism of walls with diagonal EGFRP rebars,  $\sigma = 0.5$  MPa .....298

**Figure 7-69** Failure mechanism of walls with diagonal EGFRP rebars,  $\sigma = 0.875$  MPa .....298

**Figure 7-70** Failure mechanism of walls with diagonal EGFRP rebars,  $\sigma = 1.25$  MPa .....299

**Figure 7-71** Failure mechanism of walls with diagonal SGFRP rebars,  $\sigma = 0.2$  MPa .....299

**Figure 7-72** Failure mechanism of walls with diagonal SGFRP rebars,  $\sigma = 0.5$  MPa .....299

**Figure 7-73** Failure mechanism of walls with diagonal SGFRP rebars,  $\sigma = 0.875$  MPa .....300

<b>Figure 7-74</b> Failure mechanism of walls with diagonal SGFRP rebars, $\sigma = 1.25$ MPa .....	300
<b>Figure 7-75</b> Failure mechanism of walls with diagonal AFRP rebars, $\sigma = 0.2$ MPa .....	300
<b>Figure 7-76</b> Failure mechanism of walls with diagonal AFRP rebars, $\sigma = 0.5$ MPa .....	301
<b>Figure 7-77</b> Failure mechanism of walls with diagonal AFRP rebars, $\sigma = 0.875$ MPa .....	301
<b>Figure 7-78</b> Failure mechanism of walls with diagonal AFRP rebars, $\sigma = 1.25$ MPa .....	301
<b>Figure 7-79</b> Comparison of material properties for vertical arrangements under different levels of pre-compression load ( $\sigma$ ) .....	303
<b>Figure 7-80</b> Comparison of material properties for diagonal arrangements under different levels of pre-compression load ( $\sigma$ ) .....	304
<b>Figure 7-81</b> Comparison of the most efficient models of vertical and diagonal arrangements under different levels of pre-compression load ( $\sigma$ ).....	306
<b>Figure 7-82</b> Cyclic behavior of VR7-6 model, $\sigma = 0.2$ MPa .....	309
<b>Figure 7-83</b> Cyclic behavior of VR7-6 model, $\sigma = 0.5$ MPa .....	310
<b>Figure 7-84</b> Cyclic behavior of VR7-6 model, $\sigma = 0.875$ MPa .....	311
<b>Figure 7-85</b> Cyclic behavior of VR7-6 model, $\sigma = 1.25$ MPa .....	312
<b>Figure 7-86</b> Cyclic behavior of DR8-8 model, $\sigma = 0.2$ MPa .....	313
<b>Figure 7-87</b> Cyclic behavior of DR8-8 model, $\sigma = 0.5$ MPa .....	314
<b>Figure 7-88</b> Cyclic behavior of DR8-8 model, $\sigma = 0.875$ MPa .....	315
<b>Figure 7-89</b> Cyclic behavior of DR8-8 model, $\sigma = 1.25$ MPa .....	316

## List of Symbols

$[c]$	= damping matrix
$d_c$	= exponential decay factor
$E$	= modulus of elasticity
$E_s$	= modulus of elasticity of steel
$\{F\}$	= load vector
$\{F(t)\}$	= time-varying load vector
$F_i(t)$	= generalized load of i-th mode in time domain
$F_i(f_i)$	= generalized load of i-th mode in frequency domain
$f_i$	= natural frequency of i-th mode
$F_f$	= slip tolerance factor
$F_r$	= reduced strength of FRP
$F_u$	= ultimate strength
$F_{uR}$	= strength of retrofitted wall
$F_{uURM}$	= strength of URM wall
$F_y$	= yield strength
$[K]$	= stiffness matrix
$K$	= stiffness
$K_{hs}$	= hardening stiffness

$K_p$	= penalty stiffness
$K_{URM}$	= initial stiffness of URM wall
$l_c$	= contact surface length
$[M]$	= mass matrix
$M_i$	= modal mass of i-th mode
$P$	= pressure
$P-\Delta$	= geometrical nonlinearity due to large displacements
$P-\delta$	= geometrical nonlinearity due to large deformations
$t$	= time
$\{u\}$	= displacement vector
$\{u(t)\}$	= time-varying displacement vector
$\{\dot{u}(t)\}$	= time-varying velocity vector
$\{\ddot{u}(t)\}$	= time-varying acceleration vector
$u_i(t)$	= time-varying displacement of i-th mode
$\dot{u}_i(t)$	= time-varying velocity of i-th mode
$\ddot{u}_i(t)$	= time-varying acceleration of i-th mode
$u_x$	= horizontal displacement
$u_y$	= vertical displacement
$ur_z$	= rotational displacement
$u_i(f_i)$	= peak response displacement of i-th mode

## List of Symbols

---

$\dot{u}_i(f_i)$	= peak response velocity of i-th mode
$\ddot{u}_i(f_i)$	= peak response acceleration of i-th mode
$\alpha_0$	= mean response acceleration
$\varepsilon_y$	= strain at the yield strength
$\varepsilon_r$	= strain at the reduced strength of FRP
$\rho$	= density
$\mu$	= friction coefficient
$\mu_s$	= static friction coefficient
$\mu_k$	= kinetic friction coefficient
$\sigma$	= pre-compression load
$\sigma_y$	= von Mises yield stress
$\delta$	= total slip
$\delta_a$	= allowable elastic slip
$\delta_u$	= displacement at failure of FRP for retrofitted wall
$\delta_y$	= displacement at yielding of retrofitted wall by FRP
$\dot{\delta}$	= sliding rate
$\nu$	= Poisson's ratio
$\tau$	= shear stress
$\tau_{cr}$	= critical shear stress
$\tau_{max}$	= maximum critical shear stress

## **Chapter 1. Introduction**

In this study, seismic behavior and typical damage of historical unreinforced masonry structures were investigated. The current methods of retrofitting masonry structures were discussed and the feasibility of their application for historical structures was explained. Then the appropriate method was selected and the efficiency of the method was examined numerically by adopting models using finite element method. In this chapter, history and motivation, scopes, methodology, and framework of the study are explained in detail.

## 1.1 History and Motivation

Masonry is an anisotropic, heterogeneous, and nonlinear composite material (stone, brick, adobe, and timber) that has been used so far. The properties of constitutes and loading direction can affect the mechanical properties of masonry material. The most impressive historical buildings such as cultural heritage buildings, monuments, essential facilities, and infrastructures that remained from ancient times testify the fact that these materials have been the most basic constituents of various types of structures. The structures made of masonry materials have been used for thousands of years and include more than 70% of the building inventory around the world. Masonry structures can be considered as plain (unreinforced), reinforced, and confined masonry (Zamani Ahari, 2013) (**Figure 1-1**).

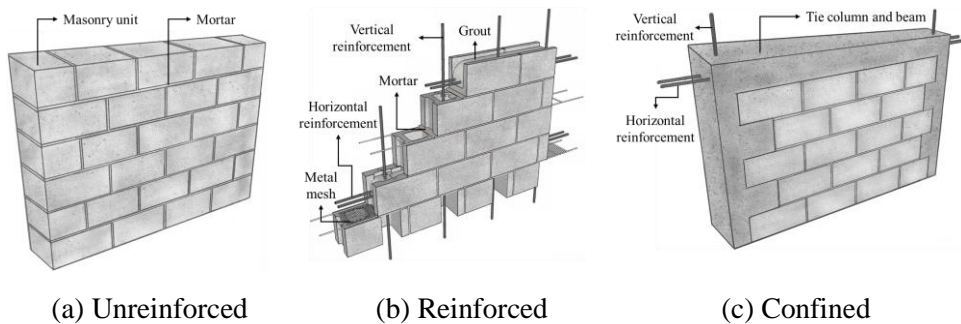


**Figure 1-1** Different types of masonry structures

Plain masonry made of adobe, stone, and brick materials can be considered as unreinforced masonry (URM) construction. Due to the large mass of these structures, the inertial forces under earthquake excitation are considerably large. On the other

hand, most of them exhibit very poor performance under lateral deformations induced by an earthquake due to poor connections between structural components, low tensile strength, etc. These factors make these valuable structures vulnerable to seismic load. Therefore, they have been selected for structural investigation in this study (**Figure 1-2**).

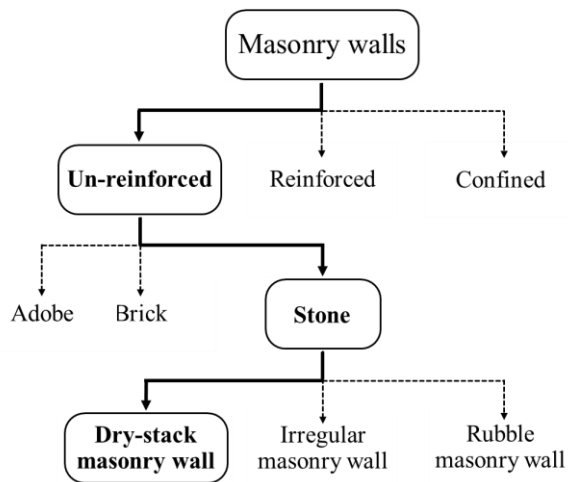


**Figure 1-2** Selected masonry structure for this study

Among all materials, stone became the major material in the construction of masonry structures such as buildings, monuments, sculptures, etc. since the early stages of human civilization. **Figure 1-3** indicates a part of a city in ancient times that most of the structures were made of stone with different configurations and shapes. The wide availability of stone in nature and the workmanship to lay stone pieces above each other are the most important factors in the application of this material in different structures. Among the three groups of masonry walls shown in

**Figure 1-2**, rubble stone walls with abundant variety in the way of arrangement can have many different configurations. Therefore, the study on this type of wall is a case-sensitive analysis and it is not possible to conduct a comprehensive study on them and generalize the results to all existing cases. In irregular stone walls, joints are made by mortar and it makes them significantly stronger than dry-stack walls with friction-based joints that have essentially zero tensile strength. Therefore, because of higher seismic susceptibility and also lack of enough study on dry-stack masonry walls, this study attempts to investigate the behavior of these structures and suitable conservation methods.

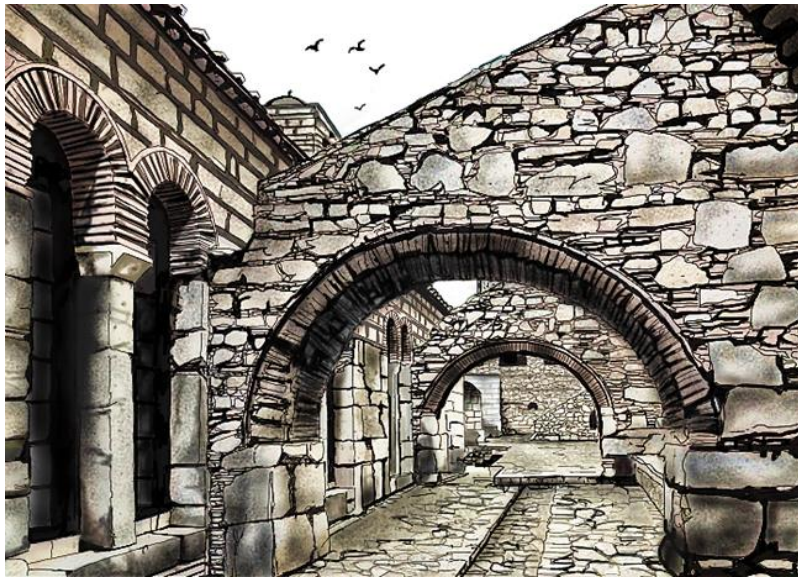


**Figure 1-3** Ancient stone masonry buildings

Despite easy construction, popularity, and continued use of ancient masonry buildings, most of them containing URM elements are very sensitive to seismic

action. These structures were built with non-engineering approaches and simple rules of construction based on the experience of the workman who did not follow any structural standard or code. Therefore, having non-engineered structural elements and applications has caused its mechanical behavior to remain unknown throughout its lifetime for scientists and engineers.

Seismic assessment of historical constructions is a difficult task due to the lack of knowledge on the existing condition of the building. Considering the diversity of URM buildings in typology, material, and constructions, different methods can be applied to assess the seismic vulnerability of the structure. Typological, mechanistic, and hybrid methods have been presented by Corsanego and Gavarini (1993). Palacios (2004) described that the seismic vulnerability of a building can be assessed by two methods as probabilistic method (observed vulnerability) and deterministic method (predicted vulnerability). On the other hand, Giovinazzi (2005) introduced three different methods to assess seismic vulnerability. It includes the observed vulnerability method which is based on the statistical observation of damage caused by past events, the analytical method to calculate the mechanical building behavior, and the method based on expert judgment.

Structural and geometrical typologies, the variability of constituent materials, construction methods, connections, intricate configuration, and the cultural and artistic specifications are the influential factors in masonry behavior particularly under seismic loads. In this regard, analysis of these complex structures with poor design has been an important topic of engineering in recent years. Accurate

evaluation of URM buildings under seismic loads requires a set of accurate information using proper methods of analysis including both experimental investigations and numerical simulations. These procedures provide a better understanding of the local and global seismic failures of the structure which can help us to choose a suitable retrofit method for the building. Tomažević (1999) has been listed some types of damage that generally can be observed in URM buildings under seismic action.

- Cracks between walls and floors;
- Cracks at the corners and wall intersections;
- The out-of-plane collapse of the perimetral walls;
- Cracks in spandrels beams and/or parapets;
- Diagonal cracks in structural walls;
- Partial disintegration or collapse of structural walls;
- A partial or complete collapse of the buildings.

A masonry structure is composed of different structural elements such as walls, arches, vaults, and domes. Masonry wall, as the fundamental part of a building that its in-plane dimension is significantly larger than the thickness, has been designed to withstand compressive loads subject to self-weight. Masonry wall with its considerable compressive strength relative to tensile strength can provide excellent support for the other elements (arches, vaults, etc.). Whereas, the low tensile strength of the masonry wall results in not desirable behavior under in-plane and out-of-plane actions caused by lateral loads. These failures are considered usually as the largest

human and economic impact caused by the earthquake. It has been proved that the failure of load-bearing walls is responsible for the major damage in URM structures which can be terminated in collapse. The poor performance of the masonry wall in out-of-plane behavior is especially due to weakness in connections between walls and walls and floors/roofs. When the floors/roofs have sufficient rigidity with high strength, the local failure happens in masonry walls as shown in **Figure 1-4**. On the other hand, flexible floors (low stiffness and strength) that are connected poorly to the walls are prone to total or partial collapse due to global behavior in walls as shown in **Figure 1-5** (Candeias, 2008).

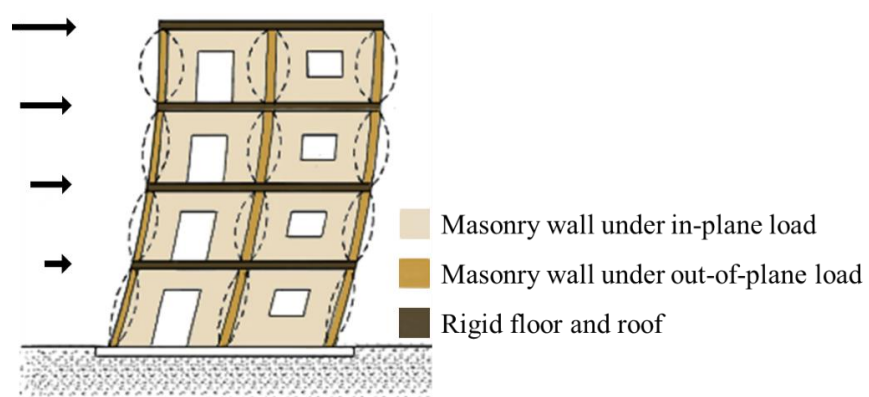


**Figure 1-4** Out-of-plane behavior of the walls of masonry buildings with rigid floors (Redrawn based on Tomažević, 1999)

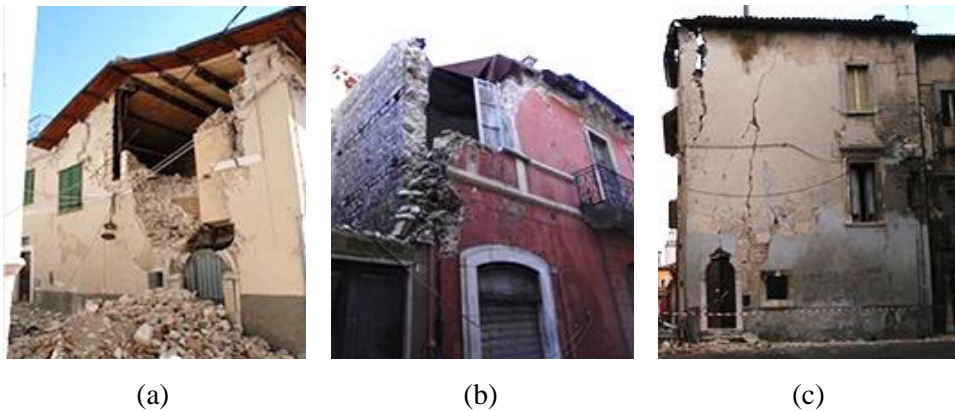


**Figure 1-5** Out-of-plane failure of old URM building (Adapted from Novelli and D’Ayala, 2019)

The in-plane failure of masonry buildings can be observed as shear (**Figure 1-6(a)**) and flexural (**Figure 1-6(b)**) failure of spandrels. Shear failure is the most serious mode among all failure mechanisms and it should be considered as the priority in the study of mechanical behavior of URM structures subjected to seismic loads (Calvi *et al.*, 1996)



**Figure 1-6** In-plane failure of old URM building: a) Shear failure of spandrels with shallow masonry arches; b) Flexural failure of spandrels (Adapted from Dazio and Beyer, 2010)

The seismic performance of a masonry structure mostly relies on the in-plane properties of walls and the in-plane stiffness of horizontal diaphragms. Nevertheless, due to the three-dimensional nature of earthquake excitation, the actual failure of URM wall is a combination of both in-plane and out-of-plane failure modes. For a better understanding of the failure mechanism and their progress in masonry walls, a set of experimental and analytical efforts should be done.

It can be concluded that the inherent structural deficiencies and material weakness of masonry structures make them quite vulnerable to seismic excitation. Therefore, fundamental measures must be taken to increase their resistance against induced loads, which is a new engineering field, and is receiving much attention recently especially in the conservation of heritage structures. Although precise codes and standards have not been designed for this purpose, it is possible to study the behavior of these structures in-depth to find their structural characteristics and vulnerabilities using various tests (Zamani Ahari, 2013).

Preservation and conservation of the built heritage are the most important government proceedings to preserve the valuable culture and tradition of a nation that must be passed down to future generations. This action requires meticulous identification of deficiencies of existing structures to provide appropriate intervention techniques. Strengthening URM elements such as a wall is the main goal in the preservation of historical buildings due to the major role of walls in surviving the building under unexpected events.

## 1.2 Scope and Methodology

As mentioned before, masonry structures show poor performance against lateral loads which highly depend on the mechanical properties of the components as well as the arrangement of stones. Thus, it is necessary to study these structures deeply with the purpose of reducing their seismic vulnerability. Despite this, few comprehensive researches have been done on the mechanics of stone masonry structures, especially under seismic load. The present study attempts to study the behavior of dry-stack stone URM walls and their deficiencies subjected to lateral loads. The main objective of this research is to evaluate the seismic vulnerability of a dry-stack stone masonry wall with different configurations based on previous experiences.

Among available and proper methods, numerical analysis based on the finite element method (FEM) was chosen for the investigation of wall behavior subjected to lateral load. To obtain reliable results using numerical simulation, it is necessary to calibrate the modeling parameters to match the results with the experiment, as much as possible. For this purpose, the result of experimental investigations on the mechanical properties of stone masonry (Characterization of granites and behavior of ancient masonry shear walls) performed by Vasconcelos (2005) has been used. He has conducted a comprehensive study on the material properties of granite stone as well as the seismic performance of stone walls made of granite and provided relatively accurate results of the experiments.

For modeling the structural behavior of the stone masonry wall, the ABAQUS (2020) software has been used, which is one of the most powerful and popular numerical simulation software to represent the behavior of a structure. Among the existing techniques for numerical modeling of the masonry walls, the micro-modeling method has been used, which is an accurate and comprehensive method for evaluating the behavior of this type of structure. In this method, all nonlinear sources including materials, geometry, and boundary conditions can be directly included in the modeling. Moreover, there are currently four main approaches for evaluating the behavior of masonry structures under seismic loads as follows: linear static, linear dynamic, nonlinear static, nonlinear dynamic methods. The most accurate method is the nonlinear dynamic analysis but it is a complex and time-consuming procedure. On the other hand, in the linear analysis methods, the nonlinear effects cannot be simulated directly. The nonlinear static analysis method has found special attention in evaluating the seismic behavior of masonry structures due to some benefits of modeling of nonlinear effects and time-cost efficiencies. Therefore, in this study, the nonlinear static method is used for the simulation of stone walls. Generally, the results obtained from analytical models of the masonry wall performance can be used in the decision process related to the strengthening possibilities of ancient structures subjected to seismic actions. In this way, a fundamental study on the available strengthening techniques for URM structures is conducted. **Figure 1-7** schematically displays the scope and methodology of the study.

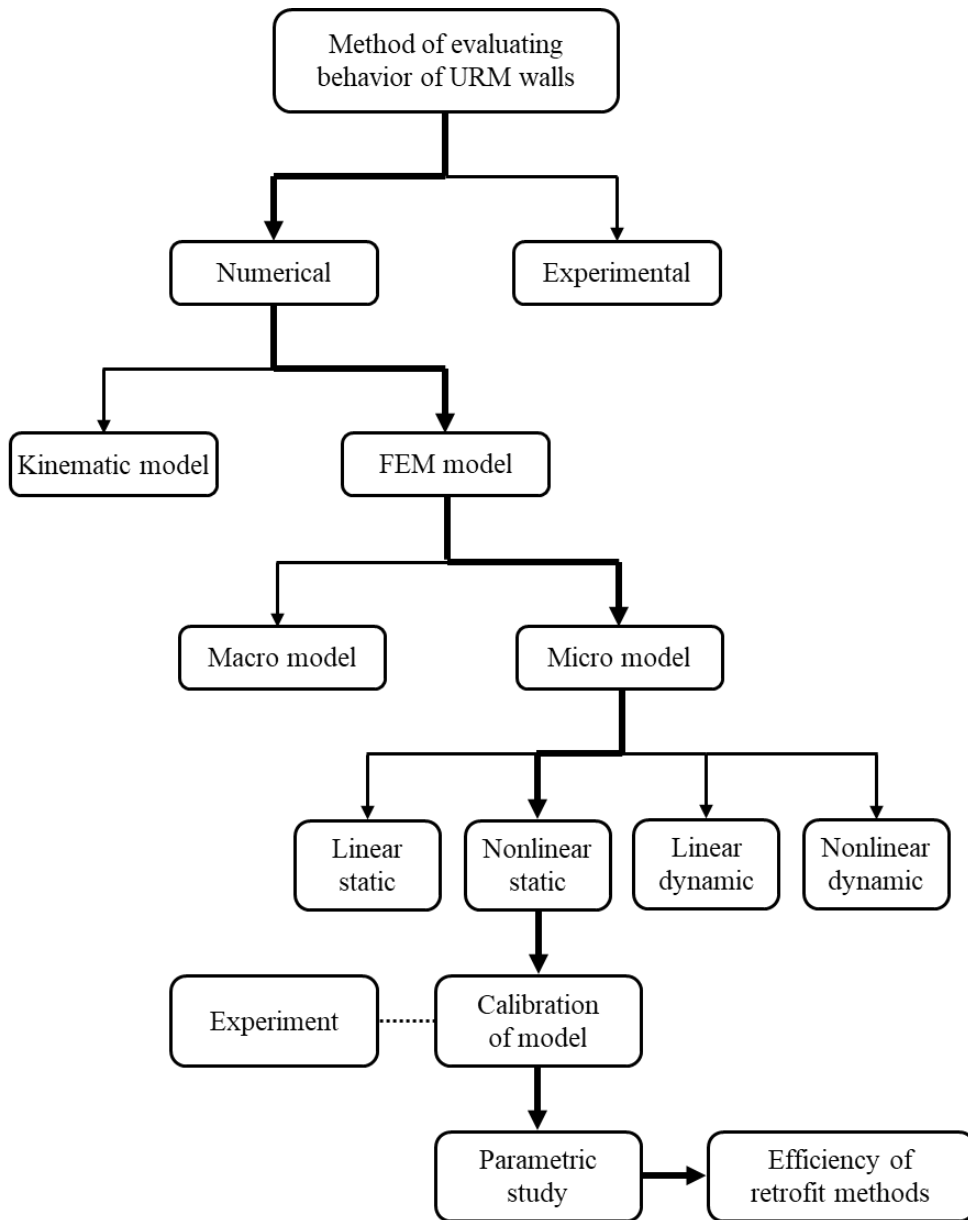


**Figure 1-7** Scope and methodology of the study

## 1.3 Organization

This dissertation is organized into seven chapters based on the steps followed during the research period plus a chapter of conclusions and suggestions for further work.

**Chapter 1** provides a general overview of masonry buildings and types of construction with the motivation for assessing the seismic vulnerability of masonry buildings. The statement of the problem, objectives of the research, and organization of this dissertation are also included in this chapter.

**Chapter 2** deals with technical investigation of historical unreinforced masonry (HURM) structures in terms of architectural and structural characterization including material classification, geometry, and components. The behavior of the unreinforced masonry wall in particular under compressive, tensile, and shear loads is investigated based on the previous studies and summarized in this chapter.

**Chapter 3** focuses on typical damage of both non-structural and structural components of HURM structures, including connections, walls, diaphragms, and foundations. Furthermore, the impact of erosion on the performance of HURM buildings, which can be generated by wind, temperature, rain, and humidity are discussed in this chapter.

**Chapter 4** introduces available conventional rehabilitation and retrofitting techniques for unreinforced masonry structures. Three different classifications can be considered for retrofitting methods: a) Improving structural integrity; b) reducing seismic demands, and c) upgrading structural components. Based on the architectural (aesthetic) and structural effectiveness and other remarkable factors, they are also compared to each other and evaluated to recommend the best approaches for HURM structures.

**Chapter 5** includes a deep study of the relevant experimental methods and numerical strategies for URM walls. Kinematic method and finite element analysis, nonlinearity sources, and type of analysis including the static and dynamic are described in this chapter.

**Chapter 6** summarizes the procedure of calibration of numerical models by applying sensitivity analysis to obtain accurate results as much as close to a set of selected experimental investigations of the stone masonry wall in previous studies. The results obtained from these calibrated numerical models were validated by the corresponding experimental data and utilized for further investigations.

**Chapter 7** deals with numerical studies on the behavior of retrofitted stone masonry walls using some of the appropriate methods.

**Chapter 8** includes the summary, major findings, and concluding remarks of this research with some recommendations for future studies.

## **Chapter 2. Technical Investigation of HURM Structures**

Masonry can be defined as the combination of units (stone, brick, or adobe) and mortar. The main use of mortar in masonry structures is filling the gaps between the units and bind them together to create a strong bond between units and mortar. However, there are plenty of unreinforced masonry buildings constructed without mortar (dry-stack method).

Unreinforced masonry (URM) structure is one of the main construction methods that can be found generally in ancient buildings all over the world. In addition, the fact that these structures have always been considered as a type of construction is due to their outstanding features such as durability, availability, biochemical properties, and many other factors that distinguish them from other materials such as steel and reinforced concrete with the lowest cost (Quiroz, 2011).

Understanding the behavior of historical masonry structures and their relevant specifications requires an in-depth study of typology, geometry, materials, configuration, and structural and construction weaknesses. This chapter attempts to introduce historical URM structures and then classify them according to the identified characteristics, and finally determine their structural behavior.

## 2.1 General Description

Generally, most historical masonry buildings were constructed with different architectural and structural features than modern masonry structures. The survey on historical buildings demonstrates that the main structural system is the load-bearing wall. This element was constructed usually in the single or multi-wythe form including interlocking brick or rubble stones between the two interior and exterior walls (**Figure 2-1(a)**). Modern structural systems (**Figure 2-1(b)**) made by curtain-wall based on steel or concrete frame have superior seismic performance without significant damage in structural and non-structural elements. Additionally, the use of reinforcement or pre-stressing elements with composite materials in modern masonry buildings provides higher stability and strength in comparison with unreinforced historical masonry structures. The seismic behavior of modern masonry buildings can be also improved by using a sufficient “wall density” or amount of walls and reinforcements, built with good quality materials following the recent codes and standards. However, adoption of such resistant systems is associated with tradition and local technological developments in each area. Modern and historical masonry buildings can also exhibit significant variations in constituent materials and foundation. The water absorption, thermal, and moisture transmission factors are the parameters related to material properties with their advantages or shortcomings for both traditional and modern materials. The diversity in materials and technology makes the structural analysis complex.

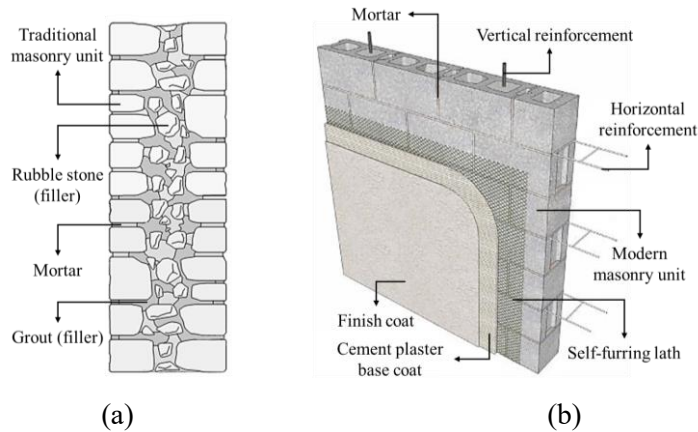


**Figure 2-1** Masonry wall types: a) Traditional masonry wall (Redrawn based on Wood and Burns, 2019); b) Modern masonry wall (Redrawn based on IMI, 2011)

## 2.2 Architectural Characterization

The study of historical structures in the preservation process is necessary to understand the originality and validity of the construction through historical, archaeological, and architectural documentation and information. This investigation helps us to establish a detailed strategy, from the construction time to the present day, to choose the appropriate retrofitting method. The restoration project requires in-depth knowledge of historical construction. It includes manufacturing methods, materials and techniques, alteration throughout history, characteristic elements, structural morphology, and the current static conditions that can be accompanied by a historical-critic survey (Voto, 2009). In fact, this survey makes it possible to detect true characteristic features that only the structure can reveal. Despite this, in the structural survey, the damage condition of the building and the soil underneath the structure has to be considered to avoid unexpected dangerous situations. In the

following sections, historical masonry structures are classified based on the constituted materials as well as geometry. These characterizations can allow a better understanding of the mechanical behavior of the historical structures, which is necessary for seismic evaluation and execution of retrofitting methods.

### **2.2.1 Material classification**

A preliminary and fundamental step in structural analysis is the material survey to define the mechanical properties of the structure for future restoration works. The structural behavior of masonry buildings is highly dependent on the mechanical properties of constituent materials. The method of construction and the use of various materials in historical unreinforced masonry (URM) structures depend on several factors such as environmental, climatic, geographical, and economic conditions or the building activity. Therefore, understanding the constituent materials in historical structures dealing with natural disasters like earthquake or wind load, deterioration, temperature impacts, chemical and biological attacks caused by air pollution can make an accurate evaluation of the mechanical behavior of the structure and better decision in using retrofitting methods. Two main categories are defined here to identify the materials used in historical structures: Masonry structures including adobe, brick, and stone structures; and wooden structures (timber structures).

This study is focused on masonry constructions and they are described in more detail below.

**a) Masonry structures**

The most common materials used for historical constructions in the Middle East and Mesopotamia were adobe and clay brick. While in Egypt, Greece, America, Mexico, and Peru, carved stone using dry-stack method had been used. The combination of carved stone with mortar made of burnt fragments of limestone had been used in Maya. Later, with the rise of urbanization and the advancement of technology, Romans surpassed the construction of larger and more complex structures using enhanced mortars and innovative techniques for the construction of walls, arcs, vaults, and domes (Quiroz, 2011). Adobe units, clay bricks, and stones have been used in building construction as the basic and the most used construction material all over the world for generations. Sometimes they were used individually or sometimes mixed with several layers in different constructions and elements. Adobe or clay brick unit is integrated sun-dried blocks with a mixture of water, sand, earth (soil), and straw which is formed by hand in wooden or metal mold (**Figure 2-2**). Adobe units have a regular shape with different sizes, which have been used since the third millennium BC until now in different constructions such as ziggurats, pyramids, and different structural elements such as massive walls, vaults, and arches. Today, this technique is updated and obtained high scientific and technological levels to be able as a good acoustic and thermal element (Roca *et al.*, 2019).



(a) Sieving of the soil



(b) Preparation of mud



(c) Stabilized mud



(d) Mold coating



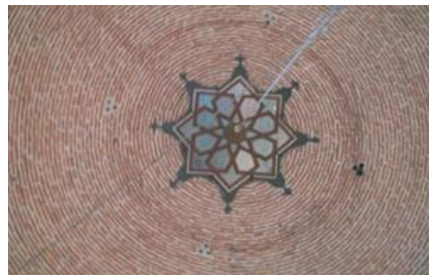
(e) Placing the mixture into the mold



(f) Bricks left to dry



(g) Composite walls



(h) Clay dome (Virgin Mary Church)

**Figure 2-2** Preparation and use of clay brick (Adapted from Dalkılıç and Nabikoğlu, 2017)

Low cost and low embodied energy and carbon, availability of construction materials, and easy construction process without advanced equipment and expertise are the advantages of this material. The main disadvantage of adobe structures is that they are highly susceptible to collapse during earthquakes (Bhattacharya *et al.*, 2014).

Placing brick units on top of each other with a dry method or by using mortar to tighten the bond between them is a common construction method, which has been used for many years (Roca *et al.*, 2019). **Figure 2-3** illustrates the various types of bonds in brick masonry walls that have been used in different historical periods.

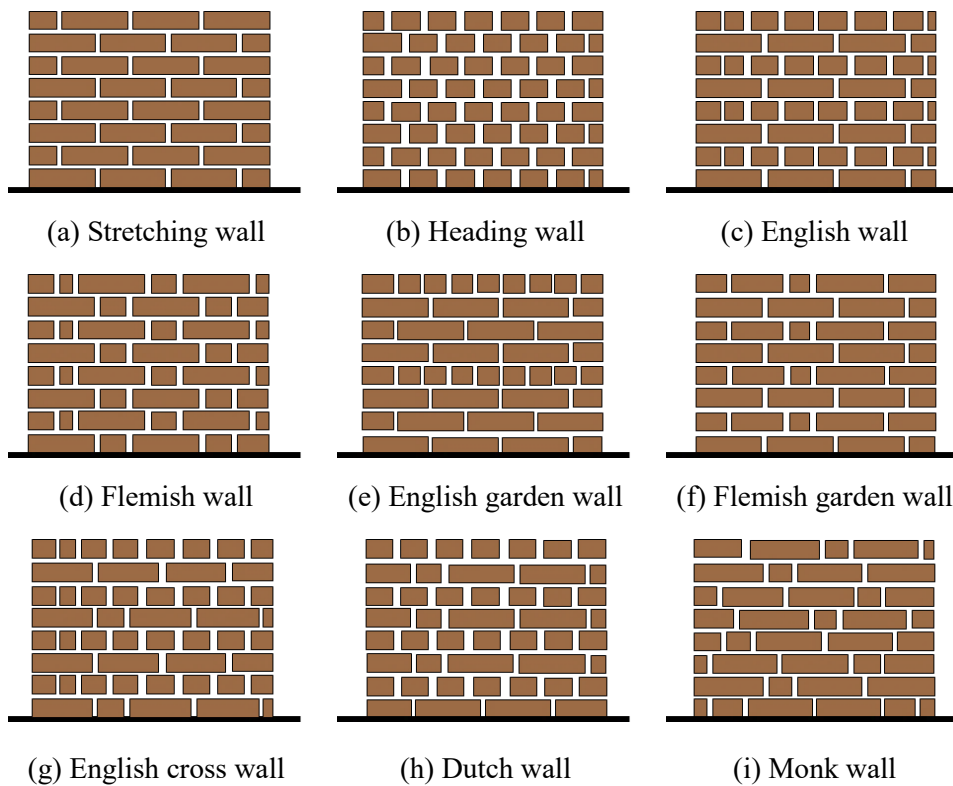


**Figure 2-3** Brick masonry walls with various bond types (Redrawn based on Lat, 2020)

The strength of brick units as the main role in the seismic behavior of masonry structure highly depends on the purity of the soil used in the preparation of bricks and the temperature at which the bricks are dried and made (Bhattacharya *et al.*, 2014). Brick materials are still common in residential constructions all over the world. Most of the masonry buildings made of bricks are vulnerable to collapse under seismic loading. Therefore, many types of research have been done by engineers in the field of retrofitting historical and non-historical URM buildings to improve the seismic behavior of the structure.

The necessity to use tall and huge structures made the stone very popular in the construction industry in the past with the straight availability of raw materials that could be found near the construction site. Durability over time, high resistance against fire, water, and insect damage, easy access, recyclability, high strength, and stiffness in comparison with adobe or brick units are the advantages of stone units. The negative aspect of this material is the inability to resist or develop elastic deformations, unlike burned clay bricks. Juhásová *et al.* (2008) stated that ductile lime mortar causes better load distribution by reducing the effect of stress concentrations, which depends on the thickness of the bed layers.

Stone had been extremely used in Asia, Middle East, North Africa, Mediterranean Europe, India, Nepal, etc. Among different types of stones, granite was the most common material used in historical construction. **Figure 2-4** shows a segment of two stone heritage.

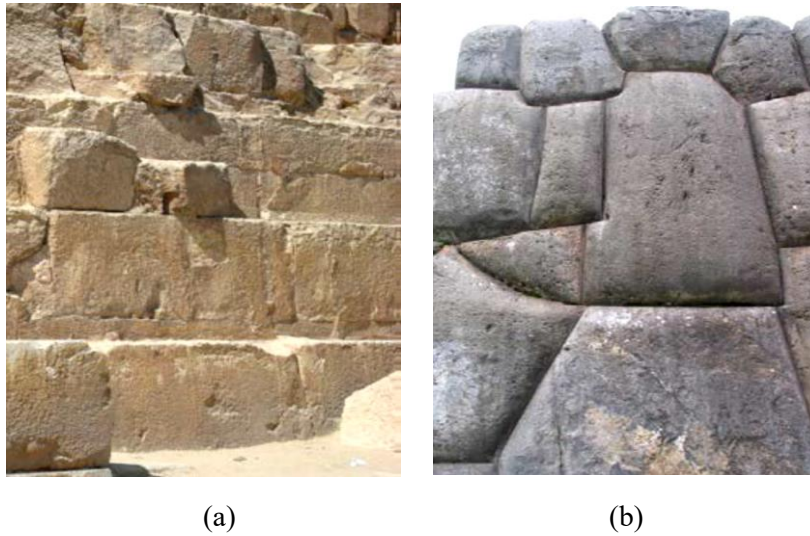


**Figure 2-4** Segment of stone heritage: a) Pyramids of Cairo in Egypt; b) Inca wall in Peru (Adapted from Quiroz, 2011)

## **b) Timber structures**

Due to the purpose of this study on the investigation of historical masonry structures, only a brief description of wooden structures is given here, which shows what types of materials were used in historical structures.

In some areas with favorable vegetation, wood is widely used in construction. It is observed that timber as one of the oldest building materials with large tensile strength had been used on the whole structure or adopted extensively for building horizontal elements such as beams, ceilings, and floors in ancient times. The main advantage of this material is its availability in nature.

### **2.2.2 Geometry**

One of the important factors which play an important role in how a building behaves during an earthquake is the geometry and shape of that building. The geometrical survey coupled with the historical analysis of masonry heritage is necessary to determine the behavior of both structural and architectonic decorative elements or all the modifications on the building during its history. This survey including topographic survey and photogrammetric survey represents a combination of elements and features specifying the structure with detailed graphical documentation. Furthermore, this information helps us to classify historical masonry structures according to the geometry and configuration of the building to choose the best retrofit method.

Historical structures can be geometrically categorized depending on several factors. The availability of materials (stones, clay bricks, and mortars), structural elements (walls, domes, arcs, vaults), architectural usage (palace and monastery), constructive techniques, and appearance are some of the factors that can influence the arrangement or assemblage methods of the constitutive units. The arrangement means the way that units and mortar could be placed on top of each other to constitute a structural element (Quiroz, 2011).

Three main categories can be defined based on the previous documentation and researches on historical masonry structures to describe the geometry and the type of configuration.

Regular masonry of bricks or carved stone uses head and bed joints of mortar to form a structural element or uses the dry-stack method to place units on top of each other. The implementation of dry unit construction relies on the gravity load and the friction resistance between the units (**Figure 2-5(a)**). Round, square, or rectangular structural elements have greater resistance to damage during an earthquake because their geometry allows for equal resistance of lateral forces in all directions.

Irregular masonry structure includes a combination of units without a complete carving (rubble) and mortar as the matrix. The units are distributed irregularly in the mortar (**Figure 2-5(b)**).

The third arrangement is three-layer masonry (three-leaf masonry) with the combination of the regular arrangement for external layers and the composition of rubble stones with mortar to infill the inner part of the construction. (**Figure 2-5 (c)**) (Quiroz, 2011).

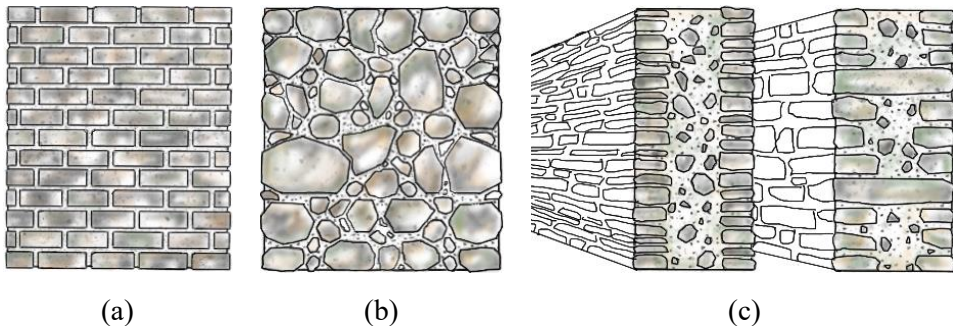


**Figure 2-5** Types of arrangements of historical masonry constructions: a) Regular masonry; b) Irregular masonry; c) Three-layer masonry

Buildings with irregular configurations are more vulnerable during an earthquake because of unfavorable strength, stiffness, and ductility.

Different classifications can be found in other scientific sources. Croci (1998) has divided the historical masonry structures into six different groups. According to his classification, the first group includes constructions of units (bricks of fired clay or carved stones) with regular mortar joints. Stones in their natural type and shape form the second group of structures. Three-layer or three-leaf masonry can be placed in the third group. A combination of bricks and stones makes another type of masonry construction. Dry-stack masonry of units without mortar is one of the most popular methods in stone structures. The last group includes bricks of sun-dried clay (adobe) with mortar of the same material (Quiroz, 2011).

### **2.3 Structural Characterization**

Historical URM structures represent a different response to earthquake excitation in comparison with modern structural systems, such as reinforced concrete and steel frame structures. Having high stiffness and brittle behavior along with flexible floor diaphragms, which are the characteristics of historical masonry structural systems, making them vulnerable to ground accelerations (Moon, 2003).

Investigation of the structural components (foundation, wall, and vault) and masonry components (units, mortar, and grout) of historical masonry structures is

necessary to understand the response of each historical element under earthquake excitation for future restoration works.

### **2.3.1 Structural components**

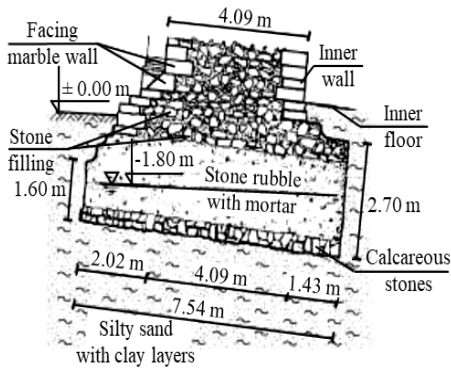
As aforementioned above, the study of structural components of historical structures can help us to understand and predict the mechanical behavior of the elements under seismic loads. Here, the main structural components are categorized into four various groups of elements that are mostly seen in historical structures. They also play an important role in the structural behavior of historical buildings.

#### **a) Foundation**

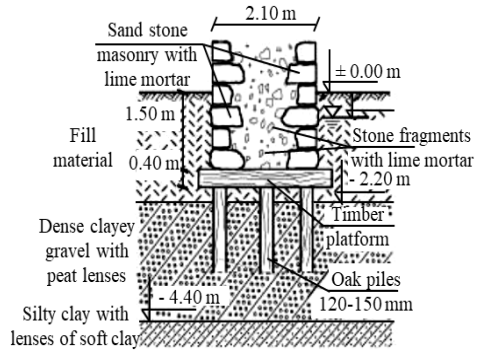
Archaeological, historical, and bibliographical information relating to the foundation building of historical constructions proves that it is one of the oldest human activities. Previous experience, ancient rules, and intuition have been influential factors in the construction and development of the foundation process in the past. Nevertheless, they were not enough to design all further constructions with different usage and different materials. The lack of proper building techniques, various problems in the subsoil condition, and poor soil-structure interaction did not lead to the advancement of foundation engineering science. However, later significant progress appeared in foundation engineering during ancient Rome by the development of new materials such as pozzolanic concrete and steel.

Some other factors such as various soil conditions in particular geographical regions, various architectural styles and availability of materials also have a contribution in using different foundation techniques. Nevertheless, foundation engineering has received less attention in the field of building technology in comparison with structural engineering science (Przewłócki *et al.*, 2005).

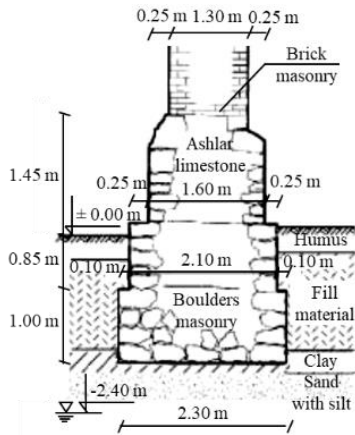
Many historical buildings had lost their resistance and finally collapsed due to many reasons, including natural disasters (flood, earthquake, and wind), war, exhaustion, and deterioration. Some others suffer from poor stability and existing cracks in structural elements that need preservation to prevent unexpected failure. In between, the foundation of numerous historical buildings remains and/or supports the outstanding structure. Therefore, investigation of the current stage of the foundation of historical constructions and its interaction with the structure and underlying subsoil is required for the structural analysis and the application of proper retrofitting methods (Przewłócki *et al.*, 2005). In **Figure 2-6**, several types of historical foundations are illustrated in various architectural and historical eras.



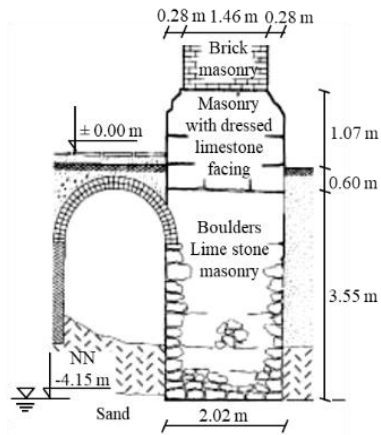
(a) Tower of Pisa (Romanesque)



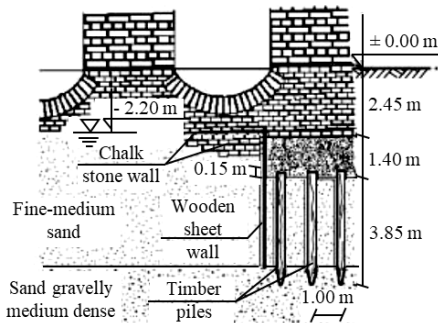
(b) Cistercian Lure Abbey



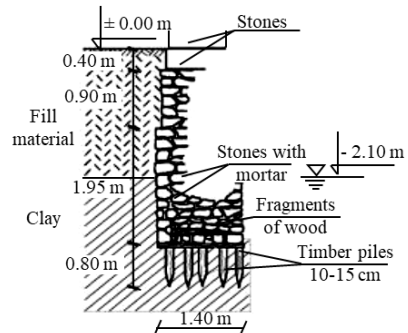
(c) Church in Trzemeszno (Gothic)



(d) Saint Maria church (Gothic)



(e) Reichstag building in Berlin



(f) Greater Savina monastery

**Figure 2-6** Foundations types of historical structures (Adapted from Przewłócki *et al.*, 2005)

**b) Wall (bearing, shear, flexural, and non-structural)**

Four principal types of URM walls are defined structurally in this study as bearing, shear, flexural, and nonstructural walls. Unreinforced load-bearing masonry wall bears the gravity load and transfers it to the foundation. This can be the major load resisting system of historical URM structures. A partial or total collapse of URM structures can be generated by inducing damage in these types of walls. Shear wall resists in-plane lateral loads such as earthquake load through shear behavior. Earthquake excitation is assumed to be exclusively transmitted into the structure through the in-plane walls. Senthivel and Lourenço (2009) categorized historical stone masonry shear walls into four different types (**Figure 2-7**) as follows:

- a) Sawn dry-stack or dry-stone masonry without bonding mortar;
- b) Regular stone masonry with bonding mortar;
- c) Irregular stone masonry with bonding mortar;
- d) Rubble masonry with irregular bonding mortar thickness.

Flexural wall resists out-of-plane lateral loads through flexural behavior. However, the low strength of this type of wall against lateral loads limits their capacity to transfer forces. Non-structural wall has no significant effect on load-bearing capacity and usually is used as decorative and partition elements.

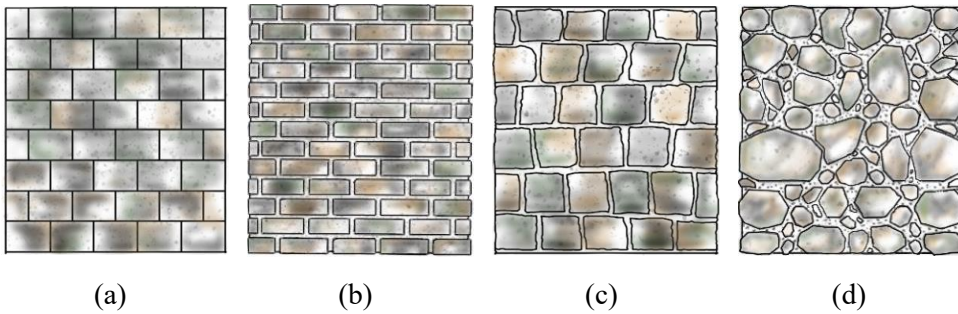


**Figure 2-7** Historical masonry walls: a) Sawn dry-stack wall without bonding mortar; b) Regular stone wall with bonding mortar; c) Irregular stone wall with bonding mortar; d) Rubble wall with irregular bonding mortar thickness

### c) Arch, vault, and dome

Arch, vault, and dome are known as one, two, and three-dimensional elements, respectively, to bridge an opening between walls. These structural components are made of sun-dried bricks, fired bricks, or stones with different types of mortar. They have been used as a complex geometric form to create attractive and valuable buildings in terms of architecture and aesthetics with open covered spaces. They were widely used in the countries of the Middle East and Egypt to keep the desired temperature of the interior spaces. As a result, the environment made by these components can adapt to the most varied climatic conditions such as rainy and.

There are different types of arches, vaults, and domes, each designed for a specific purpose. Some are designed to overcome structural problems and others for aesthetic and architectural issues as a decorative element (**Figure 2-8**).

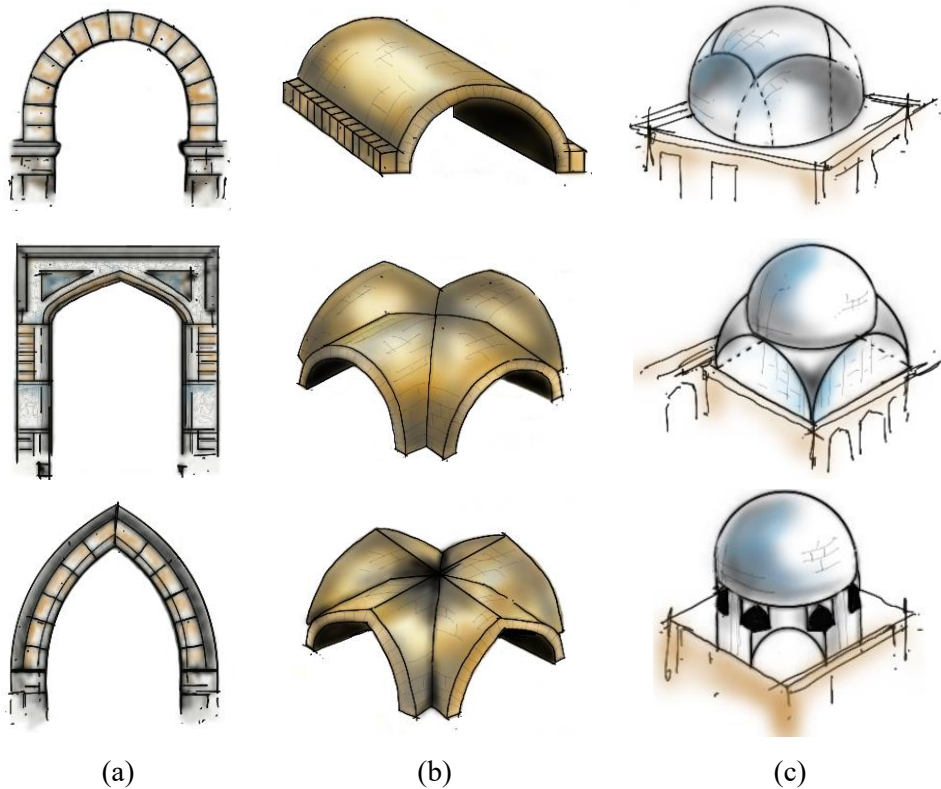


**Figure 2-8** Curved structural components: a) Arch; b) Vault; c) Dome

By repeating arches resting on pillars, arcades can be obtained to cover large open spaces. Arcature or blind arches had been used to reduce the mass of masonry structures or for decorative purposes (**Figure 2-8(a)**). Vault is a structural member made by the arrangement of arches. The barrel vault is a consecutive series of arches that should be buttressed along its entire length. To cover a rectangular space a groin (or cross) vault can be used which is made of the perpendicular intersection of two barrel vaults repeated in series (**Figure 2-8(b)**). A dome is a semi-circular, segmental, ogival, and conical structure with a circular plan that can be obtained by rotating an arch (**Figure 2-8(c)**).

It is possible to use a combination of these three types of structural elements. More types of arches, vaults, and domes can be found in the literature.

From the structural point of view, they are vulnerable to seismic effects and cause damage to the structural system. The thrust actions transmitted by arches, vaults, and domes cause damage to walls and piers, and in severe cases, it may lead to tilting and deformation of the supporting system. The outward thrust caused by arches on thin pillars can easily push or tilt the pillars over with large forces similar to the case that happened in the roof of Kings College Chapel (England). Use of thick walls as buttresses behind the supporting walls or addition of partial arches on the side of the main arch (flying buttress) are the solutions to resist the outward thrust (Figures 2-9(a) and (b)).

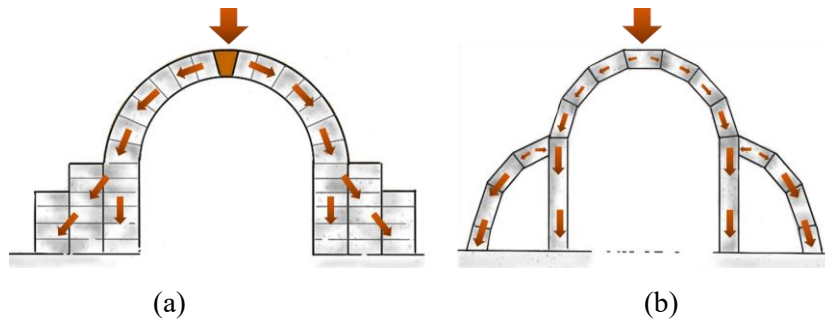


**Figure 2-9** Buttresses: a) Adding a thick wall behind the arch; b) Adding partial arches on the side of the main arch

Later, designing pointed arches by Gothic architecture caused less thrust action at the base. Nonetheless many arches, vaults, and domes subjected to moderate earthquakes had survived the effects of earthquakes with no or an acceptable degree

of damage (Mahdi, 2016). In general, the evaluation of these types of structures is complex and needs numerical and experimental analysis to obtain accurate results.

#### **d) Beam and column**

Historical structures are identified by a complex geometry consisting of straight (pier or wall) or curved members (arch, vault, and dom). In most historical structures, the load-bearing system is the wall. Therefore, beams and columns as the structural elements did not exist in these structures. Beams made of wood to cover ceilings and columns (piers) as decorative or monumental ornaments were commonly used. In recent decades, vertical and horizontal ties have been added to improve the seismic behavior of the structure, which can be defined as beams and columns. However, due to the poor connection between the horizontal and vertical ties, they cannot be considered as moment-resisting frames. The tie bar increases structural integrity and improves the bearing capacity of the structure. In the next chapter, this system is further explained.

### **2.3.2 Masonry components**

Masonry is a composite of anisotropic components including units, mortar, grout, and accessory materials (Tanner and Klingner, 2017). Each component has its specific properties that make masonry construction a non-homogeneous assemblage (Zamani Ahari, 2013). Therefore, the geometry and material properties of the masonry components (units and mortar), the way they are assembled, and the

dimension or shape of the units are the main factors to identify the mechanical behavior of a masonry structure. Understanding the material properties of the masonry component is difficult due to the variability and heterogeneity of the material. However, it helps us to identify the periods of the construction, type, and stage of the damage, strength, and stability of the material to choose proper intervention for conservation works.

### **a) Units**

Units are the principal constituent elements of a masonry structure with high resistance to compressive loads. The type and configuration of a masonry assemblage are determined by the type of unit arrangements. Many old structures are built in the form of dry-stack masonry by simply placing units on top of each other. However, the low tensile strength of units has caused using mortar or reinforcement between them to increase the stability of the structure.

### **b) Mortar**

The function of the mortar in masonry is to make a better coherence between units and hold them together at a specific distance. Mortar is usually made of different compounds that can vary depending on the type of structure or environmental and climatic conditions. The composition of lime or clay with water was mainly used in historical constructions. Moreover, some materials such as fibers of vegetation and the blood of animals had been added to the mortar to increase its

resistance, adherence, and durability. The manufacturing of new material (pozzolana) from a combination of lime enhanced with the addition of volcanic ashes by the Romans made significant progress in the field of construction. That caused the Romans to develop the first concrete and built huge construction. By creating Portland cement, mortar with very high strength and high elastic modulus was made. They could reduce the time for hardening and increase the stiffness of the structure (Quiroz, 2011).

Later, with the advancement of science and technology, some standards for the construction and use of mortar in building structures were considered. ASTM C270-12 (2012) is one of those standards which classify the type of mortar as follows (Tanner and Klingner, 2017):

Type M: High compressive strength and tensile bond strength;

Type S: Moderate compressive and tensile bond strength;

Type N: Low compressive strength and tensile bond strength;

Type O: Very low compressive and tensile bond strength;

Type K: No longer used

### **c) Grout**

Grout usually is used to filling the voids and spaces in a masonry assembly or to cover reinforcements and anchors to prevent corrosion and weathering (Tanner and Klingner, 2017).

## 2.4 Wall Behavior

Experiences from past earthquakes demonstrated that historical masonry structures suffered severely from damage which may lead to the collapse of the whole structure. Its response and failure mechanisms rely on the structural integrity (the connections between structural elements), the behavior of shear walls, material properties, and thickness of bearing walls. Therefore, evaluation of the seismic vulnerability of these valuable buildings using the experimental or numerical investigation is essential for restoration work, which is one of the most important topics in structural engineering in the last decades.

Two main approaches can be considered to assess the seismic vulnerability of a building. The first approach is the general methodology and is based on using a simple methodology for a large group of buildings in a qualitative manner. The second approach is the refined methodology which evaluates the seismic behavior of a building in a quantitative manner by considering its detail. Therefore, the selection of a proper approach depends on the objective of the study and the reliability of the expected results (Quiroz, 2011). A historical URM structure is known as a composite structure with high specific mass and low ductility due to weak tensile and shear strength. In general, the main character of ancient masonry structures is the high ratio of compressive strength to gravity loads, i.e., excellent behavior in compression (Lourenço *et al.*, 2011). Generally, walls and diaphragms are the main structural elements in historical URM buildings.

Therefore, the structural responses are defined by the out-of-plane and the in-plane behavior of the walls and diaphragms. Further, seismic performance of URM buildings highly depends on the ability of the structure to redistribute the horizontal loads between the structural elements. The connection between orthogonal walls, the connection between walls and diaphragms, and the flexibility of the horizontal diaphragms are the most influential factors to improve the load redistribution between structural elements (Lourenço *et al.*, 2011).

As shown in **Figure 2-10(a)**, poor connection between structural components or weak out-of-plane strength of the walls results in the overturning of walls (local failure) and is considered as the out-of-plane behavior of the building. The in-plane behavior of walls and horizontal diaphragms control the box-type behavior of the structure and protect it from global failure or collapse (**Figure 2-10(b)**) (Simões, 2018). Based on the above discussion, the in-plane behavior of walls is the most critical factor in the global behavior of the historical URM buildings. Hence, the in-plane behavior of walls under compressive, tensile, and shear loads is discussed in the following sections.

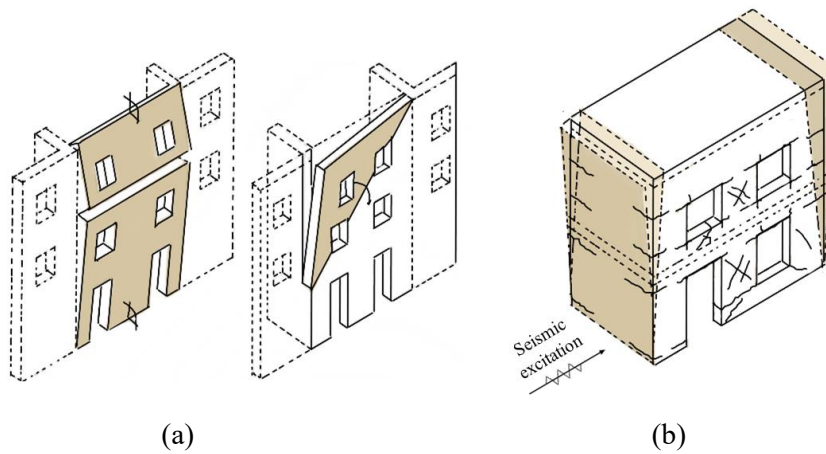


**Figure 2-10** Seismic performance of URM buildings: a) Local damage mechanisms; b) Global response (Redrawn based on Simões, 2018)

### 2.4.1 Wall behavior under compressive load

URM structures are known as high strength construction subjected to compressive loads. The performance of historical masonry structures under high vertical (compressive) loads depends on several factors. The typology of the construction (regular or irregular configuration), the way of assemblage (dry-stack or using mortar to attach the units), the joint behavior (interaction between units and mortar) and material properties are effective in resistance of the construction (Quiroz, 2011). Where the wall is under a uniaxial compressive load, an interaction is formed between units and mortar. Since the unit is stiffer than mortar, it allows less deformation and constraints the strains of the mortar. So, it produces a state of stresses represented by tension in the unit and compression in the mortar. If the compressive stresses are elevated, they could exceed yield strength, and as a

consequence, increase the probability of collapse. Meli (1998) states that under high compressive loading, typically there are three types of failure mechanisms in historical URM walls, which mainly depend on the arrangement type of the wall elements (**Figure 2-11**). In the regular walls, the failure mode is represented by vertical propagation of cracks in units and mortar (see **Figure 2-11(a)**). The pattern is generated by transversal tension as the above explanation. The second failure mechanism is the crushing in the mortar matrix and detachment of the stones in the disorganized masonry as shown in **Figure 2-11(b)**. The third failure mode is a special case presented in the three-layer masonry by separation in vertical elements due to cracking propagation in the weak middle layer (**Figure 2-11(c)**). These three failure mechanisms could seriously cause the collapse of the building. This failure mechanism presented in the three-layer wall, with separation of two vertical layers due to the weak infill material, results in a brittle failure in the wall and progressive or unexpected collapse of the building. The sudden collapse of the historical civic tower of Pavia, Italy in 1989 is one typical example of such failure. Croci (1998) described that the presence of a severe cracking parallel to the direction of loading (transversal tension) is the most commonly observed failure in URM walls under high compression, similar to the case of historical construction. If the rest of the elements is not able to compensate for the damage, this local failure could represent catastrophic consequences to the structure due to unstable conditions, resulting in the global failure of the structure (Quiroz, 2011). Note that mortar is not used in dry-stack walls and the above-mentioned failures are not of concern.

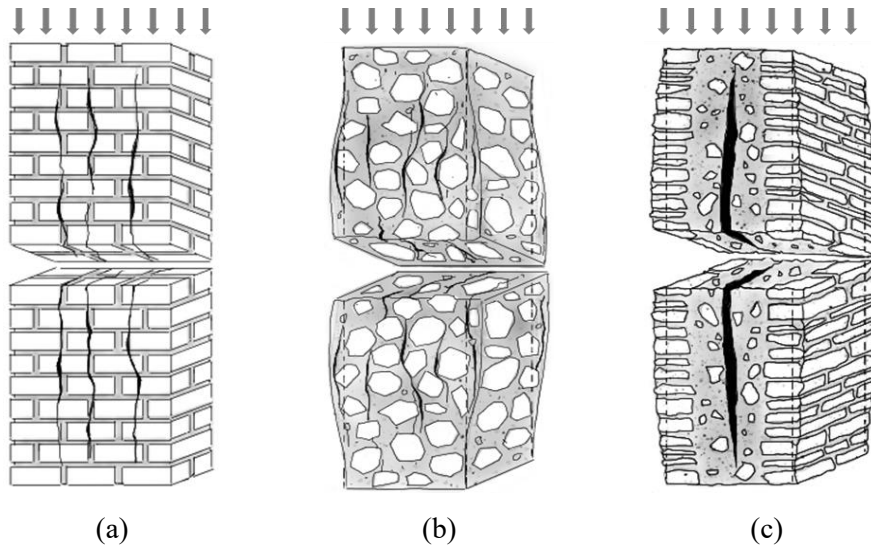


**Figure 2-11** Failure modes due to high vertical loading: a) Transversal tension; b) Crushing; c) Separation due to weak plane (Redrawn based on Meli, 1998)

## 2.4.2 Wall behavior under tensile load

The performance of unreinforced masonry structures under tensile stress is quite weak in comparison with that under compressive stress. Resistance of a historical URM structure in tension highly depends on the bond behavior between its elements such as cohesion and the strength of the units and mortar. In the case of the dry-stack walls, the tensile strength is zero due to lack of mortar, and therefore elements are simply disjointed under tensile load.

Quiroz (2011) has defined three different failure mechanisms for masonry construction subjected to uniaxial tensile loading perpendicular to the bed joints (**Figure 2-12(a)**). The first failure is generated in the interface plan of the units and mortar (at bed joints) due to the weak bond or lack of conjunction between them

(Figure 2-12(b)). The second failure is due to the cracks generated inside the unit elements. It usually occurs where tensile stress exceeds the allowable limit and the cracks appear horizontally through the units (Figure 2-12(c)). The third failure mechanism can be observed by the cracks in the mortar due to the exceedance of tensile strength under uniaxial tensile loading (Figure 2-12(d)). In most historical masonry structures, a combination of these three failure mechanisms can be perceived.

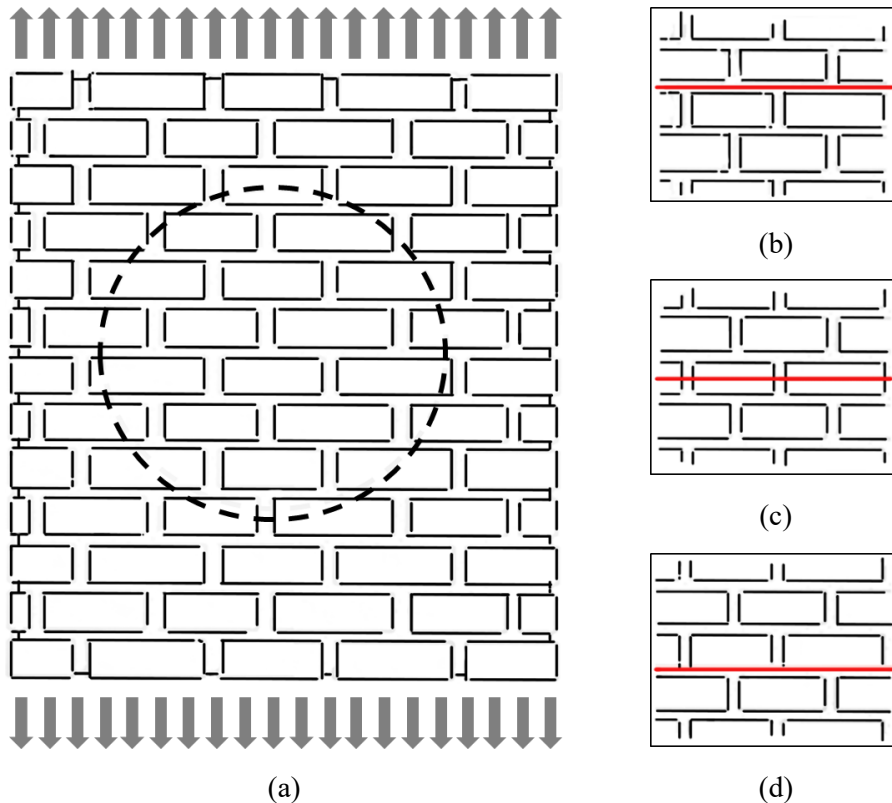


**Figure 2-12** Failure mechanism of masonry under tensile loading: a) Masonry wall under tension; b) Failure of the bond; c) Failure of the units; d) Cohesion failure (Redrawn based on Meli, 1998)

### 2.4.3 Wall behavior under shear load

Historical masonry structures under lateral loads such as wind or earthquake excitation usually confront a combination of shear and compressive forces. The mechanical behavior and the performance of masonry structure under shear force depend on the adhesion, friction, and tensile strength of the mortar joints and the units (Quiroz, 2011).

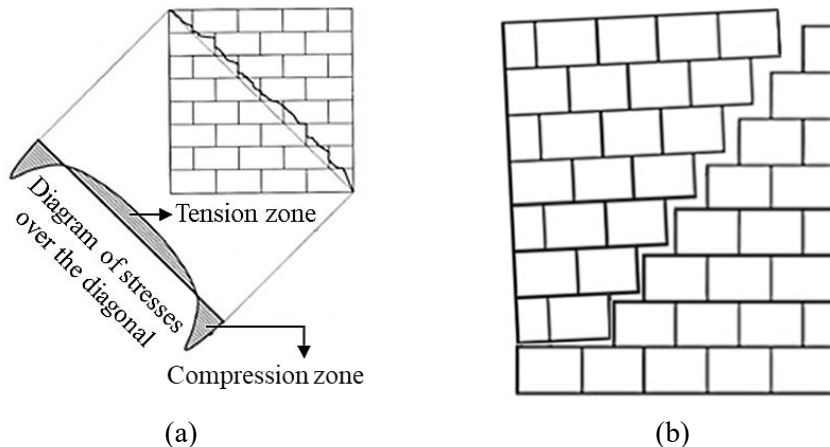


**Figure 2-13** Failure of wall under diagonal tension (shear): a) Wall with mortar; b) Wall without mortar (dry-stack) (Redrawn based on Meli, 1998)

When a URM wall is subjected to lateral loading in its plane (shear load), a state of tensile stresses is induced in the normal direction along the diagonal line (**Figure 2-13(a)**). Due to the low tensile strength of masonry, the failure mechanism is presented by cracking distributed along the diagonal line (about 45 degrees) that tends to separate the structural element into two parts. The position of the diagonal

crack depends on the direction of the loading, and in the figure, it acts from the left top to the right bottom of the wall. Due to the alternation of the seismic loading in masonry walls subjected to earthquake excitation, the cracking by two diagonals forming an “X-shape cracking” is commonly observed. In this case, as shown in **Figure 2-13(b)**, the dominant sliding line is formed at the unit interface along the diagonal line, and during the cyclic loading the direction is changed, forming an X-shape similar to the former case.

## 2.5 Summary

In this chapter, historical structures were investigated from various aspects such as constituent material, configuration, geometry, and components. Unreinforced masonry (URM) walls are one of the most common structural components in historical structures. Therefore, its behavior under different types of loading was discussed in more detail. In general, URM walls have excellent behavior under compressive loads. Whereas, because of zero or low tensile strength, the behavior of URM walls under tensile and shear loads is not desirable, and appropriate techniques are required to improve the behavior.

## **Chapter 3. Typical Seismic Damage in HURM Buildings**

The significant parts of Unreinforced Masonry (URM) structures may damage or collapse if they are not usually designed and constructed to withstand unpredictable events such as earthquake load. Historical Unreinforced Masonry (HURM) buildings are even more vulnerable due to the lack of adequate structural design for lateral loads. Understanding the mechanical behavior of a historical structure and possible damage mechanisms is an essential step in preservation work. In this chapter, typical seismic damage in non-structural and structural components of HURM buildings is described. Besides, erosion damage and its influence on the performance of HURM buildings are discussed.

### 3.1 Typical Damage of HURM Structures

Major structural elements of URM buildings under earthquake excitation may damage or collapse if they are not usually designed and constructed to withstand unpredictable ground motions. HURM buildings are more vulnerable to seismic events because their structural elements were not usually designed for lateral load. Also, mechanical properties have weakened due to the deterioration of materials over the years. As discussed by Aguilar (2016), some of the main parameters that are required for describing how and why historical buildings are damaged in an earthquake can be listed as follows:

1. Depth of the earthquake
2. Duration of the earthquake
3. Distance between the building site and earthquake epicenter
4. Building construction type (structural systems and materials)
5. Building design type (plan, elevation, and interior space configuration, nonstructural elements, overall mass)
6. Existing building condition (maintenance level)
7. Site and soil conditions

Restoration of historical structures depends on the correct intuition of the potential vulnerabilities in deficiencies of the structural components as well as the nonstructural components of the building.

Also, detection of various types of hidden and obvious defects on the structure as well as the evaluation of its mechanical performance are essential to select proper retrofitting techniques.

To prevent the collapse of the whole structure or irreparable damage, some priorities in the preservation process are defined by Shad (2015). In comparison with elements that may cause partial failure, the preference is to preserve elements with a higher rate of degradation or under a greater and longer duration of load, major structural elements, and elements that may result in the loss of a major feature. The type and the location of damage, as well as the failure mechanism, are determined by the variation on the typology, physical, chemical, and mechanical properties of the material, history, occupancy and use, and seismic hazard of the site. Furthermore, in conservation works the compatibility of materials for rehabilitation with the base material is very important to prevent the concentration of stress on a part of structure and failure (Quiroz, 2011). In fact, failure or collapse is usually caused by a combination of several types of damage or degradation in several parts of a structure. Therefore, understanding the mechanical behavior of a historical structure and possible damage mechanisms is an essential step in preservation work (Shad, 2015). In this chapter, typical damage in HURM buildings' components due to earthquake excitation is discussed in two categories of non-structural and structural elements. Furthermore, it will be discussed how erosion and other environmental factors influence the performance of HURM buildings.

## 3.2 Damage in Non-Structural Elements

In the last decades, preservation and conservation of both structural and architectural elements of historical masonry structures is one of the important objects in the engineering field. For assessment of the structural conditions, one needs to pay attention to materials, decay conditions, construction methods, and other factors to define operation planning and a series of conservation methods. Damage of non-structural elements due to earthquake excitation may contribute to the entire building's destruction and also can cause injuries or death of occupants. In historical masonry structures, which are more vulnerable to the ground motions, the non-structural and content damage can be increased during the aftershocks (Dhakal, 2010). Therefore it can increase the cost and time of repair. So the connection between non-structural elements and structural elements should be evaluated properly, taking necessary steps to improve the behavior if it is required.

The non-structural components include chimneys, parapets, ceilings, facades, internal walls, partitions, windows, doors, etc. The sensitivity to deformations, accelerations or both can cause damage to these elements. However, the type, configuration, history, age, and usage of the building can affect the type as well as intensity of damage (Baird and Ferner, 2017). Some examples of damage in non-structural elements are shown in **Figure 3-1**.



**Figure 3-1** Damage in non-structural elements: a) Severe damage of RC cornice; b) Poorly connected balcony; c) Timber joists attacked by termites (Adapted from Jiménez *et al.*, 2018)

### 3.3 Damage in Structural Elements

The poor performance and high seismic vulnerability of URM structures are evident from the damage that the structures have experienced during past earthquakes. Wall stability, type of roof system, quality of the mortar, and geometrical features are the main cause of the collapse of walls or the entire building, and determine the overall performance of URM buildings. For instance, shear cracks in the walls starting from the corners of openings, poor connection of joints, and the failure of load-bearing walls can cause a partial or complete collapse of the structure (Zamani Ahari, 2013).

Many experimental and numerical types of research have been conducted in recent decades to understand the causes and mechanisms of the failure in HURM structures by Deppe (1988), Boussabah and Bruneau (1992), Bruneau (1994), and Tomazevic (1999).

As described by Moon (2003), common types of damage in structural elements of HURM structures that were reported in the past earthquake events can be generally categorized as the following failure modes:

1. Connection failure
2. Wall failure
3. Diaphragm failure
4. Foundation failure

These failure modes are discussed in more detail in the following subsections.

### **3.3.1 Connection failure**

Connections between structural components are the most critical elements which can determine the type and extent of damage. It can be said that global responses of a structure to earthquake excitation are critically influenced by the type of connections and interactions of each structural component.

Based on Eurocode 8 (EN 1998:2005-1), special attention should be paid to the adequacy of connection between floor systems and walls, and it should be provided by steel ties or reinforced concrete ring beams. For masonry structures, the code requires that: “Non-ductile lintels should be replaced, inadequate connections between floor and walls should be improved, and out-of-plane horizontal thrusts against walls should be eliminated”. Tomažević (1999) explained that code prescriptions were determined based on the fact that the box-like behavior of URM

structures is ensured by well-connected bearing walls. In this condition, rather than local failure due to disintegration, lateral loads can be distributed among structural members according to their relative stiffness.

An analytical model was developed by D'Ayala and Speranza (2003) to identify more possible failure mechanisms in URM structures based on building geometry, materials, and connections. The model is based on an extensive database of on-site observations collected after seismic events. Based on the model, the poor quality of connections between walls or part of them often results in the collapse of the building façade. Similar observations were also obtained by the analytical model developed by Felice and Giannini (2001).

Based on D'Ayala and Paganoni (2011), continuous and efficient connections prevent out-of-plane mechanisms of walls, enhancing active in-plane shear capacity. Indeed, boundary conditions of the walls determine the response of walls, i.e. in-plane or out-of-plane response.

Another critical and damage-sensitive element of URM structures is the connection between perpendicular walls (corner connection) due to stress concentration. Where the two walls at the corner are unrestrained, instability problems are observed because the corner section is free to move. In this condition, one wall may remain very stiff because of in-plane action, and the other rock out-of-plane. It can result in the growth of gaps between the walls and even vertical cracks in the out-of-plane wall.

Usually, these kinds of damage are not critically serious from a life-safety perspective. Nonetheless, in the case of large damage, walls can become fully isolated and behave as freestanding walls. Consequently, the probability of collapse or overturning is greatly increased and seriously endangers life safety (Shad, 2015).

Vertical cracks at the corner due to the interaction of perpendicular walls are usually results of flexural and tensile stresses due to out-of-plane motions. It would be more dangerous if it occurs on both faces of the wall which results in the collapse of the wall. In addition to vertical cracks in out-of-plane walls, diagonal cracks at the corners due to shear forces acting on in-plane walls can be initiated from the top corner and grow laterally and downward. Repairing this type of damage is tough and so reconstruction may be required or could be a better option. A combination of vertical and diagonal cracks in the corner dramatically increases the possibility of collapse.

The connection between the diaphragm and out-of-plane walls is another critical component in URM buildings. In the case of poor connection, out-of-plane walls as a cantilever system could result in unstable behavior and eventually partial or complete collapse of the wall even under minor earthquake (Bruneau, 1994). The condition would more be critical if the connection between in-plane walls and the diaphragms fails since out-of-plane walls should support all lateral load (Moon, 2003).

### 3.3.2 Wall failure

The two main failure modes of URM walls are in-plane and out-of-plane modes (**Figure 3-2**). The other failures may eventually cause out-of-plane or in-plane failure in the structure (**Figure 3-3**). For example, poor connections cause separation between the structural elements or the out-of-plane collapse of the walls. Also, the damage due to insufficient load-bearing capacity of the walls causes diagonal cracks and may result in the disintegration of the walls and partial or complete collapse of the structure. Nonetheless, historical buildings usually experience a combination of both failure modes (Asteris *et al.*, 2005).

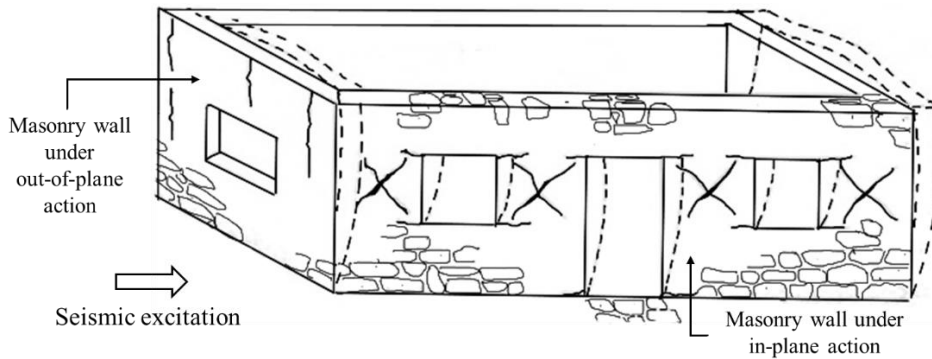


**Figure 3-2** In-plane and out-of-plane failure mechanism of URM walls (Redrawn based on Zamani Ahari, 2013)

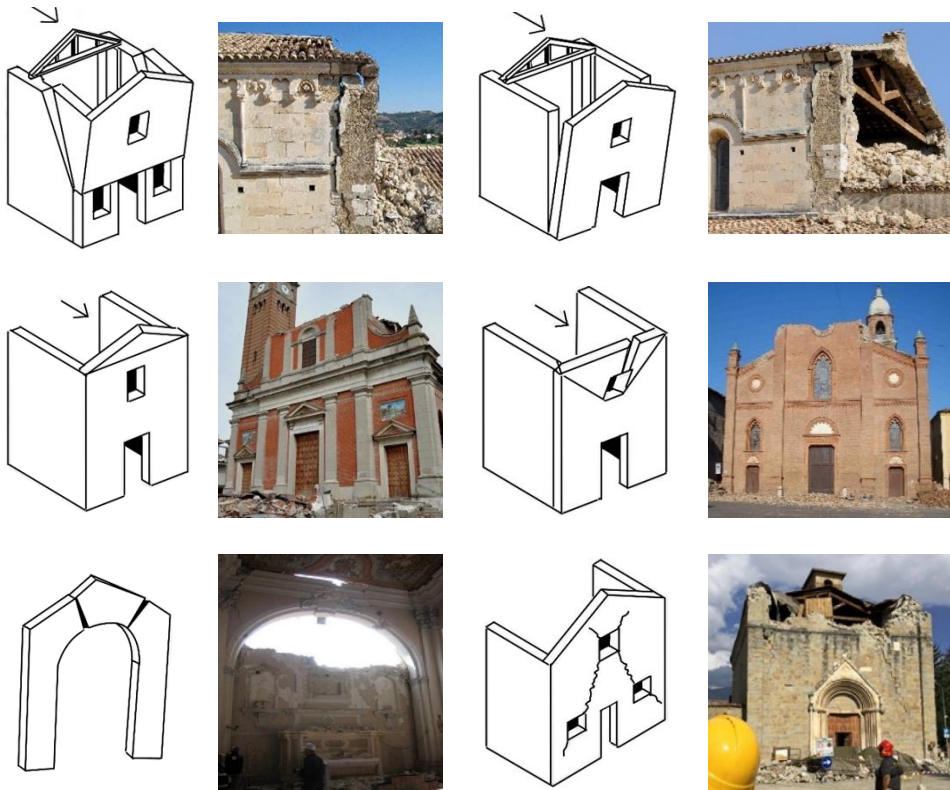


**Figure 3-3** Typical in-plane and out-of-plane failure of URM buildings (Adapted from Malena *et al.*, 2019)

As discussed before, if walls are not well connected at the corners, they can behave individually in the out-of-plane mode under lateral loads such as an earthquake. If sufficient anchorage and strong connections are provided, lateral forces can be transferred from the out-of-plane wall to the diaphragm. In this condition, out-of-plane walls can span between floors, and their slenderness is reduced. Therefore, stability is improved which results in minimizing damage and failure of out-of-plane walls (Bruneau, 1994).

In the case of multilayer walls, layers (wythes) also should be properly tied together by using adequate header courses. Otherwise, cracks can develop through the collar joint (interface of layers) and lead to independent out-of-plane motion of wythes. Another vulnerable element to out-of-plane failures is parapets which behave as a cantilever system attached to the roof (Moon, 2003). Cupolas and vaulted roofs in HURM buildings usually have a considerable mass and can transfer large inertia forces to the supporting walls. Therefore, special attention should be considered if such elevated components with high mass are supported by out-of-plane walls (Quiroz, 2011).

URM walls made by adobe units are so sensitive to flexural stresses and cracks due to out-of-plane wall motion. The cracks usually appear in a wall between two transverse walls and initiate at each intersection, grow downward vertically or diagonally to the bottom of the wall, and then develop horizontally along wall length. In this condition wall rocks (rotates) about the horizontal crack at the base (Shad, 2015).

The major parameters that control out-of-plane behavior can be considered as wall thickness and the slenderness ratio, connection between wall and roofs, load-bearing or non-load-bearing type, distance between intersecting walls, and wall support condition. Whereas, erosion in support elements (results in reducing load-bearing area), excessive moisture content (results in reducing strength), and wet-dry cycles (results in adobe strength reduction) can intensify the vulnerability of out-of-plane walls (Shad, 2015).

In-plane failure is a result of excessive in-plane shear or flexural forces placed on the components of URM walls. Masonry walls with openings (e.g. windows or doors) are composed of two main elements of piers and spandrels. Piers are shear walls between openings and spandrels are deep beams above and below openings. Typically, in-plane failures occur in only one of these elements. Usually, where the damage in the first component occurs, it changes the wall behavior and results in preventing the failure of the other component. Based on a study by Calvi *et al.* (1996), the collapse of URM structures is due to the failure of piers in most cases. As shown in **Figure 3-4**, in-plane failure of walls (and piers) have been studied for many years and are classified into four major groups.

Under flexural stress, if cracks widely develop at the top and bottom of the wall (or pier) and lead to the base and top disconnection, then the wall starts to rotate as a rigid body about the compressive toe. Toe crushing is a result of excessive compressive stress at the toe of the wall (or pier) and is usually observed along with the rocking motion. The level of vertical stress on the compression side is significantly increased by rocking motion and resulting in an explosive failure due to the crushing of the compressed zone. In case that horizontal shear forces are larger than joint capacity, horizontal shear crack is formed at the joint and results in bed-joint sliding failure. In this condition, the wall (or pier) slides horizontally along the bed joint, and the resistance relies only on friction. Although bed-joint failure is usually taking place at the bottom, it can occur in the middle or other locations along the height depending on factors such as the strength of joints.

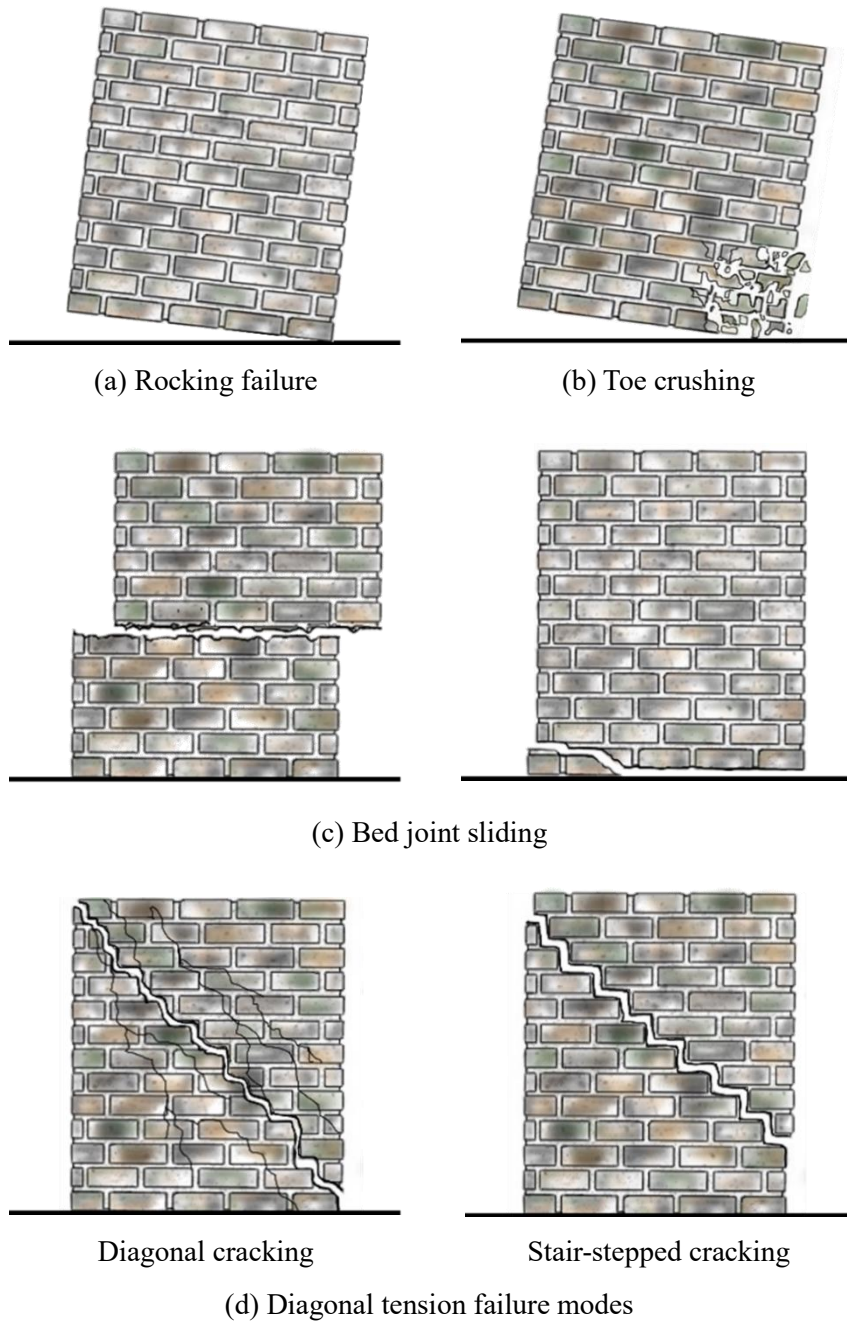


**Figure 3-4** Principal in-plane failure modes of HURM walls

Diagonal tension failure is one of the most common types of wall (or pier) failure under in-plane shear forces. Theoretically, the maximum principal tensile stresses in the wall under lateral in-plane load form along the diagonal line with about 45 degrees to the horizontal. Where these stresses exceed the tensile strength, x-shaped (diagonal) cracks occur under cyclic ground motions. In the case of URM walls, the cracks can form as stair-stepped through the joints or may propagate directly through the bricks, or in a mixed combination. The formation of diagonal cracks highly depends on the strength of mortar, bricks, and brick-mortar interfaces. If cracks propagate in the form of a stair-stepped pattern, damage would be usually less severe in comparison with the other cases. Under severe earthquake load, diagonal shear cracks along with the action of gravity load can cause extensive damage (Shad, 2015).

The results of many studies and experiences show that there are several influencing factors on the failure mechanism of walls under in-plane load. The most important factors are vertical load, slenderness, support conditions at the top (constrained or free rotation), and material properties (Sperbeck, 2008). Based on ATC (1999), the level of gravity load is one of the most determining factors in the behavior of walls. Similarly, observations from experimental studies conducted by Lourenço (1996), Rots (1997), Ötes and Löring (2006), and Mistler (2006) draw a conclusion that level of vertical load and properties of mortar and units are the most influential factors in determining in-plane failure mechanisms.

Generally, the mode of in-plane failure for walls under low levels of vertical stress is rocking or sliding and walls exhibit large displacement capacity. Low horizontal shear capacity due to weak mortar with a low friction coefficient produces the bed-joint sliding failure mechanism. Studies by Ötes and Löring (2006) and Mistler (2006) showed that rocking failure usually occurs in compact and slender walls with weak mortar under low vertical load and eventually results in toe crushing at the compression side. In contrast, where the level of vertical stress is high, diagonal cracking and toe crushing are usually the main failure modes which are typically considered as brittle failure mechanisms. Nonetheless, if diagonal cracking forms as stair-stepped type (i.e. along joints rather than units), the behavior is usually ductile with large deformation capacity due to the sliding deformation (Moon, 2003).

In-plane cyclic behavior of URM walls was studied by many researchers by conducting either using static cyclic tests (Mistler, 2006; ElGawady *et al.*, 2007) or dynamically by shaking table tests (Toranzo-Dianderas *et al.*, 2004; Badoux *et al.*, 2002). General hysteretic behavior observed in the experimental test is shown in **Figure 3-5**. Stair-stepped cracking failure induced a very ductile response but quite small strength, because of limited damage due to the crack formation in joints. Closing and opening of cracks under cyclic load resulted in high energy dissipation, forming the enclosed area with fat hysteresis loops. On the other hand, sudden failure by diagonal cracking without steps is associated with high strength capacity with low ductility.

Brittle behavior due to stiffness degradation results in hysteresis loops with a small enclosed area and so less energy dissipation. Under the rocking motion (rigid body rotation), the wall can present a large capacity for lateral displacements without damage, but the horizontal strength is relatively small. Under the rocking motion, responses form S-shape hysteresis loops with a narrow enclosed area (small energy dissipation). Transferring energy to the support through impact in each cycle (recontacting of the wall and the base) is the main source of energy dissipation during the rocking motion (Quiroz, 2011).

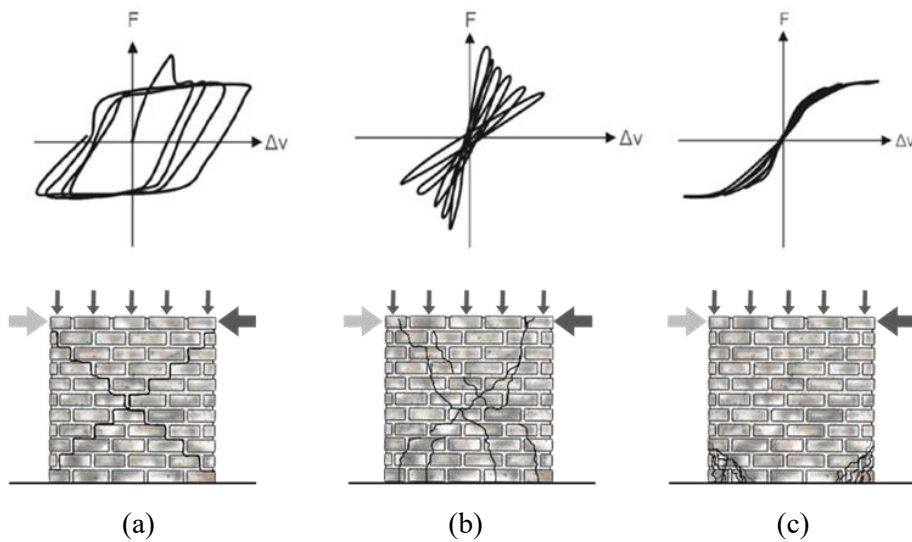


**Figure 3-5** Typical hysteresis loops of URM walls: a) Stepped cracking; b) Diagonal cracking; c) Horizontal cracking and crushing (Redrawn based on Mistler, 2006)

### **3.3.3 Diaphragm failure**

The roof system in some of the HURM structures is made of weak elements and work as a shelter for environmental impacts. However, it is essentially constructed to work as a vertical load-bearing system. Usually, these systems also have a good behavior under in-plane load and work as the horizontal diaphragm, and play an important role in transmitting lateral loads to the vertical structural elements. The mechanical behavior of the diaphragms is similar to simply supported beams (Moon, 2003). Usually, diaphragms have a large deformation capacity and experience less damage during an earthquake. Yet, they can cause damage to other structural members, especially in their connection with vertical load-bearing members. Therefore, investigation of diaphragm rigidity and their connection to other members is a very important part of the preservation program.

### **3.3.4 Foundation failure**

The vulnerability of a historical structure to ground motions highly depends on seismic hazard and soil conditions of the site as well as foundation type. The seismic hazard of a site depends on proximity to the source and intensity of the earthquake and probability of occurrence of an earthquake. Fault rupture, liquefaction and other soil failures, landslides, hazards from adjacent buildings, and tsunami are some other seismic hazards that can influence the soil condition and mechanical behavior of buildings.

Furthermore, the soil condition including geology, typology, and topography affect the ground motion and consequently the vulnerability of the structure on it. Liquefaction is one of the geotechnical matters due to ground motion and instability conditions by soil settlements that cause failure in many constructions and infrastructures (Quiroz, 2011). One of the famous examples of poor soil conditions is unstable subsoil with a thin foundation set under the leaning tower of Pisa, Italy. This tower was constructed in three stages over 177 years. Due to the soil irregularities and subsidence, the tower angled 5.5 degrees (about 4 meters) from which it was completely vertical (**Figure 3-6**).



**Figure 3-6** Leaning Tower of Pisa, Italy (Adapted from Quiroz, 2011)

Soil type also filters frequency content of earthquakes and can dramatically increase the vulnerability of the historical structures, depending on the condition. Soft soil intensifies low-frequency content and filters high-frequency content. Hence, the vulnerability of slender structures like towers with a low natural frequency increases on soft soil. On the other hand, stiff soils intensify high-frequency contents

of earthquake excitation and so mainly amplify the responses of structures with a high natural frequency such as historical buildings (Quiroz, 2011).

### **3.4 Impact of Erosion on the Performance of HURM Buildings**

The effect of erosion and earthquake can be considered as a comparison of damage that undergoes continuously during the lifetime of a structure and extreme disasters that occur only a few times in a lifetime. Earthquakes are unique among other natural hazards since they are coming without warning and their occurrences are relatively rare. Erosion (decay or deterioration) is mainly related to physical or chemical actions, and usually initiates from the outer surface that is directly exposed to the environment and propagates inward the material. Generally, it leads to reducing material strength, increasing brittleness and porosity, and also loss of material (Langenbach, 2008). All buildings are designed for a predefined lifetime, either implicitly or explicitly, and it may be considered from decades to centuries based on parameters such as functionality, convince, and maintenance costs. Historical buildings are exposed to environmental impacts for a much longer period, usually in the order of several centuries. They also probably faced one or more extreme hazards such as earthquakes which strictly reduce the performance of structures (Crocì, 1998; Shad, 2015).

Erosion can be defined as a phenomenon that occurs gradually due to environmental impacts on the structure. Many factors cause erosion, including temperature, humidity, chemical and physical factors, air quality, deposits of the soil,

and so on. Adobe and wooden structures are very susceptible to moisture, humidity, temperature, and wind action. In some areas, the rate of temperature and climate change is rapid. These alterations accelerate the growth process of decay due to the crystallization of salts and worsen the conditions for the structure. Also, the effect of the abrasive action of wind, plant growth, and burrowing by insects or animals on the erosion rate of the structure should not be ignored. Humidity is another influential factor in the reduction in strength of the historical structures mostly in adobe structures. In comparison with other materials such as stone, bricks, clay, and adobe units are more susceptible to decay. The high flexibility and deformability of adobe units in repeated wet-dry cycles significantly reduce resistance to loads even after drying. Therefore, in earthquake excitation, the weakened bond between the adobe material can result in a partial or total collapse of the structure (Shad, 2015).

Damaged structures caused by deterioration and erosion lose much of their mechanical strength against the loads imposed on them, and it can increase the risk of collapse. The connections between the structural elements provide an integrated behavior of the structure against the loads. Hence, deteriorated mortar joints can dramatically weaken the performance of the structure (Aguilar, 2016). It was observed that well-maintained buildings even without reinforcement show better performance during earthquakes. Furthermore, unrepaired cracks from previous earthquakes or decayed materials caused by erosion can increase the risk of greater damage and partial or overall building collapse during the earthquakes.

The main factors that accelerate erosion in the structure are wind, temperature, rain and humidity, biological intervention, and human intervention (Shad, 2015). These factors and their actions are explained in more detail in the following subsections.

### **3.4.1 Wind**

In general, the effects of wind flow on the structure can be investigated in two terms of loading and erosion. The velocity pressure of wind flow induces forces on the building faces, and if natural frequency is close to the dominant frequency of pressure fluctuation resonant action can occur. In this condition, the dynamic vibration is considerable and results in larger deformations and stresses. Commonly, structures with a natural frequency of less than 1 Hz are considered dynamically sensitive structures concerning wind (AIJ, 2015; ASCE, 2017; KBC, 2016). The natural frequency of HURM structures is usually larger than this threshold and so these buildings are not susceptible to dynamic wind action. Therefore, it is generally said that historical structures are more susceptible to earthquakes (which their dominant frequency is less than 1 Hz) than wind loads. However, in addition to global loading, the local effect of wind load can be considerable especially on architectural detailing that is attached to the outer surface of the structure. So the connection should be checked to prevent the collapse of these elements. Wind and sand storms also can cause surface evaporation and mechanical abrasion and are the main factor in the decaying of the surfaces (Shad, 2015). Accordingly, more attention should be

paid to material properties of outer structural elements which directly interact with the environment in wind prone area.

### **3.4.2 Temperature**

Daily or annual changes in temperature play a major role in structural strength and crack expansion and propagation. Temperature changes cause physical and chemical reactions, resulting in deterioration and decay of materials. Physical changes include the expansion and contraction of materials, and chemical changes include the interaction of materials to their strength and physical properties. The intervention used for restoration should be compatible with the constituent materials to prevent structural disintegration (Shad, 2015).

### **3.4.3 Rain and humidity**

Water in liquid and frozen form has a devastating effect on the structure and its seismic resistance. The destructive effect of water on the strength of the structure is not always obvious. Water in the form of rain, snow, ice, and groundwater interacts with the structure in various ways. The way rain and snow affect the structure is that it penetrates the holes or cracks produced by earthquakes in the material and increases the moisture content of the material and thus reduces strength. Moreover, heavy rain flows over the surface and washes away the material, destroying the structure over time. Porous materials such as masonry, plaster, and wood are more prone to this phenomenon. In cold weather, the infiltrated water freezes inside the

cracks, and it causes the cracks to widen and deepen in the structure. Furthermore, condensation of water vapor in the air contains the atmosphere pollution and affects the structure by rain leaking through roofs and other surfaces.

Splashing up the groundwater against the base of the wall or capillary action can propagate the water inside the main structure; therefore, the resistance of the wall to carry the loads may be reduced (Shad, 2015).

It can be concluded that regardless of the type of water erosion, the material loses its strength due to these phenomena, and if the lateral load such as earthquake is suddenly applied to it, the structure may collapse completely.

### **3.4.4 Biological damage**

Corrosion due to the biological pollution of historical masonry structures is very common. Natural materials such as wood and clay units reinforced by straw are more susceptible to biological attack by insects, molds, and the mechanical action of roots. The high temperature and some type of climate can increase the rate of corrosion by harmful termites, rodents, and snakes (Shad, 2015).

Decay by biological contamination can damage both structural and non-structural elements; however, the foundation is more prone to biochemical and moisture attacks due to its position in the soil and can destroy the building strength and cause overall collapse.

### **3.4.5 Human intervention**

The factors including usage, war, false interventions, incompatible retrofitting materials with the original structure. play a role in generating damage by humans. The lack of engineering knowledge of the structure causes mistakes in design, restoration work, and seismic performance of the structure. Changing the usage of historical buildings usually causes severe damage to the architectural elements as well as the structure of the building. Also, it can intensify the rate of erosion of the old constituent materials of historical constructions. The preservation work without reliable provisions and regulation has a negative influence on the structural behavior of the building. Furthermore, some political challenges make a serious threat to historical structures (Shad, 2015).

### **3.5 Summary**

In this chapter, typical seismic damage to HURM structures was discussed in detail. Damage is classified and discussed into two main categories of damage in non-structural and structural elements. Moreover, the influences of erosion on the behavior and performance of these structures were discussed. The information and explanation provided in this chapter emphasize the type and location of critical damage in elements based on past experiences and researches. It can accelerate the process of damage detection and overall assessment of existing buildings which are primary steps in preservation work.

## **Chapter 4. Technical Issues and Methods of Preservation for HURM Structures**

Historical structures are valuable heritages that must be preserved to pass aesthetic, cultural, social, archaeological, and technological values to future generations. Preservation and restoration of historical monuments and structures is one of the scientific topics that have prevented the destruction of valuable buildings by providing various methods. Accordingly, experimental and numerical studies are needed to investigate the structures as accurate as possible and provide the appropriate restoration method according to the vulnerability conditions, authenticity, and credibility parameters. In this chapter, various preservation methods for URM structures are introduced and categorized, and the application to HURM structures is discussed.

## 4.1 Preservation Techniques for HURM

Historical structures are of great importance due to transmitting many value contexts such as aesthetic, cultural, social, archaeological, and technological issues to the future generation as a human civilization's treasure. The Historical Unreinforced Masonry (HURM) structures are defined generally as a building constructed by masonry units such as clay, stone, brick, etc. These structures may have sufficient strength against vertical loads including compressive stress. However, they are vulnerable to seismic loads imposed by earthquakes and behave in a brittle manner (Sayin, 2019). Lateral forces cause large shear and tensile stresses in the structures, which over time reduce the structural strength, bearing capacity, eventually causing collapse. Furthermore, destructive activities such as unauthorized demolishing and excavations to build new constructions, as well as environmental factors such as deterioration and weathering, have destroyed or damaged many historical structures. The main objective in reinforcing and strengthening HURM structures is to improve the structural system up to a sufficient level and increase the strength and durability of the structure against all destructive factors. Preservation as a young science is an important scientific issue to protect the value and authenticity of historical constructions. Therefore, the study of rehabilitation and strengthening methods for HURM buildings has been a topic of experimental and numerical researches. Nonetheless, many historical structures have either been destroyed or are in danger of destruction throughout time.

Akçay *et al.* (2016) carried out a study to assess the strengthening intervention for load-bearing walls and slabs to increase the seismic strength of historical masonry structures. A study was conducted by Akçay *et al.* (2017) on the wall ruined from the early Byzantine period and the arched vault ruined from the Ottoman period. They analyzed the properties and problems of the materials gathered from the ruined structure by on-site examination and laboratory analyses. Then they proposed the conservation and repair methods for implementing on the masonry ruin. They expressed that the intervention should reflect the original status of the ruin; otherwise it should be avoided due to unknown parts of the structure. Therefore, a technical intervention to repair the deterioration parts of the structure is needed for the conservation and restoration of ruins. Furthermore, the ruin should provide good information about civilization and be available for visitors.

HURM buildings usually have very small ductility, and in many cases, the behavior is completely brittle. In this regard, it is very important to provide appropriate retrofitting methods according to the vulnerability conditions, compromise the authenticity of the building as much as possible, and maintain its credibility and validity.

There are various types of retrofitting methods to improve the mechanical behavior of the structure. These methods can be categorized in different ways. Sayin *et al.* (2019) believed that these techniques can generally be classified into two groups as conventional and non-conventional preservation methods. The former attempts to improve the load-bearing capacity of the system by eliminating or

reducing the negative effects caused by the design or construction process. Shear walls, infill walls, and steel braces can be placed in this category. Base isolation, local retrofitting, jacketing, and confinements are categorized in the latter group. Though, understanding which method is more suitable for restoration work needs more profound research and analysis. Some factors such as economy, sustainability, and buildability influence the choice of restoration and implementation methods (Bhattacharya *et al.*, 2014).

The purpose of this chapter is to introduce and classify recent preservation techniques of HURM buildings. According to the types of buildings, current status, and existing methods, retrofitting methods can be divided into three main categories as follows:

1. Improving the structural integrity
2. Reducing the seismic demands
3. Upgrading the structural elements of the existing building

Each category is explained in detail through each related section. Merits and drawbacks of the techniques are compared in terms of their structural action, aesthetics, and ease of implementation to identify more suitable methods in different conditions.

## 4.2 Improving Structural Integrity

Maintaining the originality of a building by improving the integrity of the structure is the main priority for the preservation of valuable historical buildings. Some of the retrofitting techniques such as confinements, fiber or textile reinforced mortar and concrete walls belong to this category. Utilizing these methods has a significant influence on improving the behavior of the entire structure under seismic loading and increasing energy dissipation. Tomažević and Klemenc (1997) by studying a masonry retrofitted with vertical tie-columns indicated that this method prevents disintegration and improves the ductility of the masonry when it is subjected to severe seismic loading. Tie bars reduce the out-of-plane and in-plane wall deformation by improving the poor connections and joints. Spina *et al.* (2004) have suggested using the combination of horizontal and vertical tie bars to increase energy dissipation. In the following subsections, all these methods are described in detail.

### 4.2.1 Confinements

Although HURM buildings have some inherent resistance to the lateral load, they are designed and constructed basically for gravity loads. Therefore, the resistance of these structures under lateral load should be improved by a proper method. One of the basic approaches in retrofitting historical structures is using a grid of horizontal, vertical, and diagonal elements to confine the structure and control

inelastic deformations. A significant part of energy caused by the earthquake can be dissipated in the joint of masonry elements and confinements.

Paikara and Rai (2006) carried out analytical and experimental work on the behavior of URM structures confined by reinforced concrete ties. They used the finite element model to simulate the performance of half-scale masonry walls under cyclic loading by using ABAQUS. The results showed that confinements can increase the energy dissipation and deformability of the wall for the in-plane behavior and also improve the mechanical behavior of the structure.

### **a) Tie column and tie beam**

Tie column (constructional columns) or tie beam (ring beam) as a boundary element to the masonry structure can improve the building integrity and increase strength for both out-of-plane and in-plane behavior. **Figure 4-1(a)** displays a reinforced tie column that confines the wall at the corner and intersection of two perpendicular walls. It improves the performance of the masonry building under earthquake excitation. This technique also can be used to confine the vertical borders of the door and window openings (ElGawady, 2004). The study on confined masonry with vertical tie-columns conducted by Tomažević and Klemenc (1997) showed that the constructional columns generally prevent disintegration. Also, it can increase lateral resistance, ductility, and energy dissipation of the masonry when subjected to severe seismic loading.

Using ring beams shown in **Figure 4-1(b)** improves the mechanical behavior of the structure in connections and joints. Masonry confined with ring-beam has a larger load-carrying capacity where is subjected to seismic loading (Borri *et al.*, 2009). Connecting constructional columns to ring beams at each floor level can help to have higher integrity in the structure as shown in **Figure 4-1(c)**. Okail *et al.* (2016) carried out an experimental and analytical study to investigate the behavior of confined masonry walls subjected to lateral loads. Confined walls with both tie columns and tie beams were tested under a combination of vertical load and monotonic pushover up to the failure. The results showed the confining elements increase the ductility and ultimate resistance of the walls, and the strength is boosted significantly by increasing the number of confinements.

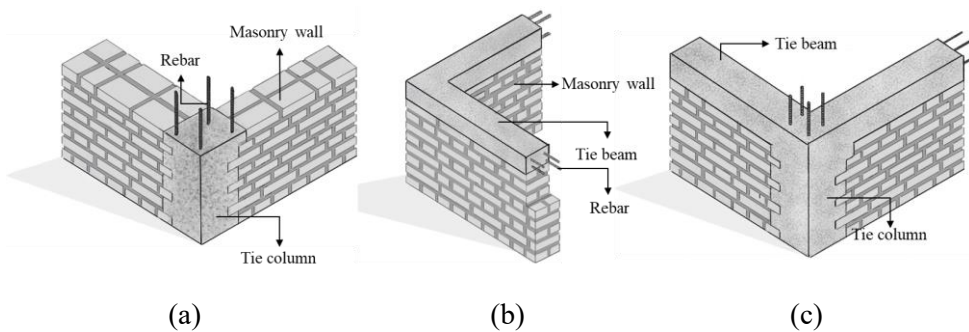


**Figure 4-1** Confining of masonry wall: a) Tie column; b) Tie beam; c) Combination of tie column and beam

Despite the advantages of this method, it is not suitable for use in historical structures due to the hard implementation and high cost. Furthermore, the incompatibility of concrete and masonry material requires an adequate connection

to the underlying masonry. Besides, additional mass is added to the top of the building. Therefore, it is recommended to use this method for confining new constructions (Wang *et al.*, 2018).

### **b) Tie bars**

The method of using tie bars (or strips) is a retrofitting technique mainly used to minimize the horizontal thrust of arches, vaults, and roofs. It improves the connectivity between structural elements such as the poor connection between walls or walls and floors. Similar to the post-tensioning technique, tie bars create compressive stresses in structural elements and cause a box-type behavior of the entire structure.

This technique can be applied horizontally and vertically to prevent out-of-plane and in-plane wall deformation (**Figure 4-2**). Spina *et al.* (2004) suggested using the combination of horizontal and vertical tie bars to improve the behavior of the entire structure under seismic loading and increase energy dissipation. In addition, this technique may be helpful to return the buildings to the vertical direction that has inclined due to soft soil and uneven settlement of the foundation. Since corrosion reduces the strength of the bars and weakens their function, they should be covered with a suitable coating (Wang *et al.*, 2018).

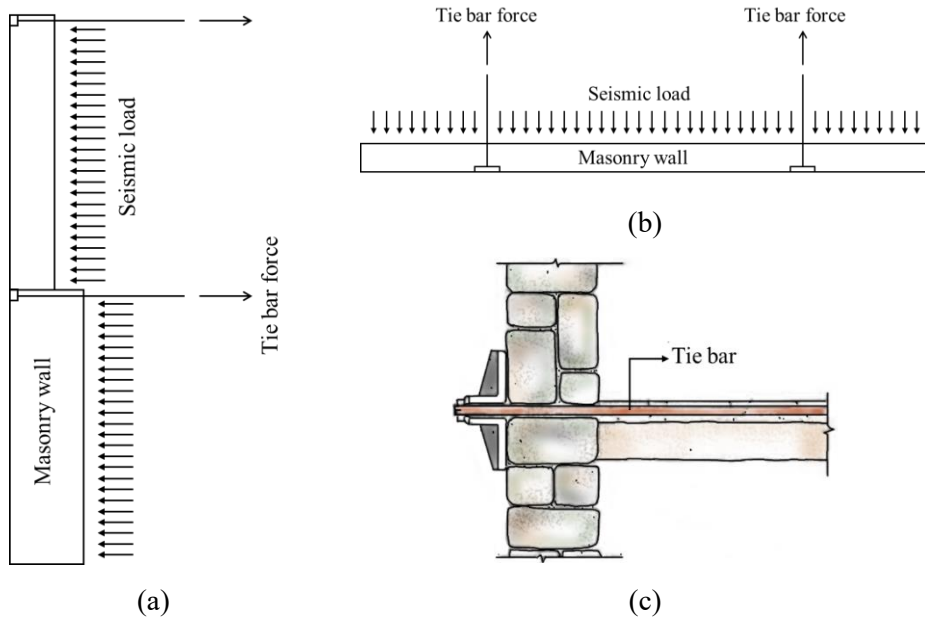


**Figure 4-2** Tie bars retrofit method: a) Section; b) Plan; c) Details of the tie bars constraint against seismic actions (Redrawn based on Spina *et al.*, 2004)

Darbhanzi *et al.* (2014) used two vertical steel ties on both edges of two masonry walls. They examined the mechanical behavior of the walls under a combination of vertical and cyclic lateral load. The results indicated that the addition of vertical steel bars for the specimen with an aspect ratio of 0.7 increases yield and ultimate strength by 210% and 280%, respectively. The bars also increase the ductility with an average value of 270%. In general, the use of vertical steel strips on both sides of the masonry walls improves the seismic capacity of the structure.

### 4.2.2 Transversal anchorage

The middle layer between multi-layer walls shown in **Figure 4-3** is typically composed of rubble stones of low quality and binding materials that primarily serve as fillers. Transversal anchorage systems prevent separation during an earthquake and significantly increase the strength of the structure by providing a connection between the two surfaces.

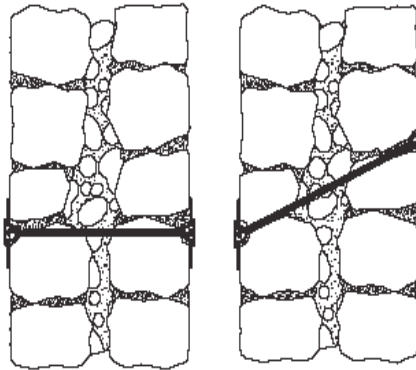


**Figure 4-3** Transversal anchorage system in multi-layer masonry walls (Adapted from Meireles and Bento, 2013)

### 4.2.3 Strengthening of junction

L-shaped steel reinforcement is an easily available and cost-effective material to retrofit URM shelters (**Figure 4-4(a)**). In the experimental study conducted by Dutta *et al.* (2013), L-shaped steel reinforcement was used to strengthen the poor junctions of URM walls. Unidirectional sinusoidal load using a shaking table was applied to investigate the performance of URM walls including the failure patterns

and failure acceleration levels of the specimens (**Figures 4-4(b)** and **(c)**). The average peak acceleration level of 0.60g was achieved for the specimen retrofitted by L-shaped steel reinforcement. The results also indicated the lateral load-bearing capacity of masonry junctions reinforced with dowels was increased 2.4 times the unreinforced wall.

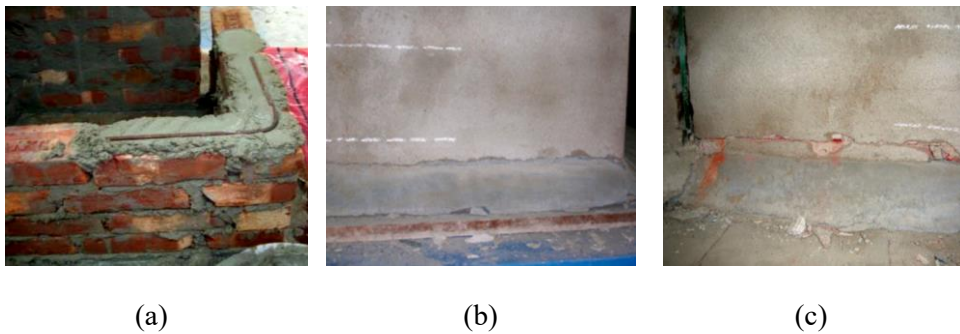


**Figure 4-4** L-shaped steel bars: a) Reinforcing masonry junctions; b) and c) Failure patterns observed retrofitted walls at the corner with L-shaped steel bars (Adapted from Dutta *et al.*, 2013)

#### 4.2.4 Textile reinforced mortar and steel reinforced grout

Masonry units have low tensile and flexural strength in comparison with compressive strength. The tensile strength of existing mortar in HURM structures is generally negligible in comparison with the masonry components. Due to the poor quality of the mortar, it is suggested to increase the tensile and flexural strength by mixing new additives into the mortar.

Fiber or textile reinforced mortar (TRM) or steel reinforced grout (SRG) are used to increase the resistance of masonry structures under tension and flexural stresses. Furthermore, the integrity of the structure can be improved by adding reinforced mortar. However, using these methods has a restriction for historical buildings with heritage value and aesthetic appearance. TRM is reinforced mortar by fiber or textile additives to increase tensile strength. Steel reinforced grout (SRG) involves ultra-high tensile strength steel cords (**Figure 4-5(a)**) embedded in a mortar matrix (**Figure 4-5(b)**). The application of this method is very similar to re-pointing or grout injection (Wang *et al.*, 2018).

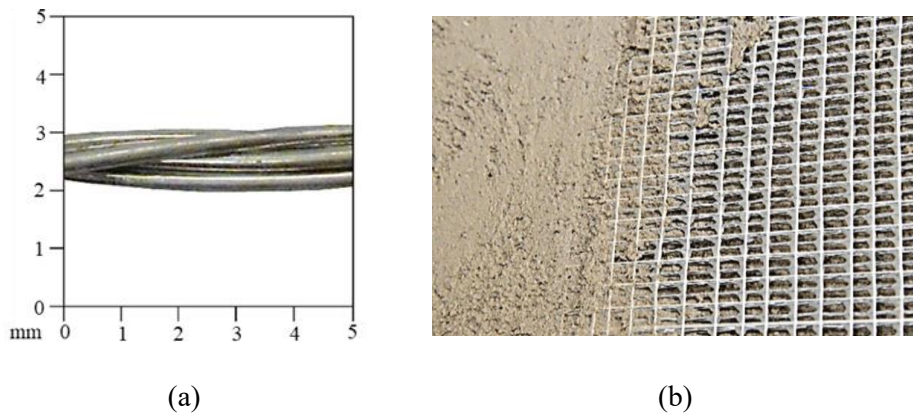


**Figure 4-5** Steel reinforced grout (SRG) system: a) Ultra-high tensile strength steel cord; b) Steel cord embedded in the mortar (Adapted from De Santis, 2017)

Da Porto *et al.* (2013) conducted experimental work on clay unit masonry infill walls for framed structures. The clay unit masonry infill wall was strengthened by hybrid glass fibers cast in an extra fiber-reinforced plaster layer. The wall was tested under in-plane cyclic load and out-of-plane monotonic load. The results

demonstrated that this strengthening technique was effective to prevent out-of-plane expulsion of masonry panels. Moreover, it reduced global in-plane damage.

The textile-reinforced mortar technique (TRM) was used by Martins *et al.* (2015) to strengthen masonry infill walls. To investigate the mechanical performance of the masonry strengthened by TRM bending tests were performed. The results showed this approach improves the out-of-plane resistance of masonry and enhances ductility. Furthermore, it can be applied to avoid brittle failure and minimize material damage.

Experimental investigation on the bond behavior of SRG applied to convex masonry substrates was done by De Santis (2017). Full-scale masonry vault specimens reinforced by SRG were provided to evaluate the bond behavior and resistance mechanism of the structure. The results showed the performance of SRG depends on the roughness of the masonry surface and the curing conditions.

#### **4.2.5 Mortar joint treatment**

Mortar in historical masonry structures is more prone to destruction and deterioration over time in comparison with units. Sometimes the mortar between the units is destroyed completely or has no function to withstand the applied loads. In this case, the mortar can be replaced or refilled by new material with higher strength. This method of preservation is called mortar joint treatment including grout injection or re-pointing the material into the narrow cracks to large voids and empty joints.

The main purpose of using this method is to maintain the original integrity and appearance of the structure. Filling the voids and cracks also prevents further physical and chemical deterioration or mechanical actions (Sayin, 2019).

Although this technique is used as a preservation method of masonry structures, it does not have a significant effect on increasing the strength and stiffness of the structure. Nonetheless, it is very effective in preserving the structure in a stable condition without physically altering external aesthetics. Therefore to improve the effectiveness of this technique on structural resistance, it is preferable to combine it with other retrofitting techniques (Wang *et al.*, 2018). The study conducted by (Tinazzi *et al.*, 2000) indicated that combining FRP rods and re-pointing techniques on masonry structures is one of the most impressive retrofitting techniques.

As mentioned, in the preservation of historical structures, retention of the original aesthetics is the most important concern. To reach this goal the material used in restoration work should be compatible with the masonry in terms of physicochemical and mechanical performance in the environment of the structure and under stress. Use of incompatible material causes further destruction and accelerates the decay mechanisms. Many research studies have been done to investigate the material compatibility in the restoration of historical buildings to ensure the long-term durability of the structure. In order to select the optimum material for earthquake-resistant design of historical structures, Apostolopoulou *et al.* (2017) established a methodology to assess the compatibility and performance of retrofitting mortars for historical masonry structures (**Figure 4-6**).

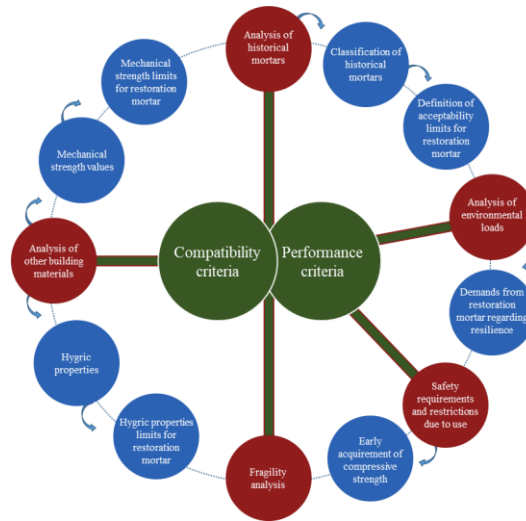


**Figure 4-6** Compatibility and performance criteria (Adapted from Apostolopoulou *et al.*, 2017)

The criteria were defined based on the investigation of material properties used in the structure of a historical monument and the results of fragility analysis (**Figure 4-7**). This technique can be used for most types of masonry buildings, especially for heritage buildings. Another application of this method is in the retrofitting of multi-layer masonry walls by inserting the mortar inside the poor connection between layers or filling the voids in the dry rubble stone’s inner core. Having the least detrimental effects on the initial masonry, preserving aesthetic features, easy implementation, and sustainability are the most important advantages of this method (Wang *et al.*, 2018).

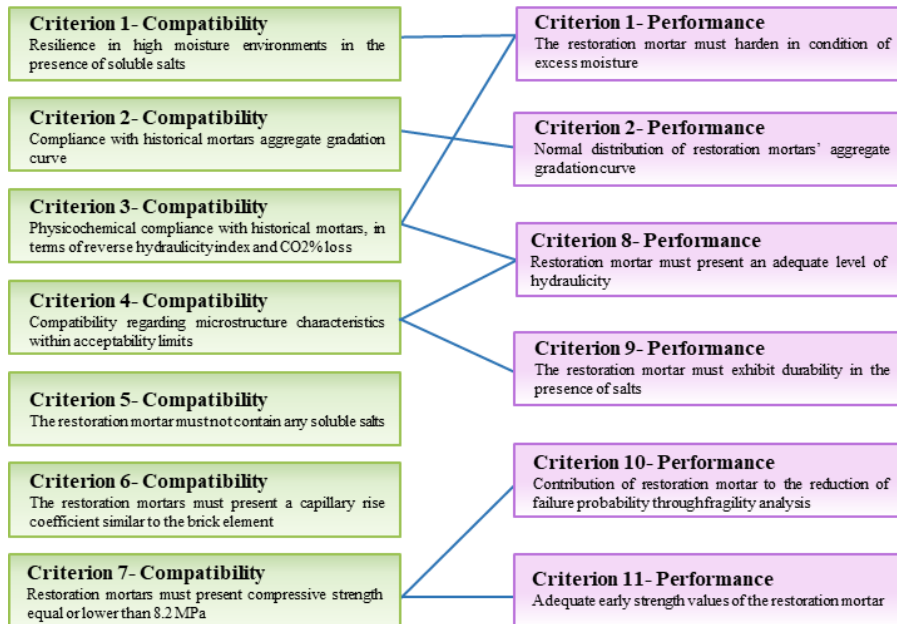


**Figure 4-7** Criteria set from the methodological approach for the selection of the restoration mortar (Adapted from Apostolopoulou *et al.*, 2017)

### a) Stitching and grout/epoxy injection

As mentioned above this method is used to repair masonry structures by injecting grout or epoxy into the voids and cracks that are appeared over time (**Figure 4-8**). The cracks can be also stitched together by steel ties and then filled with mortar to provide better stability. Epoxy resin is used for relatively small cracks (less than 2 mm wide), while cement-based grout is preferable mostly for larger cracks and voids (ElGawady *et al.*, 2004a). Ideally, this technique can recover the lost strength and stiffness of the structure up to the initial value. Schuller *et al.* (1994) examined

different types of grouts for the mortar injection to repair masonry structures with a set procedure. In most cases, grout injection did not increase the masonry strength.

However, it could restore the compressive strength up to about 80% of the original masonry strength. The in-plane stiffness can be restored up to 0.8-1.1 and in-plane lateral resistance up to 0.8-1.4 of the un-retrofitted wall. Further, cement-based grout injection can increase the interface shear bond of multi-wythe stone walls by a factor of 25-40. Although the masonry retrofitted with epoxy injection is stiffer about 10-20% than the un-retrofitted masonry, but the increase in stiffness is not significant as much as an increase in strength (ElGawady *et al.*, 2004a).

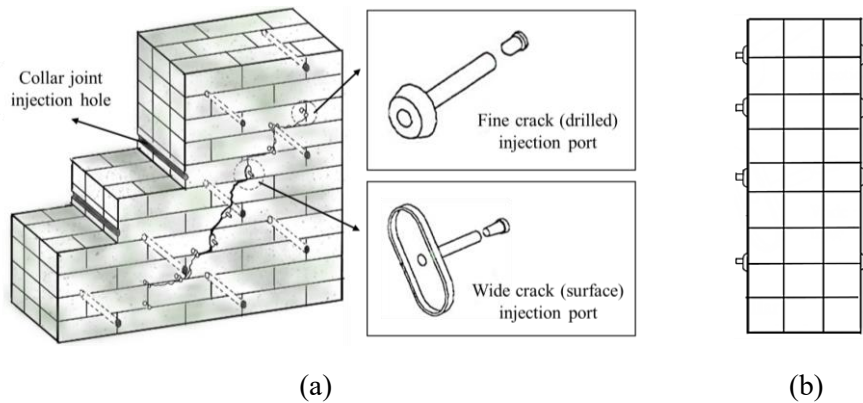


**Figure 4-8** Detail of grout injection technique: a) 3D view; b) Elevation (Redrawn based on Schuller *et al.*, 1994)

Easy implementation without requiring complex technologies, availability of material, and minimal cost cause the wide use of this method. Furthermore, the sustainability of materials makes it more appropriate in preservation works. This

technique can be successful only if the compatibility of material in terms of mechanical, physical, and chemical properties is provided (Bhattacharya *et al.*, 2014).

### **b) Re-pointing**

Higher-strength mortar is used for retrofitting the structures with weak mortar. Addition of 2% ordinary portland cement to the mortar has almost no significant increase in ultimate resistance. However, the low cost, easy implementation, and less destruction of the original form of the structure cause the wide use of this technique all over the world. The compatibility of the new material with the constituent material of the structure should be provided to achieve successful preservation (Bhattacharya *et al.*, 2014).

## **4.2.6 Strengthening of roof diaphragm**

Roof diaphragm plays an important role in structural performance and distribution of seismic loads to vertical load-bearing elements. Plywood is a multilayer wooden panel that can be used to strengthen roof diaphragm as an intervention. Existing roof systems can be replaced or upgraded by plywood in many cases. In comparison with concrete slabs, plywood provides large stiffness, is lighter, and is typically more compatible with building materials in heritage structures. **Figure 4-9** depicts an example of roof diaphragm application using three layers of plywood (21 mm or 0.83 in. thick) which are glued with polyurethane glue and connected to purlins employing chemically anchored connectors.

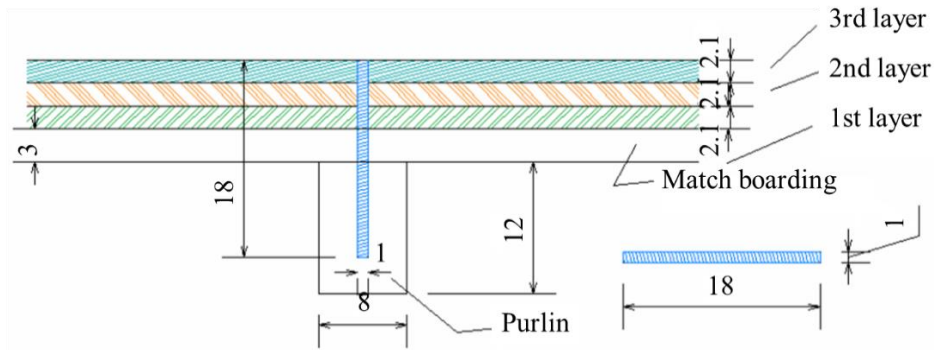


**Figure 4-9** Application of roof diaphragm system (Adapted from Meireles and Bento, 2013) (Unit: cm; Conversion: 1 cm = 0.394 in.)

### 4.3 Reducing Seismic Demands

There are two common approaches to reduce seismic demands for historical structures. The base isolation system reduces the level of entrance energy of earthquake motions from the ground to the structure by increasing the fundamental time period and also dissipation of energy through damping. Seismic dampers can be installed in the structure to damp the shaking of the building and reduce the vulnerability to seismic loading by converting kinetic energy into thermal energy (Branco and Guerreiro, 2011).

#### 4.3.1 Base isolation

Base isolation is a bearing system, which separates the building from the ground. This system reduces the frequency of earthquake motions from the ground to the structure and causes the structure to behave like a stiff body (Branco and Guerreiro, 2011). A flexible pad should be inserted between the foundation and masonry

building to transmit only a small portion of the shaking force from the base to the superstructure. This is the main idea of base isolation as demonstrated in **Figure 4-10**. The base isolation technique can be widely used in different types of buildings. However, lower efficiency and performance are acquired if the system is used for tall buildings and other flexible structures with small natural frequencies in comparison with other more rigid structures. Additionally, the application of the system should be carefully investigated for buildings on a site with soft soil which intensifies low-frequency contents of earthquake motions. It can be used for HURM buildings or other non-structural objects to confront earthquake forces. Maintaining the original appearance of the structure is one of the benefits of this approach. Nevertheless, its difficult implantation can destroy the whole structure all of a sudden. The installation of a new hybrid base costs about 3% of the total construction cost. As a result, this technique is more suitable for newly built constructions (Wang *et al.*, 2018).

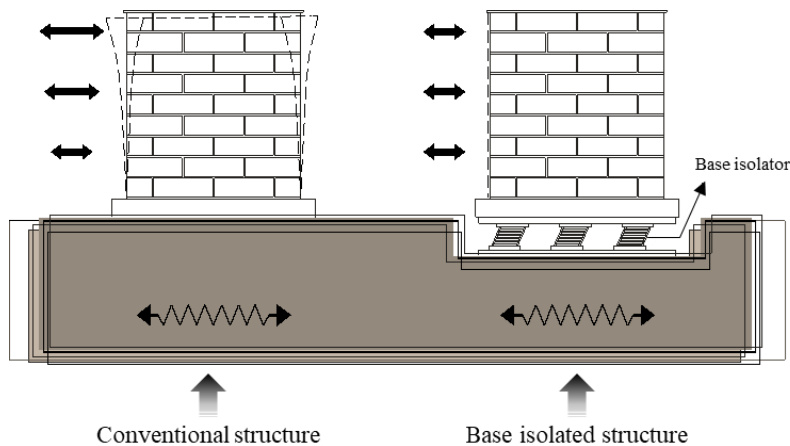


**Figure 4-10** Base isolation technique for masonry walls

### **4.3.2 Seismic damper**

To improve the seismic behavior, dissipate, and convert the kinetic energy caused by earthquake excitation into thermal energy, seismic dampers are installed. It is used to damp the shaking of the building and reduce the vulnerability of the structure. This system is also very common in bridges (Branco and Guerreiro, 2011). The most commonly used dampers in low rise buildings are viscous dampers (transform the earthquake energy to heat and friction), friction dampers (maintain the integrity of the building by rectifying floors to their original positions), and yielding dampers (yield earlier than floors by absorbing the energy) (Wang *et al.*, 2018). Along with all these advantages, it may not be suitable for HURM structures due to the disturbance on the facade of the structure. Further, it is very expensive to use a seismic damper due to the required advanced equipment and techniques.

## **4.4 Upgrading Structural Components**

The overall strength of the structure against external load is affected by the failure of a structural member and consequently leads to total collapse. Upgrading the structural components of historical masonry structures improves the load resistance of the whole structure. Various types of retrofitting methods are available to upgrade the elements' strength. Therefore, the investigation of damage type and its location is necessary to apply an appropriate method for conservation.

### 4.4.1 Reinforced concrete wall

One of the retrofitting methods to increase the global stiffness and control inter-story drifts in the structure is concrete wall. In this method, steel elements are sealed in the existing masonry structure and anchored in the concrete walls to ensure that they simultaneously resist earthquake forces (**Figure 4-11**).

An important principle for further adaptation of the concrete wall to the masonry structure is having the compatibility of modulus of elasticity, hygroscopy, and thermal expansion. To obtain more adhesion and accommodate different behaviors, mortar is used between the concrete wall and structure (Branco and Guerreiro, 2011). However, such a method has a restriction for historical buildings with heritage value.

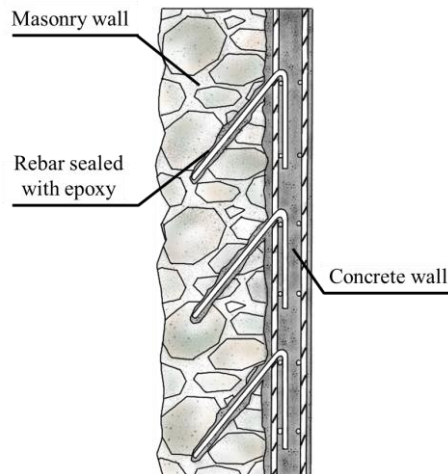


**Figure 4-11** Concrete wall (Adapted from Branco and Guerreiro, 2011)

#### 4.4.2 Moment and braced frames

Moment and braced frames are two types of structural elements used to reinforce masonry structures. Moment frames consist of beams and columns which can be applied as a local and customizable retrofitting method. This system provides full visual and physical access without any disruption between each side of the frame. Retrofitting a masonry structure using moment steel frames requires a sufficient level of compatibility between the frame and the existing structure. Because of the difference in stiffness of steel and masonry materials, special attention should be paid to provide compatibility between the frame and original structure. Frames should be properly connected to the walls and diaphragm to ensure steel and masonry are activated simultaneously under earthquake loads. One advantage of using steel moment frames is their reversibility, which makes them very efficient in comparison to concrete frames. This type of frame relies on mechanical connection and requires small ties to connect to the existing structure with the least possible destruction. **Figure 4-12(a)** shows RC moment frame used for a URM building. This system has higher rigidity than moment frames; however, it is not suitable for façade walls with openings and not compatible with building's architectural character (Meireles and Bento, 2013). **Figures 4-12(b)** and **(c)** show two different applications of steel braced frames in masonry structures.

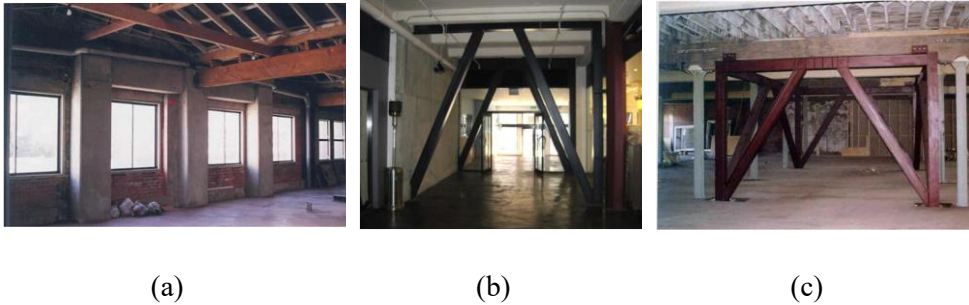


**Figure 4-12** Application of: a) Concrete moment frame; b) Eccentric bracing in walkway; c) Eccentric bracing core (Adapted from Meireles and Bento, 2013)

### 4.4.3 Surface treatment

The surface treatment approach includes confining the exterior side of construction with steel or polymer grids and then coating with a layer of high-strength mortar. The weight ratio of reinforcement varies between 3% to 8% of the construction, depending on the loading condition and required resistance. The steel or polymer grids can be replaced by fly-ash or rice-husk-ash to reduce the cost. This method can increase the structure's ultimate lateral load resistance and also improves the out-of-plane resistance of masonry buildings. Although this method is very convenient and inexpensive, the lack of voids for breathing on the surface covered by mortar causes material deterioration and rotteness (Bhattacharya *et al.*, 2014). It is also not recommended for retrofitting historical structures due to the destruction of the architectural façade. Shotcrete and Ferro-cement are the most frequently used approaches in the surface treatment of masonry structures.

### a) Application of shotcrete

Spraying the mortar over a mesh of wire is called shotcrete. The process involves removing dust, filling voids, installation of a wire mesh on the masonry surface, and then spraying shotcrete over the mesh (**Figure 4-13**). The thickness of shotcrete varies from 70 mm to 150 mm. Shear dowels are used to transfer shear stress between the masonry wall and shotcrete interface. The roughness and cleanliness of the surface have a significant role in the effectiveness of this retrofitting method (Wang *et al.*, 2018).

This technique can be applied on both sides of masonry walls to reduce tension by an average of 50%. While the application of shotcrete on one side of masonry reduces the tensile stress by about one-third (Karantoni and Fardis, 1992). An experimental study was carried out by ElGawady *et al.* (2006) by conducting cyclic tests to investigate the in-plane behavior of URM walls retrofitted with shotcrete. The walls were retrofitted on a single side using a 40 mm thick layer of shotcrete and on a double side using the same shotcrete thickness and reinforcement. The lateral load was applied and gradually increased to the point of failure. The results showed that the ultimate lateral load resistance of the walls was approximately increased by a factor of 3.6. Retrofitting the specimen in the double-side improved the ductility and energy dissipation. Moreover, this method can increase the load-carrying capacity of the structure.

However, this method destroys the aesthetic appearance of the building then it is not suitable for the restoration of historical structures.

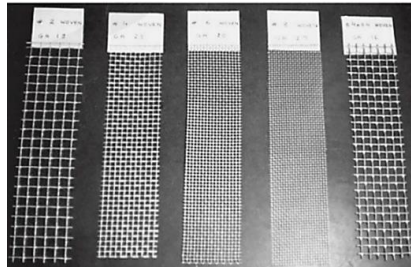


**Figure 4-13** Application of shotcrete to URM wall (Adapted from El Gawady *et al.*, 2006)

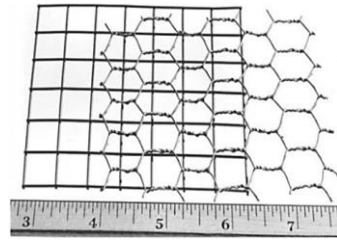
### **b) Ferro-cement**

The placement of closely spaced multiple layers of fine rod meshes in cement mortar is also called ferro-cement (**Figure 4-14**). The ratio of reinforcement varies between 3% to 8%. The thickness of the mortar is between 10 to 50 mm with a strength of 15-30 MPa. Adding a low-cost fiber such as polypropylene with a ratio of 0.5-1% can improve the strength of the mortar, although the mesh property is the key factor to define the mechanical behavior of ferro-cement (ElGawady *et al.*, 2004a). In-plane behavior can be improved through better confinement that is provided by the meshes of ferro-cement. Abrams and Lynch (2001) by doing several static tests showed that this technique could improve the in-plane lateral resistance

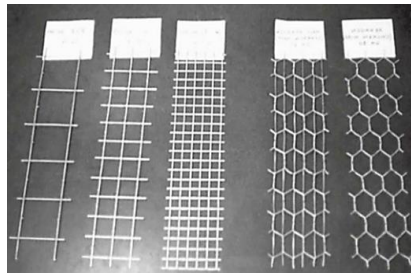
by about 150%. Besides, the strength in the out-of-plane direction by installing only 0.29% reinforcement in the longitudinal direction can be increased about 10 times (Kadam *et al.*, 2015).



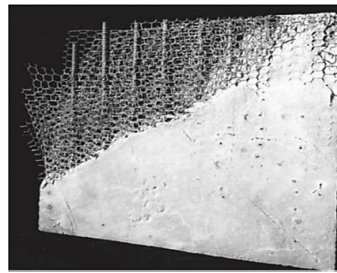
(a) Woven wire mesh



(b) Size of mesh



(c) Hexagonal and welded wire mesh



(d) Typical ferro-cement section

**Figure 4-14** Ferro-cement retrofitting method (Adapted from ACI, 2018)

It can be concluded that the surface treatment method improves the strength and stiffness of the masonry structures. Furthermore, it increases the in-plane lateral resistance and out-of-plane stability as well as the arching action. However, this method has a time-consuming process and destroys the aesthetic appearance of the building; therefore, it is not suitable for the restoration of historical structures (Wang *et al.*, 2018).

#### **4.4.4 External reinforcements**

Earthquake excitation causes many cracks in masonry structures. Over time, these cracks spread along with the structure and may result in total destruction. The weak masonry structures need to be reinforced to improve the structural system. Installation of reinforcing elements next to the structural elements of the masonry building is known as the external reinforcement technique. The reinforcement and masonry elements can be tied together to improve the mechanical behavior of the building. The external reinforcement consists of stronger elements that carry the external loads. This reinforcement system can control the propagation of cracks with its large stiffness (Wang *et al.*, 2018). It must be considered that the relative rigidities of the original masonry structure should be compatible with the new reinforcement system (Hamid *et al.*, 1994).

This approach may not be suitable for HURM structures due to changing the aesthetics of the original form. Further, the high cost of its implementation is another concern that should be considered (Wang *et al.*, 2018). Various types of external reinforcements that can be used for strengthening a masonry structure are introduced and explained in the following subsections.

##### **a) Steel reinforcement**

One of the retrofitting techniques with modern materials is external steel reinforcement. It consists of some steel elements (structural steel bracing, flat steel

bar straps, or steel shear plate) to install next to the masonry wall. Steel reinforcement improves in-plane strength, ductility, seismic behavior, and energy dissipation capacity of the structure. Taghdi *et al.* (2000) carried out an experimental study on retrofitted masonry walls with diagonal and vertical steel strips. The test was done under a combination of gravity load and incremental in-plane lateral deformation. The results showed this system was effective to improve the structural behavior of the masonry wall, and the load resistance of a structure can be improved significantly using high-strength steel elements.

#### **b) Bamboo, cane, and plastic tubing reinforcement**

The vertical and horizontal elements such as bamboo, cane, and plastic tubing can be utilized to build a network of reinforcements to improve the performance of the structure (**Figure 4-15(a)**). This system has little capacity to prevent crack propagation along with the structure. Nonetheless, it can delay the structural collapse in adobe structures.

Horizontal and vertical bamboo stems are attached externally to the masonry wall and tied together to create an integrated matrix. The details of connections are indicated in **Figures 4-15(b)** and **(c)**. This system restrains movement and distributes energy in the structure under seismic loads. Easy implementation, low cost, availability of materials are the advantages of this method mostly in developing countries. Dowling *et al.* (2005) used the combination of a ring beam and bamboo stems with vertical reinforcement to confine the U-shaped adobe wall panels. They

conducted a shaking table test for the 1:2 scale model to transient dynamic loading for investigating the structural response. The test result showed a significant increase in seismic resistance of the structure. All specimens maintained structural integrity under high-intensity simulation. Also, the results showed that by increasing the reinforcement ratio a significant improvement in resistance can be obtained.

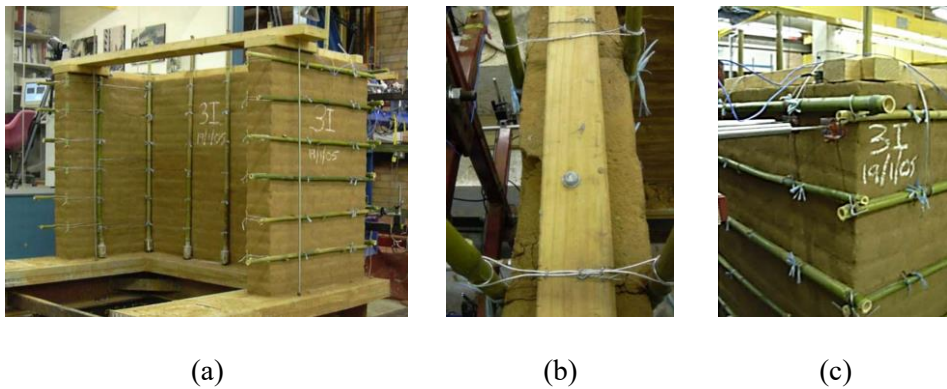


**Figure 4-15** Bamboo reinforced wall: a) External horizontal and vertical bamboo; b) Connection of ring beam, wall, and bamboo; c) Connection of external horizontal bamboo at the corner (Adapted from Dowling *et al.*, 2005)

### c) Seismic wallpaper or FRP reinforcement

Modern techniques and innovative materials such as fiber-reinforced polymers (FRP) are often proposed and allowed in current practice. It is also utilized for the restoration of historical constructions, in which essential preservation criteria must be taken into account. The main objective of the seismic strengthening of URM buildings is to improve the strength of the structures against lateral forces such as earthquakes. Fiber-reinforced polymers (FRP) are a class of materials (carbon, glass,

and aramid) that significantly improve the structural behavior of buildings in seismic actions and modify the collapse mechanisms by increasing the structural resistance. The earthquake excitation causes tensile stresses in the structures. Therefore, the FRP reinforcements are applied to the tensile sections of structural members to enhance the load-bearing resistance and increase the ductility against seismic effects (Sayin, 2019).

**Figures 4-16(a) and (b)** show an example of HURM structures retrofitted by FRP composites. Many research studies have been done to investigate the efficiency of different types of FRP retrofitting methods on the seismic resistance of masonry structures. An experimental study was carried out by Ehsani *et al.* (1999) on three half-scale URM solid brick walls retrofitted with vertical composite strips. The specimens were subjected to cyclic out-of-plane loading and displacement via an airbag loading system. The strips were bonded on both faces of the wall using epoxy resin. The results showed that the ultimate flexural strength of all specimens was significantly increased. The retrofitted walls were capable to support a lateral load of 32 times the weight of the wall. A deflection of about 2.5% of the wall height was observed.

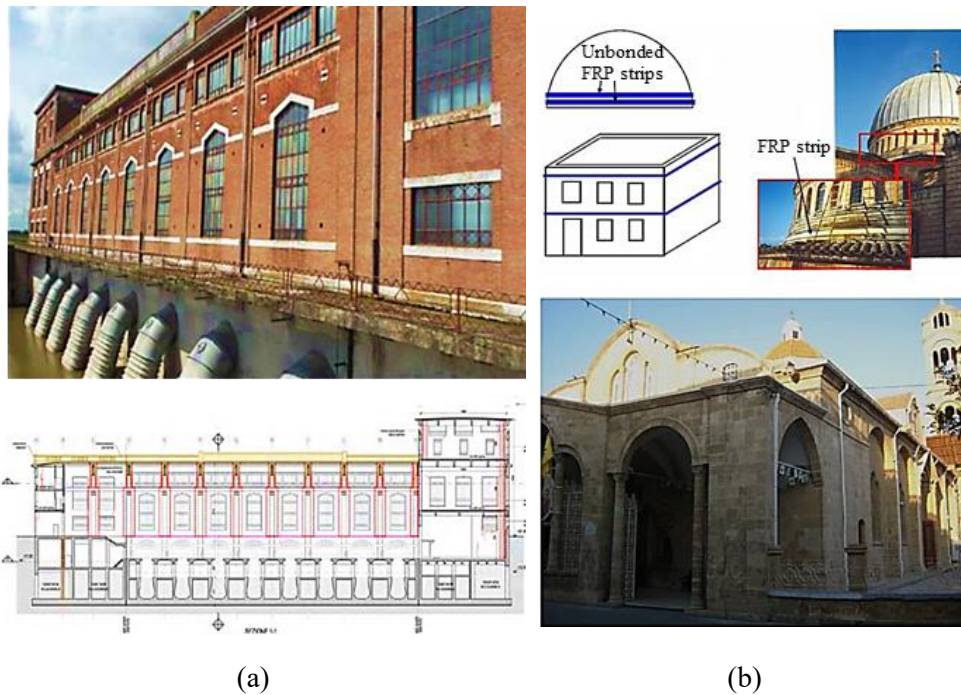


**Figure 4-16** Application of FRP in retrofitting of historical structures: a) FRP strips in Siro Pumping Station, St. Benedetto Po, Italy; b) FRP Tendons in the Church of Panaghia Faneromeni, Greece (Adapted from Abdulsalam and Ali, 2014)

This study proved that GFRP composite strips are good retrofitting techniques against lateral loads. This retrofit method increased the tensile yield strength and the ductility up to 2 and 7.5 times its original value, respectively. Further, GFRP reinforcements work more effectively when they are arranged at  $45^\circ$  to the horizontal line (**Figure 4-17**).



**Figure 4-17** Retrofitting of URM wall using GFRP (Adapted from Bhattacharya *et al.*, 2014)

Seventeen URM clay brick walls were strengthened with glass FRP fabrics and carbon FRP (CFRP) plates by Mahmood and Ingham (2011). The diagonal compressive force was applied to testing the behavior of the walls. Five un-retrofitted specimens were produced to compare the results of the tests. It was observed that the shear strength of the walls increased up to 325%. The ductility and the toughness were also enhanced by applying FRP, especially the walls that failed by diagonal shear cracking.

The study also indicated that the application of vertical or diagonal FRP retrofit maintained the specimens from sliding. However, there were no significant changes in increasing stiffness. ElGawady *et al.* (2004b) expressed that the in-plane lateral resistance and the out-of-plane resistance of the wall retrofitted with FRP were increased by a factor of 1.1 to 3 and 7, respectively. In general, it can be concluded that the application of FRP composite material increases the ultimate load-carrying capacity, lateral resistance, energy absorption, and ductility in retrofitted walls. This

retrofitting method also improves the sudden failure pattern in URM walls and causes a gradual failure pattern (Bhattacharya *et al.*, 2014).

Despite the high cost, high technology for installation, and distortion of the appearance of the structure, its valuable benefits cannot be ignored. The little added mass, low disturbance, and relatively high improvement in strength are the main advantages that come with it. However, FRP composites have illustrated poor performance in high-temperature environments when they are assembled directly to member's faces (EB technique) (Soudki and Alkhrdaji, 2005).

Unless a fire protection system or insulation, a water-proof barrier and prevention of the natural transpiration of the masonry structure should be created. To overcome these drawbacks of the EB method, the near-surface mounted (NSM) technique with cementitious adhesive or fabric-reinforced cementitious matrix (FRCM) system has been developed as an alternative technique. Cementitious material is less expensive and preferable as a bonding agent due to its compatibility with the masonry substrate (Turco *et al.*, 2006). One important advantage of the NSM method is that it has a very low intervention on the aesthetic form of the building. Also, easy implementation makes it favorable in comparison with other rehabilitation techniques. In the experimental study by Griffith *et al.* (2013), the flexural behavior of masonry walls strengthened by carbon fiber-reinforced polymer (CFRP) using the NSM method was investigated. The experimental results of this study indicated that the spacing of FRP strips played an important role in controlling the out-of-plane flexural behavior and displacement of the specimens. Increase in

the fiber reinforcement ratio has resulted in higher strength capacity and reduction in deformation. However, if the fiber reinforcement ratio keeps constant, increasing the space between strips leads to improved wall strength, reducing displacement response. The investigation by Al-Jaberi *et al.* (2015) showed a similar observation for the out-of-plane behavior of reinforced masonry walls with FRP implementing the NSM method.

The 1886 Birdcage Tavern (**Figure 4-18(a)**) is a two-story unreinforced masonry heritage building. Since the tavern was relocated as part of a highway extension project, it was needed to strengthen the building before running the project. NSM CFRP strips for retrofitting four unreinforced masonry chimneys were selected as an effective seismic strengthening approach to provide a cost-effective and minimally intrusive project. In the retrofitting process, vertical grooves were cut into two sides of the chimneys. The grooves extended beyond the base of the chimneys, and then CFRP strips were inserted into the epoxy-filled groove (**Figure 4-18(b)**).

**Figure 4-18(c)** shows Campbell Free Kindergarten (CFK) located in central Auckland (New Zealand) retrofitted by NSM CFRP strip technique. The building has significant heritage value as it is the earliest purpose-built free kindergarten in New Zealand. Due to the high risk of collapse in this building which was deteriorated seriously, NSM CFRP strips were used for strengthening the structure. URM walls were strengthened with horizontal strips and parapets with vertical to improve structural integrity out-of-plane resistance, and to retain their heritage characteristics.

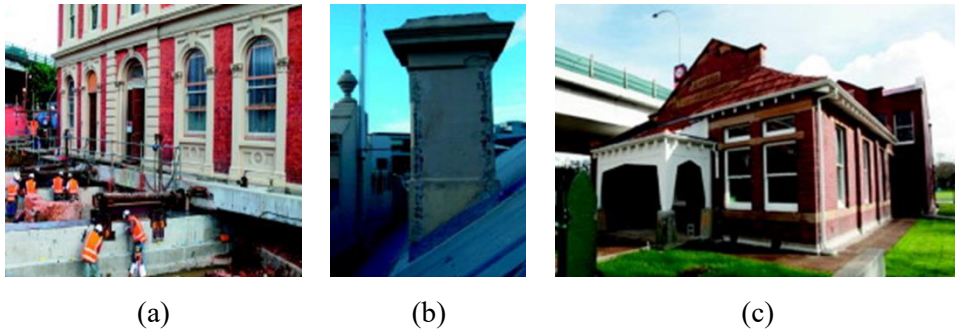


**Figure 4-18** Implementation of NSM CFRP retrofit: a) 1886 birdcage tavern (New Zealand); b) Rear chimney; c) Campbell free kindergarten (CFK) (Adapted from Dizhur *et al.*, 2014)

In general, near-surface mounted (NSM) FRP offers more advantages over externally bonded (EB) FRP. Maintaining the aesthetic form of the building, debonding at higher strains in comparison with EB FRP, reducing surface preparation, and better protection from UV exposure and vandalism are the most important advantages. Therefore, NSM FRP leads to more efficient use of the FRP material (De Lorenzis and Teng, 2007).

**Figure 4-19** schematically illustrates the process of the implementation of FRP strips, steel, and titanium reinforcement bars using near-surface mounted in a historical stone masonry building. The figure describes the possibilities of using the NSM method in the interior or exterior side of the construction.

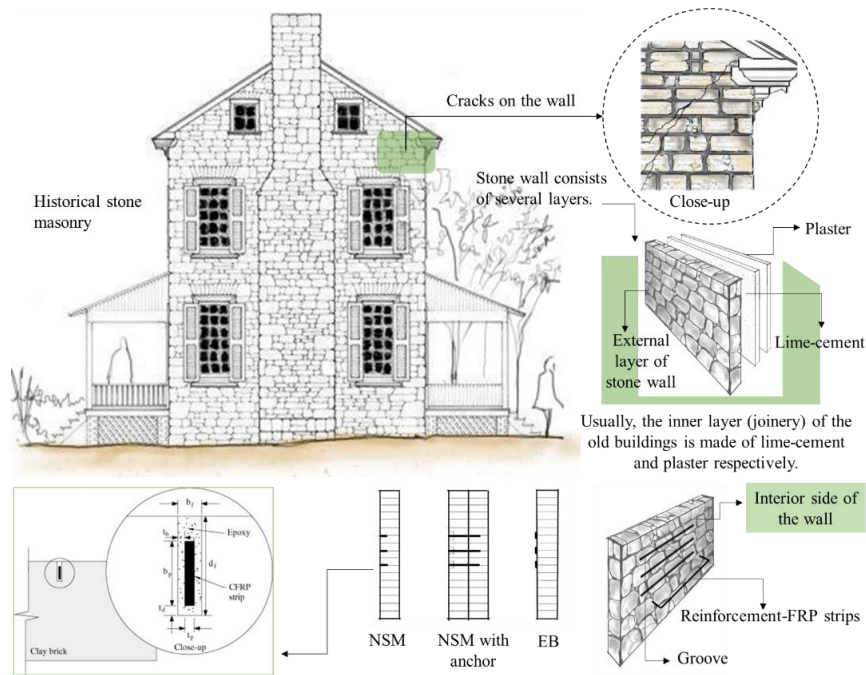


**Figure 4-19** Process of implementation FRP-NSM in stone masonry building

In some cases such as Mireuksaji stone pagoda (South Korea) which a part of the structure has collapsed, the NSM method can be used to reinforce the fallen stones. The grooves can be created at the side of the stone which is not visible on the architectural façade and then FRP strips can be placed into the grooves with the higher bonding strength. The process of implementation is shown graphically in **Figure 4-20**.

In summary, the preservation of historical construction by FRP reinforcement is a preferable technique in many countries. However, the appropriate selection of a proper reinforcement and intervention is a challenge for historical masonry structures because they must be highly compatible with the existing structure.

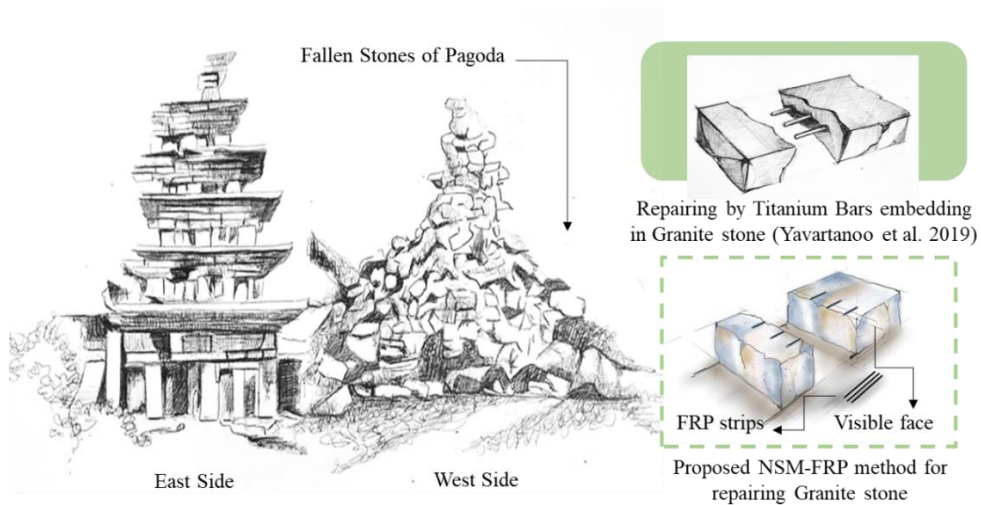


**Figure 4-20** Proposed NSM-FRP method for retrofitting historical buildings such as Mireuksaji stone pagoda (Iksan, South Koea, 1915)

#### 4.4.5 Post-tensioning

The main concept of post-tensioning method is to improve the strength and ductility of lateral load resisting system. To introduce this technique in detail, three possible approaches are described. In the first approach, a hole is drilled in the masonry wall and the pre-stressed reinforcements are placed vertically in the drilled hole as shown in **Figure 4-21(a)**. The pre-stressed reinforcement provides a compressive force that can counteract the created tensile force in the masonry wall. This mechanism can double the lateral load resistance of unreinforced masonry walls. The center core, as the second approach, consists of a reinforced core that is installed in the vertical direction of the masonry walls. The reinforcements are put in the hole, and the hole is filled with polyester or epoxy grout. Though this method is very similar to the former method, the only differences are that the steel bars are not pre-

stressed and the hole is larger. Further, it can successfully increase the strength of a masonry panel about two times under a static cyclic test (Wang *et al.*, 2018). Use of the center core approach increases the ductility and resistance of the masonry against distributing cracks caused by applied loads (Paret *et al.*, 2008).

Employing scrap rubber tires, which have an embedded steel mesh, is also proposed as a possible retrofitting method. **Figure 4-21(b)** shows the assembling of tires in detail. Half-cylindrical wooden logs are placed at the top of the wall to avoid stress concentration at the corners. The main property of rubber is to stretch after a while and lose strength to a great extent. Therefore, bolts should be tightened after 3 days to ensure that enough compressive force is applied to the structure (Bhattacharya *et al.*, 2014).

Many research studies have been done to investigate the performance of the post-tensioning method in retrofitting masonry structures. The implementation of this approach on masonry walls in the out-of-plane direction displayed that the post-tensioning technique does not significantly affect the ductility of the reinforced masonry panel. Nonetheless, it can increase both initial flexural stiffness and strength (Amiraslanzadeh *et al.*, 2012). A cyclic static test was carried out by Liu *et al.* (2015) on the seismic performance of brick masonry structures reinforced by vertical post-tensioning bars.

The results showed that post-tensioned prestressed reinforcement improves shear bearing capacity, ductility, and energy dissipation of the system. Observation

revealed that under large axial force, provided by the prestress reinforcement bar, ductility was less. Accordingly, the pre-stress load should be limited to have optimum ductility.

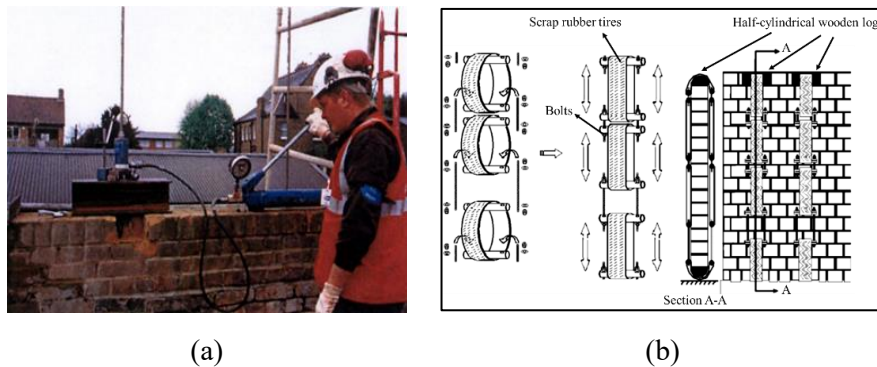


**Figure 4-21** Post-tensioning technique: a) Post-tensioning reinforcement (Adapted from Amiraslanzadeh *et al.*, 2012); b) Post-tensioning strap (Adapted from Turer *et al.*, 2007)

Post-tensioning technique can be employed to enhance the seismic performance of RC frame infilled with masonry wall. Soltanzadeh *et al.*, (2018) applied similar quasi-static cyclic loading on specimens to investigate the response of the structure which is reinforced by post-tensioning method. The results indicated higher initial stiffness, ultimate lateral strength, and ductility for the retrofitted infilled frame in comparison with un-retrofitted infilled frames. Further, failure was delayed and the rate of stiffness degradation was reduced. The smaller strain was observed for the retrofitted frames in their critical zones. A research project was conducted by Turer *et al.*, (2007) on earthquake strengthening of masonry houses using elastomeric straps applied by the post-tensioning technique. The performance of post-tensioning

rubber straps at several different masonry configurations was investigated. The test was carried out on 1:10 scale models using a simple shaking table. The results showed a significant improvement in the structural behavior of reinforced models with vertical post-tensioning rubber straps. The improvement in crack distribution and ductile response was observed remarkably. This method also improves out-of-plane stability and in-plane strength by a factor of 5 to 6. Furthermore, the specimens had even better performance where a combination of vertical and horizontal straps was used.

It can be concluded that the post-tensioning method is suitable for seismic retrofitting of historical masonry constructions. It keeps the architectural value and quality of the wall with less added mass and causes low disturbance for the original form.

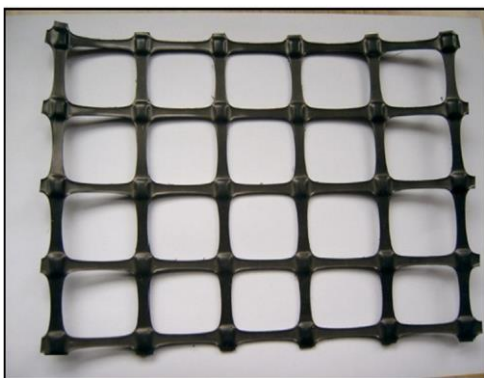
#### **4.4.6 Mesh reinforcement**

The main role of mesh reinforcement is to overcome the shortcoming of some of the above approaches. As mentioned, FRP composite is one of the favorable and efficient approaches in strengthening masonry structures. Use of a mesh of FRP composite improves structural performance. Using grid strips provides a better stress redistribution that results in crack spreading and less brittle failure. It is possible to use the mesh reinforcement not only in reinforcing the vertical masonry structures but also it can be applied to horizontal elements like vaults and arches. However, the application of a mesh of FRP on masonry structures increases the cost of preservation

which is a concern in developing countries. Therefore it is proposed to use the polymer mesh reinforcement, Polypropylene (PP) band, and bamboo meshes as good alternatives. PP band is used as a cheap and available reinforcing material which has significant elongation capacity (Wang *et al.*, 2018). In the following subsections, the detail of these materials is explained.

### a) Polymer mesh reinforcement

Polymer grid is a reinforcement material in retrofitting masonry structures. It has fundamental effects on preventing diagonal cracks. This method also increases shear tension resistance and ductility of mortar. The industrial geo-grid and soft fence are two types of polymer mesh reinforcements that have been used in the preservation of URM structures. The soft fence is a weaker mesh that is usually used in construction sites (**Figures 4-22(a)** and **(b)**).



(a)



(b)

**Figure 4-22** Polymer mesh reinforcement: a) Geogrid; b) Soft fence mesh  
(Adapted from Blondet *et al.*, 2006)

Blondet *et al.* (2006) tested three variations of the geo-grid (100%, 75%, and 50% area coverage) and one soft mesh system (80% area coverage) on the masonry wall. Mesh reinforcements were wrapped around the wall and then plated with mud plaster. Results showed that using mesh reinforcement provided displacement control and caused better stress distribution in the structure. Further, the wall was able to keep its integrity during the test. Juhásová *et al.* (2008) introduced polymer grids inserted into horizontal bed mortar as an alternative method for reinforcing masonry structures using fiber lime-cement plaster. They examined the contribution of polymer grids to the dynamic performance of the structure. This method can be implemented in the horizontal bed mortar between stone units regardless of the regularity or irregularity of the stone (**Figure 4-23**). This implementation shows higher integrity between components and better behavior under seismic load and other dynamic actions (Juhásová *et al.*, 2008).

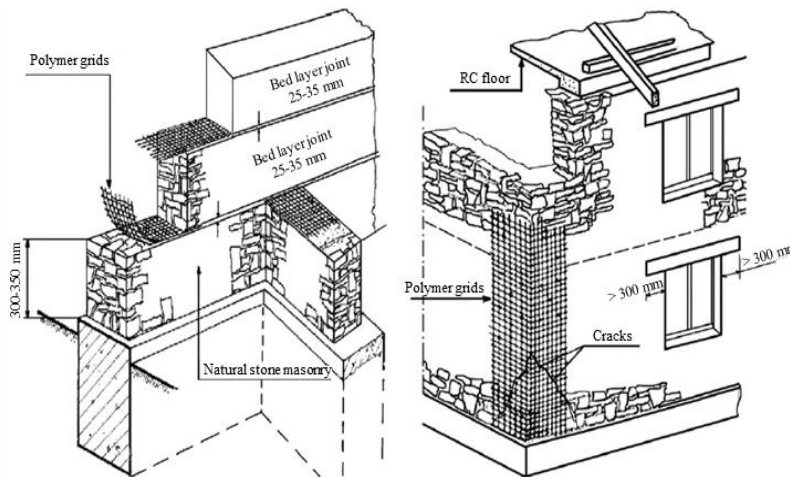


**Figure 4-23** Application of polymer grids combined with fiber lime-cement mortar in stone masonry structures (Adapted from Juhásová *et al.*, 2008)

## **b) PP packaging strip mesh reinforcement**

PP (polypropylene) packaging system consists of intertwined strips attached to the wall surface. The process includes drilling and installing the mesh provided by intertwined strips. Use of PP-bands is one of the cheapest and easiest methods that has been used in poor countries and is most often used in packaging industries (Oskouei *et al.*, 2018). Sathiparan *et al.* (2005) carried out an experimental study on the in-plane and out-of-plane behavior of masonry wallets retrofitted by PP-band meshes with two different arrangements. As shown in **Figures 4-24(a) and (b)**, the tests were carried out as the diagonal compression test. This method of retrofitting increased the strength up to 2.5 times and deformation capacity up to 45 times larger than the bare masonry wallets. Also, a large residual strength was observed after the initiation of the first diagonal shear cracks. Macabuag (2007) tested a retrofitted masonry wall under static load using a diagonal compression machine. The results indicated that the horizontal strips keep the masonry units in the same row to prevent separation. Vertical strips increase the normal stress between the masonry units, preventing sliding due to the enhancement of frictional resistance. Moreover, the results showed that shear resistance of the specimens under static loads was increased. The dynamic was conducted with the same condition by Meguro *et al.* (2005). The results of the test reveal how effective this method is in increasing the load resistance and ductility of the specimens. Using PP mesh prevents the masonry unit's destruction and provides enough deformation without failure (Macabuag *et al.*, 2012). Furthermore, this retrofitting method prevents the loss of material and retains

the wall integrity. It is also suitable for low-strength masonry structures. However, the effectiveness of the application of PP bands will be much less significant in the case of the high-strength masonry structure (Wang *et al.*, 2018).

Using polymer and PP packaging strips is not suggested for HURM buildings due to the restriction for the aesthetic and valuable face of the building historical buildings with heritage values.

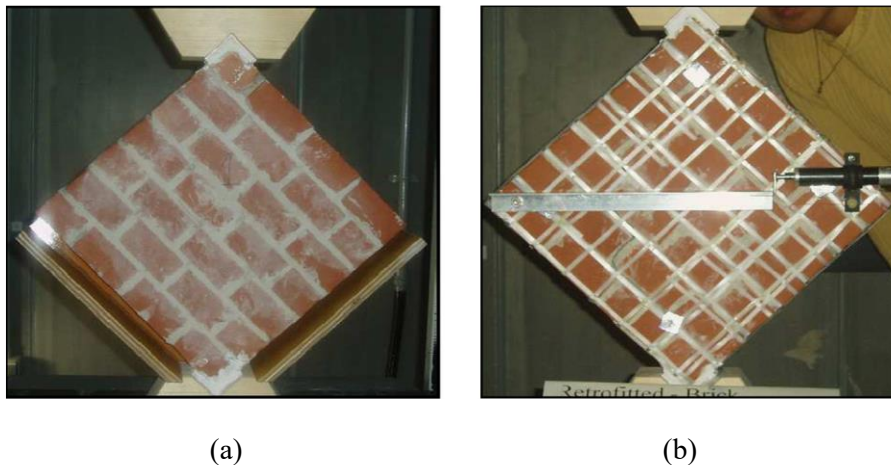


**Figure 4-24** Application of PP packaging strip mesh: a) Non-retrofitted; b) Retrofitted wall panel (Adapted from Macabuag *et al.*, 2012)

#### 4.4.7 Reticulatus system

Reticulatus system is a strengthening technique recently suggested for stone structures with regular and irregular shapes. It consists of a grid mesh with 300-500 mm width (smaller than the wall thickness) of high-strength steel or composite cords inserted in the mortar joints. The cords are stripped off about 40-60 mm, connecting

two faces of the wall. Then the mesh is anchored to the wall by transverse metal bars (5-6 per m<sup>2</sup>). Finally, the cords and the heads of the transverse bars are covered to preserve the fair-faced aspect of the masonry (Wang *et al.*, 2018). It is proposed to use an epoxy mortar or in some cases shrink cement-based mortar for the coverage. This system can also be applied in combination with other techniques (Corradi *et al.*, 2016) to take more advantage. The details of Reticulatus system are illustrated in **Figures 4-25(a) and (b)**.

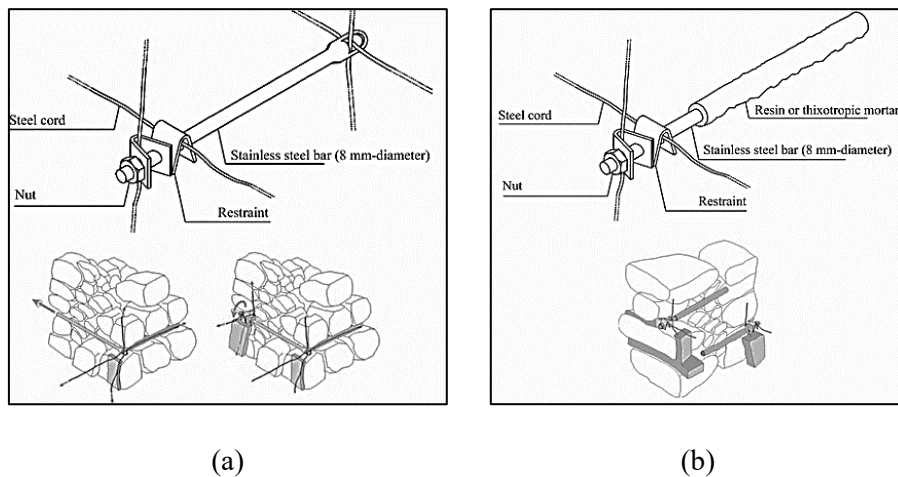


**Figure 4-25** Application of Reticulatus system: a) Detail of a through connector; b) Detail of a not-through connector (Adapted from Corradi *et al.*, 2016)

According to the studies conducted by Borri *et al.* (2011), the compression, shear, and flexural strength of the stone wall reinforced by the Reticulatus system can be improved considerably. The effectiveness of the Reticulatus technique highly depends on the reinforcement mesh embedded in the mortar joints and different masonry structures. Csikai *et al.* (2014) applied the Reticulatus system on historic

masonry structures to investigate the flexural strength. The results indicated that using this method not only improves the overall integrity of the wall but also increases the stiffness and strength of the structure. Despite this, to improve flexural strength and initial stiffness, a proper level of pre-tension is required. Fonti *et al.* (2017) introduced the Reticulatus system made of fiber-reinforcement to retrofit the historical building. As shown in **Figures 4-26(a)** and **(b)**, the reinforcement was applied to the external surface of the panel and provided a cross interlock to resist against tensile strength produced by lateral forces. Corradi *et al.* (2016) investigated the effect of four types of cord reinforcement on strengthening the square wall panels. All specimens were strengthened on both faces. Diagonal compression tests were carried out on-site and in the laboratory on full-scale walls with a different configuration. The results showed substantial increases in shear strength. For the panels retrofitted on-site, the shear strength was increased up to 170% in comparison with un-retrofitted panels. However, for the laboratory panels, the increase in shear strength was achieved 17% for stone masonry and 40% for pebble masonry. It can be observed that the increase in strength highly depends on the mechanical characteristics of the masonry (Corradi *et al.*, 2016).

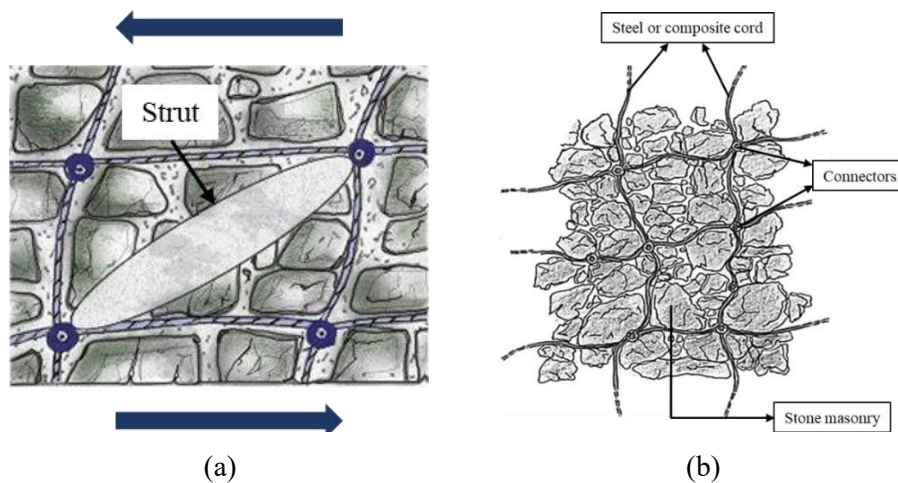


**Figure 4-26** Reticulatus system: a) Strut-and-tie model for a reinforced portion of a wall subjected to an in-plane load; b) Reinforcement layout (Redrawn based on Corradi *et al.*, 2016)

Use of Reticulatus method has almost no effect on the original aesthetic of the building. Therefore, it is suitable for retrofitting historical masonry structures with valuable features. But, this system can be only applied to the stone/rubble/pebble masonry structure (Wang *et al.*, 2018).

## 4.5 Technical Comparison

Preservation is a multidisciplinary task that requires certain criteria and provisions to provide an effective strengthening approach. This becomes even more important when dealing with historical buildings. Each retrofitting approach possesses its advantages and shortcomings; therefore, the “best approach” does not have a meaning. To select an appropriate retrofitting technique, understanding the mechanical behavior, material and the current stage of the building is important. For

example, the retrofitting technique for adobe masonry structures with weaker properties is not applicable for stone structures. Besides, the different failure mechanisms and locations may be influential to choose different types of strengthening techniques. In some cases, only a small part of a structure is damaged and preservation of the whole structure may not be really needed. Historical masonry structures may be exposed to different types of loading. In this regard, various types of retrofitting methods are needed to resist each type of loading condition. The connector which connects the retrofit material to the base structure is another important factor that can improve the performance of the selected approach. Therefore, the details of the connections should be provided to increase the effectiveness of the strengthening approach. Furthermore, to determine whether the chosen retrofitted method can resist the applied load and perform well under seismic excitation, both experimental and numerical analyses are needed. The real structure is complex and it may encounter different issues; therefore, a group of professional engineers and architects have worked to do the analysis and propose a certain solution for strengthening the structure. In addition to the above criteria, the effectiveness, cost, and available implementation technology should be considered in the selection of the most appropriate and cost-effective method. In this section, the performance of each method is defined based on the results of many scientific works conducted by engineers and scholars, and reported in **Tables 4-1** and **Table 4-2**. It can be revealed that considering all advantages and disadvantages each method performs differently in various conditions.

**Table 4-1** Advantages of URM retrofitting methods

Retrofitting methods		Advantage	
Improving structural integrity	Confinement	Tie column and beam	Increases lateral resistance by about 1.5 times, energy dissipation, integrity, in-plane and out-of-plane resistance, and deformability by about 50% (Wang <i>et al.</i> , 2018).
		Tie bar	Increases yield, ultimate strength and ductility by about 210%, 280%, and 270%, respectively.
	Transversal anchorage		Increases integrity, strength, connection between two wall surfaces, and separation prevention. Low cost.
	Strengthening of junction		Increases lateral load-bearing capacity of masonry junctions up to 2.4 times that of unreinforced wall.
	TRM and SRG		Increases resistance of masonry structures under tension and flexural stresses. Prevents out-of-plane expulsion, and reduces global in-plane damage.
	Mortar joint treatment	Grout/epoxy injection	Suitable for heritage buildings - ease of implementation, availability of material, low cost, low disturbance, high sustainability, restoration of original stiffness and strength. Improves shear and compressive strength, and out-of-plane stability.
		Re-pointing	Low cost, ease of implementation, and limited disturbance to the original form. (It can only restore its original stiffness and strength.)
	Strengthening of roof diaphragm		Distributes seismic loads to vertical elements. Can be replaced and upgraded. Low disturbance, light material, and compatible with original material.
Reducing seismic demands	Base isolation		Can be used in different building types. Dampens shaking and reduces applied lateral forces by a factor of 5 to 6 times.
	Seismic damper		High energy absorbance, easy to install. Reduces seismic induced vibrations and improves the overall behavior of the structure.
Upgrading structural components	Reinforced concrete wall		Increases global stiffness and controls inter-story drifts in the structure.
	Moment and braced frame		Customizable and reversible. Provides full visual and physical access, and requires small ties to connect to existing structures.
	Surface treatment	Shotcrete	Low cost, high durability, uniformity, and available materials, applicable on both surfaces of masonry walls. Reduces tension on an average of 50%. Increases ultimate lateral load resistance of walls by a factor of 3.6, and improves the ductility and energy dissipation.
		Ferrocement	Improves in-plane lateral resistance by about 150% and in out-of-plane direction about 10 times.
	External reinforcement	Steel reinforcement	Increases lateral load resistance of the wall.
		Bamboo reinforcement	Controls crack propagation. Increases load carrying capacity. Maintains structural integrity. Low cost, low technology, and low increase in mass.
		FRP composite	Increases in-plane lateral resistance and the out-of-plane resistance of the wall by a factor of 1.1 to 3 and 7, respectively. Low mass, low disturbance, and available materials.
	Post-tensioning		Suitable for seismic retrofitting of heritage masonry constructions. Maintains architectural value and quality of the wall with less added mass and low disturbance. Increases initial flexural stiffness, strength, shear bearing capacity, and energy dissipation. Improves out-of-plane stability and in-plane strength by a factor of 5-6 (Turer <i>et al.</i> , 2007), and doubles load carrying capacity.
	Mesh reinforcement	Polymer mesh	Low weight, high tensile strength to weight ratio. Increases integrity between components.
		PP band	Increases shear resistance under static loads. Prevents masonry unit's destruction. Prevents loss of material and retains wall integrity. (It is also suitable for the low strength masonry structures.)
	Reticulatus system		Increases shear strength up to 170% (Corradi <i>et al.</i> , 2016). It has almost no effect on original aesthetics. (It is suitable for retrofitting heritage masonry structures.)

**Table 4-2** Disadvantages of URM retrofitting methods

Retrofitting methods		Disadvantages	
Improving structural integrity	Confinement	Tie column and beam	High cost, additional mass, along with demolition and reconstruction of the original structure. Incompatibility of concrete and original masonry material requires design and use of adequate connections.
		Tie bar	High cost. Corrosion reduces strength of the bars and weakens their functionality over time. (It needs a suitable coating.)
	Transversal anchorage		Anchorage and corrosion problems. Disturbance to the original structure due to anchoring installation.
	Strengthening of junction		Low corrosion resistance of steel reinforcement.
	TRM and SRG		Somewhat inexpensive as only mortar and fibers should be considered (Wang <i>et al.</i> , 2018).
	Mortar joint treatment	Grout/epoxy injection	Successful if compatibility of material in terms of mechanical, physical, and chemical properties is provided.
		Re-pointing	Compatibility of the new and existing material is required. (No significant improvement in performance under dynamic loads.)
	Strengthening of roof diaphragm		Connection problems in case of heritage buildings, high cost, low moisture resistance, and prone to termites.
Reducing seismic demands	Base isolation		Implantation can cause destruction of the whole structure. Costs about 3% of total construction cost. Low efficiency and performance for tall buildings and other flexible structures with small natural frequency. Complicated application for sites with soft soil.
	Seismic damper		Not suitable for heritage structures. High cost and need for use of advanced equipment and techniques.
Upgrading structural components	Reinforced concrete wall		Materials may not be compatible with the original structure.
	Moment and braced frame		Low compatibility with existing structures. Needs high technical analysis to ensure steel and masonry are activated simultaneously under earthquake loads. (Not suitable for heritage buildings.)
	Surface treatment	Shotcrete	Affects aesthetics of the architecture. High disturbance. Needs treatment. Requires finishing. Expensive to install given need for special equipment as well as manufacturing of concrete and use of steel. Lack of voids for breathing on the surface covered by mortar may cause material deterioration and rotteness.
		Ferrocement	Time-consuming process. Destroys the aesthetic appearance of the building and therefore may not be suitable for the restoration of heritage structures.
	External reinforcement	Steel reinforcement	Damages the aesthetic face of structure and requires relatively high cost due to steel usage (Wang <i>et al.</i> , 2018).
		Bamboo reinforcement	Not available everywhere. Affects architectural value due to high disturbance.
		FRP composite	High cost, high technology for installation. Affects architecture. Requires finishing. Poor performance in high-temperature environments.
	Post-tensioning		High cost. Requires high technology. Anchorage problems, low corrosion resistance, and no effect on ductility.
	Mesh reinforcement	Polymer mesh	Susceptible to degradation and brittle failure. Sensitive to impact, notching, etc.
		PP band	Effectiveness of PP bands becomes less significant in the case of high-strength masonry structures (Wang <i>et al.</i> , 2018).
Reticulatus system		Requires reinforcement mesh and some re-pointing mortar.	

## 4.6 Summary

Most of the HURM buildings have an acceptable behavior under gravity load. Nonetheless, they have shown poor performance during past earthquakes due to many reasons such as deteriorated material, weak strength, and low ductility under lateral load. Therefore, many techniques have been developed for improving the behavior of these systems for seismic load. Some techniques are developed to retain integrity, strength, and stiffness. Others can essentially upgrade the behavior to a significantly higher level than the original structure, which is more favorable in a sense of modern engineering. However, in addition to the cost issue and compatibility of the retrofit method with original material, preservation of the valuable appearance of historical structures is a substantial factor to select a proper technique. In this chapter, it has been attempted to provide a list of the most common retrofit methods and classify them based on their action. The implementation, advantages, and drawbacks of each method, as well as the applicability of the method for HURM structures, were discussed in detail. This information can be used as a practical reference in the primary stage of the retrofitting project for selecting more suitable methods.

## **Chapter 5. Experimental and Numerical Methods for HURM Structures**

To understand the behavior of masonry structures, a comprehensive assessment of the mechanical behavior of structures is required by conducting an experimental test. However, the number of cases that can be investigated by the experiment has some limitations such as cost issues. With the advancement in numerical technique and emerging high-performance computers, numerical simulation can highly assist in evaluating structural behavior. To obtain reliable results from numerical simulation, it should be properly calibrated with experimental or theoretical results. In this chapter, appropriate experimental and numerical methods for masonry structures were discussed. The focus of this chapter is on the existing numerical technique for HURM structures such as the equilibrium method, structural element method, continuum method, and discrete element method. Also, regarding the required simplicities or complexities of the structure, the more appropriate method and the possibilities for improving the methods are discussed.

## 5.1 General Description

Several experimental and numerical techniques for the evaluation of seismic behavior of masonry walls are available. To investigate the behavior of the structure, a combination of both experimental and numerical approaches is required. Experimental techniques such as material and structural tests can be used based on the current situation of the building. Besides, with the advancement of simulation techniques and emergence of high-performance computers, the mechanical behavior of the structure can be investigated numerically. Therefore, these methods and their application are explained in detail in the following subsections. The considered topics in this chapter are shown schematically in **Figure 5-1**.

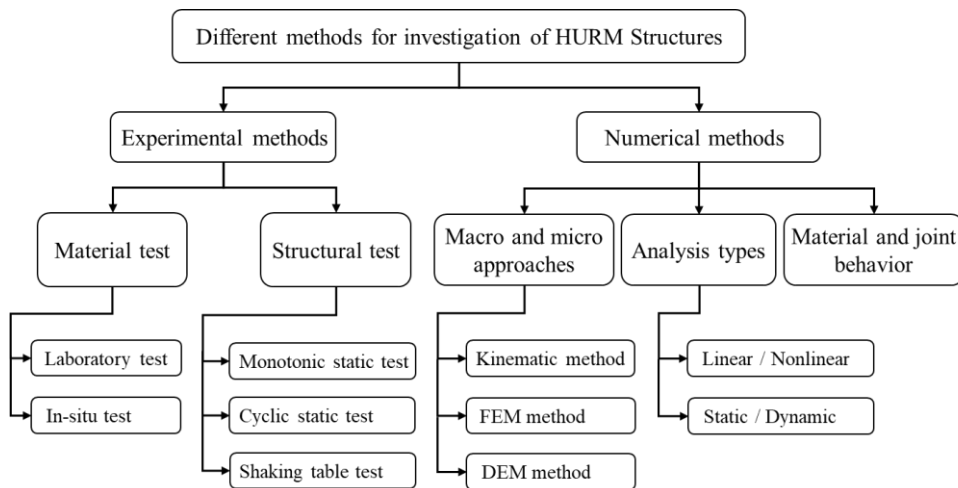


**Figure 5-1** Different methods for evaluating structural behavior of HURM buildings

## 5.2 Experimental Method

Masonry is a heterogeneous material composing of units that are connected by dry or mortar joints. Various configurations generated from the different combinations of units and joints result in a more complex structural behavior in comparison with other materials such as concrete or steel. In order to achieve reliable results in the numerical analysis including advanced constitutive models of masonry structures, it is necessary to calibrate the model with accurate experimental results (Oliveira, 2003). In general, experimental tests can be described into two categories of material tests and structural tests. The main purpose of material tests for masonry structure is the estimation of elastic and inelastic parameters of the constituent material of units and joints such as stiffness, strength, and ductility. In this series of tests, component behavior is investigated rather than the entire structure. These results are essential information that is required to evaluate structural behavior by using experimental tests or numerical simulations. On the other hand, the response of the structure is the main scope of conducting structural tests. Where making a full-scale model is not possible, the test is done on scaled-down prototypes. However, making a complete structural model is complex and requires more advanced facilities to perform the tests. Therefore, in most cases, critical structural components such as walls, columns, etc. were chosen, and the structural tests were done on these elements. In the following sections, more information regarding each approach is provided.

### **5.2.1 Material test**

The material tests can be classified into two main groups of in-situ and laboratory tests. Facing ancient buildings, non-destructive, and minor destructive tests in the group of the in-situ test are very interesting and useful. However, it does not provide enough information about the characterization of the structural material required by advanced modeling. On the other hand, performing destructive tests on ancient constructions is not possible despite providing a good result. Laboratory tests on masonry specimens representative of real constructions can be a good alternative approach (Oliveira, 2003). As an example, in the work by Yavartanoo *et al.* (2020), the specimens made of granite stones were provided from the quarries close to the Mireuksaji stone pagoda, and the required experimental test was carried out. However, this method is somewhat complicated because it is almost impossible to provide a sample that is fully compatible with the original material.

#### **a) Laboratory test**

Monotonic tests are usually carried out to investigate the most important features of material behavior including uniaxial behavior which is observable in the stress-strain diagram. Strength, stiffness, energy dissipation, and softening behavior are properly characterized to investigate the mechanical behavior under a continuous increase of imposed displacement. Softening occurs after peak strength for all frictional materials and causes a gradual reduction of the strength which can be observed in uniaxial compressive, tensile, and shear failure. Therefore, instead of

force-controlled, the test is usually conducted under displacement-controlled conditions which can be continued in the softening part. In comparison with monotonic tests, cyclic tests are more costly and time-consuming and require more advanced facilities. However, it can accurately capture cyclic hardening or softening of the material and stiffness degradation. The results of the monotonic test are close to the envelope of cyclic results. Selection between these two approaches is a matter of many factors such as cost, time, available facilities, required accuracy, the complexity of the material behavior, etc.

Generally, the basic material tests are the compressive test, tensile test, and shear test. In compressive test, a masonry specimen (stacked bond prisms or wallets) is placed under uniaxial compression employing displacement-control to assess the uniaxial compressive strength. The size of the specimen and the boundary conditions affect the strength and cracking behavior, respectively (Vermeltfoort, 1997). In the case of mortar joint masonry, the mortar tends to expand laterally under uniaxial compressive stress more than the units; however, the continuity between units and mortar results in lateral confinement to the mortar.

Shear stress at the interface of mortar and unit causes triaxial compressive stress in the mortar and bilateral tension coupled with uniaxial compression in the units. As a result, the failure will occur by developing cracks in the bricks along the loading direction. However, by providing an appropriate slenderness ratio a uniaxial stress condition in the center of the specimen can be observed. Concerning the mechanical behavior of dry joint masonry under compression, a lower compressive strength is

observed in comparison with mortar joint specimens due to the lack of interlayer material (Oliveira, 2003).

Although masonry structure has high compressive strength, it behaves very weakly under tensile stresses. Tensile behavior of masonry joints is very important in both monotonic and cyclic behavior of masonry structures. In the case of walls with dry joints, the tensile strength is zero. The tensile bond strength of the unit and mortar interface is an important factor in the nonlinear behavior of the structure originated by cracking in the mortar joints. To investigate this factor, two main tests can be carried out in the form of direct tensile bond strength test and flexural bond strength test as shown in **Figure 5-2(a)** and **(b)** (Jukes and Riddinton, 1998; ASTM, 2015).

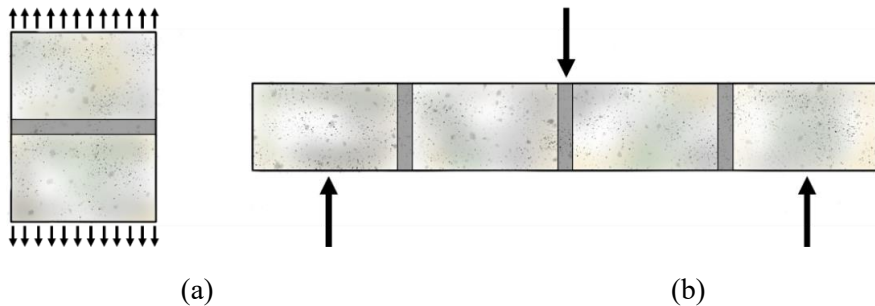


**Figure 5-2** Possible bond strength tests: a) Direct tensile bond strength test; b) Flexural bond strength test (Redrawn based on Oliveira, 2003)

The direct tensile test applies a uniformly distributed stress at the unit-mortar interface to investigate the in-plane behavior of the specimen. Van der Pluijm (1997) carried out direct tensile tests on masonry specimens made of solid clay and calcium-

silicate under a monotonic increase of deformation. It was observed that the behavior of units and mortar joints under tension is very similar to that of concrete. Mojsilović (2011) conducted direct tensile tests on two hollow clay block masonry prisms to investigate the tensile strength. The specimens subjected to direct tension in the z and y directions behaved linear-elastically up to brittle failure. A relatively large scatter was observed due to the initial cracking of units.

On the other hand, the flexural test is used to obtain tensile bond strength at the edge of the mortar joint by imposing the bending force on the specimen up to the failure (Oliveira, 2003). Jefferson and Mills (1998) carried out cyclic flexural tests on notched concrete cylinders with mortar joints to calibrate with the numerical model. The computed responses obtained in the numerical models were close to those of the original tests.

Lateral loads produced by wind or earthquake excitation cause shear mechanisms in masonry structures. However, a degree of confinement caused by gravity load leads to a combination of shear and compression mode of failure. This is an important factor that should be considered in the test of direct shear load accompanied by normal loading. The direct shear test applies a uniform state of stress to the joint which is constant during testing. One of the standard methods to carry out the test can be found in EN 1052-3 (2002). There are different configurations of shear test shown in **Figure 5-3** which are explained in detail by Jukes and Riddinton (1997). The direct shear test or couplet test shown in **Figure 5-3(a)** includes two units and one joint under shear-compression loading. In the triplet test shown in

**Figure 5-3(b)**, a prism made of three units and two joints is subjected to shear-compression loading. A different arrangement was developed by Van der Pluijm (1993) for the case of the couplet shear test (**Figure 5-3(c)**). In this method, the specimen should be attached to the steel loading elements to produce constant compressive stress upon shearing.

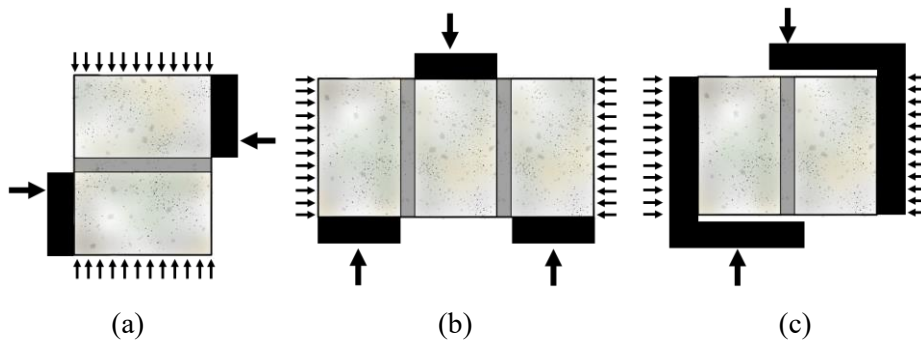


**Figure 5-3** Shear-compression loading test: a) Couplet test; b) Triplet test; c) Test set-up developed by van der Pluijm (1993) (Redrawn based on Oliveira, 2003)

Important properties such as cohesion, friction angle, dilatancy angle, and fracture energy are required to calibrate shear behavior in the numerical model. Some of these factors can be obtained by sketching the shear stress-displacement diagram. Stiffness degradation is an additional parameter for the cyclic shear test that should be considered. However, experimental results obtained from the cyclic shear test are almost rare, even almost none when dealing with dry joint masonry structures. Nonetheless, no considerable stiffness degradation was observed in former studies for the cyclic shear test of dry joint masonry walls (Atkinson *et al.*, 1989; Oliveira, 2003).

Masonry is not only a heterogeneous material because it is composed of units and mortar with different material properties, but also is an anisotropic material due to different behavior in tension and compression. This behavior is more significant if the units also represent anisotropic strength properties. Further, the discontinuity nature of masonry makes it very vulnerable to imposed loads, which is more evident for dry joint masonry structures. Concerning these characteristics, behavior under uniaxial loading conditions cannot thoroughly express the behavior of masonry under biaxial stress states (Lourenço, 1996). Because of anisotropic characteristics, the biaxial strength envelope of masonry is described by a three-dimensional surface, either in terms of full stress vector in a fixed set of material axes or by using the two principal stresses and the rotation angle between the principal stresses and the material axes (Oliveira, 2003). Page (1981) carried out a series of experimental studies to evaluate the biaxial behavior of masonry structures. The half-scale brickwork specimens made of solid clay units were subjected to proportional biaxial load. The principal compressive stresses are oriented at various angles to the bed joints. The results showed that the strength and failure modes were affected by the orientation of the principal stresses relative to the material axes and the principal stress ratio. The specimens were broken and failure occurred at mid-thickness in a plane parallel to its free surface, independent of the orientation of the principal stresses. However, the results obtained by Page (1981) do not apply to all types of masonry constructions. The diversity of material, shape, and configuration causes different biaxial strength envelopes and different failure modes. Although biaxial strength envelopes are useful for understanding the behavior of the masonry structure,

in advanced numerical models, information about softening behavior for the analysis is more important (Oliveira, 2003). In practice, the results of biaxial and cyclic tests are rare, and usually, results of monotonic uniaxial compressive, tensile, and shear tests are the main available data to be used in numerical simulation.

### **b) In-situ test**

For HURM structures that have experienced various unexpected events during their lifetime, complementary in-situ tests are very useful to investigate the accurate characteristics of historical structures. Because they can provide important information on the damage or current stage of the structure. Before applying in-situ tests, a complete structural survey is needed to provide correct data about the structure. The survey includes an accurate geometrical survey to determine the geometry of the structure with its irregularities. Moreover, a damage survey should be performed to investigate the existing cracks as well as the factors that threaten the stability of the structure. Further, the information and documentation of construction history should be provided to identify the structural building stages, the construction techniques, and possible strengthening interventions that had been performed in the past (Oliveira, 2003). The in-situ test investigates the mechanical properties of a structure in different ways including non-destructive, minor destructive tests, destructive tests, and monitoring.

Non-destructive and minor destructive tests are used to evaluate the mechanical characteristics of those structures that are of great importance, such as national

heritage that should not be damaged in any way. The non-destructive test applies an indirect action such as sonic or ultrasonic impulses and high-frequency waves to determine the defects of the structure. The application process highly depends on some characteristics of masonry such as its homogeneity and configuration.

In general, the non-destructive test is a somewhat cheap and simple technique. Nonetheless, the obtained qualitative results provide only a preliminary evaluation of the mechanical characteristics of masonry. Conversely, the minor destructive test can be applied to the masonry structure to provide a quantitative determination of mechanical properties such as Young's modulus, shear strength, etc. The slight and temporary damage produced by this method can be easily repaired after testing. Therefore, using this method is also preferable for historical masonry constructions. Two common approaches to perform a minor destructive test are coring and flat-jack techniques. The former technique is often used for those of masonry composed of multilayers by producing a deep and narrow hole and taking the samples of the most significant parts, which can be mechanically tested in the laboratory. Also, the video survey is carried out by inserting a camera inside the hole to provide technical information about the internal cavities and cracks. The latter technique is usually used to evaluate the shear strength along the mortar joints, the compressive stress state, and the compressive deformability properties of masonry. It is also possible to compute the friction angle and the cohesion of the mortar joints by accomplishing this test on various locations on the structure with different compressive stress states (Oliveira, 2003).

To evaluate the response of the structure under a given earthquake excitation, dynamic properties of the structure (mass, stiffness, and damping ratio) are required. For this reason, dynamic identification can be used that is one of the useful and promising techniques in the category of the non-destructive test (Fanelli and Pavese, 1993; Doebling *et al.*, 1996). In this method, vibration response of the structure is measured in terms of amplitude and frequency content to a given excitation. The measurement can be used to monitor the structure, either locally (response of single structural component) or globally, by measuring its overall properties (e.g. displacement at the roof) under pulse excitation. The technique is based on the fact that the dynamic response of the structure to natural excitations of the environment (e.g. wind) or artificial excitations (e.g. railroad traffic, vibrodyne) is a function of the stiffness, mass, damping, and boundary conditions.

Destructive tests are carried out on the original material of the structure to obtain valuable data such as strength, stiffness, and deformability properties. The specimens in this technique are provided by removing a part of the structure or collecting fallen and broken parts of the structure to perform laboratory tests. The obtained experimental results can be used for further researches on other masonry structures with similar materials and building techniques. As an example, a set of destructive tests had been conducted on masonry specimens of the Civic Tower of Pavia, which collapsed in 1989 (Macchi, 1992).

Monitoring system is used to investigate the mechanical behavior of the structure with time. This method includes some instrumentation which is applied to

monitor and observe cracks' movements, vibrations, and deformations of the building. The sensors can be assigned to the structure or just the vibration and deformations can be recorded by camcorders and image processing. Then the results can be updated several times under the events (earthquake, wind, or other excitations) that may happen during the tests to calibrate the numerical analysis with more precision. These reliable results obtained by the monitoring system contribute to a better understanding of the mechanical behavior of the structures as the most preferable method for heritage structures (Oliveira, 2003). Currently, extensive monitoring systems have been mounted on some of the famous historical structures including the Florence Cathedral, the Pavia Cathedral, the Pisa Tower, and the Mexico City Cathedral (Macchi, 1997).

### **5.2.2 Structural test**

In general, two classes of structural tests to evaluate the performance of structures are static tests including monotonic (or push-over) and cyclic (or quasi-static) tests, and dynamic tests (shaking table test). Within them, the shaking table test is considered the most accurate state-of-the-art technology to evaluate responses of the structure to earthquake excitation. The size and weight of the specimen are some of the concerns due to shaking table capacity.

Although there are some large facilities, in many cases it is not possible to conduct the test on a full-scale model. Also, the technique is considerably more costly than static tests. Typically, monotonic and cyclic tests provide valuable results

to understand the behavior of the structure with less cost. In the following sections, each approach is discussed in more detail. Note that another approach that is called hybrid or pseudo-dynamic is also available in which structural tests and numerical analysis are conducted simultaneously to capture responses of structure more accurately. Generally, this approach includes three main components: experimental facilities, numerical tools, and connection units (including corresponding hardware and software). Discussion about connection units is out of the scope of this study, and since numerical and experimental techniques are the same as a conventional approach, no more discussion is provided in this chapter.

### **a) Monotonic static test**

In the monotonic static test (or push-over test), the applied load is increased incrementally to the specimen in a given direction to identify its properties in terms of the relation between force and displacement (stress and strain).

To capture the post-peak behavior, it is necessary to carry out the test under displacement-control conditions. The monotonic test provides the response of the structure under static loads and the result in terms of the force-displacement curve is of the most practical property to determine structural behavior. This curve is representative of structural capacity and several crucial parameters can be extracted from it including initial stiffness, yield and ultimate strength, ductility, and overstrength. However, this method is not able to precisely evaluate stiffness degradation and possible cyclic hardening or softening. Further, this laboratory test

is more common to be performed on structural elements such as beam, column, wall, etc. than on a full structure. The fact that it is easy to perform and less time-consuming in comparison with other types of testing leads to wide use of this method in many research and studies for many years.

### **b) Cyclic static test**

Cyclic static test (or quasi-static test) is carried out on the structural elements or in some cases on a small scale of full structures. In this method, the load is applied slowly (quasi-static state) under force or displacement control. This test tries to simulate earthquake excitation by increasing or decreasing the amplitude in both ways to evaluate the dynamic behavior of the structure. One of its main advantages over the monotonic test is that it can directly measure strength and stiffness degradation and also cyclic hardening and softening behavior. Also, performing a static cyclic test doesn't require very complex equipment and is not as costly as a shaking table test (Mendes, 2012). Ideally, any displacement imposed on the structure should be determined by considering the interaction between the input excitation and the response of the structure, and it cannot be considered in the cyclic static test. Therefore, a set of standard protocols were defined to be used as load history in cyclic tests. ATC-24 protocol (ATC-24, 1992), SAC protocol (Clark *et al.*, 1997), FEMA 461 (FEMA, 2007), and SPD protocol (Porter, 1987) are some examples of such developed protocols (**Figure 5-4(a), (b), (c) and (d)**).

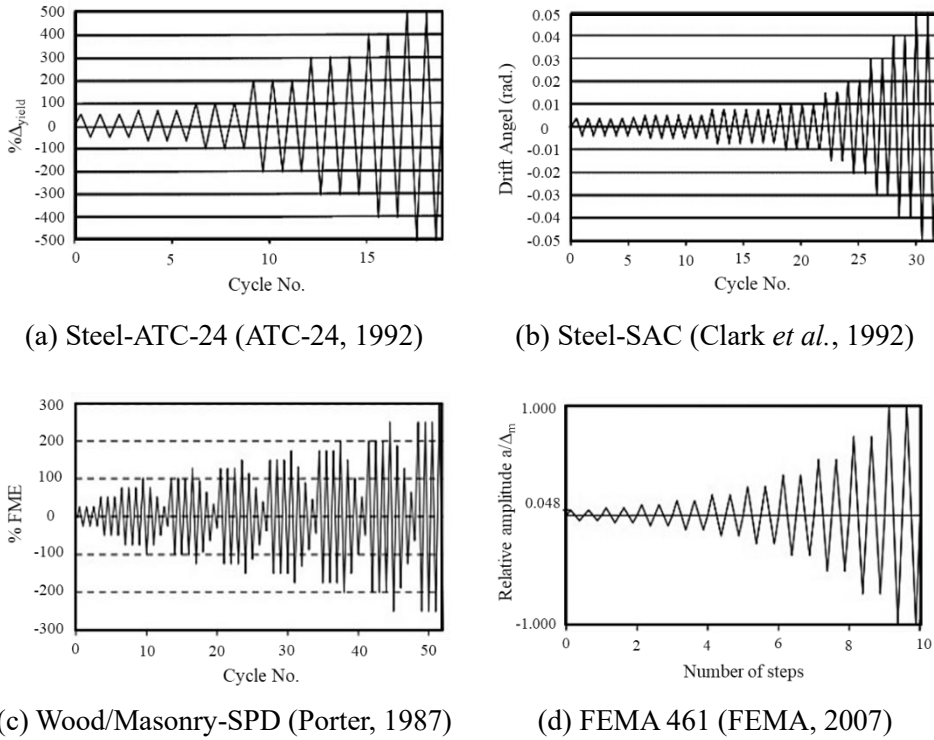


**Figure 5-4** Examples of standard protocols for cyclic test

### c) Shaking table test

The shaking table test is considered the most accurate laboratory method to reproduce the load under earthquake excitation. The shaking table consists of a rigid platform that is connected to hydraulic actuators to produce shaking motions. In some cases it is possible to conduct shaking table tests on a full-scale model, However, a simplified model commonly known as Mock-up, is prepared to reproduce the geometrical, physical, and dynamical characteristics of the prototypes. The mock-up is prepared with a small scale of full structures, however, it should be able to reproduce the dynamic behavior of the real structure. Besides the most

important parameters such as geometry, the relationship between stresses and strains of the materials, mass and gravity forces, and boundary conditions should be properly matched with real conditions. Although this test is the most adequate method in seismic investigations, the cost of the experiment facility and mock-ups preparation is quite high (Mendes, 2012).

### **5.3 Numerical Analysis Methods**

The high vulnerability of historical masonry structures requires that their seismic behavior be investigated under different conditions. Numerical methods are so beneficial techniques since they can minimize the intervention caused by experimental assessments. Numerical studies have been increasingly used to predict the response of structures in the last decades even more for historical masonry structures that are extremely vulnerable to seismic loading. In case of conditions that are impractical to conduct experimental tests (e.g. destructive test for historical masonry buildings), numerical methods can be used as computational laboratory tools to predict the response of the structure (Mendes, 2012).

Numerical models are aimed to represent the real behavior in different types of structures ranging from simple to complex geometry subjected to static, quasi-static, or dynamic loads to determine the strength and stability of the structures. The numerical investigation of historical masonry structures with their complex structures, high anisotropy, and inelastic behavior is a very demanding procedure in some cases. Hence, the studies related to the analysis of historical structures are less

than modern structures made of concrete or composite materials. Therefore, to determine the most proper and efficient techniques for simulation, the advantages and disadvantages of existing methods must be well understood before its application (Dejong, 2009).

Several methods and computational tools are available to evaluate the mechanical behavior of historical masonry structures (**Figure 5-5**). The methods can be used based on the different levels of complexity and availability in the matter of the required time and costs (Lourenço, 2002). Besides, these methods must be able to simulate the behavior as close as possible to the real structure concerning the computational demands as an important criterion (Pappas, 2012).

It should be also considered that carrying a complete set of displacement-control tests is required to obtain the necessary properties for advanced numerical models with a successful result. However concerning all these criteria, the results of different methods might also be different, and it does not mean that a more complex method always gives a more accurate answer. Lourenço (2002) specified some important factors that should be considered in numerical investigations as follows:

- Adequacy between the analysis tool and the sought information;
- Available engineering should be compatible with the analysis tools;
- Available financial resources and time requirements.

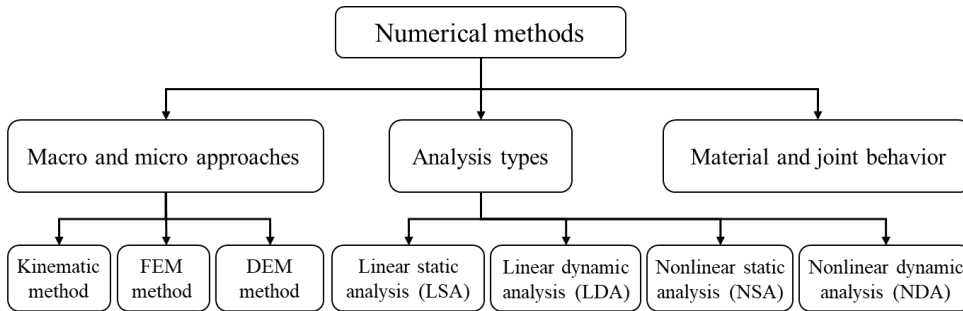


**Figure 5-5** Numerical methods for analyzing the behavior of HURM structures

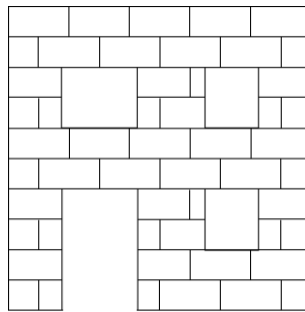
Masonry is anisotropic material with a combination of units and mortar. The mortar joint has distinct directional properties and acts as a plane of weakness under loading conditions and these features require an accurate engineering analysis. Depending on the level of accuracy and the simplicity desired, different approaches are available for the numerical analysis of the masonry structures with linear elastic or nonlinear inelastic material behavior (Rots, 1991). These methods can be applied to simulate the structure at a macro or micro level and present the stage of damage using different ways and constitutive laws (Pappas, 2012). Lourenço (1996) proposed a computational approach laying on separate brick and mortar layers to model masonry structures. The approach was enhanced by introducing the brick-interface model (Lourenço and Rots, 1997) and anisotropic continuum model (Lourenço *et al.*, 1998). Gambarotta and Lagomarsino (1997a and b) proposed a brick-mortar damage model and homogenization techniques to be applicable for cyclic loading. The proposed model was updated with a more effective iteration technique by Brasile *et al.* (2007) to be more practical for complex models. In the

study by Valente (2003) a more complex method based on fracture mechanics was adopted to model seismic failure of masonry structures. In the study by Yi *et al.* (2006), masonry structures were modeled as a combination of elastic continuum parts connected with contact elements at predefined crack locations. The strength of the material is only assessed at these contact elements.

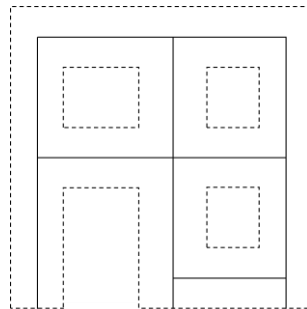
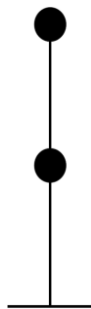
Following this approach, analysis is simplified considerably and convergence problems and computational costs are reduced effectively. As discussed by Dejong (2009), this approach is effective if crack locations are known with an acceptable level of certainty. In the study by Milani *et al.* (2006a, 2006b) an approach based on limit analysis and homogenized material was proposed. The approach was improved by Milani *et al.* (2007) to be applicable for 3D masonry structures under lateral seismic load. In some of the research, a simplified approach for modeling masonry structure is proposed by considering equivalent frames with the ability to develop plastic hinges (Magenes and Della Fontana, 1998; Kappos *et al.*, 2002; Salonikios *et al.*, 2003).

### **5.3.1 Concept of macro and micro approaches**

In general, being macro- or micro-modeling is a relative term, and it is determined based on the level of details that are included in the model in comparison with the other possible methods. Some of the common modeling approaches and the main corresponding responses that can be obtained are illustrated in **Figure 5-6**.

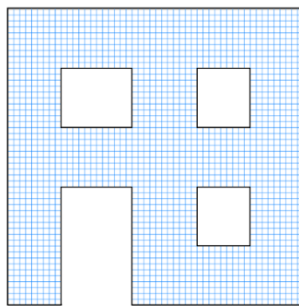


(a) Original structure

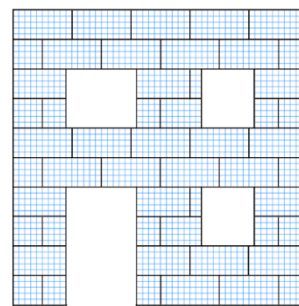


(b) Overall yielding of base and stories

(b) Plastic hinges within members



(c) Failure in the domain



(d) Failure in the units and joints

**Figure 5-6** General definition of macro-and micro-modeling

In the state of the engineering's art in the field of masonry structures **Figure 5-7(a)**, macro-and micro-modeling have a more specified meaning.

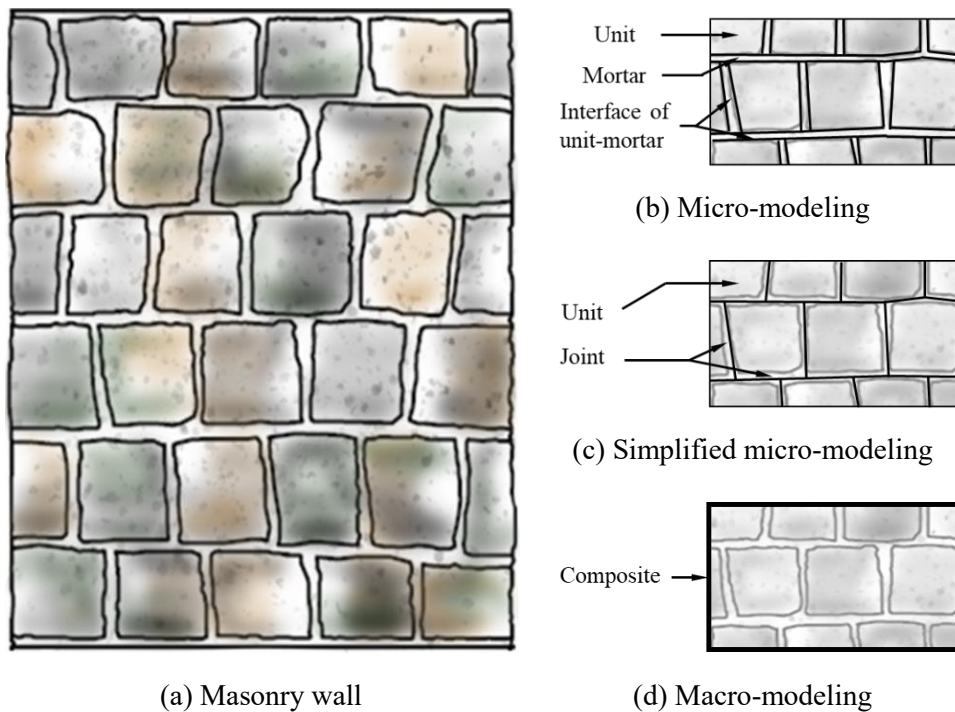


**Figure 5-7** Micro- and macro-modeling approaches for masonry structures

### a) Micro-modeling

The micro-modeling method can simulate the models which are composed of multiple materials under a heterogeneous state of stress or strain. In this method, units and mortar in the joints are simulated as continuum elements either with elastic or inelastic properties, whereas the interface of unit-mortar is represented by discontinuum or interface elements with the ability to appear local slip or crack phenomena (**Figure 5-7(b)**).

The interface elements are considered to model potential crack/slip planes with a dummy stiffness to restrict the interpenetration of the continuum. Therefore, the

combined action of the unit, mortar, and interface can be monitored under a magnifying glass (Lourenço, 2002). In this approach, elastic properties such as modulus of elasticity and Poisson's ratio, and for more accurate model inelastic properties such as yield and ultimate strength of both unit and mortar should be considered (Lourenço, 2002). If inelastic parameters are not considered, the model is not able to represent the failure in units and mortar, and only interface failure can be directly observed. In this case, the stress and strain should be checked individually to control possible cracks (under tensile load) and crushing (under compression load). Therefore, it is necessary to investigate the behavior of the constituent materials (units and mortar), and their interface with proper experiments on the original or similar structural elements or structures. Despite the many advantages of this method including accurate and detailed results, it requires considerable computational effort to perform analysis which would cause a vastly time-consuming process (Pappas, 2012).

### **b) Simplified micro-modeling**

This model is used for simplifying analysis to minimize time and cost, in particular for complex models such as historical masonry structures. As it is shown in **Figure 5-7(c)**, units are expanded up to the half-thickness of the mortar and represented by continuum elements (with either elastic or inelastic material), whereas the behavior of the mortar joints and the unit-mortar interface is considered as discontinuum or interface elements.

In fact, an artificial interface is supposed in the middle of each joint consisting of mortar and the two unit-mortar interfaces, which are lumped into an average interface.

Therefore, masonry is considered as a set of blocks bonded by potential fracture/slip surface at the joints. Thus, the properties of the joint can be considered as the representative behavior of mortar and the unit-mortar interface. The simplified micro-modeling is not as accurate as the micro-modeling approach, because of the exclusion of Poisson's effect of the mortar in the analysis (Lourenço, 1996). Note that, where the mortar thickness is so smaller than the dimension of units, very fine mesh should be used to get reliable results from the micro-modeling approach. It considerably increases computational cost and reduces the efficiency of the approach. However, simplicity, less computational cost, and relatively accurate results (which is enough information in many cases) lead to the widespread use of a simplified micro-modeling approach by engineers and researchers.

### **c) Macro-modeling**

In this method, units, mortar, and unit-mortar interfaces are considered as a homogeneous continuum (**Figure 5-7(d)**). The homogenized model can be either elastic or inelastic as well as isotropic or orthotropic. The properties of the homogeneous material should be representative of the mechanical behavior of the units, mortar, and unit-mortar interface (Lourenço, 2002).

To obtain the properties for macro-model analysis with good accuracy, the experimental tests should be carried out with an appropriate size of specimens to be used for calibration of the modeling parameters.

The geometrical and mechanical properties of each component obtained from experimental tests can help us to predict the mechanical behavior of the composite body in numerical analysis. Several approaches were proposed by the researchers to obtain homogenized property. Lourenço (1996) proposed a technique for homogenization based on matrix formulation for easy implementation in numerical simulation. In this method, masonry is assumed to be a layered material that considerably simplifies the complexity of the simulation. Note that the accuracy of the analysis highly depends on the size of mesh elements, which means the larger the mesh size, the less accurate the results (Pappas, 2012). Therefore, with less time and cost requirements, as well as the user-friendly mesh generation feature (due to excluding irregular shapes of mortar and units), this modeling approach is used widely in many numerical analyses. Note that in the case of dry joints, the simplified micro-model and micro model are essentially the same. Therefore, the modeling techniques for dry joints are only based on the macro-model or micro-model.

In summary, the macro-model approach is the most used method for numerical analysis of masonry structures due to its simplicity and the lesser calculation requirements (Pappas, 2012). However, it should bear in mind that generally one modeling approach cannot be preferred over the other methods. Therefore, considering the advantages of each method and different application fields, the best

case for the model should be selected. The micro-modeling method provides structural details for a better understanding of the local behavior of masonry structures, while the macro-modeling method is applied to the solid walls with sufficiently large dimensions.

According to the mentioned parameters in using any of the micro or macro models, a new division can be considered to create structural models with different levels of sophistication. Currently, the kinematic method based on limit analysis and finite element method based on direct (static or dynamic) analysis is widely used to simulate the behavior of masonry construction. These methods are explained in more detail in the following subsections.

### **5.3.2 Kinematic method**

The kinematic method (or equilibrium method) is based on limit analysis that decomposes the structural components into rigid blocks with homogeneous constructive characteristics to evaluate the seismic vulnerability of the structure. Therefore, the modeling approach by using this technique can be considered as macro modeling. The macro elements (blocks) are created based on various parameters to be representative of a possible kinematic mechanism failure (limit state) under the load. Those parameters can be defined as geometrical or structural boundaries, the mutual bond and connections between structural components, materials and configurations, and existing or expected cracks. However, in this approach, sliding between the blocks and tension are not considered, whereas the

infinite compressive strength of the masonry is a hypothesis of the analysis. An example of a possible mechanism corresponded to in-plane behavior under lateral load is schematically shown in **Figure 5-8**.

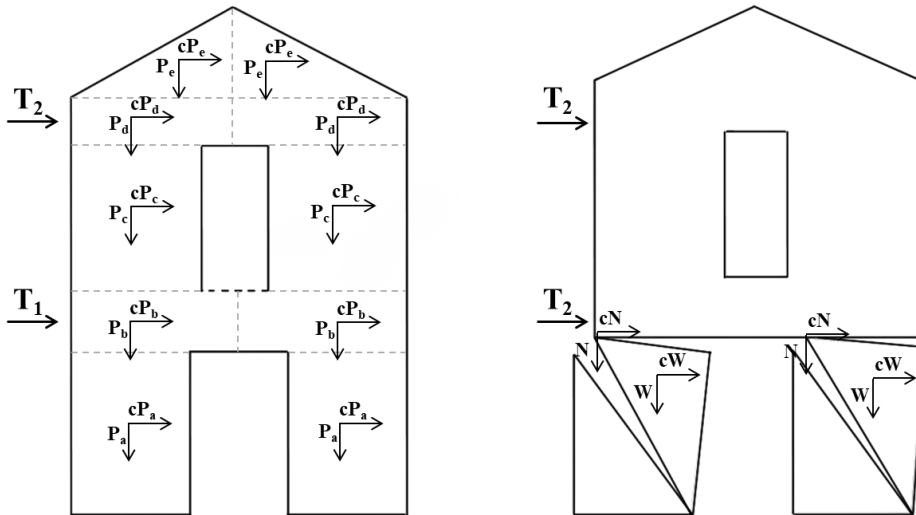


**Figure 5-8** Formation of a kinematic chain for in-plane behavior (Redrawn based on Pappas, 2012)

To have an appropriate estimation of the overall behavior of a structure under seismic load, all possible expected kinematic failure mechanisms should be analyzed. Available data surveys and experiences from the last earthquakes can be used as a reliable source to predict possible failure mechanisms for the different types of structures. In addition to gravity load, other stabilizing forces from the connections, diaphragms, or strengthening ties can be directly included in the equilibrium equation for limit analysis. By performing limit state analysis for each mechanism, a different coefficient  $\alpha_0$  will be obtained which is the mean response acceleration

for the ultimate limit state where the equilibrium is lost. Then through all the mechanisms, the case leading to failure with the lowest values of  $\alpha_0$  is identified as the most critical case. The kinematic mechanisms correspond to out-of-plane failure usually characterized by lower coefficients  $\alpha_0$  in comparison with the one correspond to in-plane failure (Pappas, 2012).

Since the first proposal for the kinematic modeling approach, the technique of the limit analysis has been upgraded. In the research by Lagomarsino (2006), limit analysis is combined with the capacity spectrum method, which leads to a more facilitated method that can be adopted with seismic codes for the design process [Italian codes OPCM 3274 (PCM, 2003); OPCM 341/2005 (PCM, 2005)]. Moreover, the kinematic analysis method has undergone some improvements by Ochsendorf (2002), De Luca *et al.* (2004), Block (2005), Block *et al.* (2006), and Roca *et al.* (2007) based on graphic oriented techniques using both kinematic and static approaches. As explained by Orduña and Lourenço (2003; 2005a; 2005b), the revised hypotheses are based on the absence of tension between the blocks, perfect plastic behavior for shear failure at the joints, and the creation of a hinge at a point, which is the result of a compressive load independent from the rotation. They proposed another significant approach which is a complete limit analysis formulation for 3D problems with an assembly of rigid blocks. The model is based on nonassociative flow rules and adopts no-tension frictional interfaces with a proposed formulation for the torsion failure mode. The numerical results were in very good

agreement with experimental results which emphasize the importance and efficiency of this method.

### **5.3.3 Finite element method**

One of the most widespread structural analysis tools in numerical analysis is Finite Element Method (FEM). It can be used to simulate simple to complex structures in both micro or macro scale with linear or nonlinear properties. However, FEM is more appropriate to simulate continuous structures under static and dynamic loads that remain somewhat connected during elastoplastic failure (Dejong, 2009).

One advantage over the kinematic approach is that by using FEM and considering proper behavior, there is no need to have prejudgment about the location and type of failure. Because depending on the condition, it will be observed in the results. However, depending on the complexity of the model and the required level of accuracy, it may not be possible always to have correct failure detection. Experience and preknowledge about the behavior of similar structures and engineering judgment assist to evaluate the reliability of the results. In this method, the complex structure is discretized into small parts that are called elements, which are connected at their nodes to create a continuum, and the assembly of these elements is commonly called “mesh”. Regarding the desired simplicity, a wide range of element types and shapes are available that can be used in macro or micro modeling within two or three dimension spaces. As a convention, elements are considered in two categories of “structural elements” including spring, truss, beam,

and shell elements and “continuum (or solid) elements”. They also can be categorized based on their geometry as following: zero-dimensional (0D) elements include spring elements; one-dimensional (1D) elements include truss and beam elements; two-dimensional (2D) elements include membrane, plate, and shell elements; and three-dimensional (3D) elements include continuum elements.

The element type is defined by its geometry, shape function (first or second order), explicit or implicit formulation, integration point (full or reduced Gaussian integration points), and active degree of freedoms (translational and rotational).

0D elements, i.e. spring elements, have a wide range of applications, such as in lumped mass-spring modeling approach, beam-column joint behavior, interface behavior between contact surfaces, a simplified model for soil-structure interaction, etc. By using spring elements, the behavior of original material and components of the part (e.g. mortars or components of connections) is replaced by its overall behavior.

1D elements, i.e. truss and beam elements, are proper to be used in the case that the member is mainly under uniaxial stress.

Truss elements have only a translational degree of freedoms (DOFs) and have resistance only under axial load. With proper material properties that can consider different behavior for tension and compression, these elements are appropriate to be used in the strut and tie modeling concept for masonry structures.

Beam elements have both translational and rotational DOF and also have axial, flexural, shear, and torsional resistance. These elements are the most widely used in structural engineering due to their simplicity. In some software, beam element is provided as two types of the element with axial-flexural deformation (which are called frame or beam-column element) and element with only flexural deformation and rigid axial deformation (which are called beam element). With this definition, truss element is beam element with axial deformation and rigid flexure. Here, “beam element” is considered in general definition having both flexural and axial resistance and deformation. Theoretically, beam elements are appropriate for modeling line-type members (e.g beams, columns, and brace) whose length is considerably larger than the dimensions of the section normal to the length. Beam elements are generally formulated based on Euler-Bernoulli and Timoshenko's theory. Euler-Bernoulli beam is appropriate for the members the ratio of length to a greater dimension of the section larger than 15. In this condition, shear deformation is negligible and excluded from the formulation. Where the ratio is less than 15, the shear deformation is considerable and considered in the formulation of Timoshenko's theory. For the members with a ratio of less than 10, even the Timoshenko elements cannot accurately calculate the response, and higher-order elements like the shell and solid elements are recommended. Shell elements can be considered as a two-dimensional form of beam elements. Shell elements are appropriate for plane-type members (e.g. slabs and walls) the thickness is considerably less than the smallest dimension of the plane size.

Similar to theoretical limitation for beam elements, where the ratio of the smallest dimension of the plane to the thickness is less than 15, shear deformation is negligible, and thin shell elements can be used. For the ratio of less than 15, shear deformation is considerable, and thick shell elements should be used. Where the ratio is less than 10, continuum elements are recommended. Shell elements have both translational and rotational DOFs and can resist in-plane normal and shear stress. In the case of thick shell elements, transverse or out-of-plane shear also can be resisted. Shell elements without flexural resistance are called membrane elements (2D form of truss elements). Also, shell elements with rigid in-plane stiffness are called plate elements.

Continuum elements are the most complete elements because their formulation is written in form of three-dimensional stress and strain state. In contrast with shell and beam elements, all dimensions are explicitly considered in continuum elements. Therefore, they do not need rotational DOFs since rotation is directly determined based on the relative translational motion of nodes with respect to each other. However, to calculate rotation properly, enough mesh should be provided that in some cases may require too many elements. To overcome this problem, a special form of solid elements is developed that is called “continuum shell element” which has both translational and rotational elements. Besides, continuum elements can be used in the two-dimensional form under “plane-stress”, “plane-strain”, and “axisymmetric” conditions. Under “plane-stress” condition, out-of-plane stress is zero (or negligible), and out-of-plane strain can be calculated based on in-plane strain

separately. In “plain-strain” condition, out-of-plane strain is zero, and out-of-plane stress can be calculated individually from in-plane stress. In “axisymmetric” condition, the stress and strain condition is the same with respect to the axis passing the centroid of the geometry. The behavior of masonry walls under out-of-plane deformation requires modeling in three-dimensional space. However, if in-plane behavior is under investigation, it can also be modeled in two-dimensional space under plane stress conditions. It effectively reduces the complexity of the model and the cost of analysis.

### **5.3.4 Discrete element method**

Using structural elements including springs, truss, beam, membrane, plate, and shell elements is one of the simplest approaches to simulate historical masonry buildings in the macro-modeling approach. They are used to represent the geometry of the pillars, columns, arches, vaults, and domes concerning homogeneous material behavior. Lourenço (2002) has proposed three different possibilities for modeling a wall with several openings using a lumped mass approach, a beam approach, and a panel macro-model (rigid blocks or shell elements).

Due to the complex geometry of historical masonry structures, using line-type elements (beam and truss elements) is not suitable to represent an accurate model of the given structures. Instead, solid elements in two- and three-dimension can be a true alternative method to model the complex buildings with massive structural parts such as piers, buttresses, arches, vaults, and domes. However, application of DEM

is mainly limited to the simulation of a partial component rather than the entire building, since it brings too much computational cost.

All mentioned methods with their advantages and disadvantages can be used along with the concept of the macro-modeling approach. In order to model the micro-modeling approach, the concept of discrete element method (DEM) developed by Cundall (1971) is utilized for an accurate understanding of each masonry constituent (unit and mortar) and their interface behavior. In DEM method, units can be modeled as either rigid or deformable blocks. In the case of using rigid blocks, analysis is significantly simplified since deformation and failure are considered only in joints, and failure of blocks itself is excluded from modeling. On the other hand, deformable blocks are discretized by using the finite element method, so deformation and failure are considered in both joints and blocks. Therefore, it can simulate the progressive failure of the masonry structures as a consequence of failure of joints and blocks. The study conducted by Page (1978) on the in-plane behavior of clay masonry walls was the first attempt to use DEM (micro-modeling) approach for masonry structures. Papastamatiou and Psycharis (1993), Baggio and Trovalusci (1995), and Psycharis *et al.* (2003) are some examples of the studies that employed DEM method for simulation of historical masonry structures. As explained by Lourenço and Rots (1997), all main failure modes of masonry walls can be captured by using DEM method, including cracking of joints, sliding, tensile cracking, and compressive crushing of units, diagonal and stair-stepped cracking. Additionally, breaking of units in tension because of mortar dilatancy under high normal stress can be effectively

included in the model. In the case of a simplified micro-modeling approach, all the mentioned failure modes can be detected except failure due to dilatancy of mortar because mortar thickness is not considered in the modeling.

## **5.4 Analysis Types**

In the state of the practice, several types of analyses are available within the software that can be used for simulation structural behavior. A well understanding of the basis of this method is of great importance to obtain reliable results. Generally, structural analysis can be categorized based on two characteristics of being linear or nonlinear and being static or dynamic. In general, three main sources are attributed to nonlinearity including geometric nonlinearity, material nonlinearity, and boundary conditions nonlinearity. Based on the condition, either one or all sources can exist. The term geometrical nonlinearity comes from the fact that changing the shape of the structure under loading can affect the response.

In a geometrically linear analysis of FEM models, the initial condition of the structure is considered for determining node coordinate. Therefore there is no need for an iterative solution, and response directly can be obtained. On the other hand, geometrically nonlinear analysis requires an iterative solution, and the loads are incrementally increased. At each increment of loading, either node coordinate is updated (direct approach) or the effects (such as extra moments) are added to the response (indirect approach). Clearly, the direct approach is more accurate because

of considering the changes in geometry due to structural deformations directly in formulating the constitutive and equilibrium equations.

The effect of nonlinear geometry can be discussed in two terms of large displacements and large deformations. The effect of large displacements can be considered as changing the action of the applied load. As an example, in the case of the building, the gravity axial load in columns or walls results in axial reaction force. Whereas under lateral load structure is tilted and now the product of gravity axial load and lateral deflection results in extra moments at the base, which is also known as  $P-\Delta$  effect and can be considered under large displacements. One common example of a large deformation effect can occur in beam-columns members that are under axial and flexural load. Where deflection of the member is large, an extra moment can be added due to eccentric axial load concerning the member's joint and is also known as  $P-\delta$  effect. Another important effect of large deformation is in the level of strain. Under small deformation, strain can be defined as the ratio of deformation and initial length, which is called engineering or nominal strain. However, if the deformation is large engineering strain is not appropriate and logarithmic strain should be considered, which is defined based on the ratio of incremental deformation and true length at that increment. Different type of buckling failure is the result of the large deformation or displacement. However, the term "large" or "small" is case sensitive and should be investigated in each case.

Some of the standards and the codes for building design such as ASCE (2017) provide some guidelines on whether the effect should be included or not. Although

it brings more computational costs, it would be more reliable if these effects directly are included in the analysis.

Nonlinearity associated with material properties can be observed due to nonlinear elastic behavior (e.g. in rubber materials), inelastic behavior (e.g. plastification, cracking), viscose behavior, creep, fatigue, and temperature. Usually, under normal conditions, linear elastic behavior is assumed for masonry structure for simplification; therefore, inelastic behavior is considered as the main source of material associated nonlinearity. Changing in internal (e.g. joints) or external (e.g. support) boundary conditions can result in nonlinearity in the response. Joint behavior is an example of nonlinearity associated with boundary conditions in masonry structures. The behavior of dry joints is the frictional type and is modeled as perfect plastic behavior. In the presence of mortar, if the micro-model is used then the behavior is defined by the assigned material and thus nonlinearity is included in the material. Whereas in the simplified micro-modeling approach, the mortar is not modeled directly and behavior is defined by interface elements. The nonlinearity is included in the boundary conditions. Inelastic material behavior and joint behavior are discussed in more detail in **Section 5.5**.

Imposed load to the structure can be considered as static or dynamic load depends on their nature and action on the structure. By definition, being dynamic or static depends on the fact that induced inertial forces are negligible or significant. If the natural frequency of the structure is close to the natural frequency of the imposed excitation, then induced inertial forces are large and dynamic action should be

considered. The action of gravity load is considered static since they are applied gradually on the structure and the dynamic action is negligible. The seismic load is the result of the transient excitation at the base of the structure due to earthquake shaking. Since the earthquake excitation has most of its energy in its higher frequency contents, structures with small frequency (including masonry buildings) are critically vulnerable to its dynamic action. On the other hand, wind load has most of its energy in its smaller frequency content, so its dynamic action is smaller on (short) masonry buildings. That is why seismic loads are usually more critical and of concern for masonry buildings than wind loads.

Currently, four types of analysis are recommended to evaluate the seismic response of masonry structures (and other structures), linear static analysis, linear dynamic analysis, nonlinear static analysis, and nonlinear time history dynamic analysis. Each method may be applied based on the required demands and current conditions of the structure. To achieve more reliable results it is recommended that all the above methods be performed sequentially for the seismic investigation of the given structure. In linear methods, the actual inelastic behavior is considered by some factors to adjust the response with a real inelastic response. While in nonlinear analysis, inelastic behavior is included directly in the model and actual nonlinear behavior can be simulated.

Nonlinear dynamic time-history analysis is considered the most accurate method among the available methods. However, its computational cost is one of the main hindrances for its application as the main analysis tool in many cases. Therefore,

a more simplified method like nonlinear static analysis may be more useful in preliminary investigation (Sar, 2014). In the following sections, more details about each approach are provided.

### 5.4.1 Linear static analysis (LSA)

A linear static analysis (LSA) or elastic analysis considers a linear relationship between the applied load and displacement. In fact, this method is only applicable to the cases where stresses remain in the linear elastic range. It is assumed that the structure obeys Hooke's law and the force is linearly proportional to deformation as well as stress to strain. There is no plastic deformation in materials because by removing the load, the material returns to its original state. Further, the boundary conditions do not vary during the application of loads. The dynamic effect (accelerations and velocities of the excited system) is neglected entirely. Therefore, the inertial and damping forces are not considered in the equilibrium equation due to negligibly small accelerations and velocities. The equilibrium equation in this condition is written in form of **Equation (5-1)**.

$$[K]\{u\}=\{F\} \quad (5-1)$$

where  $[K]$  is stiffness matrix,  $\{u\}$  is displacement vector, and  $\{F\}$  is load vector. If it is required, the effect of soil-structure interaction also can be considered by linear spring assigned to the base rather than support. Since elastic material is considered, the stiffness matrix is constant, and the solution can be obtained directly and an

iterative solution is not required. However, if the nonlinear geometry effect is considerable, it can be included which requires an iterative solution.

Seismic loads are essentially dynamic loads and should be analyzed under dynamic conditions. To simplify the process of design and analysis of the structure under seismic load, the concept of equivalent static load (ESL) is developed to evaluate the response of structures under seismic load that can be used along with LSA. In this method, seismic loads are defined as the product of the total weight of the structure and a seismic load factor. The factor is defined based on the seismic hazard of the site location, dynamic properties of the structure, soil condition, and importance of structure, inelastic behavior of the structure, etc. Inelastic behavior is introduced by adopting a response modification factor (to reduce the load) and displacement factor (to increase the displacement). LSA method by considering the concept of ESL is an efficient method for solving most structures and is widely used as the main procedure in seismic relevant codes and standards. This method is typically more accurate in regular structures under low seismic load, in which dynamic response is mostly dominated by the fundamental mode, and the contribution of higher modes and torsion is negligible. Since linear static analysis is the simplest approach that requires a short time for analysis that makes it more appropriate for general investigation of the structure in the preliminary analysis.

### 5.4.2 Linear dynamic analysis (LDA)

Linear dynamic analysis (LDA) is more accurate than LSA method to analyze the structure seismic load. Because inertial and damping force is directly considered in the equilibrium equation, LDA can be performed either as time history analysis (in time-domain) or as spectral analysis (in frequency-domain). In time history analysis, time-variation of the seismic load is considered in the equation of equilibriums (equation of motion) in the form of **Equation (5-2)**.

$$[M]\{\ddot{u}(t)\} + [C]\{\dot{u}(t)\} + [K]\{u(t)\} = \{F(t)\} \quad (5-2)$$

where  $[K]$  is the stiffness matrix,  $[C]$  is the damping matrix,  $[M]$  is mass matrix,  $\{u(t)\}$  is time-varying displacement,  $\{\ddot{u}(t)\}$  is time-varying acceleration,  $\{\dot{u}(t)\}$  is the time-varying velocity, and  $\{F(t)\}$  is time-varying load. The mass, stiffness, and damping matrices do not vary with time. Also, soil-structure interaction can be included in the stiffness matrix similar to LSA. The effects of nonlinear geometry also can be added directly in the solution process to be considered at each increment of loading.

There are two general procedures to solve time history analysis, which are the direct solution (implicit/explicit method) and modal decomposition approach. In direct solution, coupled equation of motion is directly solved by using numerical integration method. In the modal decomposition approach, it is assumed that the response of the structure is the composition of its response in each natural mode of

vibration. Thus, the system of equations can be decoupled which allows us to obtain the solution for each mode individually as a single degree of freedom system, and then it is distributed to the structure by using the mode shape function. This method considerably reduces computational cost in comparison with the direct solution. Mass, stiffness, damping value, and the force of each mode are determined based on properties of structure and each mode. Taking into account modal mass, stiffness, damping, and generalized force ( $M_i$ ,  $K_i$ ,  $C_i$ , and  $F_i(t)$ , respectively), modal responses of each mode include acceleration,  $\ddot{u}_i(t)$ , velocity,  $\dot{u}_i(t)$ , and displacement,  $u_i(t)$ , are calculated by **Equation (5-3)**.

$$M_i \ddot{u}_i(t) + C_i \dot{u}_i(t) + K_i u_i(t) = F_i(t) \quad (5-3)$$

Ideally, the accurate response can be obtained by considering all mode shapes, but it can result in too much computational cost, and reducing the efficiency of the modal analysis. The contributions of the modes in the responses are not the same; the first mode has the highest contribution, and contribution is reduced by increasing the mode number. Therefore, usually a few first modes with higher contributions are chosen for the analysis. Seismic guidelines have recommendations or requirements for selecting the minimum number of modes (e.g. minimum number of modes that have 90% modal contributions). At each instance of loading, the response is the summation of the response obtained for each mode at that moment, amplified by the corresponding modal contribution factor and distributed by the mode shape vector. Note that response modification factor should be considered either by reducing the

input load before analysis or reducing internal force after analysis as post-processing. Similarly, deformation should be increased by the deformation factor.

Reliable results by time-history analysis highly depend on earthquake records to define input loading. It is an important challenge in seismic design due to the random and indeterministic nature of earthquakes. Several recommendations are proposed to select records from the available database of past earthquakes or generated artificial records. Similar to linear time history, those records should be matched with soil condition and seismic hazard of the site and need to be properly scaled based on structural properties.

In spectral analysis, a semi-dynamic analysis is performed to obtain the response. It is defined based on the concept of seismic response spectrum. The spectrum is the peak response of a single degree of freedom system (with specific natural frequency and damping ratio) to the earthquake excitation. It can be obtained from the design spectrum defined by seismic codes or calculated based on available seismic data and past earthquake time histories of the site. In this method, instead of considering time-variation, the peak load is defined based on the response spectrum taking into account the frequency and damping ratio of each mode. Then the corresponding response to this load for each mode is calculated by **Equation (5-4)**.

$$M_i \ddot{u}_i(f_i) + C_i \dot{u}_i(f_i) + K_i u_i(f_i) = F_i(f_i) \quad (5-4)$$

It can be seen despite that the equation is written based on dynamic equilibrium similar to **Equation (5-2)**. However, instead of the time,  $t$ , the natural frequency of

each mode  $f_i$  is replaced, so are the peak response acceleration,  $\ddot{u}_i(f_i)$ , peak response velocity,  $\dot{u}_i(f_i)$ , and peak response displacement,  $u_i(f_i)$ . Therefore, it sometimes is called semi-dynamic analysis. Issues regarding minimum numbers of modes, response modification factor and deformation factor should be considered similar to time history analysis. Note that the concept of the equivalent static load is defined based on the same concept as spectral analysis by assuming only the first mode as the dominant response and some other conservatism issue. In contrast with time history analysis, the time correlation of the response in different modes is not considered directly in the spectral analysis. Therefore, after scaling the response of each mode by its modal contribution factor, they cannot be added by simple summation to avoid overestimation. Instead, a more advanced statistical method of summation like SRSS (square root of sum of squares) or CQC (complete quadratic combination method) is recommended.

Using spectral analysis considerably reduces the computational cost in comparison with time-history analysis (either by direct solution or modal decomposition), and is widely used for seismic analysis.

### **5.4.3 Nonlinear static analysis (NSA)**

When a nonlinear relationship exists between the applied loads and relevant displacements, the nonlinear static analysis (NSA) or pushover analysis can be conducted. As mentioned earlier, nonlinear effect is due to geometric nonlinearity, material nonlinearity, and boundary condition that can change stiffness under loading.

However, the stiffness remains constant in LSA, and inelastic behavior under seismic load is included by using the response modification factor and deformation factor. Whereas nonlinearities are directly included in the solution by performing NSA and sequence of yielding and failure can be observed. The idea of performing NSA or pushover analysis can be explained as follows: The energy entered the structure through seismic excitation at the base results in the vibration (deformation) of the structure, increasing the level of internal force which may exceed the yield strength. Concerning inelastic behavior, this condition can be viewed as imposed deformation to structural members without taking into account the excitation source to a target point. The target point is defined based on the fact that the level of energy in the structure should be in balance with the energy of the excitation. The static response is calculated under the load that is incrementally increased by doing the iterative procedure.

Despite the complexities and computational cost of nonlinear analysis in comparison with linear analysis, modern software and high-performance computer have made it possible to obtain a logical solution to these nonlinear problems. To increase the accuracy and validity of the analysis, sufficient skills are required to determine the appropriate model and solution parameters (Augenti and Parisi, 2009).

Between the linear methods (LSA and LDA) and nonlinear dynamic analysis, a nonlinear static approach based on pushover analysis is being applied as an effective and most economical alternative approach. NSA has been developed to model the complex behavior where due to the insufficiency and limitations of linear

seismic analysis is not capable to model. Nonlinear time-history analyses are quite complicated and time-consuming procedures. This is an efficient method to investigate the performance and the maximum response of the structures, instability, and post-buckling behavior (Remseth, 1979). The actual seismic behavior of individual masonry shear walls as well as the nonlinear response of masonry buildings can be evaluated by NSA concerning significant irregularities in plan or elevation. By performing pushover analysis, very important characteristics of the structure under seismic load can be obtained, including stiffness, strength, ductility, overstrength factor, and response modification factor. Besides obtaining these parameters that define the inelastic capacity of the structure, pushover analysis can be used as an effective tool for performance-based design. Several procedures have been suggested in the last decades to achieve the maximum benefit from inelastic capacity and the more accurate simulation of the nonlinear behavior of structures under earthquake loads. The general concept of these approaches is based on comparing seismic demand and capacity. The N2 method (Fajfar and Fishinger, 1988), nonlinear static procedure NSP (FEMA 356), and improved capacity spectrum method CSM (FEMA 440) are some of the well-known examples. Although the general concept of NSA methods is based on monotonic loading, cyclic loading can be done by introducing load protocol. Therefore, cyclic (Quasi-static) analysis (CNSA) can be considered as a developed form of NSA. However, the computational cost of CNSA is substantial in comparison with NSA method. In addition, in CNSA cyclic behavior of components should be properly introduced in

the model that can result in more complexity of analysis and convergence problems (Dejong, 2009).

#### **5.4.4 Nonlinear dynamic analysis (NDA)**

Nonlinear (time-history) dynamic analysis (NDA) is assumed the most appropriate and accurate method to fully determine the behavior of structures under seismic loads. Because time variation of the load and all sources of nonlinearity are directly and simultaneously considered in the analysis as well as dynamic magnification and interaction between vibration modes (Chambers and Kelly, 2004). Similar to the time-history LDA method, reliable results by NDA highly depend on appropriate earthquake records to define input loading. In some cases, the only way to investigate the performance of a structure is NDP despite its difficulties. Several types of structures such as stone structures, base-isolated structures, structures with supplemental damping, and pounding buildings cannot be effectively analyzed by simple conventional analysis techniques.

The use of the NDP for these types of structures can provide a reasonable representation of their seismic response. However, this approach requires a significantly larger computational cost than the other methods and restricts its wide application. Advancements in numerical technique and performance of computers can result in the more widespread application of the NDA. Therefore, the early developments in the performance-based design engineering field tended to push the NSP rather than the NDP. Using the two different methods of NSP and NDA indicates

that the former provides more conservative results in most of the cases and predicts larger displacements for the structure (Tehrani and Maalek, 2006).

Due to the complexity of masonry structures, specifically for historical structures, LSA or LDA may be useful only in preliminary investigations. Because in these methods, inelastic behavior is represented simply by the response modification factor, not the actual failure mechanism. On the other hand, due to complexity and computational cost, NDA may also not be an efficient way to investigate nonlinear behavior. Therefore, NSA is performed usually to assess the inelastic behavior and capacity of the structure. It can be used to find structural deficiencies in terms of stiffness, strength, and ductility. Based on the detected deficiencies, the proper retrofit methods are chosen and the efficiency of each method can be checked by performing NSA (Augenti and Parisi, 2009). If it is required, some or all appropriate retrofit techniques can be checked in more detail by performing NDA to have a better understanding of its performance.

## **5.5 Material and Joint Behavior**

Material behavior or relationships between stress and strain at any material point are defined by appropriate constitutive equations. These equations are available to model stress-strain relationships based on phenomenological behavior at the macroscopic level (Lee and Fenves, 1998). They are defined in a range of simple Hooke's law for elastic behavior to advanced plasticity and fracture model.

Nonlinearity associated with material properties can be observed in both elastic and inelastic ranges. The response of all materials under small loading is elastic which means deformation (strain) is fully removed by removing the load (stress). This relation can be linear (e.g. for steel) or nonlinear (e.g. for rubber material). In practice, for many engineering materials such as concrete and brick, this nonlinearity is not as much as rubber material, and so linear elastic behavior is assumed for simplicity. On the other hand, where stress exceeds the elastic limit and materials exhibit inelastic behavior, the behavior is always nonlinear. Inelastic behavior is observed due to many factors such as plastification, cracking, etc. Commonly, based on the type of inelastic behavior, materials are categorized as ductile, brittle, and quasi-brittle material. Ductile materials such as mild steel exhibit large plastic deformation before fracture (elastic-plastic behavior). While in brittle materials such as glass, stress increases with strain up to the maximum strength, and then cracks suddenly form, resulting in material failure (elastic-damage behavior).

On the other hand, the cracking process in quasi-brittle materials like concrete, adobe, and stone is a continuous forming and connecting of micro cracks (Mehta and Monteiro, 1993; Lee and Fenves, 1998). In these materials, the tensile behavior is similar to brittle material (i.e. elastic-damage behavior) and usually is modeled as a linear stress-strain relationship up to tensile strength. However, the behavior under compressive stress includes three parts of elastic, plastic, and damage. Depending on how cracks are implemented in the modeling, damage models are developed generally by two methods called “Discrete crack (DC) approach” and “Smear-

crack (SC) approach” (Ngo and Scordelis, 1967; Rashid, 1968; Cervera and Chiumenti, 2006; Pappas, 2012).

In DC models, cracks are explicitly modeled as a geometrical opening in the body of the structure, defining tensile failure criteria. In early developed models, the failure criteria were checked in each node, and critical nodes where their conditions satisfy the criteria are divided into two nodes to simulate crack opening. This process is checked at each increment of the loading, so the model can simulate crack propagation to the next node. Since in DC model cracks are formed only along the element boundaries, resulting in a strongly mesh-dependency of the responses. This problem can be overcome by implementing advanced and high-quality re-meshing techniques. However, updating the mesh considerably increases the computational cost (de Borst *et al.*, 2004).

Extended finite element method (XFEM) proposed by Belytschko *et al.* (1999), Moës *et al.* (1999) and Sukumar *et al.* (2000) is an effective approach to solve many of the drawbacks in DC model. XFEM allows propagating cracks inside the elements without updating the mesh. In this approach, by tracking the advance of the crack, elements around crack-prone areas are enriched. It means that the nodal degrees of freedom are continuously updated to represent both the displacement corresponding to crack opening and developed singularity at the crack tip. On the other hand, SC models are based on implicit modeling of the cracks. In this approach, the structure is modeled as a continuum model and the impacts of cracks are implemented as strength and stiffness degradation where stress conditions satisfy the failure criteria.

Therefore, influences of crack are smeared in the broader area of the integration point and are introduced in constitutive equations as damage models (de Borst *et al.*, 2004). Thus, interface elements are not required and there are no restrictions about the direction and location of the cracks, and they can be calculated at any integration point inside the domain. Also, since SC models do not consider discontinuities in the topology of the model, re-meshing is not required. Because of the simplicity of this concept and its implementation as a material constitutive model, it is widely used in engineering problems.

A summary of SC model development was reported by Pappas (2012). This approach was originally proposed by Rashid (1968), and by developing the idea different constitutive models have been proposed for modeling damage based on SC approach. Hillerborg *et al.* (1976) include a fictitious crack in the model by utilizing the formulation of cohesive crack models that were developed in nonlinear fracture mechanics. Bazant and Oh (1983) improved the model to make it more compatible with the common procedure used in the finite element codes. Saetta *et al.* (2000) enhanced the model by implementing an orthotropic damage model for brittle failure. Clemente *et al.* (2006) modified the model by assigning a scalar damage model by introducing auxiliary algorithms for tracking the progress of the localization band in the mesh that can model localized individual cracks.

As discussed by Pappas (2012), the main drawbacks of SC approach in modeling masonry structures are related to considering the damaged material as a vast volume which is not matched with the reality of the damage in masonry

structures. Although the susceptible region can be detected with an acceptable level, the local behavior at joints (as a line of weakness) is not modeled effectively.

Therefore, it can be concluded that the results of modeling based on SC approach is acceptable in terms of representing overall damage in masonry structures with large volumes. More detailed modeling is required for structures with high irregularity or where the purpose is to study structures with smaller volumes (Silva, 2008a).

Application of SC and DC models in the field of masonry structure, along with the specific definition of macro-and micro-modeling approaches, can be explained as the following. In the case of the macro-modeling approach where topology is modeled as a continuum, SC model can be used as a homogenized material. The concept of DC model is used in the micro-modeling approach by introducing a discontinuity in joints and assigning an appropriate behavior to them. Additionally, SC model can be assigned to the units as a homogenized material. Although adopting DC models for the units such as enriching by XFEM elements is possible, it can result in impractical computational cost. Since dry-stack joints essentially have zero tensile strength, no tensile stress is transferred to the units. Therefore, a more simple material constitutive model may be utilized along with a micro-modeling approach. The joints are generally modeled by using contact (or interface) elements with cohesive or/and frictional behavior. Frictional behavior is defined by introducing the frictional coefficient following Columb friction theory and considering zero tensile strength. Normal stress is calculated during analysis at nodes that are in contact

which each other, and critical shear stress is defined as the product of normal stress and frictional coefficient. Sliding occurs if the shear stress is larger than critical stress; otherwise, nodes did not slide on each other (commonly known as stick state). Cohesive behavior is defined by introducing cohesive stiffness, tensile normal and shear strength of the joint, failure criteria (based on stress or deformation), and damage evolution law. In this model, it is usually assumed that the joint behavior is linear up to the level where failure criteria are not satisfied. The corresponding nodes in contact move with each other based on the assigned cohesive stiffness, and stress is completely transferred between nodes. Where failure criteria are satisfied, corresponding nodes in contact start to move individually and stress transferred within them decreases following the damage evolution law and finally reaches zero. In order to model cyclic behavior, cohesive and frictional behavior can be mixed in a way that initial joint behavior is only based on the cohesive model, and after failure, the behavior is defined based on only the frictional model (ABAQUS, 2020).

## 5.6 Summary

In this chapter, experimental and numerical techniques for evaluation of seismic behavior of masonry walls were discussed in detail. Besides the experimental approaches, numerical simulation can provide much useful information. To obtain logical results from the numerical model, it is very important to calibrate the parameters of the model with the experimental data. The concept of macro, micro, and simplified-micro modeling of the masonry walls was discussed. Within developed numerical methods, finite element method and kinematic method are widely used in the field of masonry structures. Therefore, these methods and their application were systematically described in detail. The main sources of nonlinearity including material, geometry, and boundary condition were discussed. Also, common analysis procedure and their advantages and drawbacks for simulation of seismic load were examined.

## **Chapter 6. Numerical Modeling of Stone Wall**

In this chapter in-plane behavior of stone masonry walls is investigated numerically. The ABAQUS software, one of the most powerful and popular tools for numerical simulation, has been used for modeling stone shear walls. Two-dimensional (2D) nonlinear finite element models based on the micro-modeling approach were constructed, and behavior under seismic load was explored by performing pushover analysis. The results of experimental tests carried out by Vasconcelos (2005) have been considered for calibration and validation of numerical models. The effects of critical parameters on the behavior of the walls were assessed on the calibrated model by conducting sensitivity analysis. Parametric studies have been done by making a set of models with different aspect ratios (walls and units), following characteristics of calibrated models, to understand the behavior of the walls more comprehensively.

## 6.1 General Descriptions

Masonry wall consists of units (stone, brick, or adobe) and mortar. The variety in stacking units on top of each other can create different types of wall configurations. The unreinforced stone-masonry wall is the most popular and widely used ancient structure in monumental and traditional buildings all over the world throughout the ages due to its remarkable benefits. This element plays an essential role in determining the strength of the structure under lateral loads. High durability, fire resistance ability, availability, and easy construction make it resist seismic loads.

Ancient masonry walls are considered vulnerable structures to withstand seismic actions that should be strengthened properly. Therefore, the assessment of the mechanical behavior of HURM structures by evaluating the structural resistance and failure mechanisms is needed for the rehabilitation and retrofitting process. Furthermore, understanding the seismic behavior of masonry stone walls provides good knowledge in the design of new masonry structures which are still used for (residential) buildings.

The possible configuration of stone walls can be categorized into (i) sawn dry-stack or dry-stone masonry without bonding mortar; (ii) irregular stone masonry with bonding mortar; (iii) rubble masonry with irregular bonding mortar thickness; and (iv) a combination of the three techniques (Vasconcelos, 2005).

Mortar has two main roles in masonry structures as an adhesive to sticks and holds the units together more tightly and as a filler between the units. Using perfectly cut and regular stones in the larger dimensions (with high gravity load) makes it possible to build high-strength structures without mortar. This kind of arrangement is called dry-stack masonry wall for which the strength of the structure relies on the skill of the workmanship as well as the frictional resistance of the stone units.

The masonry structures built by unit-mortar arrangement are the most popular construction in most regions. The capacity of these structures to resist seismic loads is comparatively low. Old masonry structures using bonding mortar may have partially or completely lost the mortar due to weathering effects. Therefore, in rubble stone masonry walls where mortar plays a major role in holding the stones, the loss of even a part of mortar causes a significant reduction in wall strength.

Due to the scarce studies on regular dry-stack stone masonry walls, this study attempts to assess the structural performance of this type of wall arrangement using finite element modeling. Lourenço *et al.* (2005) conducted a comprehensive experimental and numerical study to assess the behavior of historical dry stone masonry walls under combined compression and shear loads. The test was done under the displacement control condition by applying monotonic loads on the wall specimens. Furthermore, some numerical analyses have been carried out to model the seismic behavior of dry masonry walls using rigid block limit analysis and discrete element analysis by Azevedo *et al.* (2000) and Orduña and Lourenço (2003).

In this chapter, after introducing details of selected experimental tests and ABAQUS software, the numerical modeling procedure and results are explained in detail. **Figure 6-1** illustrates the main components of the modeling procedure in this chapter.

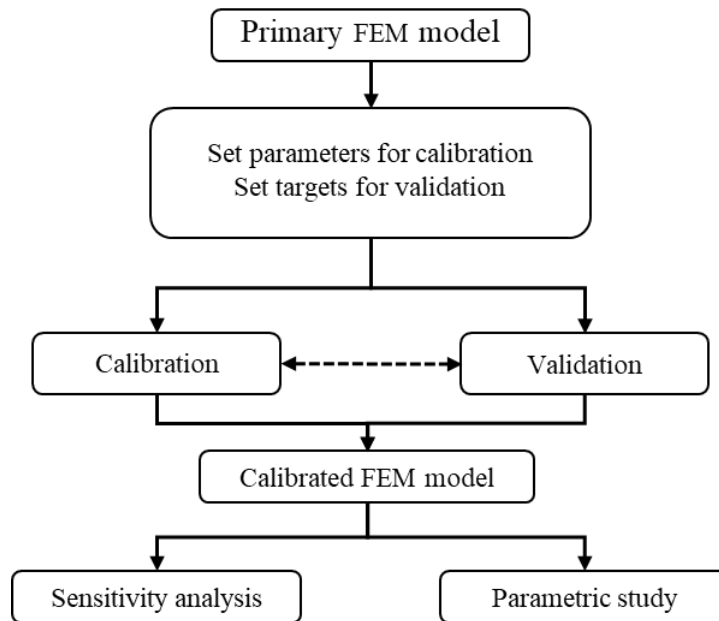


**Figure 6-1** Modeling procedure dealt with in this chapter

## 6.2 Experimental Research Program

In contrast with mortar-based walls, research on the analysis of dry-stack masonry buildings is almost nonexistent. On the other hand, performing destructive tests on historical construction is usually impossible and most researches on masonry

structures are based on laboratory tests. Therefore, any research in this area may provide a better understanding of the complex behavior of this type of structure.

Here, some of the available experimental researches are introduced, and among them the most comprehensive one is selected for calibration and validation.

One of the most relevant experimental investigations was carried out by Lourenço *et al.* (2005) at the Structural Technology Laboratory of the Technical University of Catalonia, Barcelona, in cooperation with the University of Minho. The experiment consists of the characterization of the in-plane structural behavior of dry-stack walls. Seven dry stone masonry shear walls ( $1\text{ m} \times 1\text{ m} \times 0.2\text{ m}$ ) made of Montjuic stone were subjected to combined vertical and horizontal loads. All the tests were carried out under monotonic loading. The horizontal in-plane load was increased monotonically until the failure of the wall was reached. Significant features of the mechanical behavior of the walls along with their ultimate capacity and failure mechanisms were discussed in their work. The results showed that the modulus of elasticity of the walls increased with increasing the vertical load.

It can be understood that the dry-stack stone masonry structure has a specific elastic nonlinear behavior, with increasing stiffness upon compressive loading. Large stiffness with linear behavior retained up to almost 30% of the peak load and then, stiffness degradation could be observed by increasing deformation. Due to sudden movement or slipping of the stones, severe oscillations of the horizontal load were observed. The different levels of initial vertical load resulted in different failure

modes. For the walls subjected to lower vertical load, the upper part of the wall was rotated, and sliding along the bed joints happened in the stair-stepped diagonal crack form without visible cracking in the stone. Whereas for the walls subjected to higher vertical loads cracking of the stone units were observed and the walls exhibited a significant increase of stiffness.

The in-plane resistance and failure modes of dry-stack masonry walls were investigated and validated experimentally by Casapulla and Argiento (2018). This test consisted of the application of a monotonically increasing horizontal point-load to the side face of the dry-stack stone masonry wall specimen using a universal test machine. The point-load was applied at a variable height within the vertical midplane of the wall to transmit all possible in-plane displacements. Different loading conditions were considered to simulate both pure sliding and mixed rocking-sliding failure modes. The wall specimens had the size of  $0.8 \text{ m} \times 0.468 \text{ m} \times 0.050 \text{ m}$  (length  $\times$  height  $\times$  width) including twelve courses of stretcher blocks. The size of units was considered as  $0.1 \text{ m} \times 0.039 \text{ m} \times 0.050 \text{ m}$  (length  $\times$  height  $\times$  width) made of Neapolitan tuff stones with an average unit weight equal to  $13.1 \text{ kN/m}^3$  make it superscript. The friction coefficient between the joints was calculated experimentally equal to 0.52 using the same setup of the wall. These experimental test results were performed to validate the results of the analytical study on the lateral strength of dry-stack stone masonry walls under in-plane loading based on an existing macro-modeling approach using limit analysis methods.

Uzoegbo and Ngowi (2003) conducted an experimental investigation on dry-stack interlocking block wall systems to evaluate the structural behavior of the system under in-plane loading. The walls were made with a  $3\text{ m} \times 2.50\text{ m} \times 0.22\text{ m}$  (length  $\times$  height  $\times$  width) dimension. The first row was laid in mortar and cured for three days in unloading condition. The rest of the courses was made by the dry-stack method. A steel beam was used to distribute the pre-compression load evenly at the top of the wall. The test results showed that dry-stack masonry wall under uniform compression load usually fails by the development of tension cracks parallel to the axis of loading along the midsection of the wall. At ultimate state, cracks also appeared on the faces and edges of the specimen. It can be understood that an interlocking system in the dry-stack masonry buildings can improve the alignment and stability of the wall.

The frictional force between the brick joints in dry-stack masonry structures is very important in terms of energy dissipation. However, not many relevant studies have been done in this area. Lin *et al.* (2017) investigated the dynamic friction characteristics of dry bricks by conducting an experimental test to validate the advantages and stability of the novel test concept. Nine different loading speed tests were conducted to evaluate the effects of shear rate on the cyclic behavior of dry-stack masonry structures. The results showed by increasing the shear rate, the initial stiffness decreased and the hysteretic loop started to exhibit “pinch characteristics”. Based on this investigation under different loading rates a dynamic friction characteristic model of the dry brick joint was developed. This model includes five

stages as pre-sliding, softening transition, macro-slip, hardening transition, and unloading stages. Besides, the friction coefficient decreased as the loading speed increased, and also the reduction rate declined.

Elvin and Uzoegbo (2011) assessed the response of a full-scale dry-stack masonry structure (3.9 m (width)  $\times$  3.9 m (length)  $\times$  2.76 m (height)) with minimum reinforcement subjected to earthquake loads. A wall was considered for the north and west walls and a window for south and east walls. El Centro, North Ridge, and Llolele earthquake records were used to apply the seismic excitation. The damage was observed in the form of shifted bricks and some bricks were split, cracked, or crushed. The result showed that the “X” shape damage was observed in the two walls in the same direction of the base motion. Due to the free movement of bricks in dry-stack buildings, the earthquake and harmonic base motion energies were dissipated through inter-brick friction, and in some cases by bricks cracking and crushing.

The experimental program carried out by Vasconcelos (2005) in the Department of Civil Engineering of Minho University, Guimarães, Portugal was selected in this study for the validation of numerical models. The experiments were performed to evaluate the seismic performance of the ancient stone masonry shear walls with/without bonding mortar. The study includes material tests and a set of monotonic and cyclic tests with different levels of pre-compression loads on small-scale specimens. The stiffness, strength, deformation capacity and failure modes were obtained for three different wall configurations.

**Figure 6-2** indicates the three wall specimens used in experimental investigations which (out-of-plane) thickness of the wall was 200 mm. Type (I) was sawn dry-stone or dry-stack stone masonry wall without bonding material (**Figure 6-2(a)**). Type (II) was irregular stone masonry wall with bonding mortar (**Figure 6-2(b)**). Type (III) was rubble masonry wall with irregular bonding mortar joint thickness (**Figure 6-2(c)**).

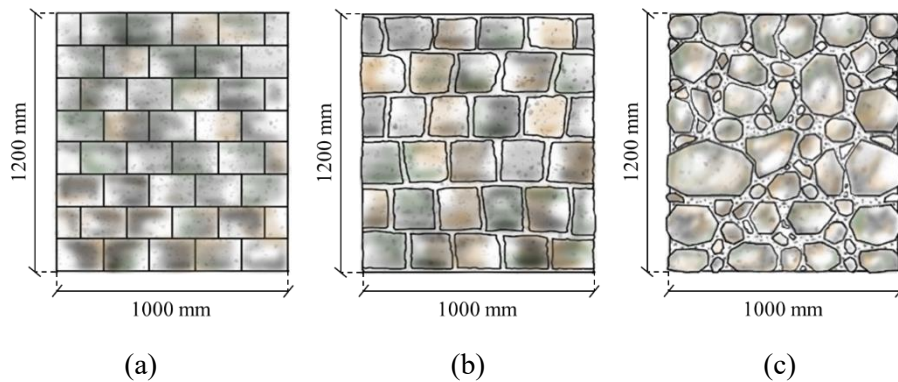


**Figure 6-2** Details of experimental test specimens: a) Dry stack sawn masonry; b) Irregular masonry with bonding mortar joints; c) Rubble masonry wall (Redrawn based on Vasconcelos, 2005)

Among all stone materials, granite is the most used stone in the construction of ancient buildings and monuments. Therefore, the wall specimens used in experimental research work were made of locally available two mica and medium grain granite stone. The average values of measured density ( $\rho$ ) and Poisson's ratio ( $\nu$ ) were 2611 ( $\text{kg/m}^3$ ) and 0.28, respectively. Also, the results showed that the mean values of the modulus of elasticity ( $E$ ) under different levels of pre-compression ( $\sigma$ )

can be calculated based on **Equation (6-1)**. The corresponding values are reported in **Table 6-1**.

$$E \text{ (MPa)} = 2352 + 1913\sigma \text{ (MPa)} \quad \text{(6-1)}$$

**Table 6-1** Mean values of modulus of elasticity ( $E$ ) of granite stone under different levels of pre-compression ( $\sigma$ )

$\sigma$ (MPa)	0.2	0.5	0.875	1.25
$E$ (MPa)	2734.0	3287.5	4068.9	4722.0

The experimental test set-up shown in **Figure 6-3** was used for conducting both monotonic and cyclic tests. The wall specimens were fixed to the steel beams (top and bottom) with two adjustable clamping angles to prevent horizontal displacement at the base. The first course of the wall (half in height) in top and bottom, which is not shown in the specimen dimension, was tied to the steel beams. The bottom steel beam was also fixed to the test floor using a couple of steel rods. To uniformly insert the vertical load from the actuator into the wall specimen, a stiff beam was used with that transfer load to the top beam by steel rollers to allow relative displacement of the wall. Steel rollers were placed to minimize the friction force between the two components during lateral deformation. An independent and dedicated oil pressure system was connected to the vertical hydraulic jack to keep axial pre-compression constant during the test.

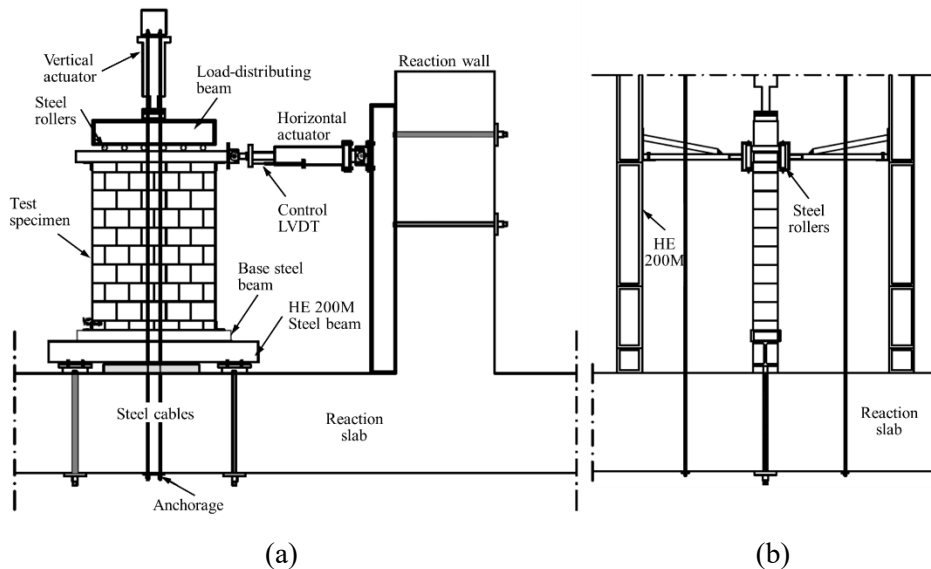


**Figure 6-3** Experiment test set-up: a) Front view; b) Side view (Adapted from Vasconcelos, 2005)

By using a horizontal actuator, the lateral load was applied to the top steel beam instead of the wall to prevent crushing in the specimen. The lateral load was applied as displacement-controlled and at the rate of 100 mm/s. This actuator was linked to the reaction wall employing a two-dimensional hinge to allow vertical displacements at the top of the wall and corresponding rotation. Furthermore, the out-of-plane movements of the wall were prevented by a set of steel tubes connected to vertical steel rollers (**Figure 6-3(b)**). Several LVDTs (Linearly Variable Differential Transducers) were placed to measure deformations of the walls.

Four levels of pre-compression ( $\sigma$ ) were considered including 0.2 MPa (40 kN), 0.5 MPa (100 kN), 0.875 MPa (175 kN), and 1.25 MPa (250 kN).

In the current study, results of monotonic tests for walls with dry-stack joints under all four pre-compression levels were selected to be used for the validation of numerical models. The typical failure mechanism and force-displacement curves of these walls are shown in **Figure 6-4**.

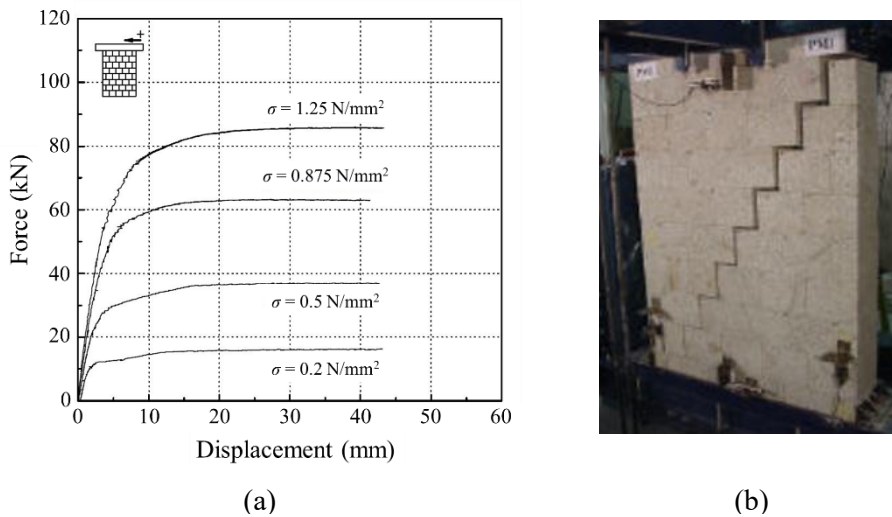


**Figure 6-4** Results of monotonic test for walls with dry-stack joints: a) Force-displacement curves; b) Failure mechanism (Adapted from Vasconcelos, 2005)

The observed behavior of walls with dry-stack joints under all pre-compression levels was similar. The strength and stiffness of the wall were significantly increased under higher pre-compression loads **Figure 6-4(a)**. The failure mechanism of all walls was in the forms of stair-stepped (**Figure 6-4(b)**) and no substantial compressive crushing was observed in the walls. All walls could sustain a large lateral deformation which is directly related to the failure mechanism.

### 6.3 ABAQUS Software

Currently, there are many open-source and commercial software and packages worldwide for numerical simulation of structures with their advantages and disadvantages. Among them, ABAQUS is one of the most powerful and well-known software that is developed based on finite element method. The software is one of the main products of Dussault Simulia Co. and can simulate a wide range of engineering problems including continuum and porous structural modeling, computational fluid dynamic, heat transfer, electrical and magnetic problems, and topology optimization. The software allows considering multiphysics problems by providing proper analysis solver and elements with coupled degrees of freedom, such as displacement-heat elements, pore pressure-displacement-heat elements, etc. Also, it provides a variety of element types, constitutive material model, analysis procedure, constraints, and interface elements, and analysis type. All sources of nonlinearity including inelastic behavior, geometry, and boundary condition can be simply included in the model. Enhanced solvers are included in the software to attain convergence and improve the accuracy and efficiency of analysis in complex problems. All required steps for pre-processing, processing and post-processing can be done within a unified graphical user interface (GUI) that is called ABAQUS/CAE, where CAE stands for “Computer-Aided Engineering”. As an alternative approach, the model data can be provided in the format of the text file (commonly known as the input file) and directly recalled by the solver for the analysis.

The software allows adding user-subroutines (FORTRAN and C++) to add special elements, materials, and boundary conditions that are not available in the software library. Also, macro-codes (Python) can be used for manipulating the whole procedure in pre-and post-processing steps, including repeating actions, extracting results, etc. The overall framework of modeling by the software is shown schematically in **Figure 6-5**.

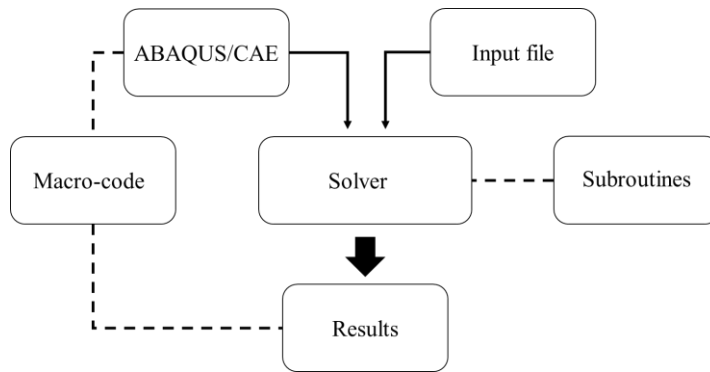


**Figure 6-5** Modeling framework in ABAQUS

In summary, the main advantages of ABAQUS are a user-friendly GUI environment (for pre-processing, processing, and post-processing), powerful mesh engine, enhanced solver, and a comprehensive library (of the element, material, and analysis). These advantages make ABAQUS one of the most popular and reliable simulation software for engineers to deal with both real problems in industry and academic research. ABAQUS/CAE provides a modular-based framework to do all the required steps for pre-processing, processing, and post-processing. This

framework facilitates to find proper actions that are required for each step of modeling. The essential modules used for modeling are shown in **Figure 6-6**.

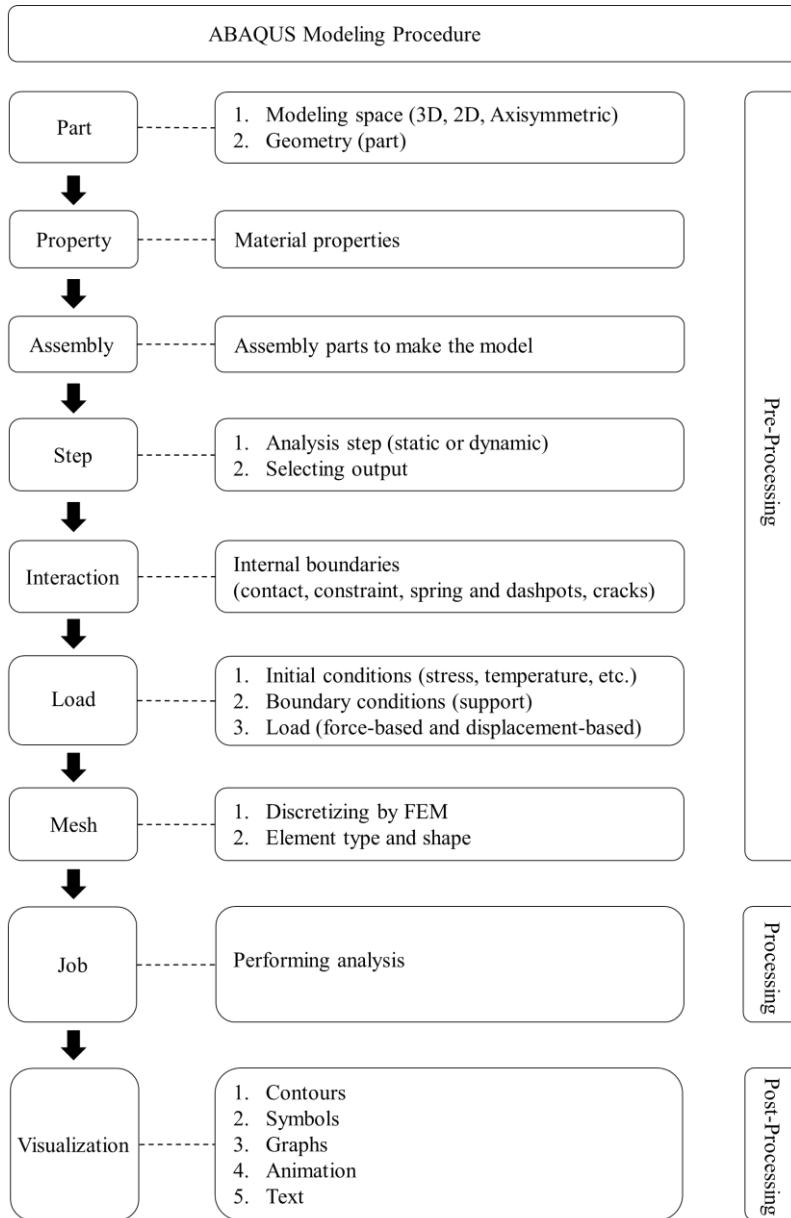


**Figure 6-6** Main modules in ABAQUS/CAE

Modeling space (3D, 2D, and Axisymmetric) and geometry of the numerical model is defined in the “Part module”. The structure can be made by a single part (continuum structure) or it can be divided, and is modeled by multiple parts, defining interaction between them.

Physical properties (mechanical, thermal, etc.) are defined and assigned to each part in the “Property module”. Physical properties along with additional required geometrical properties (that are not explicitly modeled) are defined as a section and assigned to the part. Cross-section properties of line elements (beam and truss), the thickness of shell element, out-of-plane depth of continuum element in 2D-space (plane-strain and plane-stress condition), etc. are examples of additional required geometrical properties that are not explicitly modeled. Then, these parts are mounted on each other in the “Assembly module” to make the model.

In “Step module”, the analysis procedure and desirable output are defined. Type of analysis (static, dynamic, heat transfer, and coupled analysis), small or large-displacement formulation, incremental loading framework, iterative or direct solution, etc. are determined in this module.

The relation between parts is defined in “Interaction module”. It can be defined as a constraint, linear or nonlinear springs, or assigning interactions between surfaces. All boundary conditions including initial conditions, support, and loads are defined in “Load module”.

The discretization of the geometrical-based (object-based) model is done in “Mesh module” by finite element method. A wide range of element shapes and behaviors are available, and with a powerful mesh engine a mesh of elements with high quality can be provided.

All former steps in ABAQUS are defined for a single model and each model database file can have many models. In order to do analysis, for each model in “Job module” a specific job is defined and submitted to the solver. Prerequisites for analysis such as the amount of allocated memory, normal or parallel-processing, precision (single or double) can be assigned to a job before the start of the analysis. Also, in this module, the progress of the solution can be monitored. Finally, results can be investigated in “Visualization module”. The results can be visualized as contour-based, symbol-based, graphs, animations, and text files.

## 6.4 Numerical Model

In this section, the procedure and main assumptions for modeling in ABAQUS software are briefly explained. The in-plane behavior of the wall under lateral load can be considered as plane-stress conditions. Modeling can be done in 2D-space under plane-stress conditions, which significantly reduces the computational cost. The main components of the model are shown in **Figure 6-7**.

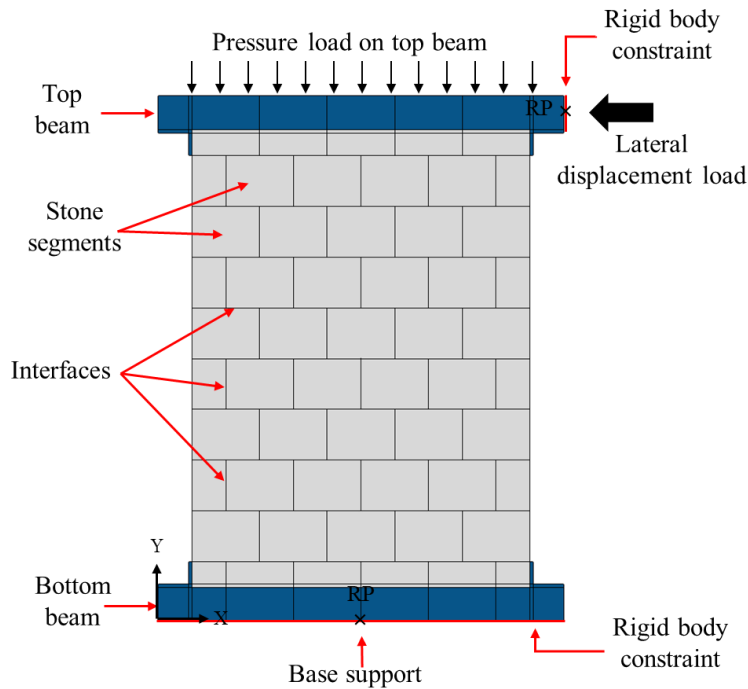


**Figure 6-7** Main components of the numerical model

Parts were modeled in 2D-space by using shell geometry, and out-of-plane thickness of the wall (200 mm) was included in section properties. Based on the results of experimental tests, inelastic behavior was not observed in stones and beams. Thus, both steel and stones are defined as homogeneous material with isotropic elastic properties, requiring only modules of elasticity and Poisson's ratio.

Joint behavior was defined by assigning contact interactions between parts. Contact interaction can be defined in two ways, surface to surface and/or general contact. In surface to surface approach, all surfaces in contact should be defined before analysis. In the general contact approach, the software, as part of the analysis procedure, considers peripheral surfaces of all parts and automatically detects

surfaces in contact with each other. So, by using general contact, not only there is no need to predefine surfaces in contact, but also if one unexpected contact occurs it will be automatically detected and is considered in the analysis. However, the surface to surface approach is generally more accurate. Regarding too many surfaces in contact with each other, the “general contact” approach was considered in this study. Contact behavior was defined by assigning tangential and normal behavior.

Normal behavior was considered as “Hard contact” with an allowance of separation. By using this approach, when the surfaces are in contact, full compression stress is transferred between two surfaces. Under tensile force, surfaces can freely separate from each other.

Tangential behavior was defined based on the “Coulomb friction model”. The basic concept of the model is to associate the maximum allowable frictional (shear) stress to the compression stress between the contacting bodies at their interface surfaces. In the basic form of the Coulomb friction model, two contacting surfaces can carry shear stresses up to a certain magnitude at their interface before they start to slide. This state is called sticking. As shown in **Figure 6-8(a)**, this model defines critical shear stress ( $\tau_{cr}$ ), at which sliding of the surfaces starts, as a fraction of the contact pressure,  $P$ , between surfaces ( $\tau_{cr} = \mu P$ ), where fraction,  $\mu$ , is known as the friction coefficient. During analysis, the stick/slip calculation determines the transition of a point from sticking to slipping or from slipping to sticking. It is commonly known that the friction coefficient at the initiation of slipping is not the same as the friction coefficient at established slipping (**Figure 6-8(b)**). The former

is typically referred to as the “static” friction coefficient ( $\mu_s$ ), and the latter is referred to as the “kinetic” friction coefficient ( $\mu_k$ ). Typically, the static friction coefficient is higher than the kinetic friction coefficient. Although the transition of friction coefficient from static to kinetic state can be defined, the kinetic coefficient obtained by the tests was used to be conservative and will be shown by  $\mu$ .

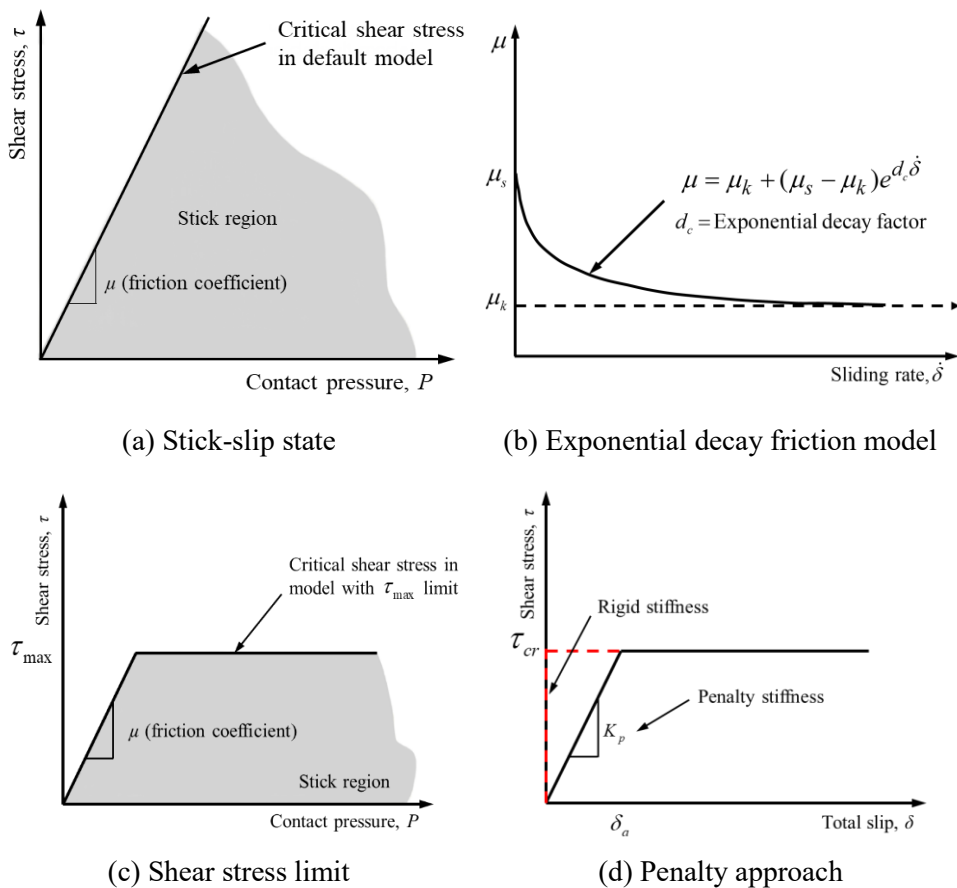


**Figure 6-8** Components of friction model (Adapted from ABAQUS, 2020)

Following the original concept of the Coulomb friction model,  $\tau_{cr}$  increases linearly by  $P$  without any upper bound limit, which is unrealistic. An upper limit can be introduced by specifying a shear stress limit ( $\tau_{max}$ ) so that sliding will initiate if the magnitude of the shear stress reaches this value, regardless of the magnitude of  $P$  (**Figure 6-8(c)**). By using this limit, where shear stress exceeds  $\tau_{cr} \leq \tau_{max}$ , sliding starts. This limit is typically considered where the contact pressure stress may become very large and  $\tau_{cr}$  at the interface exceeds the yield stress in the material close to the contact surface. As a rational estimation,  $\tau_{max}$  can be considered equal to  $\sigma_y / \sqrt{3}$ , where  $\sigma_y$  is the von Mises yield stress of the material adjacent to the surface (ABAQUS, 2020). In this study, the stone material is assumed to be elastic, therefore  $\tau_{max}$  is not considered.

Ideally, the relation between frictional shear stress and sliding is in form of rigid-perfect plastic however, it can result in convergence difficulties. Therefore, instead of initial rigid stiffness, a finite stiffness is considered and commonly known as penalty stiffness (**Figure 6-8(d)**). By including penalty stiffness, the structure shows more flexibility than the time ideal rigid behavior is considered. Note that in practice ideal rigid behavior may not be observed in many cases due to many factors such as nonhomogeneous surface conditions. So, it is very important to define the penalty stiffness ( $K_p$ ) appropriately to be matched with reality. In ABAQUS software, penalty stiffness is calculated during analysis based on the following procedure.

At any increment of loading, normal stress ( $P$ ) and corresponding critical shear stress ( $\tau_{cr} = \mu P$ ) are calculated for each set of the contact surfaces. Since  $\tau_{cr}$  is known,

$K_p$  can be defined if the corresponding sliding at critical shear stress is known, which is called the allowable elastic slip ( $\delta_a$ ). It can be specified directly or as a fraction of characteristic contact surface length ( $l_c$ ), i.e.  $\delta_a = F_f l_c$ , where  $F_f$  is called slip tolerance factor. The default value of  $F_f$  is 0.005 and has been calculated by try and error and based on a trade-off between accuracy and efficiency. Therefore, the default value of  $F_f$  is not appropriate for all cases in general and sensitivity analysis may be required.

Boundary conditions are very important in the simulation, influential in the response, and should be properly implemented in the numerical analysis. Although it is not practically possible to explicitly model all details of the experimental set-up, the effect of main components should be logically implemented in the model.

Since the model is defined in 2D-space, the effect of out-of-plane anchors in the experiment is conceptually included in the modeling. There are two main boundary conditions including the base support (below the bottom beam) and connection of the right side of the top beam to the actuators. Considering the rigidity of base support and connection details of the actuator endplate, the right side top beam and bottom edge of the bottom beam were converted to a rigid line by using the “Rigid body” constraint. Thus, the motion of all points on these edges can be defined by assigning boundary conditions to their corresponding reference point, RP.

Since the model is in 2D-space, active degrees of freedom (DOF) are  $u_x$ ,  $u_y$ , and  $u_z$ . All degrees of freedom of RP assigned to the bottom edge of the bottom beam were restrained to simulate fix support.

Loading is applied in three steps. In the first step, a self-weight load was applied by applying “gravity load” to the whole component of the model, and then the pre-compression load is applied to the top beam edge. Finally, in the third step, the lateral load (imposed by the actuator) was implemented as horizontal displacement ( $u_x$ ) to the RP assigned to the right edge of the top beam. Since both end sides of the actuator had pin connection, the other DOFs, i.e.  $u_y$  and  $u_z$ , were not restrained. Nonlinear geometry was included in the analysis by turning on “Nlgeom” option. Loading in all steps was increased gradually by setting a small increment size. FEM discretization of the domain was made by using a mesh of quadrilateral elements with a quite fine size (4×8 in big stones) that was obtained by primary sensitivity analysis (**Figure 6-9**). CPS4 element type is assigned to the mesh that is a plane stress element with 4 nodes (linear shape function) and full Gaussian integration points (4 points).

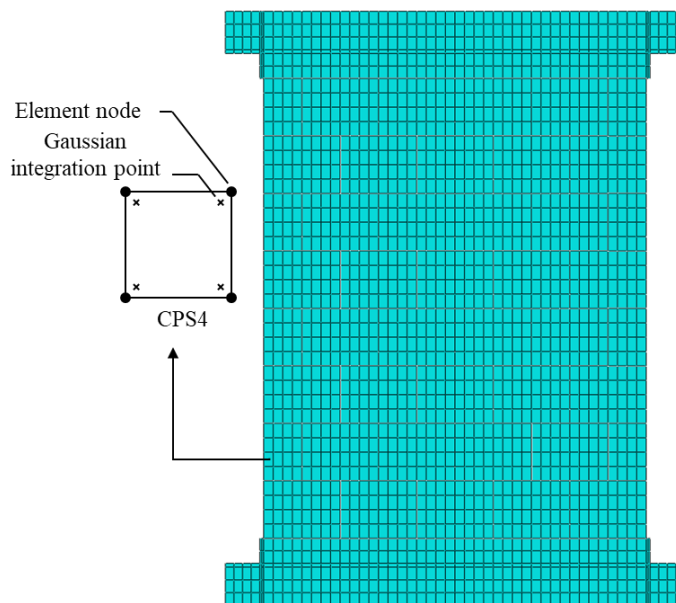


**Figure 6-9** 2D finite element model

## 6.5 Calibration and Validation of Numerical Models

In the former section, components and general assumptions used in FEM models were discussed. This section is concentrated on the detail and procedure of the framework used for checking the validity of models.

Depending on the type of characteristics of a numerical model, many parameters are included in the models. Some of these parameters are related to physical properties such as modulus of elasticity, Poisson's ratio and, density, and some of them are requirements of the numerical technique such as mesh size and load increment. In each type of modeling technique, a set of parameters are considered that can be the most influence on the solution.

To show the efficiency and validation of results by numerical methods, these parameters are calibrated (or adjusted) to reach matching as best as possible with the results of the experimental test. Instead of experimental test, a theoretical solution also may be used to check the validity of the numerical models. Though some closed-form solutions are available for URM walls under simple conditions, validation with experimental results would be necessary because of their severe nonlinear behavior.

Three important issues regarding the matching are how much the level of desirable accuracy is, what parameters should be considered for adjusting (calibration), and what should be considered as targets for matching (validation). The level of accuracy in a simple word may be interpreted as the difference between micro-and macro-modeling approaches. For instance, failure in the macro-modeling approach with a homogenized inelastic material is determined as diagonal cracking developed by plastic deformations. While the real failure mechanism is stair-stepped that can explicitly be captured in the micro-modeling approach. As a rational approach, the main parameters with a higher level of uncertainty can be selected for calibration. In the following, the main parameters and selected parameters for calibration are introduced.

Since in the experimental tests, crushing in the stone (inelastic behavior) was not observed, material properties are considered as an elastic material, with the modulus of elasticity and Poisson's ratio. The results of material tests on granite stones by Vasconcelos (2005) and Yavartanoo *et al.* (2020) showed that these parameters have a quite large variation similar to concrete material (and in contrast

with steel material). Therefore, these parameters bring uncertainty to the models. In this study, to have a logical method for comparison, a constant Poisson's ratio is considered. It is assumed that the modulus of elasticity follows the proposed fitted equation (**Equation (6-1)**) by Vasconcelos (2005).

The second set of important parameters are related to joint behavior, i.e. friction coefficient and penalty stiffness. The results of the material test showed that for dry joints, the friction coefficient is about 0.65. However, as discussed by Vasconcelos (2005), a smaller value of about 0.35 should be considered when the wall behavior is under investigation. Therefore,  $\mu$  was considered as an uncertain parameter and included in the group of calibration parameters. For simplification, Penalty stiffness was assumed to be constant and the default value in software was used.

The third group excludes details of boundary conditions in numerical models. The base is assumed to be fixed support based on set-up details. Although no special observation regarding sliding, uplift, yielding, etc., were reported in the test report, any imperfection can change the results. Similar issues can happen in the connection between the actuator and the top beam. In addition, the profile section of the top and bottom beam was not reported in the test, although it was mentioned that the same profiles were used. In 2D-space, the top and bottom beam was modeled by shell geometry, and it cannot be representative of the I-shape section profile that is commonly used in these kinds of experiments. So, to consider the correct stiffness of real profile and uncertainty in the boundary conditions, modulus of elasticity of

top and bottom beam,  $E_s$ , were included in the group of calibration parameters. A constant Poisson's ratio of 0.3 was considered for the beams.

The selection of targets for matching (validation) depends on available data from experimental results. Stress and strain distribution was not reported by Vasconcelos (2005). The main reported parameters were failure mechanisms and the force-displacement curve. Thus, two sets of targets were defined as "overall behavior" and "failure mechanism" based on available data.

The overall behavior target was investigated by comparison of the force-displacement curve and the main parameters that can be extracted from the curve, i.e. initial stiffness and ultimate strength. Note that the behavior is not perfectly plastic, so yield strength also can be extracted. Due to the complexity of digitizing yield strength, instead of direct comparison, it is compared by visually comparing the curve obtained by experiment with that calculated by the numerical model. The failure mechanism observed in the test was stair-stepped for all specimen under all pre-compression loads and is set to be a target for the validation process. **Figure 6-10** displays a summary of the procedure used for calibration and validation.

The process of calibration has been done by performing many analyses with adjusting the friction coefficient and beam properties, and results are briefly explained in the following.

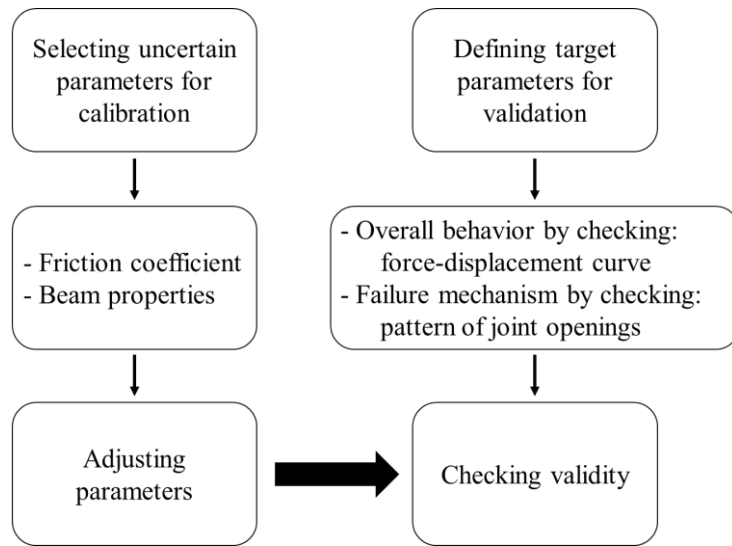


**Figure 6-10** Calibration and validation procedure

The observed failure mechanism of the wall in the experiment was stair-stepped under different levels of pre-compression (**Figure 6-11(a)**). The results of analyses revealed that the friction coefficient ( $\mu$ ) has a significant influence on the strength of the wall and also the type of failure mechanism. If a friction coefficient of about 0.35 or less is considered it results in the failure mode of sliding under all four cases of pre-compression rather than the stair-stepped mode (**Figure 6-11(b)**). Instead, if a friction coefficient of around 0.4 or more is considered, the failure mode is stair-stepped (**Figure 6-11(c)**). Values larger than 0.4 for friction coefficient result in increasing the stiffness and strength of the wall. However, utilizing the value of 0.4 results in the best fit with the force-displacement curve of the experiment and therefore was chosen as the calibrated value of friction coefficient. More results and details about sensitivity analysis to the values of friction coefficient can be found in **Section 6.6.3**.

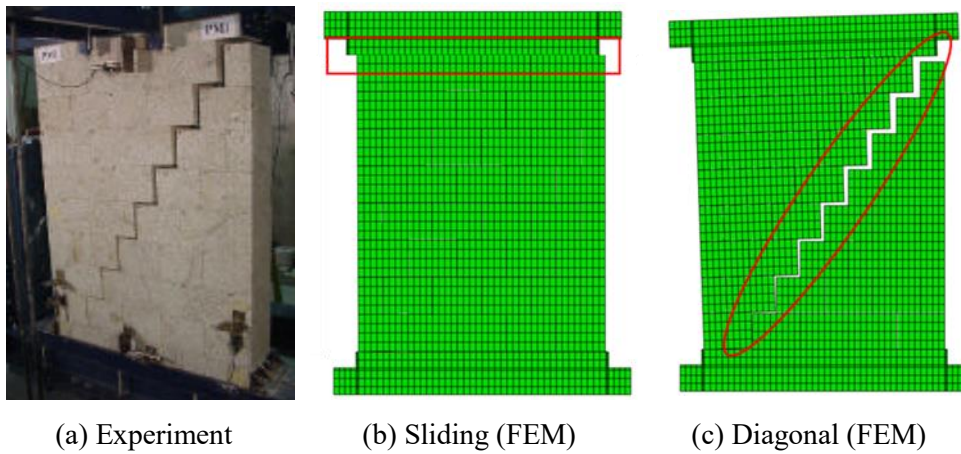


**Figure 6-11** Failure mechanism

Top and bottom steel beams have a considerable effect especially on the stiffness of the system. Essentially, these beams are designed properly to act as a rigid boundary concerning the main components which here is the wall. Since the section profile of beams was not reported in the experimental report, in the 2D modeling, the modulus of elasticity of the beam ( $E_s$ ) is adjusted to match the stiffness of the FEM models with that of the experiment. Since boundary conditions are changed by changing  $E_s$ , yield and ultimate strengths of the wall also are changed a little. The force-displacement curves of specimens with friction coefficient of 0.4 and different values of  $E_s$  are shown in **Figure 6-12**. It can be seen that by changing  $E_s$ , stiffness is considerably influenced while it does not have significant effects on values of strength. Values of stiffness ( $K$ ), and yield ( $f_y$ ) and ultimate strengths ( $f_u$ ) were extracted from the curves and are reported in **Tables 6-2 to 6-5**.

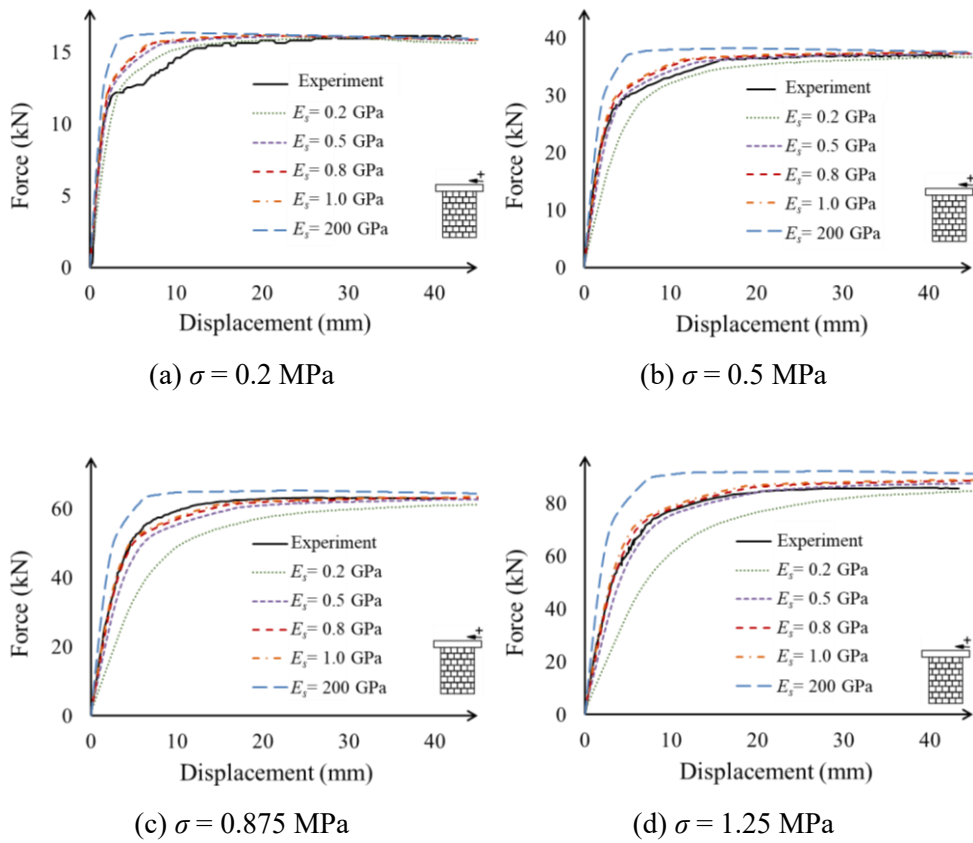


**Figure 6-12** Influence of  $E_s$  on force-displacement curves under different levels of pre-compression load ( $\sigma$ ) and  $\mu = 0.4$

**Table 6-2** Influence of  $E_s$  on mechanical properties of wall ( $\mu = 0.4, \sigma = 0.2 \text{ N/mm}^2$ )

	$K$ (kN/mm)	$F_y$ (kN)	$F_u$ (kN)
	0.2	4.49 (0.50)	12.02 (1.11)
	0.5	6.16 (0.69)	12.24 (1.13)
$E_s$ (GPa)	0.8	6.85 (0.77)	12.14 (1.12)
	1	7.14 (0.81)	12.17 (1.12)
	200	9.14 (1.03)	15.75 (1.45)
Experiment	8.81	10.81	16.13

Note: The values in parentheses are the normalized result by the value of the experiment.

**Table 6-3** Influence of  $E_s$  on mechanical properties of wall ( $\mu = 0.4$ ,  $\sigma = 0.5 \text{ N/mm}^2$ )

	$K$ (kN/mm)	$F_y$ (kN)	$F_u$ (kN)	
$E_s$ (GPa)	0.2	5.98 (0.60)	26.96 (1.00)	36.60 (0.99)
	0.5	9.21 (0.93)	28.12 (1.05)	37.22 (1.00)
	0.8	10.77 (1.08)	28.69 (1.07)	37.39 (1.01)
	1	11.45 (1.15)	28.88 (1.08)	37.46 (1.01)
	200	16.89 (1.70)	31.06 (1.16)	38.22 (1.03)
Experiment	9.89	26.73	36.94	

Note: The values in parentheses are the normalized result by the value of the experiment.

**Table 6-4** Influence of  $E_s$  on mechanical properties of wall ( $\mu = 0.4$ ,  $\sigma = 0.875 \text{ N/mm}^2$ )

	$K$ (kN/mm)	$F_y$ (kN)	$F_u$ (kN)	
$E_s$ (GPa)	0.2	6.91 (0.44)	44.38 (0.92)	61.15 (0.96)
	0.5	11.48 (0.73)	50.96 (1.05)	62.66 (0.99)
	0.8	13.91 (0.89)	48.38 (1.00)	63.14 (1.00)
	1	15.02 (0.96)	48.72 (1.01)	63.34 (1.00)
	200	24.90 (1.60)	49.67 (1.03)	65.26 (1.03)
Experiment	15.54	48.24	63.17	

Note: The values in parentheses are the normalized result by the value of the experiment.

**Table 6-5** Influence of  $E_s$  on mechanical properties of wall ( $\mu = 0.4$ ,  $\sigma = 1.25 \text{ N/mm}^2$ )

	$K$ (kN/mm)	$F_y$ (kN)	$F_u$ (kN)	
$E_s$ (GPa)	0.2	7.45 (0.44)	58.76 (0.88)	84.62 (0.98)
	0.5	12.98 (0.78)	65.79 (0.99)	87.50 (1.01)
	0.8	16.11 (0.96)	66.24 (1.00)	88.46 (1.03)
	1	17.56 (1.05)	69.15 (1.04)	88.76 (1.03)
	200	31.77 (1.90)	69.82 (1.05)	92.13 (1.07)
Experiment	16.65	66.09	85.83	

Note: The values in parentheses are the normalized result by the value of the experiment.

It can be concluded that use of 0.8 GPa for  $E_s$  results in best matching for mechanical properties with that of values obtained experimentally.

The procedure of calibration and validation results in the conclusion that the values of  $\mu = 0.4$  and  $E_s = 0.8$  GPa in the numerical model results in the best matching with the experimental results. The trend of stiffness, yield, and ultimate strength of the wall obtained experimentally and those of the calibrated models under different pre-compression loads are illustrated in **Figure 6-13**.

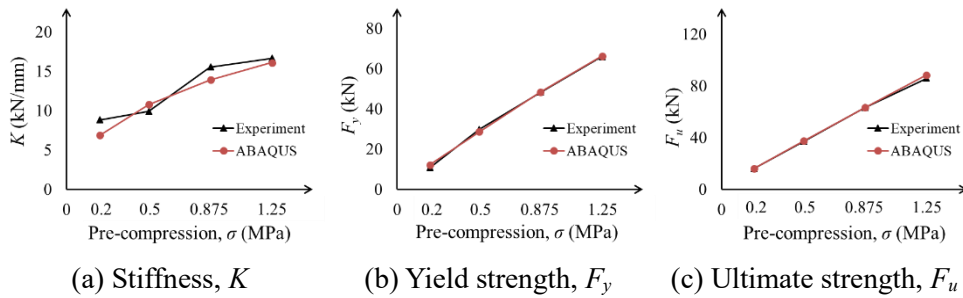


**Figure 6-13** Comparison of mechanical properties of the wall obtained by experiment and calibrated model

The graphs show that the calibrated models can simulate mechanical properties very well. Since the failure mechanism was also detected properly by the model, it can be concluded that the modeling technique was validated. This approach was used in the rest of the study for further investigation including sensitivity analysis, parametric study, and retrofitting method.

## 6.6 Sensitivity Analysis

In this section, the sensitivity of the calibrated model to the main parameters of modeling including penalty stiffness factor, mesh size, and friction coefficient. Moreover, the results of 3D modeling and 2D modeling and the results of cyclic analysis and pushover analysis are compared.

### 6.6.1 Penalty stiffness sensitivity analysis

It was discussed in **Section 6.4** that penalty stiffness ( $K_p$ ) is defined as the ratio of critical shear stress ( $\tau_{cr}$ ) to the allowable elastic slip ( $\delta_a$ ). The value of  $\delta_a$  should be chosen small enough such that the penalty stiffness can be a logical representation of ideal infinite stiffness. By introducing a slip tolerance factor ( $F_f$ ),  $\delta_a$  is defined as the product of characteristic contact surface length ( $l_c$ ) and  $F_f$ . Since  $l_c$  is a characteristic of mesh size and is constant during analysis, at any increment of loading with a specific value of  $\tau_{cr}$ , using a smaller value of  $F_f$  results in a larger value of penalty stiffness. **Figure 6-14** illustrates the force-displacement curves of the wall obtained experimentally and those of the calibrated model using different values of slip tolerance factor. It can be seen that the value of  $F_f$  has a negligible effect on the strength of the wall, as well as the failure mechanism. However, it has a quite significant influence on the stiffness of the wall.

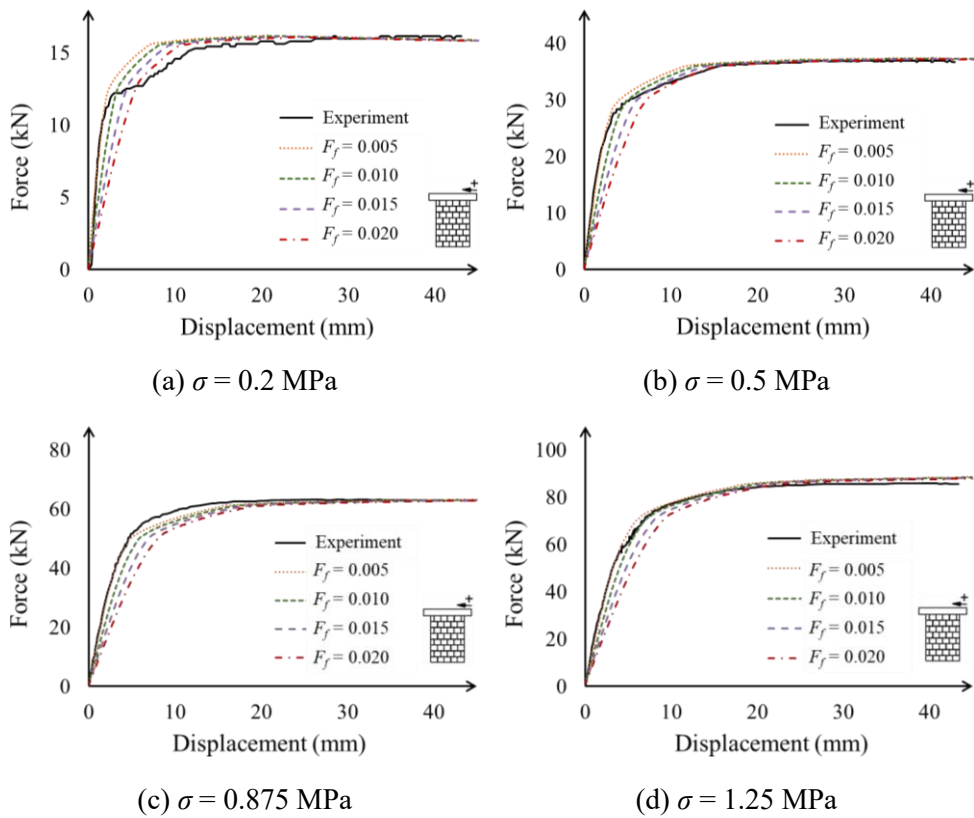


**Figure 6-14** Influence of  $F_f$  on force-displacement curves of the calibrated model under different levels of pre-compression load ( $\sigma$ )

Mechanical properties of the walls obtained from the sensitivity of analysis, extracted from the curves shown in **Figure 6-14**, are reported in **Tables 6-6 to 6-9**. Based on the results, by increasing  $F_f$  the stiffness is decreased and the best results are obtained by adopting  $F_f = 0.005$  (the default value in ABAQUS). Although more variation can be observed for both yield and ultimate strengths by changing the value of  $F_f$ , the variations are small (on average 5% and 0.4% for yield and ultimate strengths, respectively) and can be neglected.

**Table 6-6** Effect of  $F_f$  on mechanical properties of calibrated model ( $\sigma = 0.2$  MPa)

	$K$ (kN/mm)	$F_y$ (kN)	$F_u$ (kN)
$F_f$	0.005	6.91 (0.78)	11.96 (1.10)
	0.010	4.44 (0.50)	12.59 (1.16)
	0.015	3.29 (0.37)	12.21 (1.13)
	0.020	2.62 (0.29)	11.75 (1.08)
Experiment	8.81	10.81	16.13

Note: The values in parentheses are the normalized result by the value of the experiment.

**Table 6-7** Effect of  $F_f$  on mechanical properties of calibrated model ( $\sigma = 0.5$  MPa)

	$K$ (kN/mm)	$F_y$ (kN)	$F_u$ (kN)
$F_f$	0.005	10.88 (1.10)	26.90 (1.00)
	0.010	7.84 (0.79)	29.09 (1.08)
	0.015	6.16 (0.62)	28.92 (1.08)
	0.020	5.09 (0.51)	27.68 (1.03)
Experiment	9.89	26.73	36.94

Note: The values in parentheses are the normalized result by the value of the experiment.

**Table 6-8** Effect of  $F_f$  on mechanical properties of calibrated model ( $\sigma = 0.875$  MPa)

	$K$ (kN/mm)	$F_y$ (kN)	$F_u$ (kN)
$F_f$	0.005	14.06 (0.90)	48.46 (1.00)
	0.010	10.82 (0.69)	48.95 (1.01)
	0.015	8.84 (0.56)	49.21 (1.02)
	0.020	7.50 (0.48)	49.85 (1.03)
Experiment	15.54	48.24	63.17

Note: The values in parentheses are the normalized result by the value of the experiment.

**Table 6-9** Effect of  $F_f$  on mechanical properties of calibrated model ( $\sigma = 1.25$  MPa)

	$K$ (kN/mm)	$F_y$ (kN)	$F_u$ (kN)
$F_f$	0.005	16.27 (0.97)	66.92 (1.01)
	0.010	13.03 (0.78)	67.68 (1.02)
	0.015	10.93 (0.65)	69.31 (1.04)
	0.020	9.44 (0.56)	70.54 (1.06)
Experiment	16.65	66.09	85.83

Note: The values in parentheses are the normalized result by the value of the experiment.

## 6.6.2 Mesh size sensitivity analysis

Mesh sensitivity analysis should be done by addressing the effect of both element size and element behavior. In 2D plane-stress space, ABAQUS provides four types of quadrilateral continuum elements with 2D plane-stress formulation. CPS4, a first-order element (linear shape function) with full Gaussian integration points (4 points), has been used in the calibrated model. CPS4R is exactly similar to CPS4, but with reduced Gaussian integration points (1 point). CPS8, a second-order element (quadratic shape function) with full Gaussian integration points (8 points), and CPS8R, which is exactly similar to CPS8, but with reduced Gaussian integration points (4 points).

Primary sensitivity analyses showed that mechanical properties and failure mechanisms are not notably affected by the type of element and no more results are provided here. However, the mesh size has more considerably changed the results.

Therefore, a set of five mesh patterns were considered for the number of elements in width and length of stone units as shown in **Figure 6-15**. The number of

elements of the top and bottom beams is selected in accordance with the mesh size of stone units to remain the uniformity of the model.

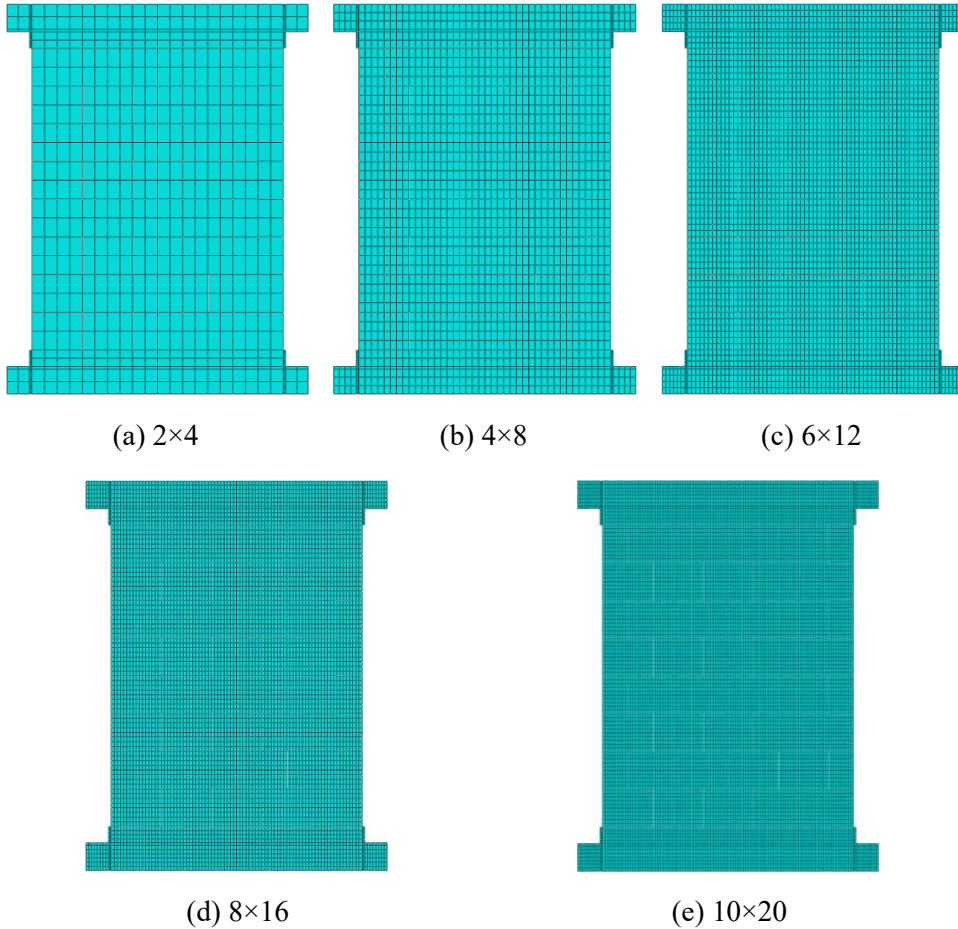


**Figure 6-15** Mesh pattern

The results of the mesh sensitivity analysis showed that mesh size does not change the failure mechanism. Assuming elastic behavior for stone units, failure is localized at joints. Therefore, reducing mesh size does not have special effects on the simulated behavior of stone units. Also, as shown in **Figure 6-16** and reported in

Tables 6-10 to 6-13, the effects of mesh size on yield and ultimate strengths can be ignored, while its effects on stiffness are more significant.

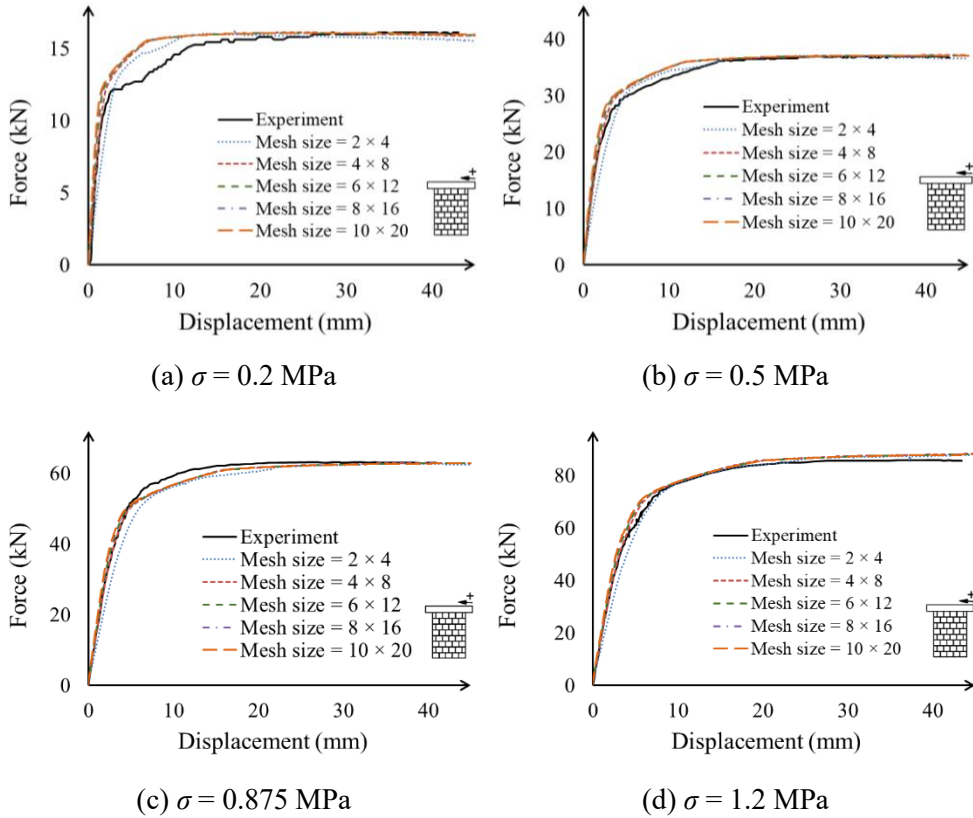


**Figure 6-16** Influence of mesh size on force-displacement curves of the calibrated model under different levels of pre-compression load ( $\sigma$ )

**Table 6-10** Effect of mesh size on mechanical properties ( $\sigma = 0.2$  MPa)

		$K$ (kN/mm)	$F_y$ (kN)	$F_u$ (kN)
Mesh Size	2×4	4.73 (0.53)	11.25 (1.04)	16.28 (1.00)
	4×8	7.21 (0.81)	11.45 (1.05)	16.13 (1.00)
	6×12	8.76 (0.99)	11.93 (1.10)	16.07 (0.99)
	8×16	9.85 (1.11)	12.18 (1.12)	16.08 (0.99)
	10×20	10.67 (1.21)	12.19 (1.12)	16.06 (0.99)
Experiment		8.81	10.81	16.13

Note: The values in parentheses are the normalized result by the value of the experiment.

**Table 6-11** Effect of mesh size on mechanical properties ( $\sigma = 0.5$  MPa)

		$K$ (kN/mm)	$F_y$ (kN)	$F_u$ (kN)
Mesh Size	2×4	8.12 (0.82)	27.04 (1.01)	37.08 (1.00)
	4×8	11.17 (1.12)	27.20 (1.01)	37.17 (1.00)
	6×12	12.70 (1.28)	27.46 (1.02)	37.11 (1.00)
	8×16	13.67 (1.38)	27.79 (1.04)	37.06 (1.00)
	10×20	14.34 (1.45)	28.09 (1.05)	37.07 (1.00)
Experiment		9.89	26.73	36.94

Note: The values in parentheses are the normalized result by the value of the experiment.

**Table 6-12** Effect of mesh size on mechanical properties ( $\sigma = 0.875$  MPa)

		$K$ (kN/mm)	$F_y$ (kN)	$F_u$ (kN)
Mesh Size	2×4	11.05 (0.71)	48.44 (1.00)	62.76 (0.99)
	4×8	14.31 (0.92)	48.55 (1.00)	62.80 (0.99)
	6×12	15.73 (1.01)	48.68 (1.00)	62.79 (0.99)
	8×16	16.59 (1.06)	49.11 (1.01)	62.79 (0.99)
	10×20	17.16 (1.10)	49.37 (1.02)	62.77 (0.99)
Experiment		15.54	48.24	63.17

Note: The values in parentheses are the normalized result by the value of the experiment.

**Table 6-13** Effect of mesh size on mechanical properties ( $\sigma = 1.25$  MPa)

	$K$ (kN/mm)	$F_y$ (kN)	$F_u$ (kN)	
Mesh Size	2×4	13.21 (0.79)	66.42 (1.00)	87.94 (1.02)
	4×8	16.47 (0.98)	66.51 (1.00)	88.17 (1.02)
	6×12	17.78 (1.06)	67.13 (1.01)	88.02 (1.02)
	8×16	18.54 (1.11)	67.39 (1.02)	87.96 (1.02)
	10×20	19.05 (1.14)	67.81 (1.02)	87.93 (1.02)
Experiment	16.65	66.09	85.83	

Note: The values in parentheses are the normalized result by the value of the experiment.

Based on the results, by increasing the number of elements (i.e. using a finer mesh), the stiffness is increased notably. The reason lies in the fact that by increasing the number of elements, characteristic contact surface length ( $l_c$ ) is reduced. Consequently, the value of allowable elastic slip ( $\delta_a$ ) results in increasing penalty stiffness. Therefore, it is similar to the sensitivity analysis for penalty stiffness, but here  $F_f$  is fixed instead of  $l_c$ .

### 6.6.3 Friction coefficient sensitivity analysis

The effect of friction coefficient on the behavior of the wall was investigated as one main component in the calibration and validation process. However, since it is the main parameter concerning the strength of the wall and failure mechanism (for elastic behavior), the variation of the mechanical properties by changing the friction coefficient is discussed in this section. As illustrated in **Figure 6-17**, yield and ultimate strengths highly depend on the value of friction coefficient ( $\mu$ ). It can be seen that in all cases with  $\mu$  less than about 0.35, the strengths are smaller. Because

for a smaller value of  $\mu$ , shear strength of the horizontal layer is small and the failure mode is sliding, which results in smaller strength than stair-stepped failure mode.

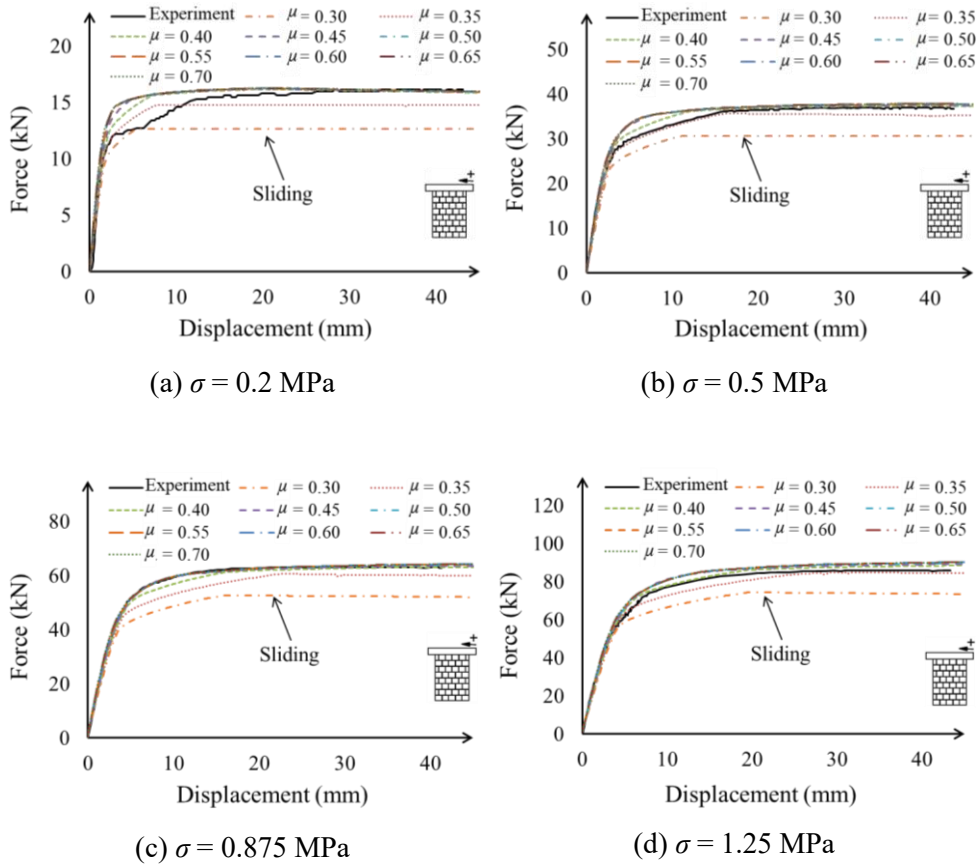


**Figure 6-17** Influence of friction coefficient on force-displacement curves of the calibrated model under different levels of pre-compression load ( $\sigma$ )

The effect of friction coefficient on the mechanical properties of the wall is reported in **Tables 6-14** to **6-17**. From the results, it can be seen that by increasing the value of  $\mu$ , the strengths are increased. For the value of about 0.4 and larger the mode of failure was stair-stepped in all models. However, by using a larger value of

$\mu$ , the increase in strength is not significant. The reason lies in the fact that the shear strength is increased by  $\mu$ , but it does not increase tensile strength. Since for a large value of  $\mu$ , the failure mode is diagonal cracking, increasing the value of  $\mu$  is not effective.

**Table 6-14** Effect of friction coefficient on mechanical properties of calibrated model ( $\sigma = 0.2$  MPa)

	$K$ (kN/mm)	$F_y$ (kN)	$F_u$ (kN)
	0.30	5.82 (0.66)	10.36 (0.95)
	0.35	6.35 (0.72)	10.80 (0.99)
	0.40	6.85 (0.77)	12.30 (1.13)
	0.45	7.31 (0.82)	13.24 (1.22)
$\mu$	0.50	7.79 (0.88)	14.16 (1.31)
	0.55	8.10 (0.91)	14.52 (1.34)
	0.60	8.44 (0.95)	14.66 (1.35)
	0.65	8.76 (0.99)	14.70 (1.36)
	0.70	9.05 (1.02)	14.73 (1.36)
Experiment	8.81	10.81	16.13

Note: The values in parentheses are the normalized result by the value of the experiment.

**Table 6-15** Effect of friction coefficient on mechanical properties of calibrated model ( $\sigma = 0.5$  MPa)

	$K$ (kN/mm)	$F_y$ (kN)	$F_u$ (kN)	
	0.30	9.53 (0.96)	23.25 (0.87)	30.67 (0.83)
	0.35	10.20 (1.03)	26.29 (0.98)	35.62 (0.96)
	0.40	10.77 (1.08)	28.43 (1.06)	37.39 (1.01)
	0.45	11.26 (1.13)	29.39 (1.09)	37.55 (1.01)
$\mu$	0.50	11.69 (1.18)	30.13 (1.12)	37.70 (1.02)
	0.55	12.07 (1.22)	30.27 (1.13)	37.79 (1.02)
	0.60	12.41 (1.25)	30.75 (1.15)	37.85 (1.02)
	0.65	12.71 (1.28)	30.84 (1.15)	37.86 (1.02)
	0.70	12.98 (1.31)	31.06 (1.16)	37.87 (1.02)
Experiment	9.89	26.73	36.94	

Note: The values in parentheses are the normalized result by the value of the experiment.

**Table 6-16** Effect of friction coefficient on mechanical properties of calibrated model ( $\sigma = 0.875$  MPa)

	$K$ (kN/mm)	$F_y$ (kN)	$F_u$ (kN)	
	0.30	12.65 (0.81)	39.72 (0.82)	52.69 (0.83)
	0.35	13.34 (0.85)	45.02 (0.93)	60.63 (0.96)
	0.40	13.91 (0.89)	48.38 (1.00)	63.14 (1.00)
	0.45	14.40 (0.92)	49.02 (1.01)	63.58 (1.00)
$\mu$	0.50	14.82 (0.95)	49.77 (1.03)	63.91 (1.01)
	0.55	15.18 (0.97)	50.04 (1.03)	64.13 (1.01)
	0.60	15.49 (0.99)	50.77 (1.05)	64.20 (1.01)
	0.65	15.77 (1.01)	51.15 (1.06)	64.21 (1.01)
	0.70	16.02 (1.03)	51.27 (1.06)	64.22 (1.01)
Experiment	15.54	48.24	63.17	

Note: The values in parentheses are the normalized result by the value of the experiment.

**Table 6-17** Effect of friction coefficient on mechanical properties of calibrated model ( $\sigma = 1.25$  MPa)

	$K$ (kN/mm)	$F_y$ (kN)	$F_u$ (kN)
0.30	14.87 (0.89)	56.93 (0.86)	74.36 (0.87)
0.35	15.55 (0.93)	63.09 (0.95)	84.96 (0.99)
0.40	16.11 (0.97)	66.24 (1.00)	88.46 (1.03)
0.45	16.57 (1.00)	66.95 (1.01)	89.26 (1.04)
$\mu$ 0.50	16.96 (1.02)	69.03 (1.04)	89.81 (1.05)
0.55	17.30 (1.04)	69.30 (1.05)	90.19 (1.05)
0.60	17.60 (1.06)	70.57 (1.07)	90.25 (1.05)
0.65	17.85 (1.07)	70.67 (1.07)	90.27 (1.05)
0.70	18.08 (1.09)	71.07 (1.08)	90.28 (1.05)
Experiment	16.65	66.09	85.83

Note: The values in parentheses are the normalized result by the value of the experiment.

Note that as reported in the tables, the stiffness also was also increased but not significantly. Because by increasing  $\mu$ , the value of critical shear stress is increased and results in increasing the penalty stiffness. However, the effect is much smaller than that of  $F_f$  and  $l_c$ .

#### 6.6.4 Comparison of 2D and 3D analyses

It was discussed that the in-plane behavior of the URM walls can be modeled in 2D model by considering the plane-stress condition. The result of the calibration and validation process shows how this method could effectively simulate both local and global failure of the wall. In this section, results of 2D and 3D models were compared comprehensively to find the main differences.

The 3D model was made by using the same assumptions as (2D) calibrated model. In order to constrain out-of-plane motion, the out-of-plane DOF of the mid-surface in all components was restrained (**Figure 6-18(a)**). The same arrangement of mesh was used and the number of elements in the width of the wall was chosen based on comparison with the in-plane dimensions (**Figure 6-18(b)**). The element type was chosen as C3D8, which is a hexahedral 3D stress continuum element with first-order shape function (8 nodes) and full Gaussian integration points (8 points).

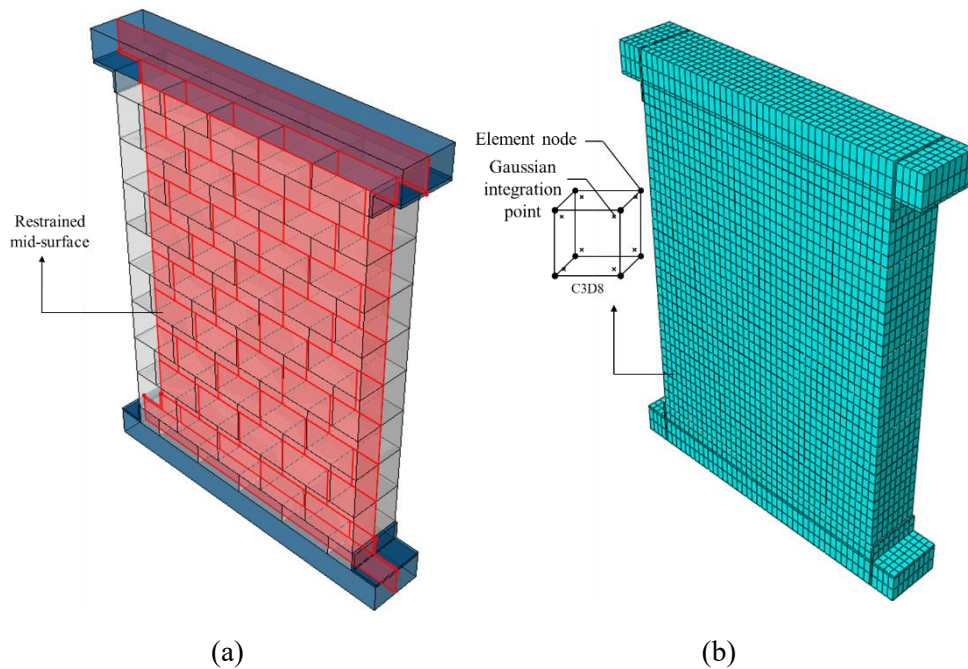


**Figure 6-18** a) Restrained mid-surface of components for out-of-plane motion; b) 3D mesh

The comparison has been done in terms of stress distribution, force-displacement curve, and failure mechanism. The force-displacement curves of 2D and 3D models along with experimental results are depicted in **Figure 6-19**. It can be seen that there is almost no difference between the results. Therefore, there is no reason to use 3D model concerning the force-displacement curve as representative of the global behavior of the wall.

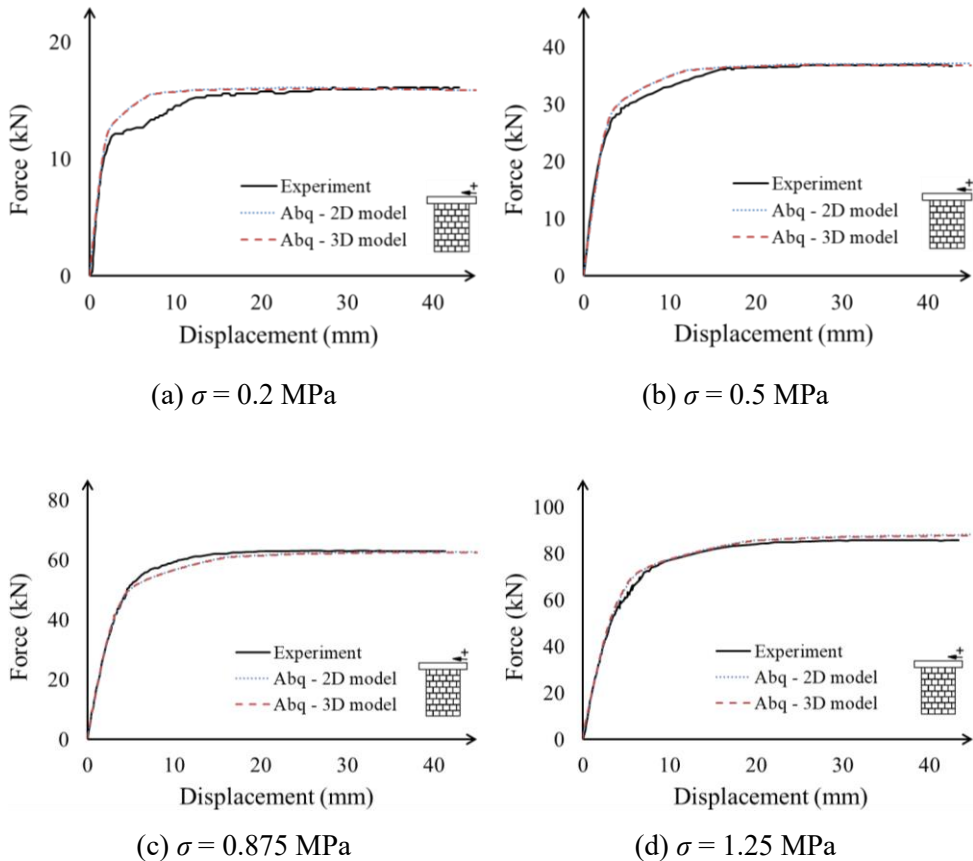


**Figure 6-19** Comparison of force-displacement curves of 2D and 3D models under different levels of pre-compression load ( $\sigma$ )

Distribution of von Mises stress in the wall under gravity load and pre-compression load, and at the target lateral displacement are shown in **Figures 6-20 to 6-22**. From the figures, it can be seen that the overall pattern is the same in all conditions. Although there are some discrepancies in local stress concentrations, the order of stress is the same, and maximum and minimum values are very close, and thus, in general, they are the same.

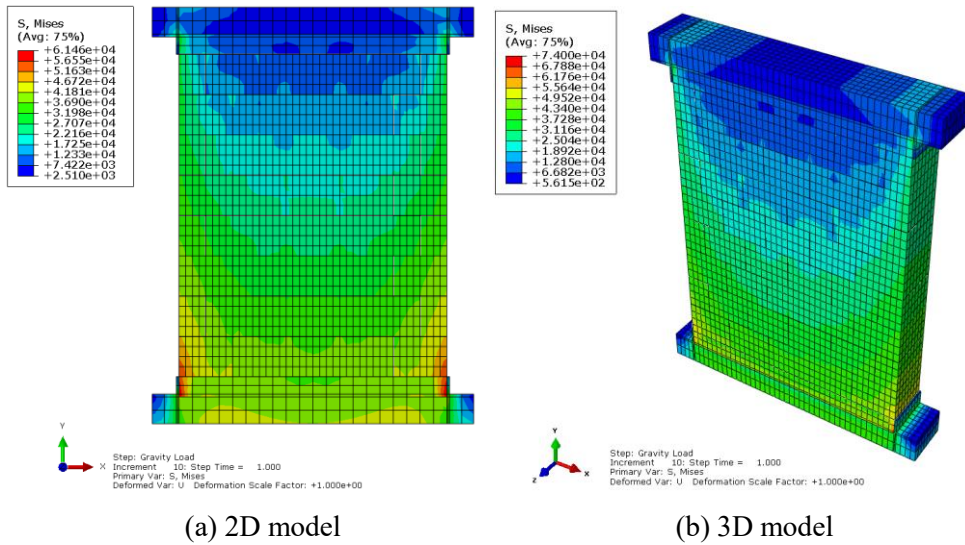


**Figure 6-20** von Mises stress distribution (MPa) under gravity load

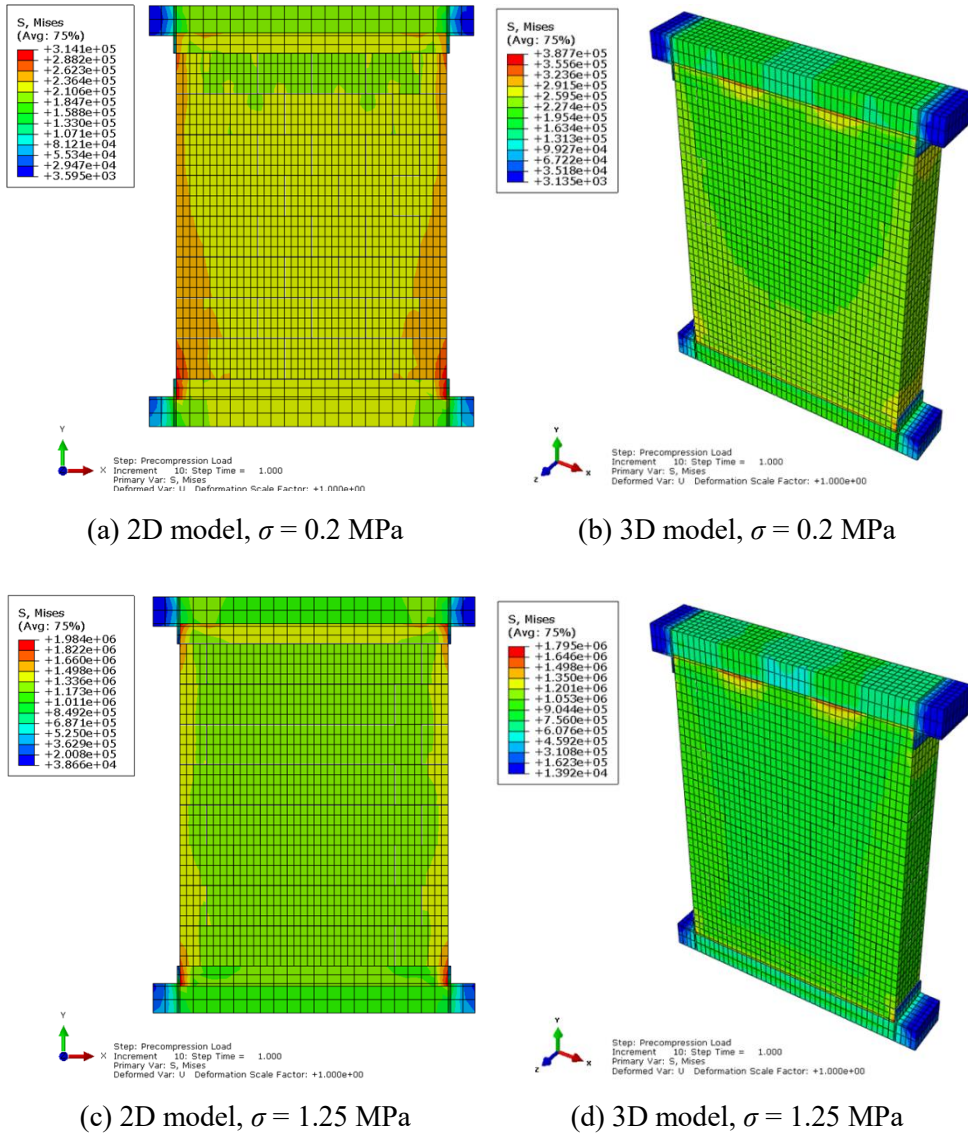


**Figure 6-21** von Mises stress distribution (MPa) under different levels of pre-compression load ( $\sigma$ )

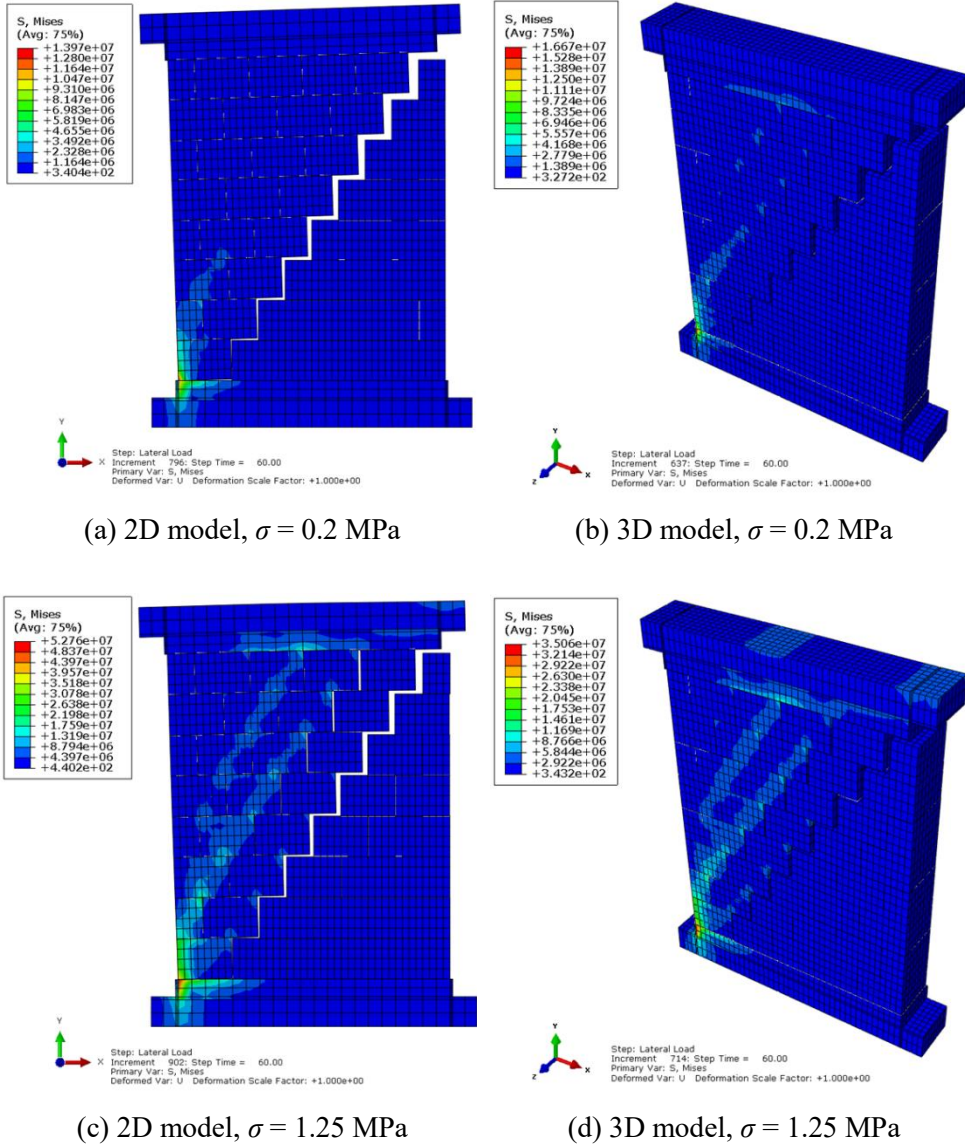


**Figure 6-22** von Mises stress distribution (MPa) at maximum lateral load under different levels of pre-compression load ( $\sigma$ )

It should be noted that the assumption of plane-stress condition is an ideal condition and due to element connectivity and Poisson's effect, there are some inherent out-of-plane restraints for some elements, which result in out-of-plane stress

in those elements. This term is directly considered in 3D von Mises stress, while is not essentially included in 2D von Mises formulation. However, no specific trends can be observed from the results where 2D or 3D models show larger values. In some cases, 2D model has higher stress, while in other cases stress is larger in 3D models. Since experimental reports do not provide any information about stress distribution, it is not possible to make a logical conclusion on the accuracy of models. Nonetheless, the results of 2D and 3D models are overall well matched with each other in terms of both stress distribution and values. It can be concluded that the stress distributions obtained by 2D models are rational and acceptable. In addition, the failure mechanism obtained by 3D model is exactly the same as 2D model as shown in **Figure 6-22**.

Note that in addition to the higher computational cost of 3D models due to the more number of elements and integration points than 2D model, its running time is also considerably larger. On average, the order of time required for analysis of 3D models was about 2 ~ 3 times that of 2D model. Therefore, based on the above discussions, it can be said that 2D model can effectively model the behavior of the wall with the same accuracy and achievement as 3D model with a less computational cost.

### **6.6.5 Comparison of pushover and cyclic analysis**

It was discussed in the experimental report that conducting a cyclic test for the wall with dry-stack joints is not easy work. Therefore, only for a few cases, it was

possible to successfully continue the test to reach the same target displacement that has been considered for pushover tests. They are still very useful since they can show the overall energy absorption capability of the walls. The loading protocol and the typical force-displacement curves obtained by cyclic tests are shown in **Figure 6-23** and **Figure 6-24**, respectively.

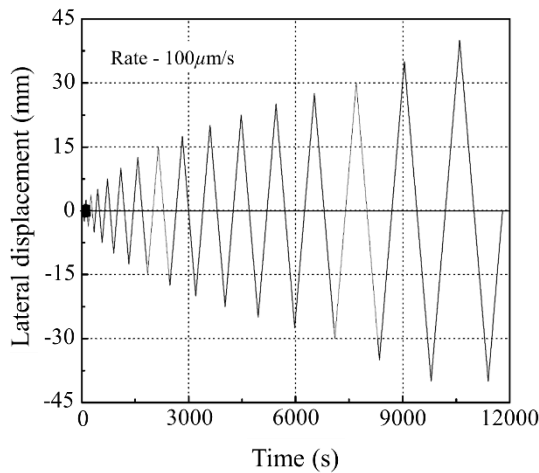
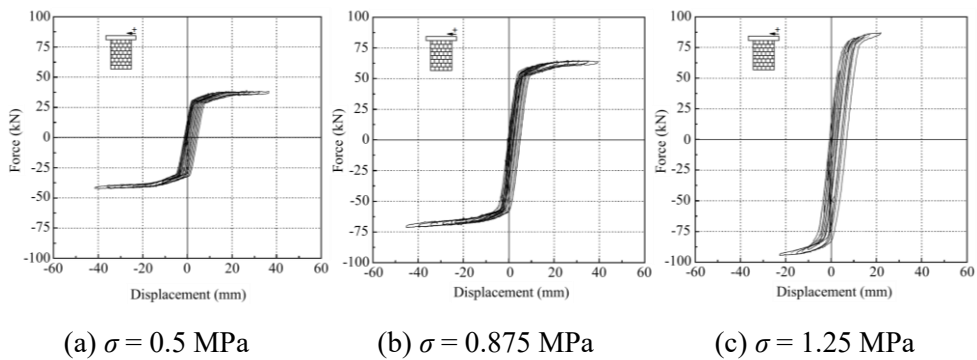


**Figure 6-23** Loading protocol for conducting cyclic test (Adapted from Vasconcelos, 2005)



(a)  $\sigma = 0.5 \text{ MPa}$

(b)  $\sigma = 0.875 \text{ MPa}$

(c)  $\sigma = 1.25 \text{ MPa}$

**Figure 6-24** Cyclic behavior of walls with dry-stack joints (Adapted from Vasconcelos, 2005)

Based on the figure, four main issues can be observed. First of all, the backbones of cycles matched well with the pushover curve obtained by the monotonic test. The second issue is that during cyclic loading the hysteresis loops are biased to one side (the direction of the first lateral load). The third issue is related to the observed behavior at the moment of reversing the load. By comparing the reverse loading mechanism on the left and right side (biased side) of graphs in **Figure 6-24**, on the biased side, there is a smaller initial sliding before the wall recovers its stiffness. The fourth issue is that in all cases, the hysteresis loops are so thin which means the cyclic energy absorption of these walls is so small. This is a very critical issue concerning seismic behavior of the wall and should be improved with an appropriate retrofit technique. In this section, the results of cyclic analyses of the wall are reported. The cyclic load protocol shown in **Figure 6-23** was introduced as amplitude in ABAQUS and used in the calibrated model instead of the formerly defined amplitude for performing pushover analysis.

In sensitivity analysis under monotonic loading, it was observed that increasing friction coefficient has no significant influence on the strength when it is equal to or larger than 0.4. However, in the analyses of the wall under cyclic loading, it was found that friction coefficient (even for the mentioned range of 0.4 and larger) is an influential parameter in hysteresis behavior during unloading and reversed loading. On the other hand, the other parameters such as mesh size and penalty stiffness had no remarkable effect on the wall behavior in unloading and reversed loading stage. Therefore, to precisely calibrate numerical models with cyclic experimental results,

sensitivity analysis on friction coefficient in the range of 0.4 to 0.6 was conducted. All the other parameters were assumed to be the same as the calibrated model for monotonic loading. **Figure 25** indicates cyclic force-displacement curves under different levels of pre-compression load and friction coefficients.

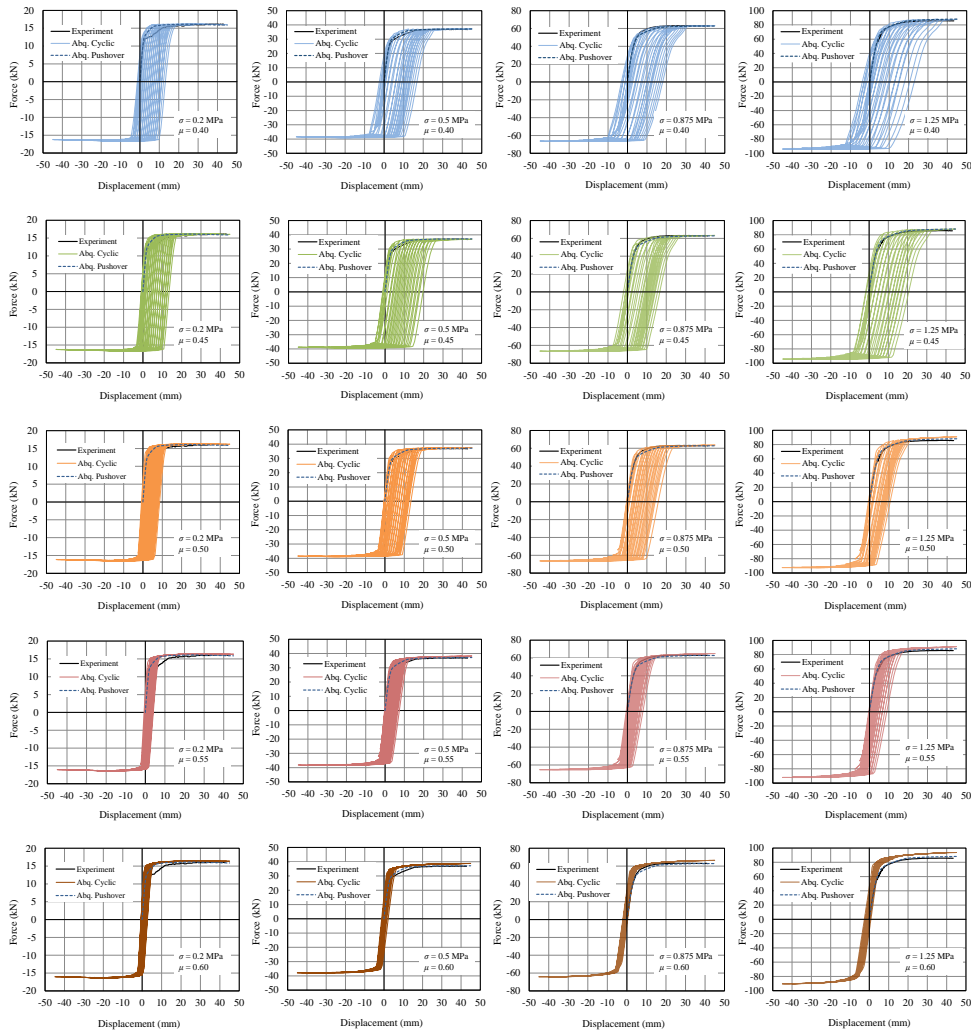


**Figure 6-25** Cyclic force-displacement curves under different levels of pre-compression load ( $\sigma$ ) and friction coefficient ( $\mu$ )

It can be seen that for small friction coefficients, hysteresis loops are too fat in comparison with the test results, which means energy absorption is considerably overestimated. For large friction coefficients, hysteresis loops are narrower and the results become closer to the test result. However, it can be seen for the case with  $\mu = 0.6$  that the direction of the biasing has been inverted. The best fit in terms of all characteristics including energy absorption and the biasing was obtained for  $\mu = 0.55$ . **Figure 26** indicates the comparison of experimental and numerical cyclic tests for the best fit value of friction coefficient ( $\mu = 0.55$ ). In small to medium displacements, the results of numerical analysis are very consistent with the experiment. Just that in the last few cycles related to large displacements, a slight difference can be observed.

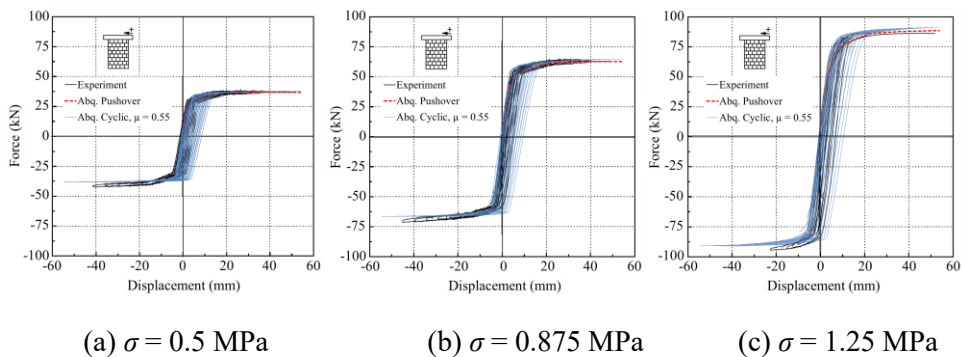


**Figure 6-26** Comparison of experimental and numerical cyclic analysis of walls with dry-stack joints

**Figure 6-27** illustrates the condition of the model at target displacement (45 mm) from cyclic and pushover analysis. It can be seen that the failure mechanism is stair-stepped similar to a monotonic test at the same place. However, the vertical

opening of the joints is larger than that of pushover analysis and more number of joints are opened. In addition, in cyclic analysis clear formation of reverse stair-stepped cracks (X-type) can be seen.

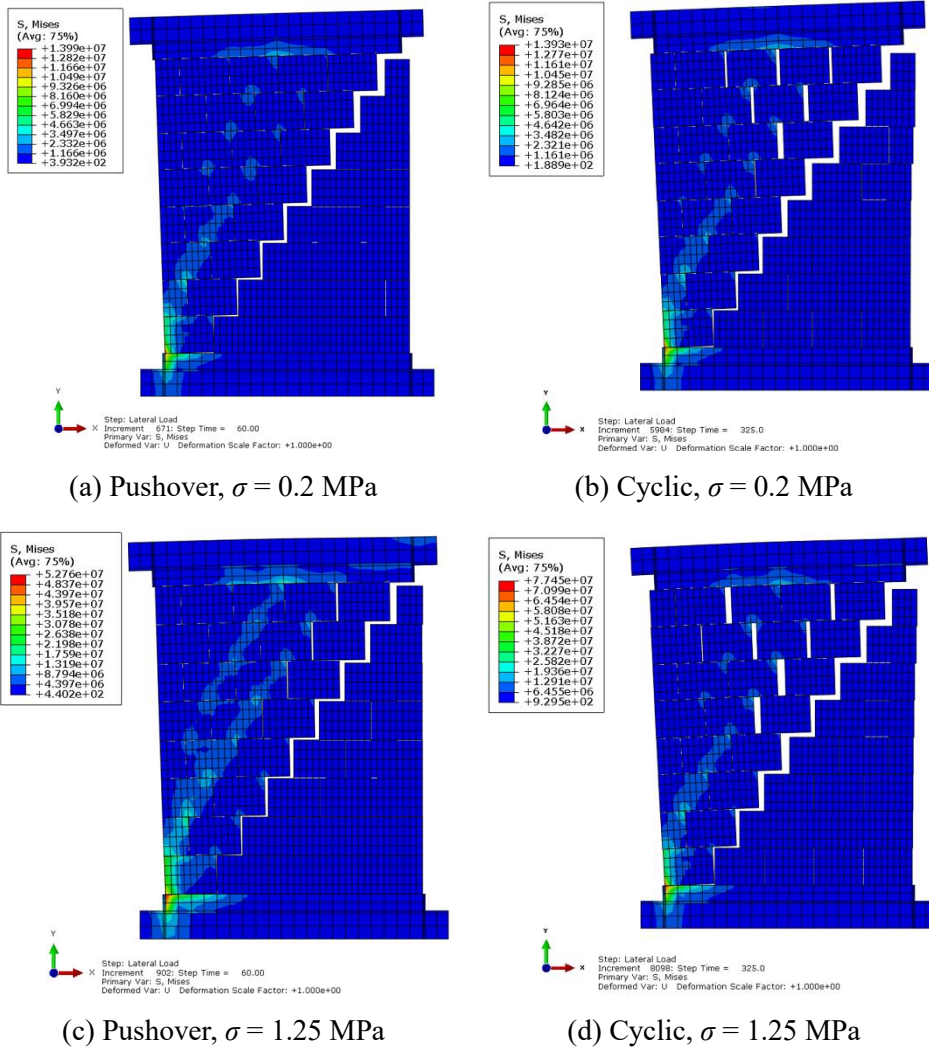


**Figure 6-27** Comparison of failure mechanism by pushover and cyclic analysis under different levels of pre-compression load ( $\sigma$ )

Force-displacement curves of the walls obtained by cyclic and pushover analysis for all pre-compression loads are shown in **Figure 6-28**. Most of main characteristics are detected within an acceptable level.

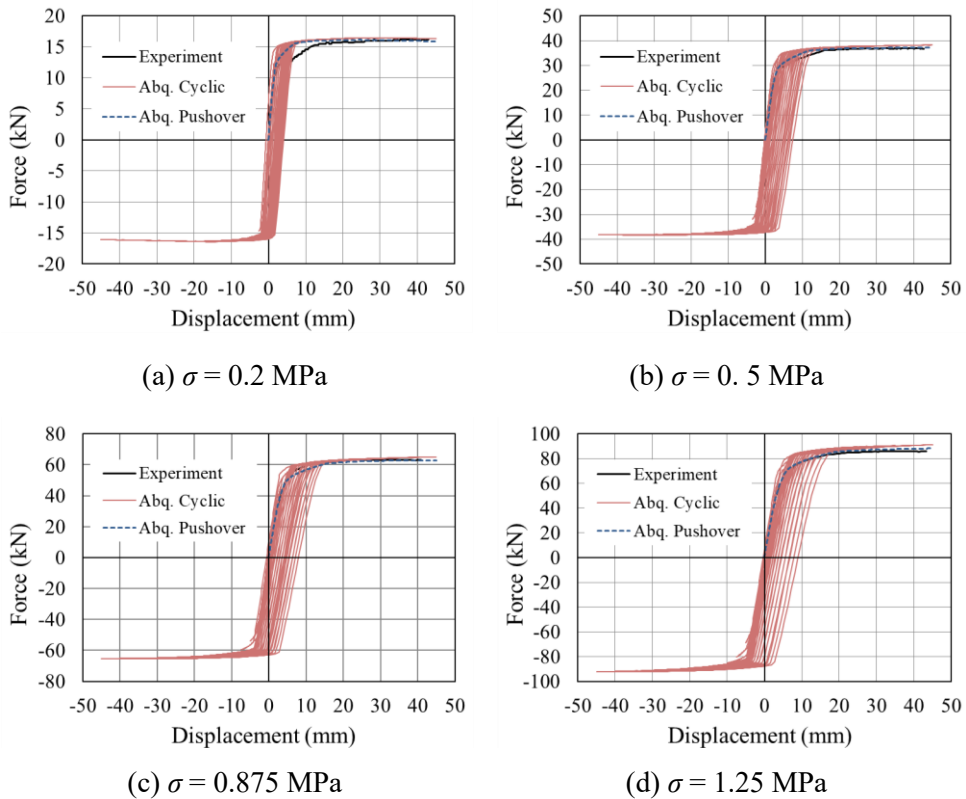


**Figure 6-28** Comparison of pushover and cyclic force-displacement curves under different levels of pre-compression load ( $\sigma$ )

Based on the results, the backbone of hysteresis loops matches well with the pushover curves. Thus, the pushover analysis can appropriately be used as representative of the backbone curve of hysteresis loops. Also, biasing toward the direction of the first lateral load is detected by the model. Delay in recovering

stiffness on both sides can be observed in the graphs and as found in the experimental test the delay in the biased side is smaller. In addition to these advantages, the time and computational cost of performing cyclic analysis are significantly larger than pushover analysis. The required time for performing cyclic analysis on average was 10 times that for pushover analysis. Therefore, in the rest of this study, pushover analysis is considered as the main tool for assessment of wall behavior, and only for a few special cases, the cyclic analysis was performed.

One of the main characteristics of the cyclic behavior is determined by the amount of dissipated energy (hysteresis energy) through each cycle. The higher hysteresis energy means that the structure can absorb higher energy during cyclic excitation. It was obtained for the wall under different levels of pre-compression load by calculating the area enclosed by each hysteresis loop. These values are reported in **Table 6-18**.

**Table 6-18** Cyclic dissipated energy of walls (kN-mm)

Pre-compression load (MPa)			
$\sigma = 0.2$	$\sigma = 0.5$	$\sigma = 0.875$	$\sigma = 1.25$
209.03	885.99	1920.15	3228.90

Note that the obtained cyclic behaviors were not exactly matched with the results of experiments and so the reported values are larger than the experiment. Since the same modeling assumptions were used for all models in this study, it can

be assumed the errors are also the same. So, the values in **Table 6-18** were considered as reference values of URM walls for comparison with results of the retrofitted wall in **Chapter 7**.

## 6.7 Parametric Study

The results of former experimental and numerical studies on masonry walls with mortar-based joints showed that the level of pre-compression load and the aspect ratio are the main parameters that determine the in-plane behavior of the walls. Based on these studies, the failure mechanism for walls with a high aspect ratio and/or under low pre-compression load is mainly flexural failure (rocking). On the other hand, walls with low aspect ratio and/or high pre-compression load is mainly shear failure (diagonal cracking) (Samarasinghe *et al.*, 1981; Anthoine *et al.*, 1995; Zhuge *et al.*, 1996; Schultz *et al.*, 1998; Bosiljkov *et al.*, 2003).

However, there were not many studies on walls with dry-stack joints, which including a large number of historical structures and which are even more sensitive in comparison with mortar-based walls. Therefore, a set of parametric studies have been done in this study, and a summary of results was briefly explained in this section.

Here, the effect of unit size and the aspect ratio (by changing height and width) of the wall was considered as the main factor for parametric study, and the results were compared with the original wall (calibrated model). All assumption for the modeling was the same as the calibrated model.

In the parametric study on the unit size, the width and height of the original wall were maintained as the original wall. Then, three cases were considered for unit size with length (mm)× height (mm) of 100×75 (fine unit), 200×150 (original unit), and 400×300 (large unit) as shown in **Figure 6-29**, and walls were assembled with these stones.

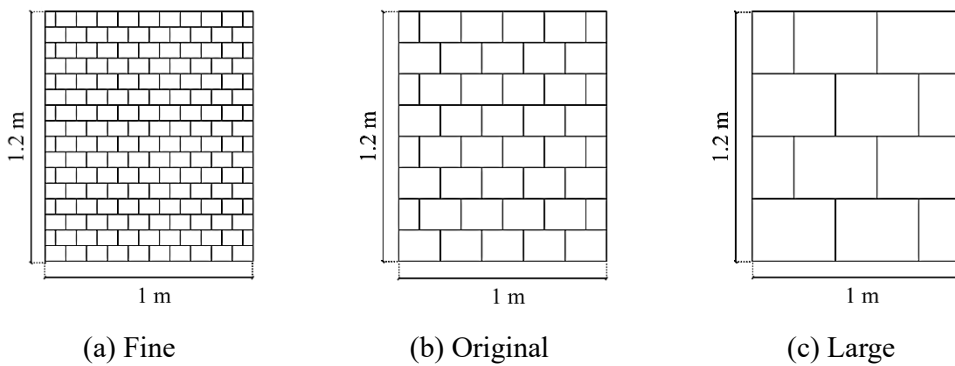
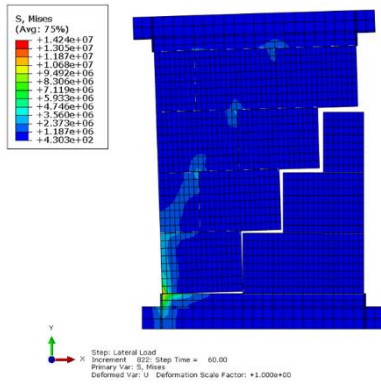
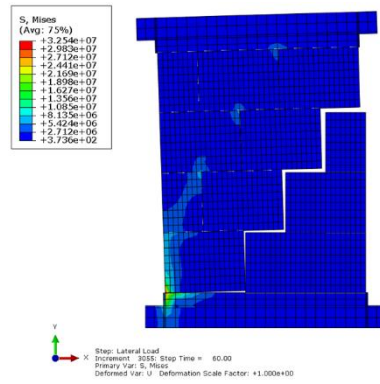


**Figure 6-29** Different size of stone unit in the masonry wall

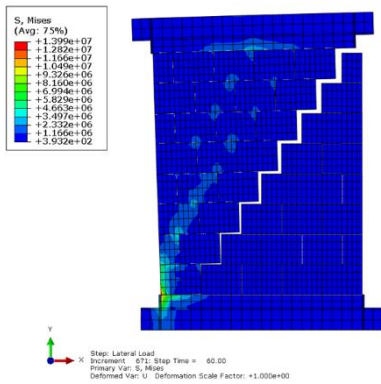
Stress distribution and failure mechanism of walls with different unit sizes are shown in **Figures 6-30 to 6-31**. It can be seen that there is no considerable difference in the stress distribution for different pre-compression loads. Additionally, the failure mechanism for both the fine unit and the large unit was stair-stepped similar to that of walls with the original unit. However, the effect of pre-compression load on the amount of opening of joints for fine mesh is greater than large mesh.



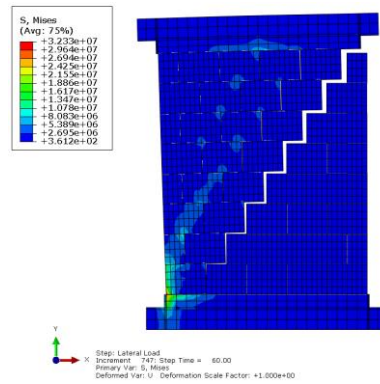
(a) Large stones unit,  $\sigma = 0.2$  MPa



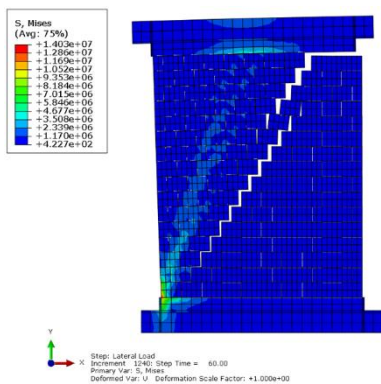
(b) Large stones unit,  $\sigma = 0.5$  MPa



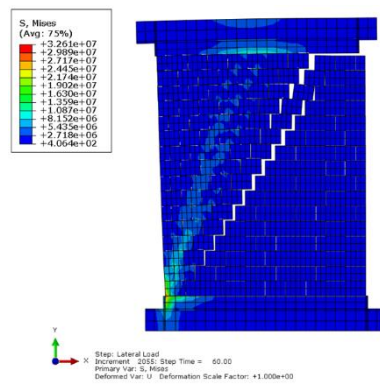
(c) Original stones unit,  $\sigma = 0.2$  MPa



(d) Original stones unit,  $\sigma = 0.5$  MPa

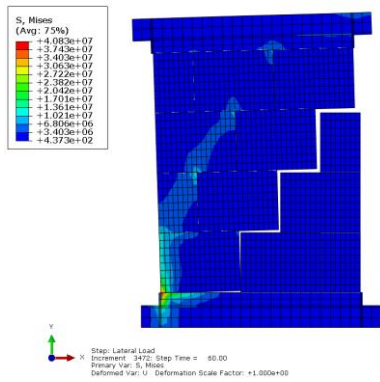


(e) Fine stone unit,  $\sigma = 0.2$  MPa

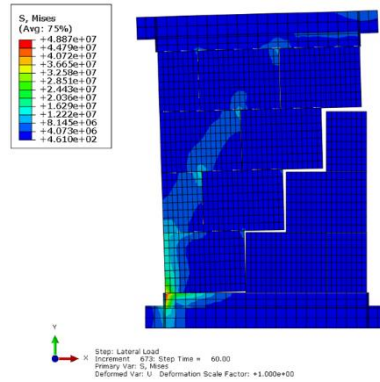


(f) Fine stone unit,  $\sigma = 0.5$  MPa

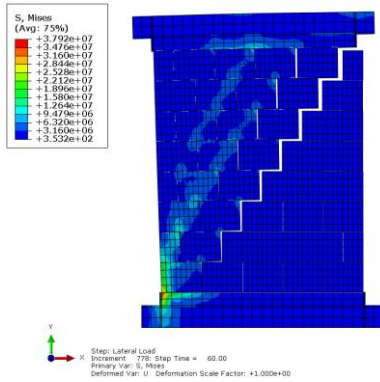
**Figure 6-30** Stress distribution and failure mechanism based on stone unit size under different levels of pre-compression load ( $\sigma = 0.2$  and  $0.5$  MPa)



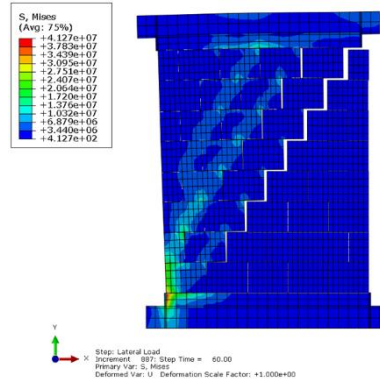
(a) Large stones unit,  $\sigma = 0.875$  MPa



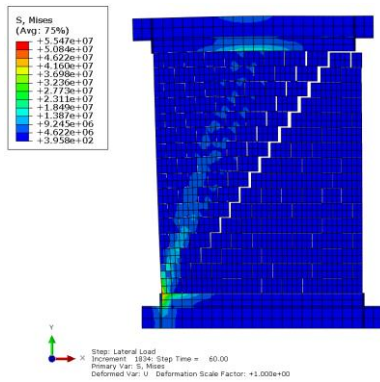
(b) Large stones unit,  $\sigma = 1.25$  MPa



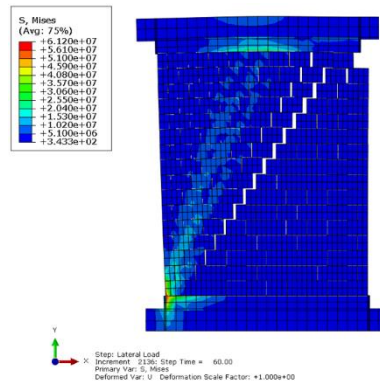
(c) Original stones unit,  $\sigma = 0.875$  MPa



(d) Original stones unit,  $\sigma = 1.25$  MPa



(e) Fine stone unit,  $\sigma = 0.875$  MPa



(f) Fine stone unit,  $\sigma = 1.25$  MPa

**Figure 6-31** Stress distribution and failure mechanism based on stone unit size under different levels of pre-compression load ( $\sigma = 0.875$  and  $1.25$  MPa)

The force-displacement curves of walls with different size units are shown in **Figure 6-32**. It can be seen that both stiffness and strength are increased by increasing the unit size, but the effect is not significant. Based on these results, it seems that unit size is not an influential parameter on the overall behavior of walls with dry-stack joints.

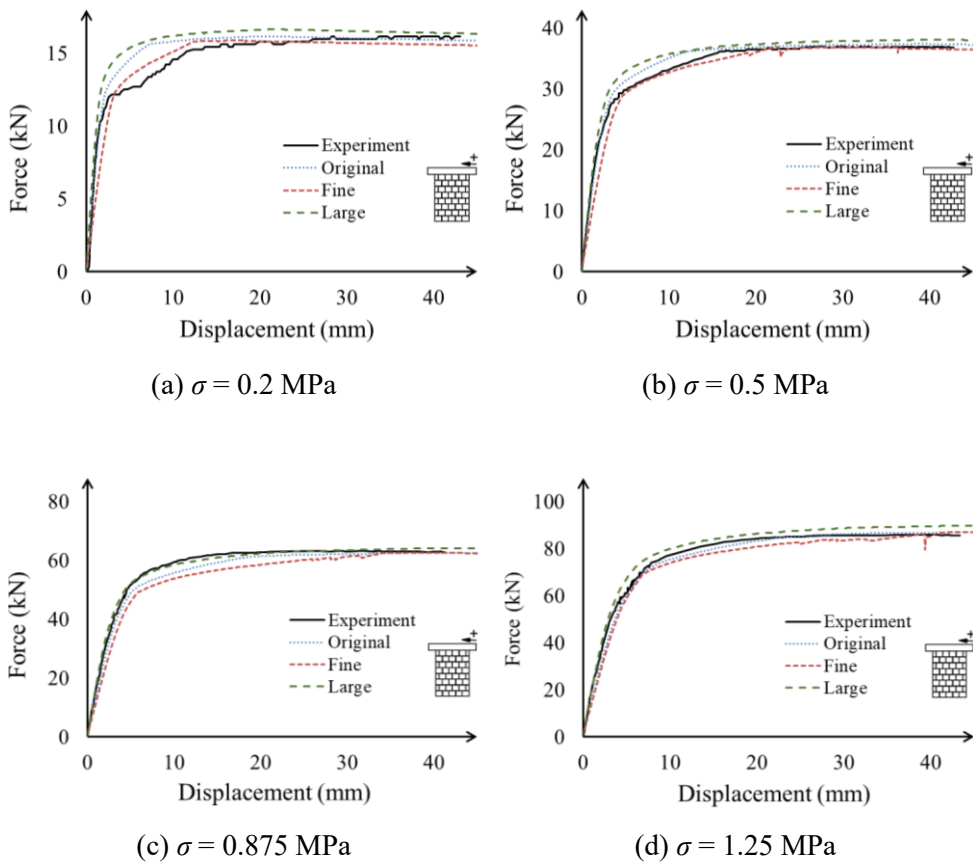


**Figure 6-32** Force-displacement curves for different size of stone unit under different levels of pre-compression load ( $\sigma$ )

The parametric study on the dimension of the wall has been done by changing the width and height of the original walls. For the parametric study, as shown in **Figure 6-33**, 9 cases (including the original wall) were considered to investigate the effects of width, height, and wall-size on the mechanical behavior of the wall. The stress distribution and failure mechanism of all 9 models are shown in **Figures 6-34 to 6-36** and the results are discussed in the following. **Figure 6-34** shows the results of the model with the height same as the original wall but with different widths. Based on the results, the failure mode of the wall was not changed by increasing the width, and the stair-stepped mechanism occurred similar to the original model. In all cases, joints were opened in stair-stepped form along an oblique line (45 degrees) that passing the compressive corner. Therefore, for walls with a width larger than the original wall, the cracks will not reach the top corner. Based on these observations it can be expected that the joints in these walls under cyclic load will be open in form of eccentric inverted V-shape (“/ \”) instead of X-shape stair-stepped.

Results for models with height larger than the original models are shown in **Figures 6-35 to 6-36**. For the taller models with an equal or larger width, the observation was similar to that of the model with original height. For taller models with the same width as the original model, it can be seen that the failure mode was also stair-stepped joint opening. However, crack is reached to the tensile face rather than the top corner, because diagonal cracks always are opened along an oblique line (45 degrees). Therefore, the failure mechanism is more like the diagonal shear failure of deep beams.

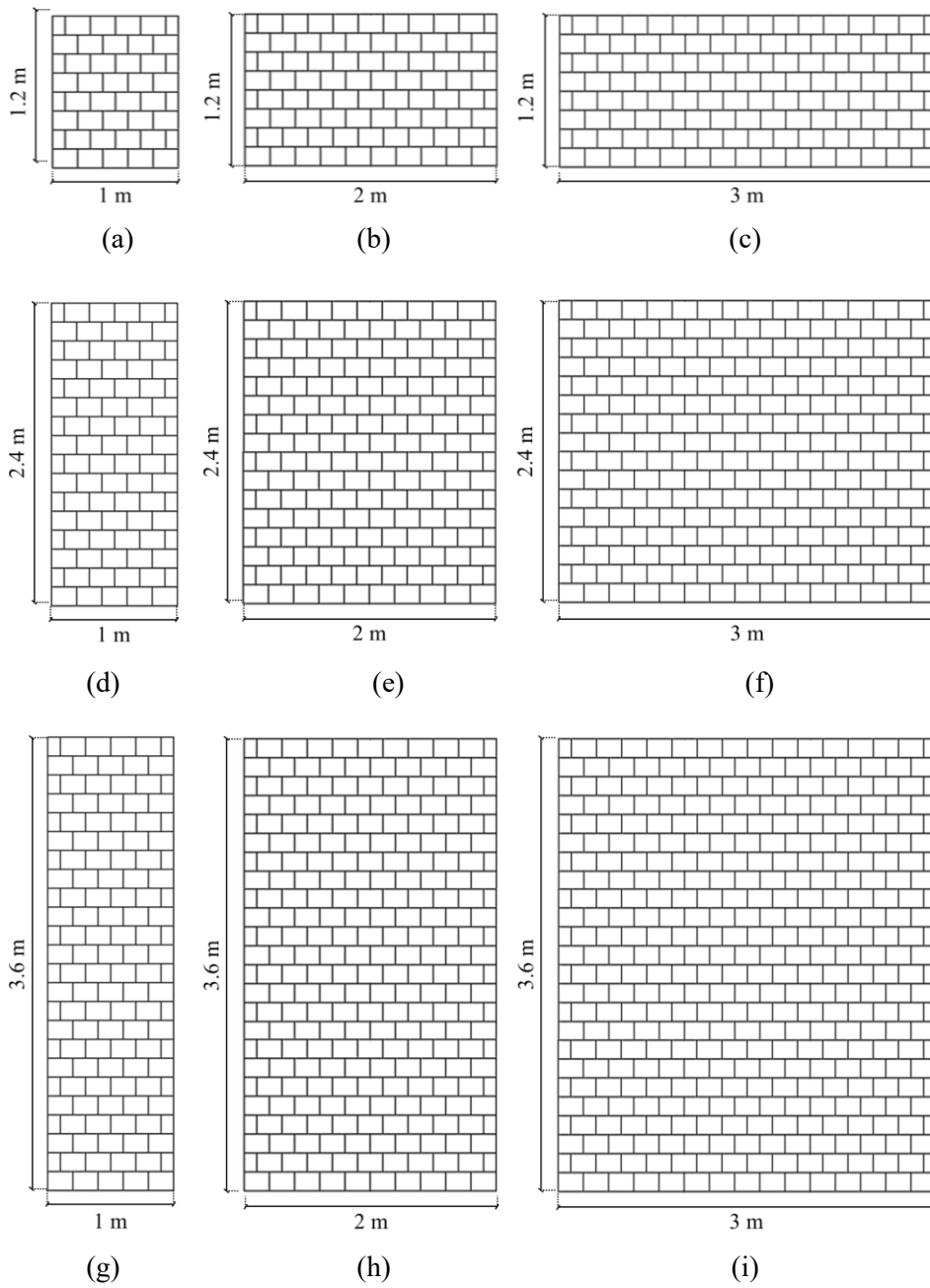
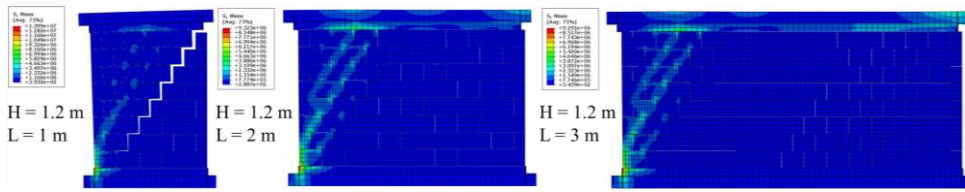
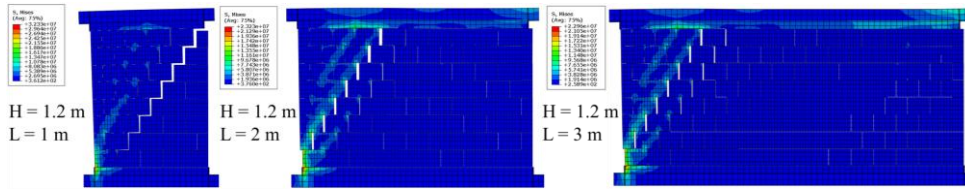


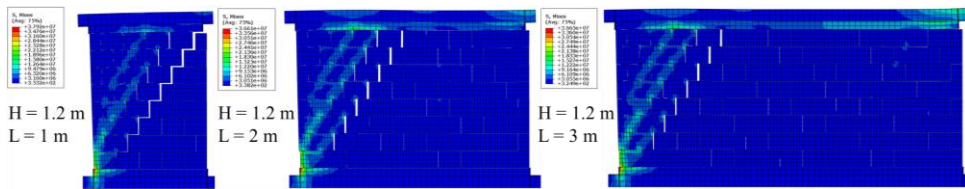
**Figure 6-33** Walls with different aspect ratios for parametric study



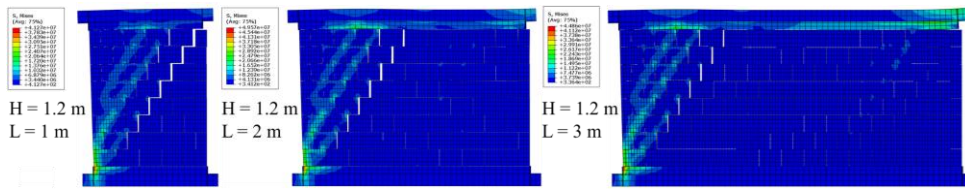
(a)  $\sigma = 0.2 \text{ MPa}$



(b)  $\sigma = 0.5 \text{ MPa}$

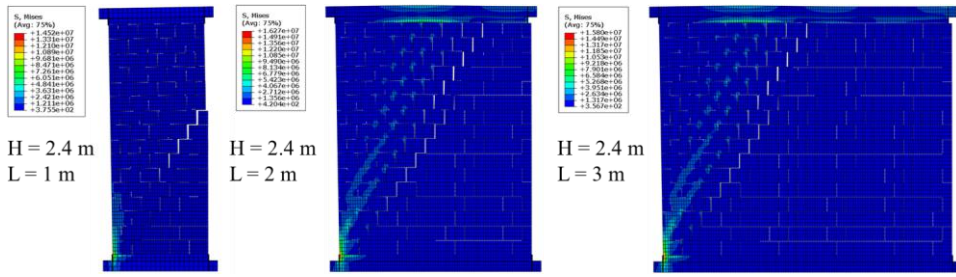


(c)  $\sigma = 0.875 \text{ MPa}$

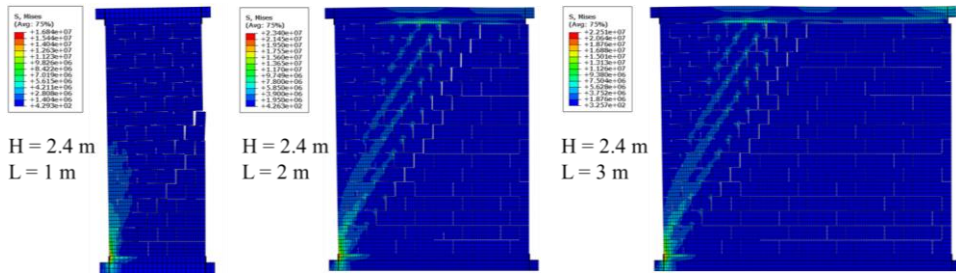


(d)  $\sigma = 1.25 \text{ MPa}$

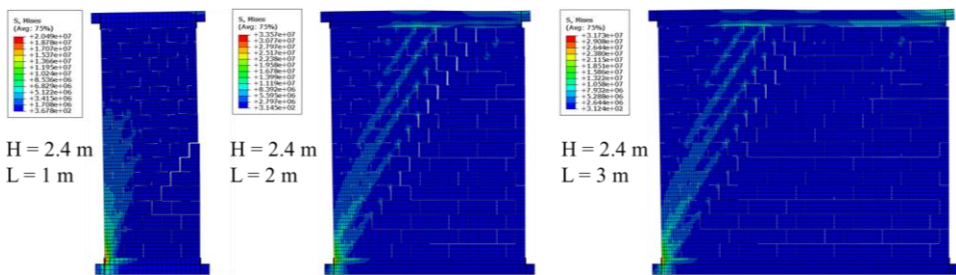
**Figure 6-34** Stress distribution (MPa) and failure mechanism of walls with  $H = 1.2$  (m) and variable  $L$  under different levels of pre-compression load ( $\sigma$ )



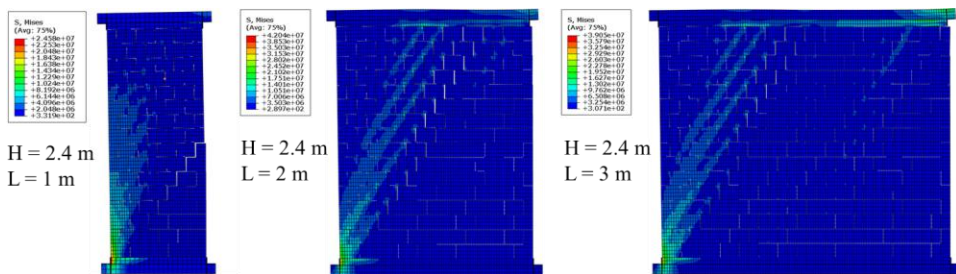
(a)  $\sigma = 0.2 \text{ MPa}$



(b)  $\sigma = 0.5 \text{ MPa}$



(c)  $\sigma = 0.875 \text{ MPa}$



(d)  $\sigma = 1.25 \text{ MPa}$

**Figure 6-35** Stress distribution (MPa) and failure mechanism of walls with  $H = 2.4$  (m) and variable  $L$  under different levels of pre-compression load ( $\sigma$ )

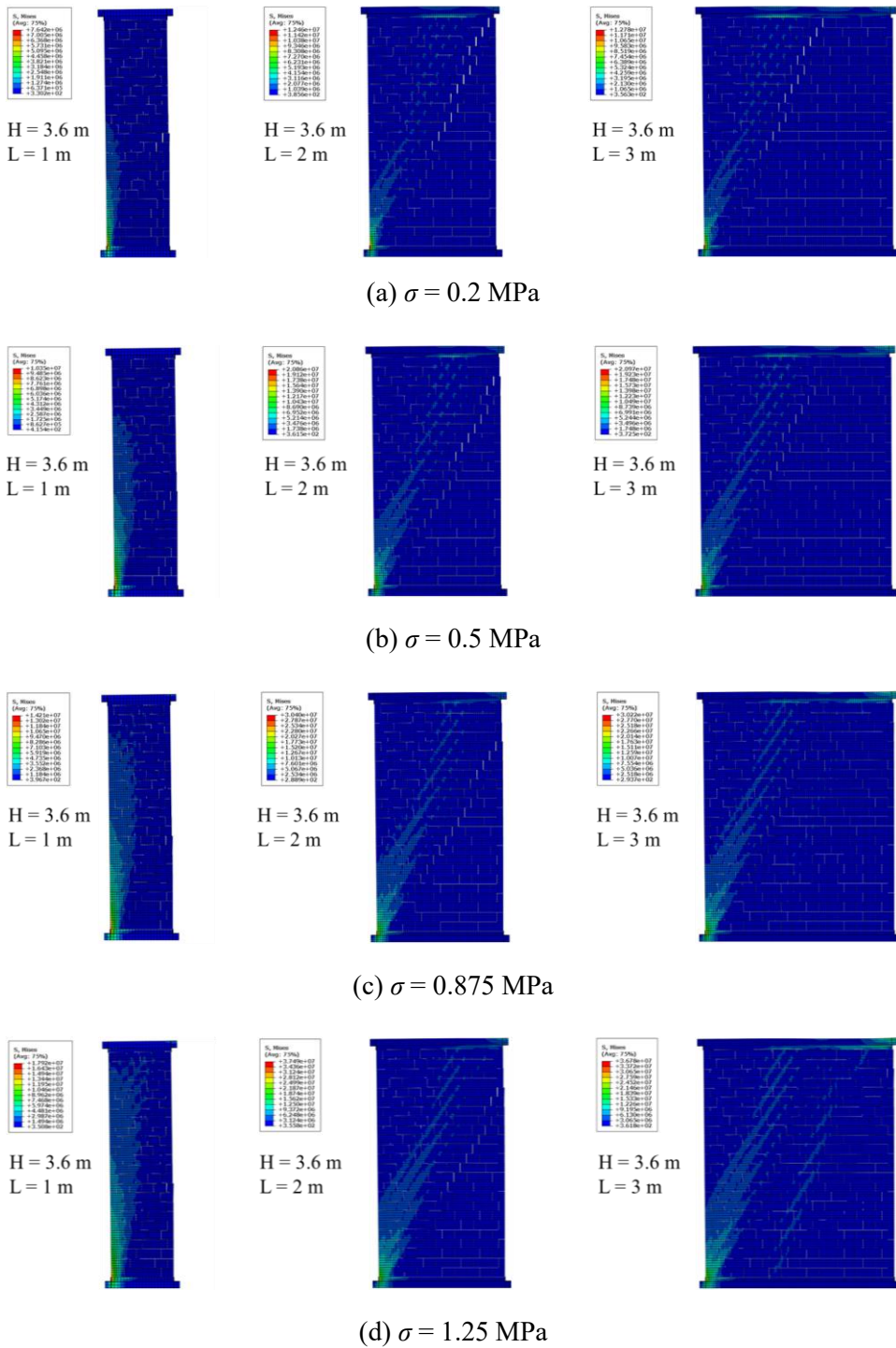
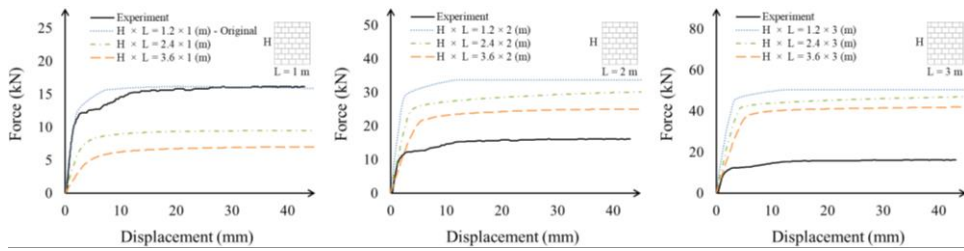


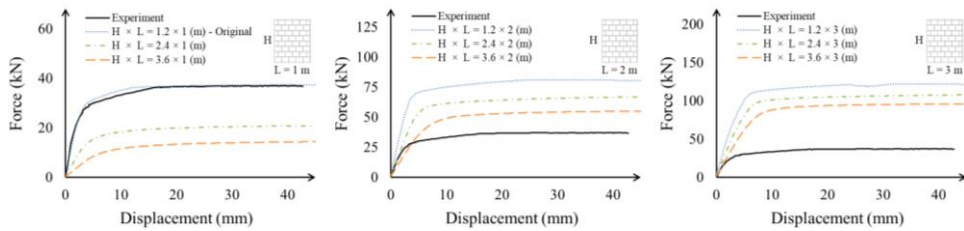
**Figure 6-36** Stress distribution (MPa) and failure mechanism of walls with  $H = 3.6$  (m) and variable  $L$  under different levels of pre-compression load ( $\sigma$ )

The force-displacement curves of walls with different heights and width for different levels of pre-compression load are shown in **Figures 6-37 to 6-38**. Based on the results in **Figure 6-37**, for a wall with a specific width, the stiffness and strengths of the walls are notably reduced by increasing the height. On the other hand, for a wall with a specific height (**Figure 6-38**), stiffness and strength of the wall are significantly increased by increasing the width.

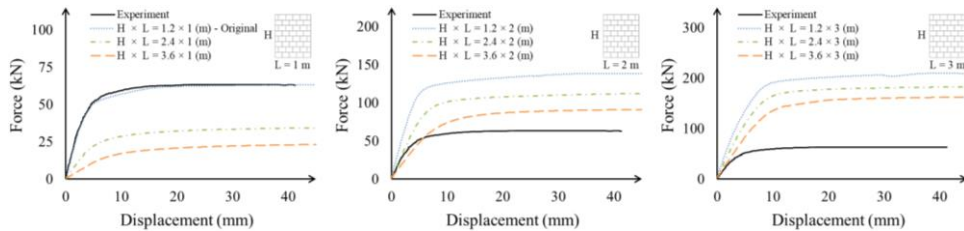
The effect of wall-size can be investigated by analyzing walls with length (m) and height (m) of  $1 \times 1.2$  (original wall),  $2 \times 2.4$ , and  $3 \times 3.6$ . The aspect ratio of the last two cases is the same as the original (i.e.  $1/1.2$ ), while the wall-size is two and three times the original wall, respectively. Based on the failure mechanism shown in **Figures 6-34 to 6-36**, it can be seen that the failure mode is stair-stepped in all cases. However, the amount of joint opening is much smaller for the larger wall. As shown in **Figure 6-39**, the initial stiffness of the walls is the same, but, the strength is quite larger for larger walls. It can be seen that the relationship between and wall-size is almost linear. The reason can be explained by considering the source of strength. In case of failure of dry-stack walls in form of stair-stepped joint opening, the main source of the strength is the weight of the lifted part. Since weight of the lifted part is increased linearly by enlarging wall-size, the strength is also increased almost linearly.



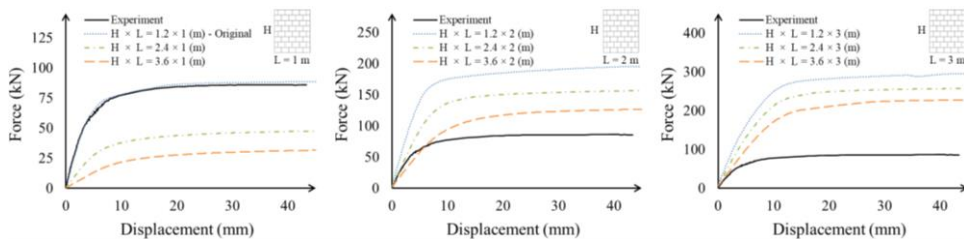
(a)  $\sigma = 0.2$  MPa



(b)  $\sigma = 0.5$  MPa

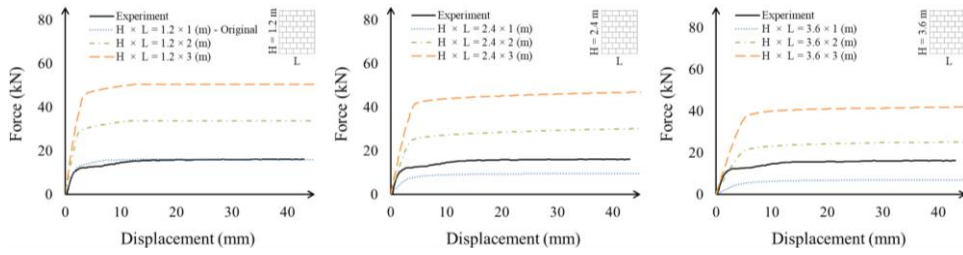


(c)  $\sigma = 0.875$  MPa

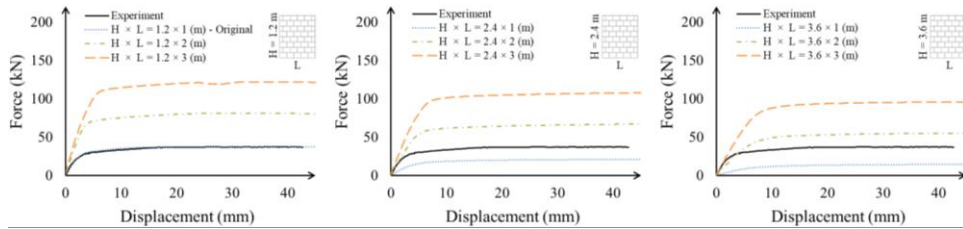


(d)  $\sigma = 1.25$  MPa

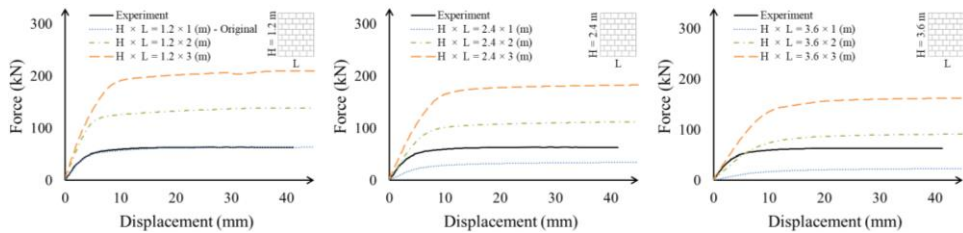
**Figure 6-37** The effect of height on the behavior of walls under different levels of pre-compression load ( $\sigma$ )



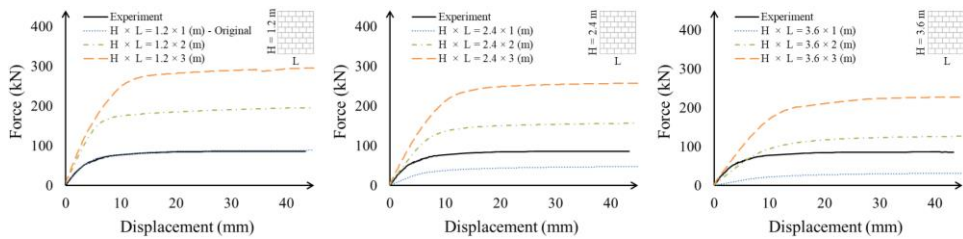
(a)  $\sigma = 0.2$  MPa



(b)  $\sigma = 0.5$  MPa



(c)  $\sigma = 0.875$  MPa



(d)  $\sigma = 1.25$  MPa

**Figure 6-38** The effect of width on the behavior of walls under different levels of pre-compression load ( $\sigma$ )

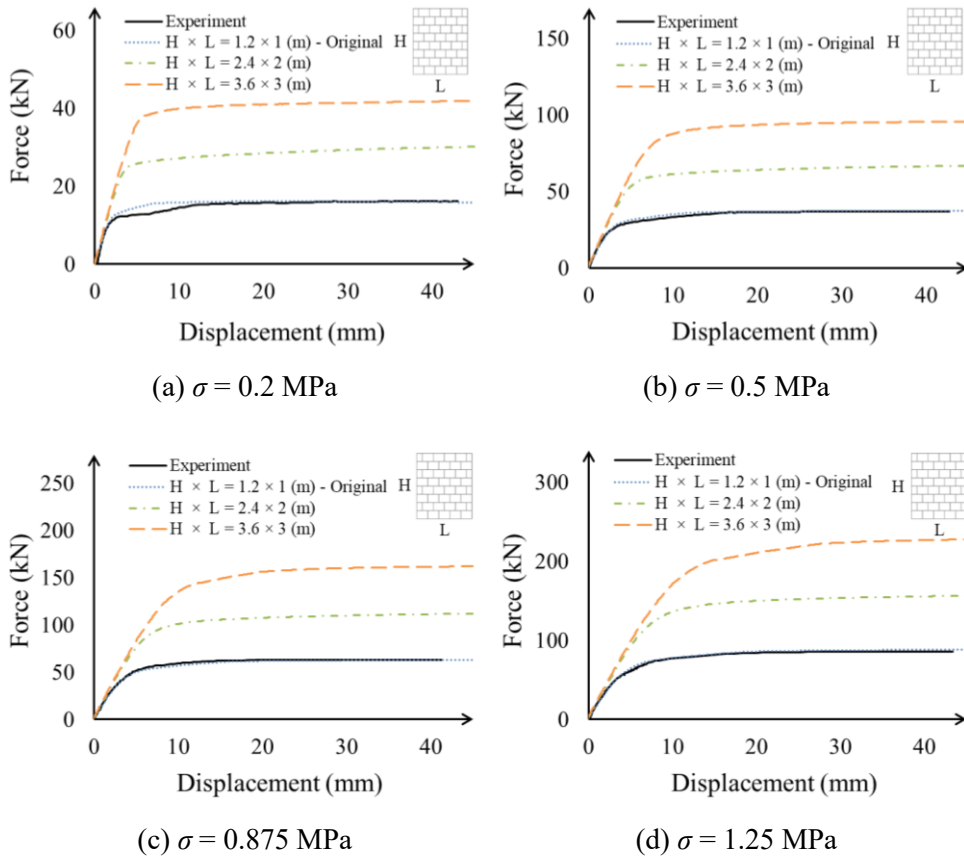


**Figure 6-39** The effect of wall-size on the behavior of walls under different levels of pre-compression load ( $\sigma$ )

## 6.8 Summary

In this chapter, behavior of URM walls with dry-stack joints was investigated by using numerical modeling. The experimental study by Vasconcelos (2005) was selected for the validation of numerical models. ABAQUS software, one of the most powerful numerical tools, was used to make the 2D finite element models, and pushover analyses were performed.

By calibrating a set of parameters, the validity of the numerical model was checked by comparing its results with the experiment. Results were compared in terms of mechanical behavior including stiffness, strength, and failure mechanism. A comparison study of mechanical behavior under different levels of pre-compressions showed that the results of the numerical model matched with that of the experiments with a high level of accuracy. The sensitivity of the calibrated model was analyzed for the main parameters, the effect of 3D modeling and cyclic analysis, and each case was discussed in detail. In addition, a set of parametric studies have been done on the unit size and aspect ratio of the wall to have a more comprehensive investigation. Based on the results, the wall with a larger unit size had higher stiffness and strength. However, the changes were not significant, and also the failure mechanism was not changed. On the other hand, mechanical behavior was considerably affected by the changing aspect ratio and wall-size. The results show that by increasing the height of the wall stiffness and strength reduce, while by increasing the width of the wall they increase substantially. It was found that by increasing wall-size, and keeping aspect ratio constant, the strength is almost linearly increased, while stiffness is not changed much considerably.

## **Chapter 7. FEM Analysis of Stone Masonry Walls Retrofitted by Rebars**

Seismic retrofitting of historical masonry structures is essential in terms of the reduction of potential damage to protect the valuable architectural and cultural features of the buildings. Among different retrofitting techniques, one of the most appropriate methods is selected in this study, and its performance is examined by FEM analysis. This method which has received great attention in the past decades includes rebars with different materials embedded in the stone wall. This method has many advantages over other techniques, including ease of application, availability, and preservation of the aesthetic appearance of the building. In this chapter, the seismic performance of the stone masonry wall strengthened with the different types of rebars are analyzed, and the most proper material and arrangement are presented based on the results of analyses.

## 7.1 Proposed Retrofit Technique

In the last decades, a better understanding of the seismic behavior of masonry and historical structures has been obtained through post-earthquake surveys and analytical studies. Accordingly, many advanced methods and techniques have been developed for retrofitting masonry structures that improve their seismic performance. Besides, the traditional systems can be upgraded by some innovative methods to increase the ductility and energy dissipation of the structure (Paganoni and D’Ayala 2015). For historical structures, these approaches can be utilized by considering their advantages and shortcomings as well as the effect that they have on the appearance of the structure. Among all methods stated in **Chapter 4**, rebars as a type of reinforcement have been successfully applied for many years in different structures so far. Therefore the numerical studies in this chapter attempt to represent the mechanical behavior of the dry-stack stone masonry wall strengthened with rebars including different materials and arrangements.

As the appearance of the structure is one of the most important issues in retrofitting historical structures, the simulations were conducted based on this assumption that the reinforcing rebars were inserted from the sides of the wall without any intervention on the aesthetic faces. Using this method to increase the strength of dry-stack stone walls can be a more appropriate and convenient technique due to anchoring or aesthetics requirements.

The anchoring process includes inserting the rebars from the side of the wall and anchors them to the supporting or side members by embedding the end part of the rebar or using an appropriate anchorage device. The embedment length can be calculated theoretically or investigated by several experimental tests. This method does not require any surface preparation work and takes minimal installation time comparing with some other techniques.

There are many types of anchorage devices used for historical masonry structures. Some of the traditional anchorage devices used for historical masonry structures in different shapes and sizes are shown in **Figure 7-1**. It can be observed in **Figure 7-2** that they are quite visible on the facade of the building which could be hidden by architectural and artistic manipulations to a certain extent.



(a) Shambles cross

(b) S Plate

(c) Cartwheel

(d) Long Cross

**Figure 7-1** Different shapes of traditional anchorage used for HURM buildings  
(Adapted from Redgwick, 2017)



**Figure 7-2** Traditional anchorage used for HURM buildings (Adapted from Palmer, 2017)

Contrary to the traditional method, in the proposed method the anchorage devices are located at the top and side of the wall instead of the face (**Figure 7-3**). They can be hidden in the roof or covered by adding a row of the same material used for masonry constructions to maintain the aesthetic form of the building.

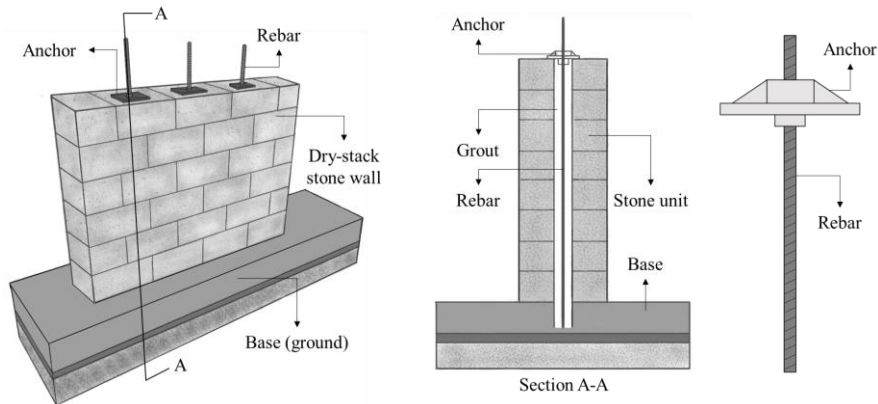


**Figure 7-3** Detail of embedding system

In the following sections, details of the retrofitting program including material properties and arrangement of rebars inserted in the stones are described.

## **7.2 Material Properties**

The study of available materials with considerably high quality and different geometry for reinforcement bars is an interesting field of engineering today. There are plenty of materials that are used for manufacturing reinforcement. Each material can be used based on its advantages including availability, durability, and cost. However, in the case of retrofitting historical structures, the current stage of damage and the constituent material of the structure are also crucial factors in selecting the most proper material to protect the building from any kind of erosion.

Stainless steel as a group of iron-based alloys has shown excellent corrosion resistance and high strength at high temperatures. On the other hand, titanium has a lower modulus of elasticity than mild steel and stainless steel, although it has large strength and lower density, thermal conductivity, and coefficient of thermal expansion. Furthermore, composites made of two or more materials (phases) of different nature are preferable for structural strengthening due to their excellent properties and availability. Among composites, fiber-reinforced polymer (FRP) is available in various forms (bars, strips, sheets) and materials (glass, carbon, and aramid). FRP has high tensile strength and high corrosion and magnetic resistance and is a lightweight material. This material is also suitable for retrofitting historical construction where the aesthetic of original structures needs to be preserved or where

strengthening with traditional techniques cannot be effectively employed. Compared with steel bars, which are widely used in practice, titanium is an effective and superior material for use in rehabilitation. In the matter of cost, stainless steel has a lower initial material cost than FRP. In contrast, the cost of installation and maintenance of FRP is less than stainless steel and titanium in the long run, which makes it more suitable to use for a lower life cycle cost overall. This matter is more important in terms of preservation and conservation projects.

In this study, the performance of walls retrofitted by inserted rebars with stainless steel (SS), titanium (Ti), and FRP materials as the most commonly used materials was investigated. **Table 7-1** indicates the properties of each material that were investigated based on the previous experimental studies. Generally, FRP composites are made by using carbon fibers, aramid fibers, and glass fibers. Carbon polymers can be made based on demands in two different forms including high-modulus (CFRP1) and high-strength (CFRP2) polymers. In the same way, FRP made by glass can be divided into two groups named E-glass (EGFRP) and S-glass (SGFRP) polymers (Islam, 2008). The polymer made by aramid is named AFRP in this study. In the following numerical analyses, all types of FRPs mentioned in the table are used.

**Table 7-1** Material property of rebars ( $d = 6$  mm) for retrofitting stone wall

Material		$E$ (GPa)	$F_y$ (MPa)	
Stainless steel (Shrestha <i>et al.</i> , 2011)		200	667	
Titanium (Yavartanoo <i>et al.</i> , 2020)		70.6	363.4	
FRP (Islam, 2008)	Carbon	High-modulus	390-760	2400-3400
		High-strength	240-280	4100-5100
	Glass	E-glass	70-80	2000-3500
		S-glass	85-90	3500-4800
Aramid		62-180	3600-3800	

**Figure 7-4** shows the stress-strain relationship of the different materials mentioned in the table. According to this figure, FRPs have higher strength than stainless steel and titanium. They exhibit a linear elastic behavior up to the strength, and then suddenly fail due to their brittle nature. On the other hand, stainless steel and titanium exhibit a large ductility before failure. In this study, all these material properties were examined to find the most efficient cases in terms of stiffness, strength, and ductility.

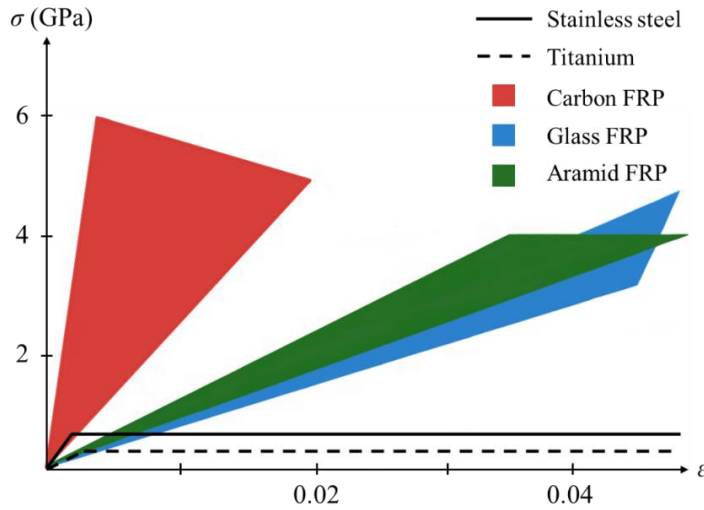


**Figure 7-4** Stress-strain diagrams for different materials (Redrawn based on Islam, 2008)

In the rest of this study, high modulus carbon, high strength carbon, E-glass, S-glass, and aramid fiber polymers are recalled as CFRP1, CFRP2, EGFRP, SGFRP, and AFRP, respectively.

### 7.3 Numerical Modeling Assumptions

In order to examine the retrofit technique, FEM models were made by adding rebars to the model that was calibrated in **Chapter 6**. Therefore, essential parameters including stone material, joint behavior, analysis procedure, and boundary conditions are exactly similar to the calibrated model. Rebars were modeled as a line geometry and discretized by T2D2 element, which is a truss element with 2 nodes (linear shape function) in 2D space. In practice, the inserted rebars should be jointed to the stones by a proper adhesive material such as resin epoxy or cement-based grouts, and this

connection is commonly called “bond”. The behavior of the bond is governed by the properties of rebars, stones and adhesive material and strength of stone-adhesive and rebar-adhesive interfaces. In this study, it was assumed that the strength of the adhesive material as well as stone-adhesive and rebar-adhesive interfaces are larger than both rebars and stones. It means that the bond behavior is determined only by the properties of rebars and stones, and other failure modes are ignored. In this way, rebars are placed inside stones by using “Embedded region” constraint of the software.

The material properties of titanium and stainless steel were defined as linear elastic - perfect plastic behavior. For FRP materials, elastic-brittle behavior was modeled as a linear elastic up to the strength ( $F_y$ ) followed by a linear softening plastic behavior to a defined reduced strength ( $F_r$ ) to model the rupture. The software automatically considers a perfect plastic behavior for the strain larger than the corresponding strain at the defined reduced strength ( $\varepsilon_r$ ). The slope of the linear softening plastic part was defined by  $F_y$  and its corresponding strain ( $\varepsilon_y$ ),  $F_r$  and  $\varepsilon_r$ . The values of  $F_r$  and  $\varepsilon_r$  are adjusted based on  $F_y$  and  $\varepsilon_y$  to be a logical representation of damaged material and also to avoid numerical instability. Therefore, a set of primary analyses have been done for this issue. Based on the results,  $F_r$  and  $\varepsilon_r$  were defined as  $0.001F_y$  and  $\varepsilon_y + 0.001$ , respectively, and were used in the main analyses.

## 7.4 Retrofitting Program

The retrofitting program contains the investigations of different arrangements of rebars with the selected types of material properties under different levels of pre-compression load. Three types are considered for the arrangement of rebars including horizontal, vertical, and diagonal. Details and results of each case are discussed in the following subsections.

### 7.4.1 Horizontal rebar models

In the first type of arrangement, rebars were placed horizontally in the stone wall in different positions. All rebars had the same length as the width of the wall. Different arrangements were examined by changing the number and position of rebars along with the height of the wall as shown in **Figure 7-5** and values of specified spacing in the figure are reported in **Table 7-2**. As shown in the table, a specific name was assigned to each model based on the number of rebars. For instance, HR1-2 model is horizontal arrangement type 1 with 2 rebars.

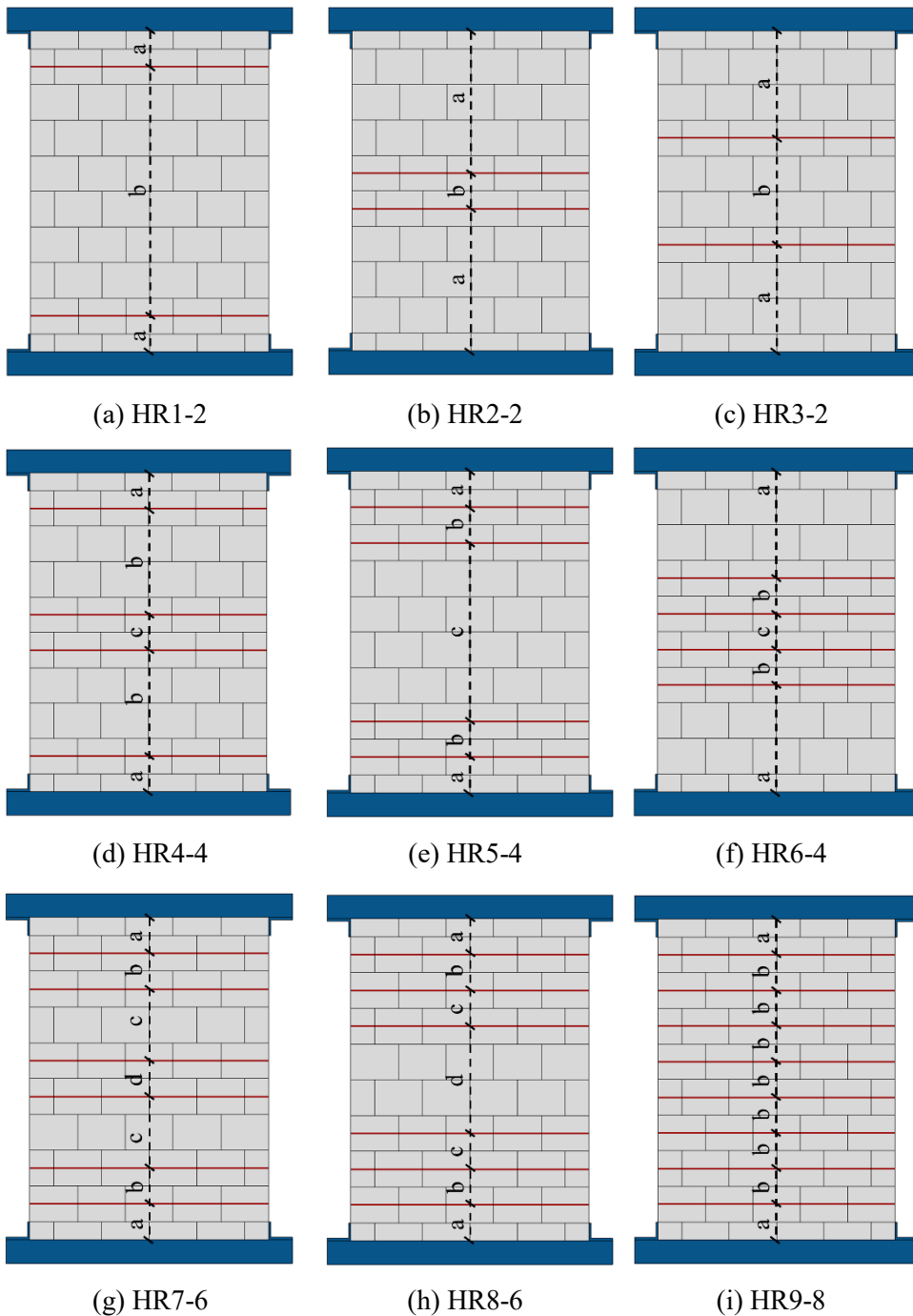


**Figure 7-5** Horizontal arrangement of rebars in the stone masonry wall

**Table 7-2** Details of finite element models strengthen with horizontal rebars

Type	Model	No. of bars	Spaces
1	HR1-2	2	$a = 15 \text{ cm}, b = 105 \text{ cm}$
2	HR2-2	2	$a = 60 \text{ cm}, b = 15 \text{ cm}$
3	HR3-2	2	$a = 45 \text{ cm}, b = 45 \text{ cm}$
4	HR4-4	4	$a = 15 \text{ cm}, b = 45 \text{ cm}, c = 15 \text{ cm}$
5	HR5-4	4	$a = 15 \text{ cm}, b = 15 \text{ cm}, c = 75 \text{ cm}$
6	HR6-4	4	$a = 45 \text{ cm}, b = 15 \text{ cm}, c = 15 \text{ cm}$
7	HR7-6	6	$a = 15 \text{ cm}, b = 15 \text{ cm}, c = 30 \text{ cm}, d = 15 \text{ cm}$
8	HR8-6	6	$a = 15 \text{ cm}, b = 15 \text{ cm}, c = 15 \text{ cm}, d = 45 \text{ cm}$
9	HR9-8	8	$a = 15 \text{ cm}, b = 15 \text{ cm}$

The force-displacement curves of the wall with horizontal rebars are shown in **Figure 7-6**. It can be seen that there is no considerable enhancement by this method in any of the arrangements. Although there is little improvement in the strength of the wall under low pre-compression load ( $\sigma = 0.2 \text{ MPa}$ ), the effect is much smaller under higher pre-compression loads. Because the horizontal rebars do not change the tensile strength at horizontal joints which tend to be open under lateral load. As a result, it cannot improve the behavior of the wall. Failure mechanisms of the walls with horizontal rebars are shown in **Figures 7-7** and **7-8**. It can be seen that, except HR1-2 model that had stair-stepped failure mode, in all other cases failure mode was in form of a combination of horizontal sliding and flexural (rocking) failure. But the

contribution of horizontal sliding failure was less under higher pre-compression loads because of larger (frictional) shear strength. Since horizontal rebars add tensile strength to vertical joints, flexural (rocking) failure mode was observed instead of stair-stepped joint opening. Based on the results, addition of horizontally arranged rebars was considered an ineffective method.

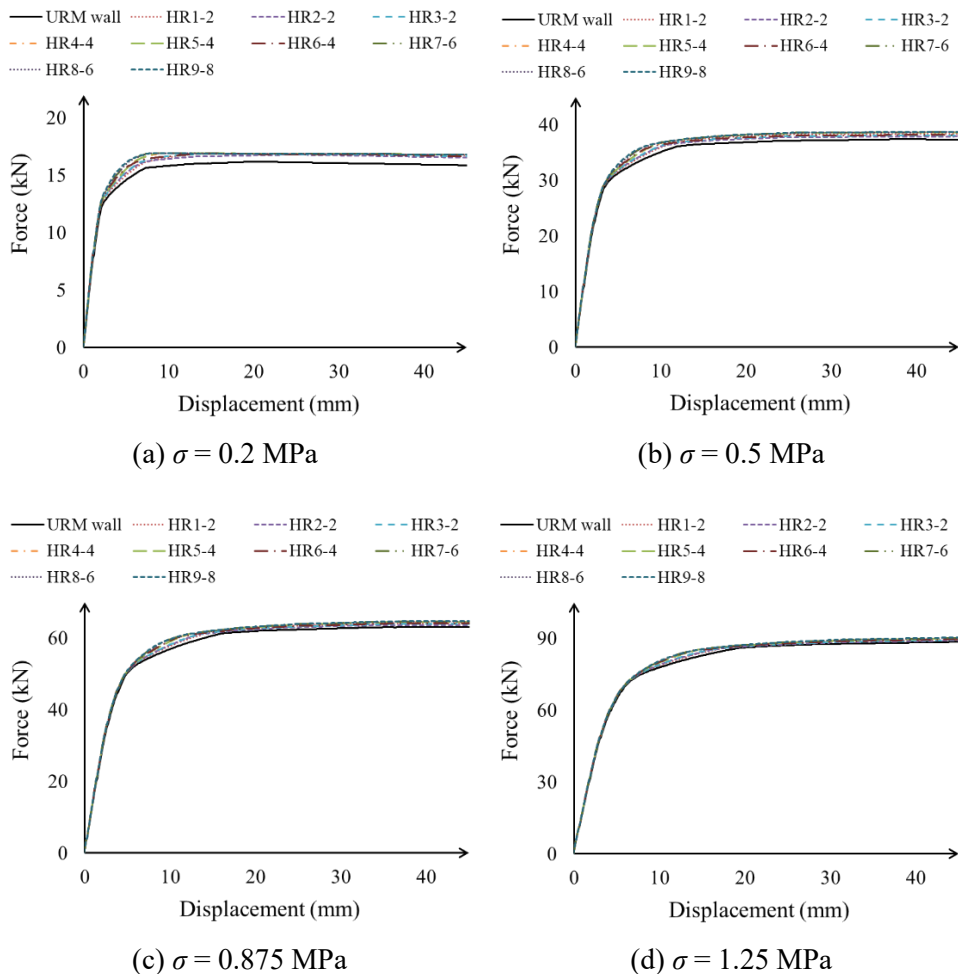


**Figure 7-6** Force-displacement curve of walls with horizontal stainless steel rebars under different levels of pre-compression load ( $\sigma$ )

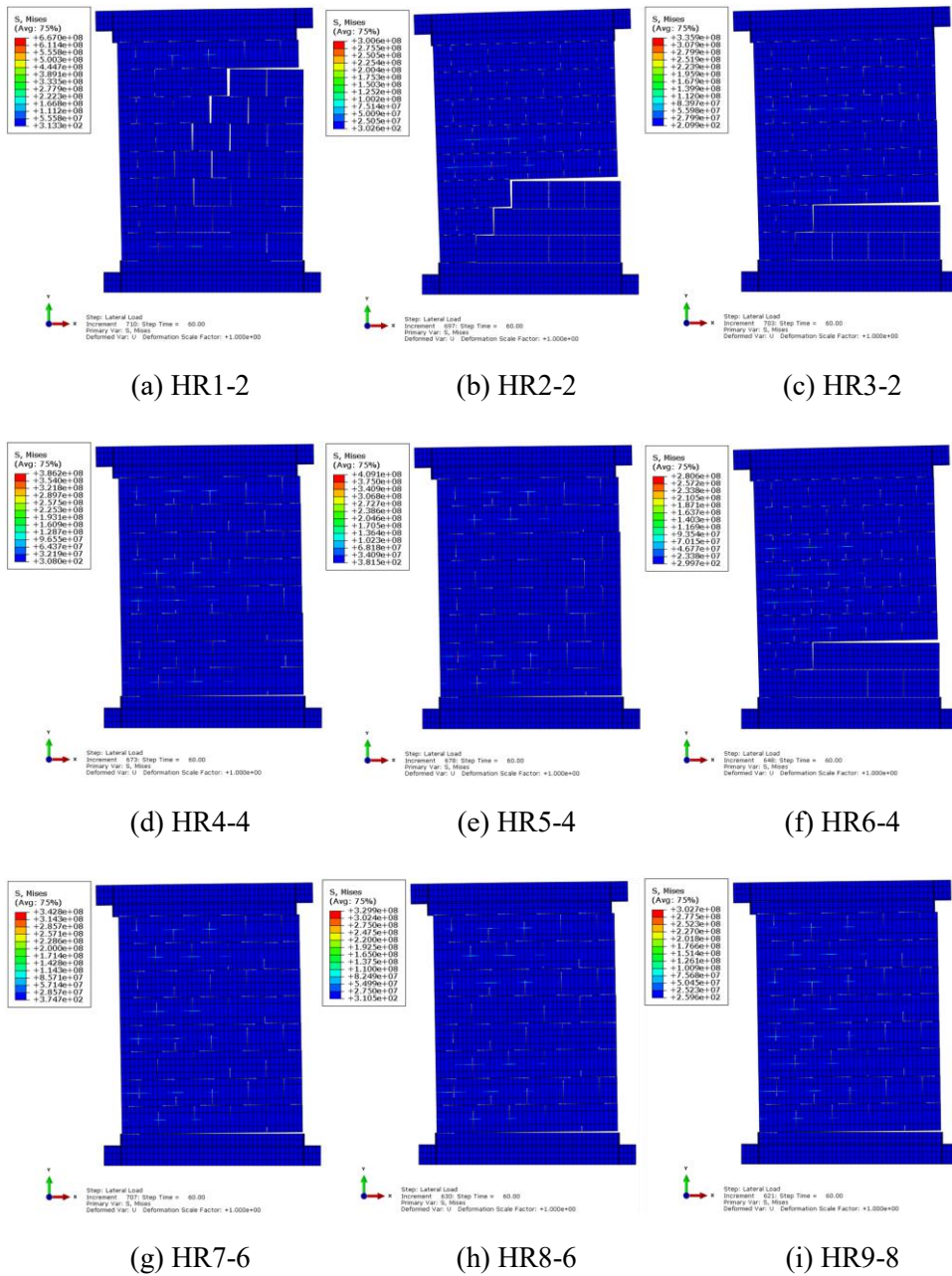


Figure 7-7 Failure mechanism of walls with horizontal stainless steel rebars,  $\sigma = 0.2$  MPa

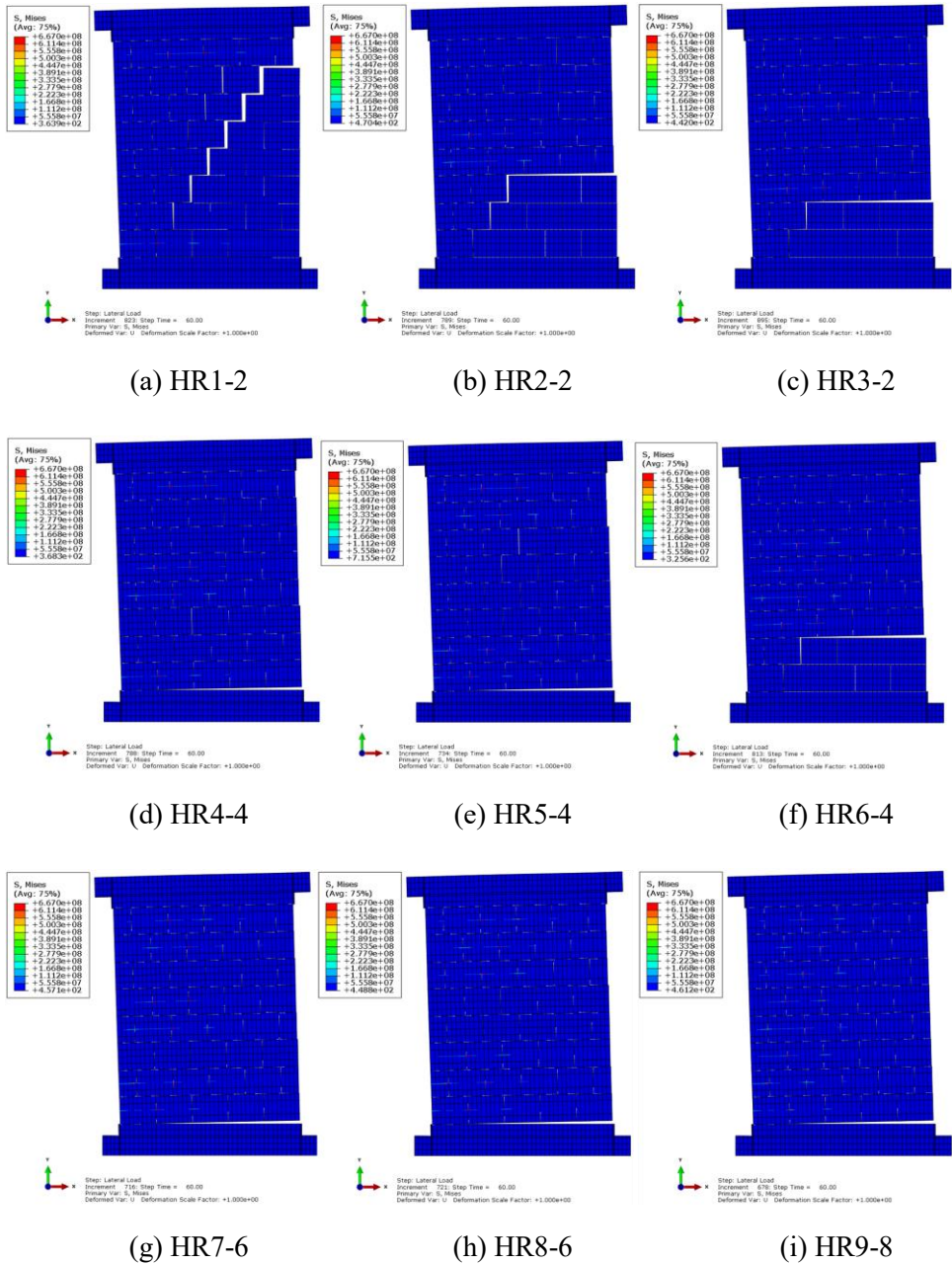
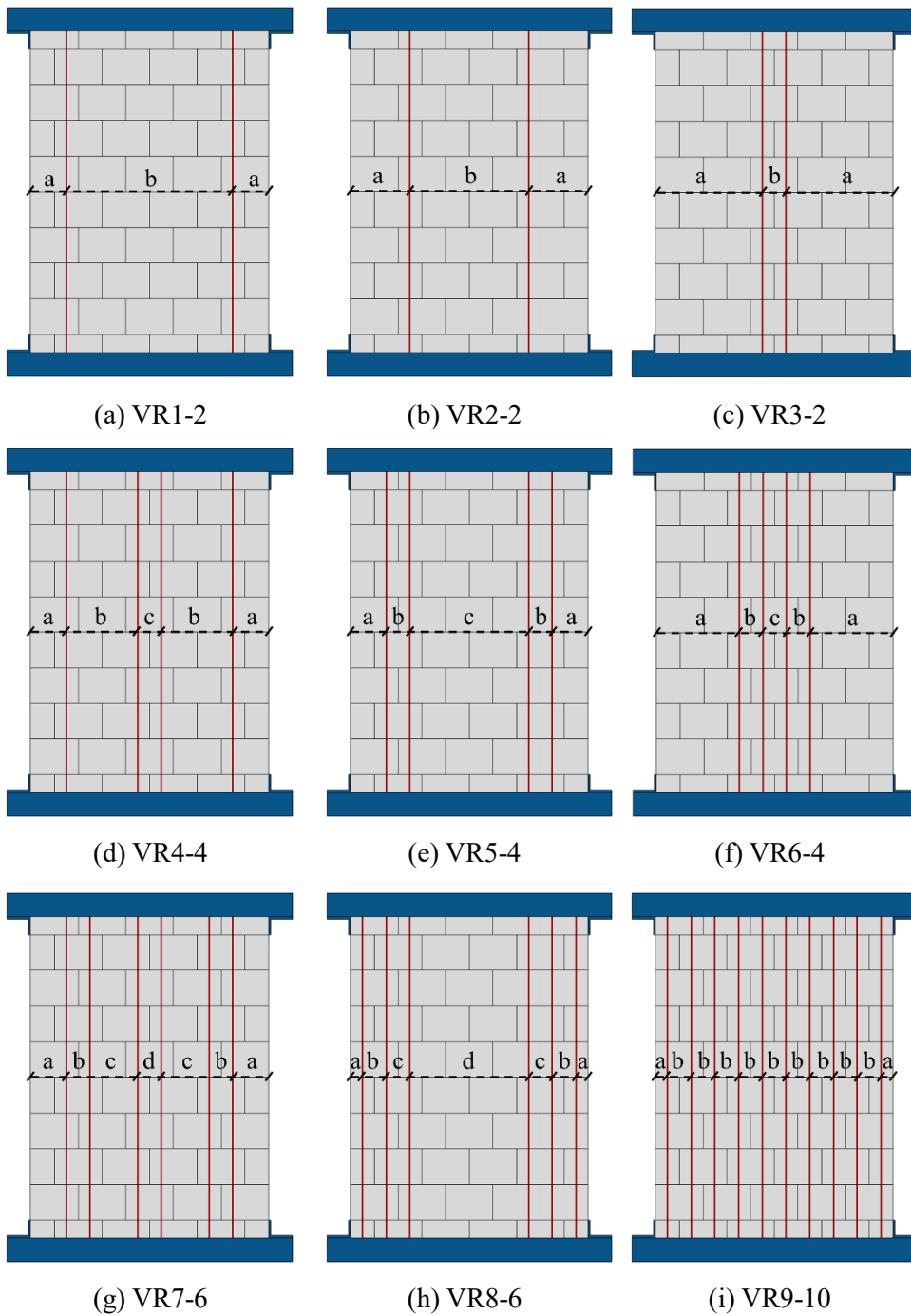


Figure 7-8 Failure mechanism of walls with horizontal stainless steel rebars,  $\sigma = 1.25$  MPa

### 7.4.2 Vertical rebar models

In the second type of arrangement, rebars were placed vertically in the stone wall in different positions. All rebars had the same length as the height of the wall. Different arrangements were examined by changing the number and position of rebars along with the width of the wall as shown in **Figure 7-9**, and values of specified spacing in the figure are reported in **Table 7-3**. As shown in the table, a specific name was assigned to each model based on the number of rebars. For instance, VR1-2 model is vertical arrangement type 1 with 2 rebars. In the following, the mechanical behavior of retrofitted walls by vertical rebars with stainless steel, titanium, and FRP materials under different levels of pre-compression load is discussed.



**Figure 7-9** Vertical arrangement of rebars in the stone masonry wall

**Table 7-3** Details of finite element models strengthen with vertical rebars

Type	Model	No. of bars	Spaces
1	VR1-2	2	$a = 15 \text{ cm}, b = 70 \text{ cm}$
2	VR2-2	2	$a = 25 \text{ cm}, b = 50 \text{ cm}$
3	VR3-2	2	$a = 45 \text{ cm}, b = 10 \text{ cm}$
4	VR4-4	4	$a = 15 \text{ cm}, b = 30 \text{ cm}, c = 10 \text{ cm}$
5	VR5-4	4	$a = 15 \text{ cm}, b = 10 \text{ cm}, c = 50 \text{ cm}$
6	VR6-4	4	$a = 35 \text{ cm}, b = 10 \text{ cm}, c = 10 \text{ cm}$
7	VR7-6	6	$a = 15 \text{ cm}, b = 10 \text{ cm}, c = 15 \text{ cm}, d = 10 \text{ cm}$
8	VR8-6	6	$a = 15 \text{ cm}, b = 10 \text{ cm}, c = 10 \text{ cm}, d = 30 \text{ cm}$
9	VR9-10	10	$a = 5 \text{ cm}, b = 10 \text{ cm}$

#### a) Stainless steel and titanium

The force-displacement curves of walls retrofitted by stainless steel vertical rebars are shown in **Figure 7-10**. It can be seen that all nine proposed arrangements result in considerable hardening and overstrength in the system. By considering the original behavior of the wall as elastic-perfect plastic behavior, the retrofitted walls exhibited elastic-hardening plastic behavior with a quite large ductility. Although the overall changes in force-displacement curves under different levels of pre-compression load were the same, two main differences can be seen. By increasing pre-compression load, the added extra overstrength is getting smaller in comparison with the original strength.

Under lower pre-compression loads (except for VR1-2, VR2-2, and VR3-2 models) there is a softening part after the peak strength. However, this softening part is changed to a perfect plastic behavior by increasing the pre-compression load.

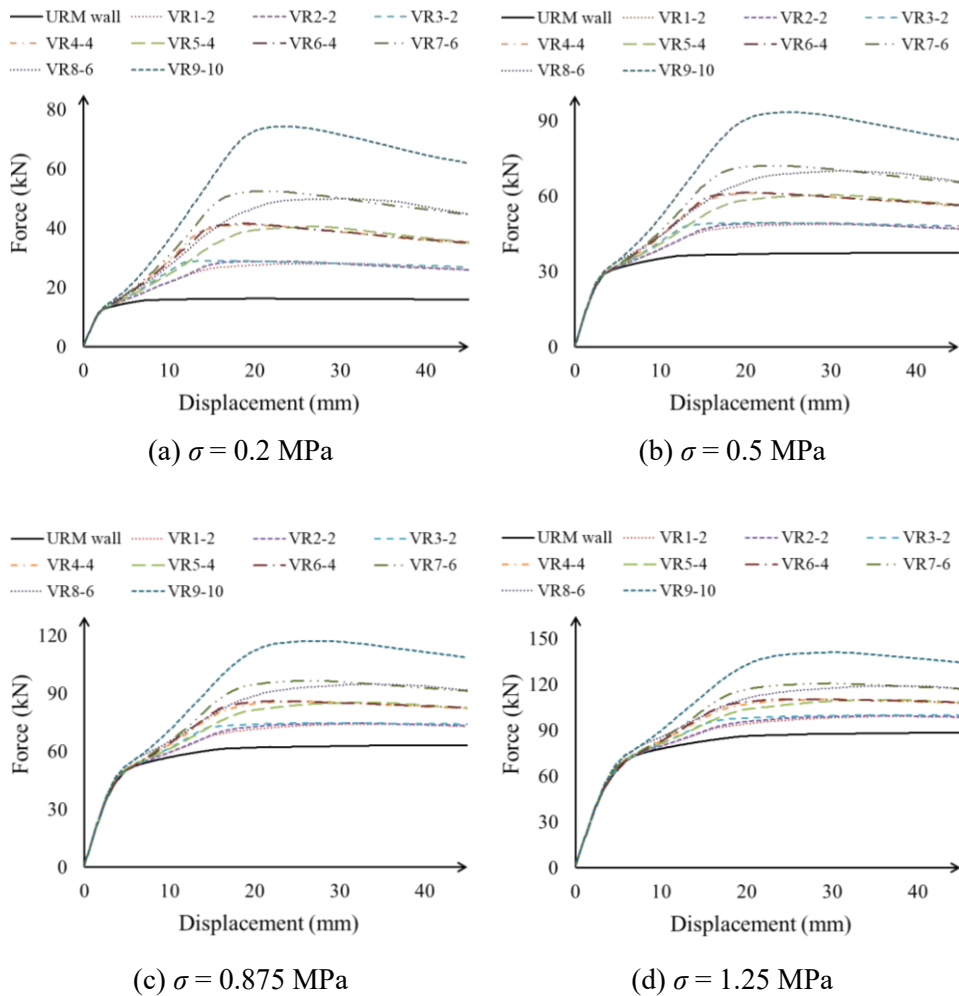


**Figure 7-10** Force-displacement curve of walls with vertical stainless steel rebars under different levels of pre-compression load ( $\sigma$ )

Based on the results, VR3-2, VR6-4, and VR7-6 models were selected within the proposed arrangements as the most efficient and practical cases. The failure mechanisms of these walls at target displacement (45 mm) are shown in **Figures 7-11 to 7-14** for different levels of pre-compression load.

The failure mechanism of both VR3-2 and VR6-4 was stair-stepped crack, however, the cracking in VR3-2 is similar to the original wall while for VR6-4 the cracks were opened in the middle height of the side instead of the top (right) corner. On the other hand, the failure mechanism of VR7-6 was mainly in form of flexural failure, and joints were opened along the baseline rather than stair-stepped pattern.

A similar observation was obtained for the walls retrofitted by vertical titanium rebars, as shown in **Figures 7-15 to 7-19**.

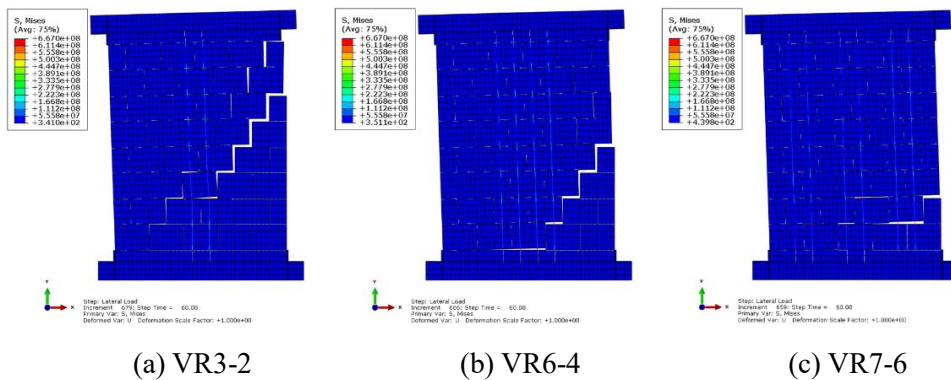


**Figure 7-11** Failure mechanism of walls with vertical stainless steel rebars,  $\sigma = 0.2$  MPa

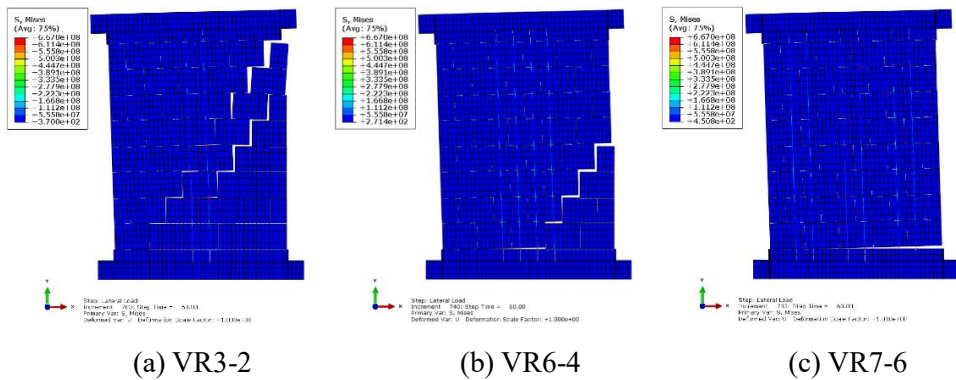


Figure 7-12 Failure mechanism of walls with vertical stainless steel rebars,  $\sigma = 0.5$  MPa

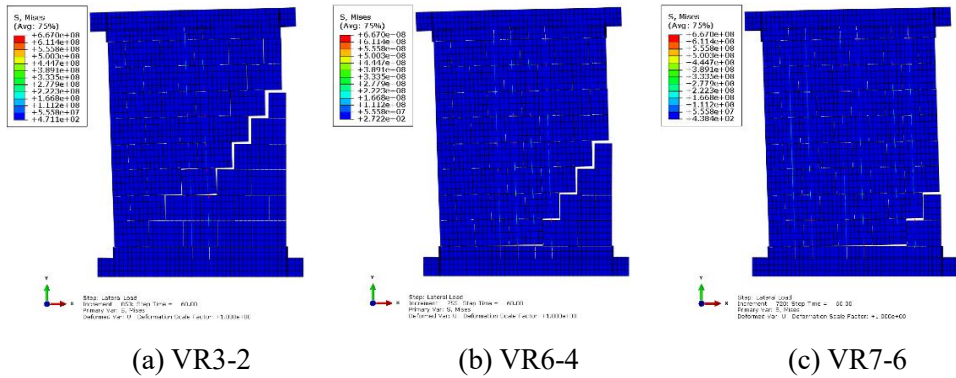


Figure 7-13 Failure mechanism of walls with vertical stainless steel rebars,  $\sigma = 0.875$  MPa

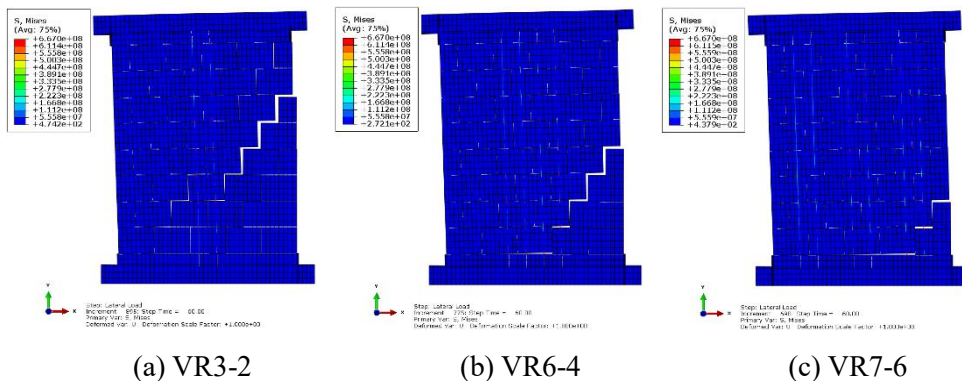


Figure 7-14 Failure mechanism of walls with vertical stainless steel rebars,  $\sigma = 1.25$  MPa

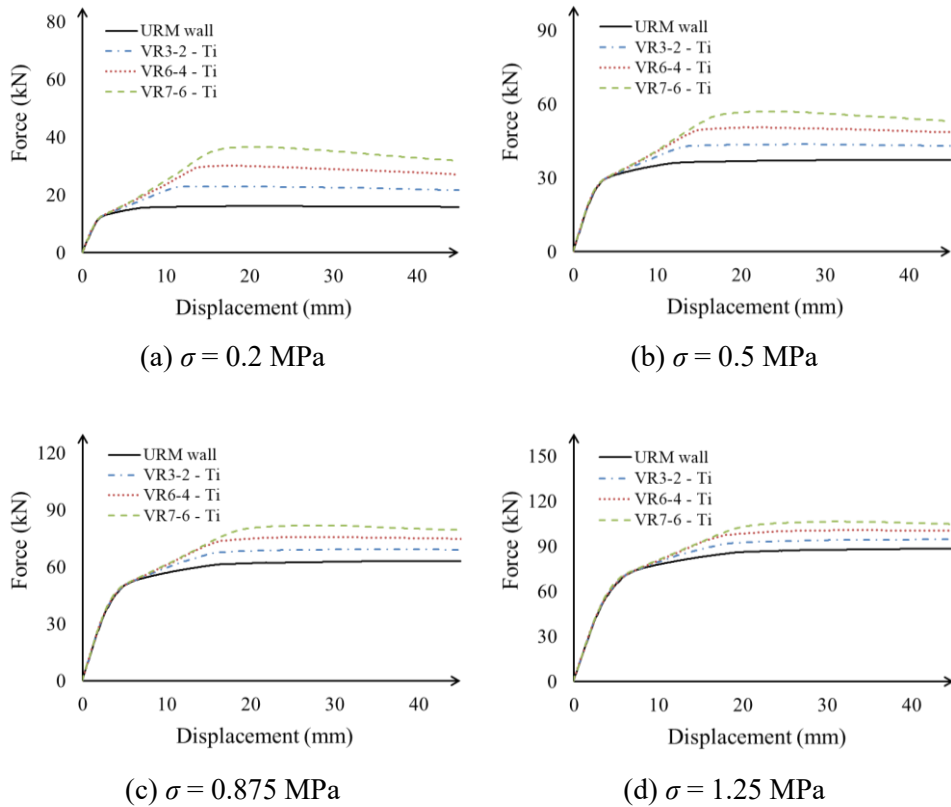


Figure 7-15 Force-displacement curve of walls with vertical titanium rebars under different levels of pre-compression load ( $\sigma$ )

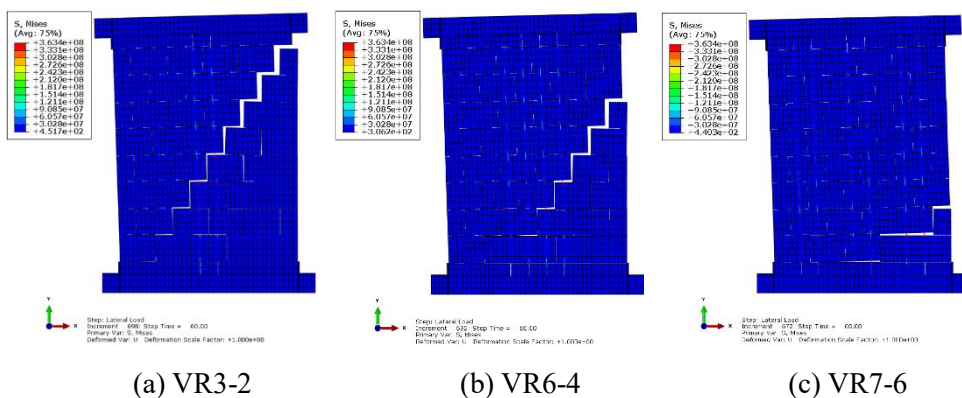


Figure 7-16 Failure mechanism of walls with vertical titanium rebars,  $\sigma = 0.2$  MPa

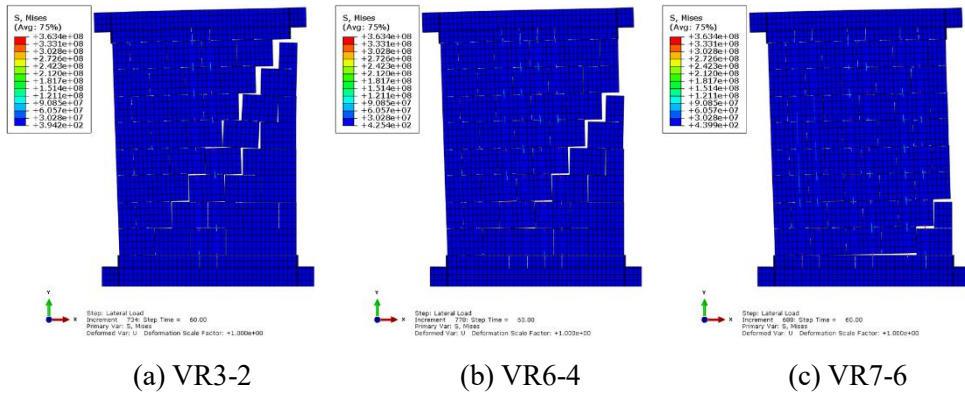


Figure 7-17 Failure mechanism of walls with vertical titanium rebars,  $\sigma = 0.5$  MPa

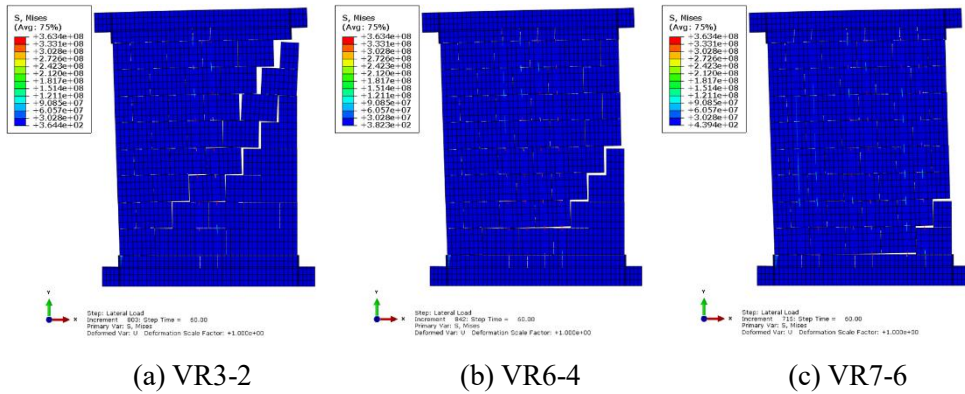


Figure 7-18 Failure mechanism of walls with vertical titanium rebars,  $\sigma = 0.875$  MPa

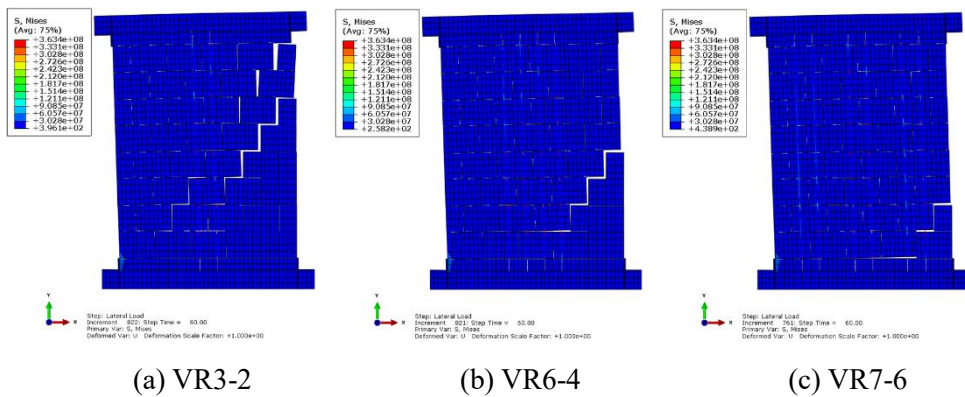


Figure 7-19 Failure mechanism of walls with vertical titanium rebars,  $\sigma = 1.25$  MPa

The ratios of ultimate strength of the retrofitted wall,  $F_{uR}$ , and the original wall,  $F_{uURM}$ , for the models with stainless steel and titanium vertical rebars are reported in **Table 7-4**.

It can be seen that for all levels of pre-compression load, VR7-6 had the highest strength. However, the strength ratio was less under higher pre-compression loads.

**Table 7-4** The strength of retrofitted wall with vertical rebars ( $F_{uR}/F_{uURM}$ )

$\sigma$ (MPa)	Material	Type		
		VR3-2	VR6-4	VR7-6
0.2	SS	1.79	2.57	3.24
	Ti	1.42	1.87	2.27
0.5	SS	1.32	1.64	1.93
	Ti	1.17	1.35	1.53
0.875	SS	1.18	1.36	1.53
	Ti	1.10	1.20	1.30
1.25	SS	1.13	1.25	1.36
	Ti	1.07	1.14	1.20

**b) FRP**

The force-displacement curves of walls retrofitted by vertical rebars with different FRP materials are shown in **Figures 7-20 to 7-23**. All cases show a significant hardening and overstrength to the behavior of the original walls, similar to the observation on the same arrangement by stainless steel and titanium materials. In all cases, retrofitted walls have elastic-hardening plastic with quite large ductility. Although the amount of overstrength by using FRPs is much larger than that obtained

for stainless steel and titanium material, the strength is suddenly dropped to the strength of the original wall after peak strength. It happened because of the brittle behavior of FRP materials. It can be seen from force-displacement curves that the displacement at yielding,  $\delta_y$ , for models with different types of FRP are almost the same with the value of 1.7, 2.9, 4.3, and 5.3 mm under pre-compression of 0.2, 0.5, 0.875, and 1.25 MPa, respectively. The corresponding displacements at FRP failure,  $\delta_u$ , are extracted from the curve, and then corresponding ductility  $((\delta_u - \delta_y)/\delta_y)$  was calculated and is reported in **Tables 7-5 to 7-8**. The ratios of ultimate strength of the retrofitted wall,  $F_{uR}$ , and the original wall,  $F_{uURM}$ , and ratios of hardening stiffness,  $K_{hs}$ , and initial stiffness of the original wall,  $K_{URM}$ , are also reported in the tables.  $K_{URM}$  was adapted from the calibrated model in **Chapter 6**. Note that the ratio of  $(F_{uR}/F_{uURM})$  can be considered as the overstrength factor of walls for the case with FRP rebars. Since the behavior of models with stainless steel and titanium rebars is in form of elastic-perfect plastic, ductility and ratio of  $(K_{hs}/K_{URM})$  are not reported in the tables. For all three examined arrangement cases (i.e. VR3-2, VR6-4, and VR7-6 models), SGFRP did not reach the failure strain at the target displacement and can be considered as the case with the largest ductility (in range of 7.57 to 25.09 under different levels of pre-compression load). CFRP1 failed sooner than all other cases and provided the minimum ductility (in range of 3.07 to 11.74 under different levels of pre-compression load). Within all FRP material, CFRP2 provided the largest overstrength (in the range of 1.76 to 11.08 under different levels of pre-compression load) and also quite large ductility and hardening stiffness were considerably large. Therefore, use of CFRP2 and SGFRP can be considered as the most efficient case.

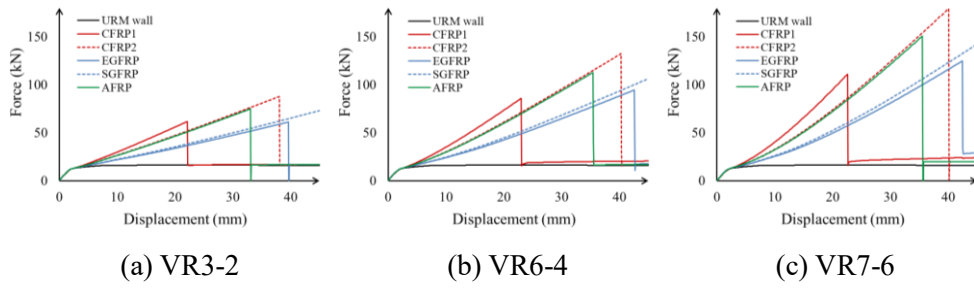


**Figure 7-20** Force-displacement curve of walls with vertical FRP rebars,  $\sigma = 0.2$  MPa

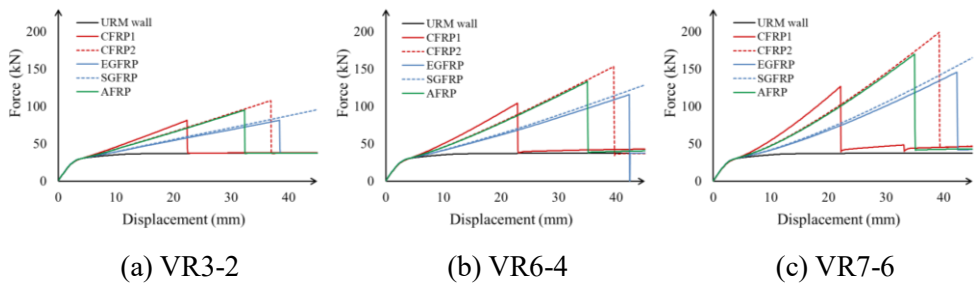


**Figure 7-21** Force-displacement curve of walls with vertical FRP rebars,  $\sigma = 0.5$  MPa

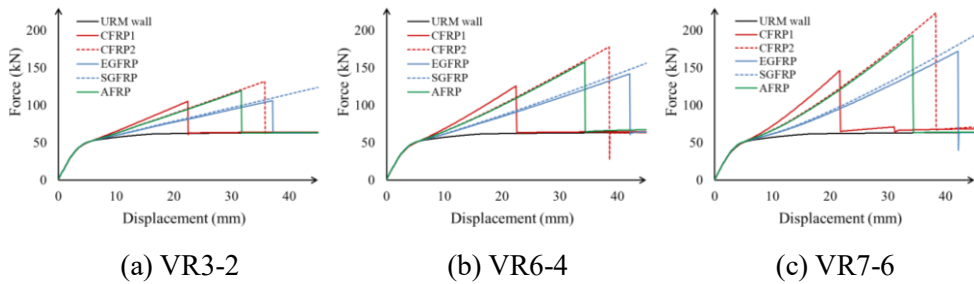


**Figure 7-22** Force-displacement curve of walls with vertical FRP rebars,  $\sigma = 0.875$  MPa

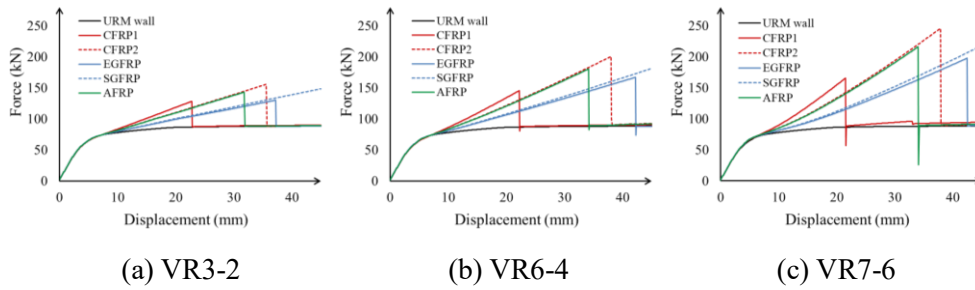


**Figure 7-23** Force-displacement curve of walls with vertical FRP rebars,  $\sigma = 1.25$  MPa

**Table 7-5** Ductility, hardening stiffness, and strength of retrofitted walls with vertical rebars,  $\sigma = 0.2$  MPa

Type	Ductility			$K_{hs} / K_{URM}$			$F_{uR} / F_{uURM}$		
	VR3-2	VR6-4	VR7-6	VR3-2	VR6-4	VR7-6	VR3-2	VR6-4	VR7-6
CFRP1	11.74	12.26	12.00	0.36	0.51	0.70	3.81	5.30	6.86
CFRP2	20.96	22.26	22.13	0.31	0.46	0.64	5.42	8.18	11.08
EGFRP	21.96	23.61	23.52	0.19	0.30	0.41	3.77	5.84	7.71
SGFRP	25.09	25.09	25.09	0.21	0.32	0.44	4.51	6.57	8.81
AFRP	18.09	19.43	19.52	0.30	0.44	0.60	4.62	6.96	9.32

**Table 7-6** Ductility, hardening stiffness, and strength of retrofitted walls with vertical rebars,  $\sigma = 0.5$  MPa

Type	Ductility			$K_{hs} / K_{URM}$			$F_{uR} / F_{uURM}$		
	VR3-2	VR6-4	VR7-6	VR3-2	VR6-4	VR7-6	VR3-2	VR6-4	VR7-6
CFRP1	6.56	6.77	6.51	0.26	0.36	0.48	2.17	2.79	3.39
CFRP2	11.56	12.49	12.38	0.22	0.32	0.44	2.88	4.10	5.32
EGFRP	12.08	13.41	13.41	0.14	0.21	0.28	2.17	3.09	3.90
SGFRP	14.38	14.38	14.38	0.15	0.22	0.30	2.55	3.44	4.41
AFRP	10.00	10.92	10.90	0.21	0.31	0.41	2.54	3.56	4.54

**Table 7-7** Ductility, hardening stiffness, and strength of retrofitted walls with vertical rebars,  $\sigma = 0.875$  MPa

Type	Ductility			$K_{hs} / K_{URM}$			$F_{uR} / F_{uURM}$		
	VR3-2	VR6-4	VR7-6	VR3-2	VR6-4	VR7-6	VR3-2	VR6-4	VR7-6
CFRP1	4.18	4.18	4.01	0.23	0.31	0.44	1.66	1.99	2.32
CFRP2	7.28	7.93	7.88	0.19	0.27	0.37	2.09	2.81	3.53
EGFRP	7.55	8.77	8.77	0.13	0.18	0.24	1.68	2.25	2.72
SGFRP	9.47	9.47	9.47	0.13	0.19	0.26	1.96	2.47	3.06
AFRP	6.34	6.95	6.95	0.19	0.26	0.35	1.89	2.49	3.07

**Table 7-8** Ductility, hardening stiffness, and strength of retrofitted walls with vertical rebars,  $\sigma = 1.25$  MPa

Type	Ductility			$K_{hs} / K_{URM}$			$F_{uR} / F_{uURM}$		
	VR3-2	VR6-4	VR7-6	VR3-2	VR6-4	VR7-6	VR3-2	VR6-4	VR7-6
CFRP1	3.31	3.20	3.07	0.22	0.29	0.37	1.45	1.64	1.87
CFRP2	5.74	6.21	6.20	0.18	0.25	0.34	1.76	2.27	2.78
EGFRP	6.07	7.04	7.06	0.12	0.17	0.22	1.47	1.89	2.23
SGFRP	7.57	7.57	7.57	0.13	0.18	0.24	1.68	2.05	2.46
AFRP	5.03	5.47	5.46	0.18	0.24	0.32	1.62	2.04	2.44

Failure mechanisms of walls retrofitted by vertical rebars with different types of FRP materials at the target displacement are shown in **Figures 7-24 to 7-43**. In the case of VR7-6 model and for all FRP materials, the failure mechanism was in form of flexural failure, and joints were opened along the baseline, similar to that of stainless steel and titanium materials. However, joint opening for EGFRP and SGFRP was quite smaller than for the other FRP materials due to their larger ductility. The failure mechanism of VR6-4 models in most cases was mainly due to flexural

failure. It was in contrast with the observation for the stainless steel and titanium material. In addition, the failure mechanism of VR3-2 for most of the cases was similar to the failure mode of VR6-4 of stainless steel and titanium material. The reason can be associated mainly with the larger hardening stiffness of walls retrofitted by FRP materials, which increase the shear strength of the wall and do not allow the formation of a stair-stepped joint opening in the wall.

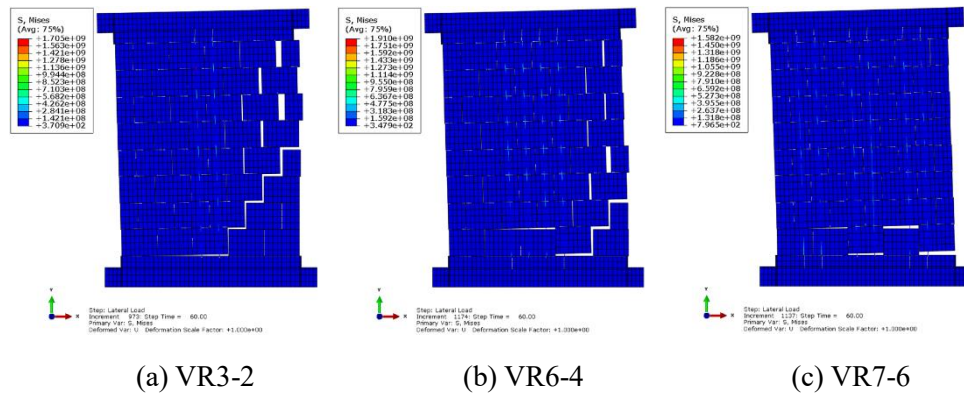


Figure 7-24 Failure mechanism of walls with vertical CFRP1 rebar,  $\sigma = 0.2$  MPa

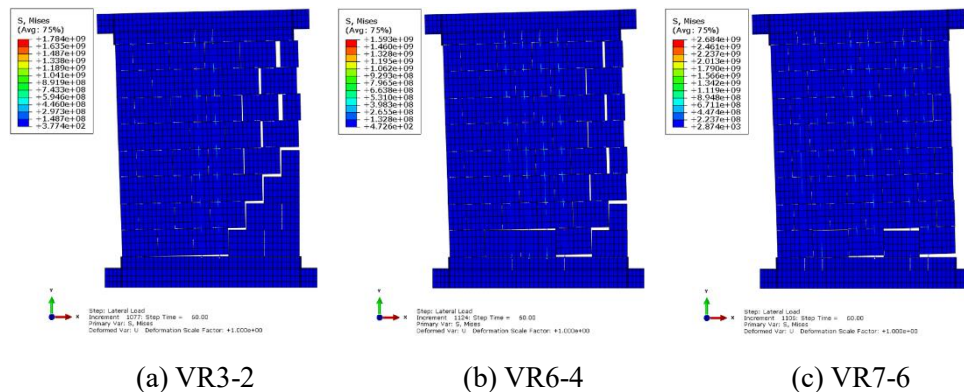


Figure 7-25 Failure mechanism of walls with vertical CFRP1 rebar,  $\sigma = 0.5$  MPa

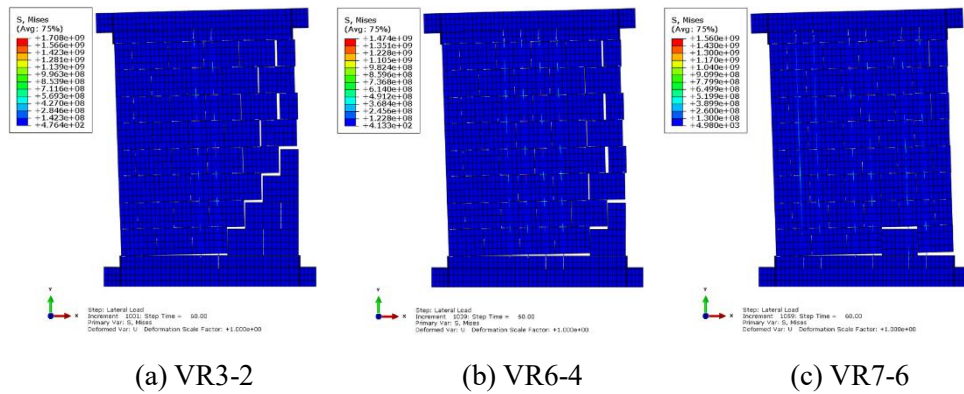


Figure 7-26 Failure mechanism of walls with vertical CFRP1 rebars,  $\sigma = 0.875$  MPa

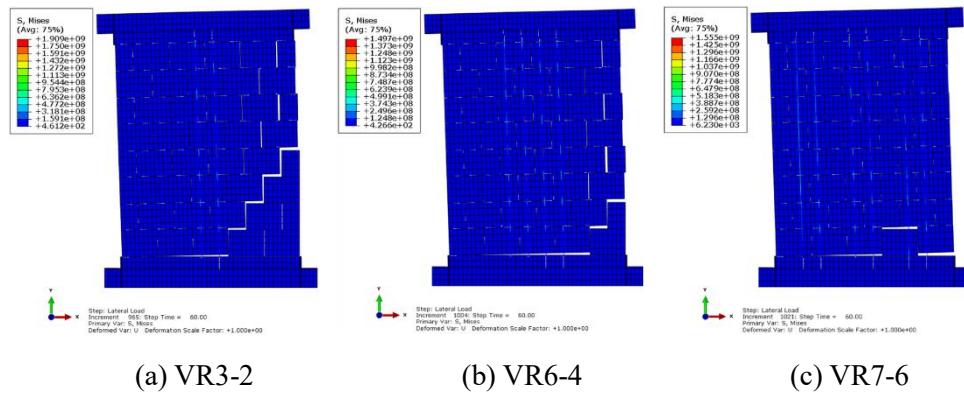


Figure 7-27 Failure mechanism of walls with vertical CFRP1 rebars,  $\sigma = 1.25$  MPa

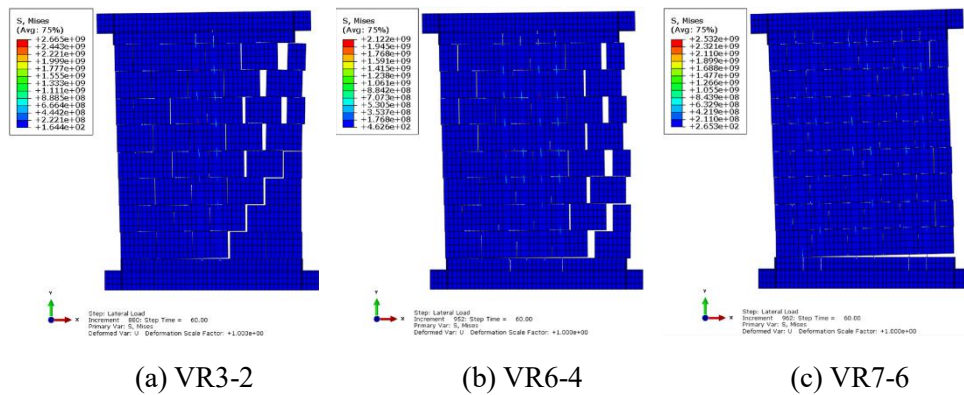


Figure 7-28 Failure mechanism of walls with vertical CFRP2 rebars,  $\sigma = 0.2$  MPa

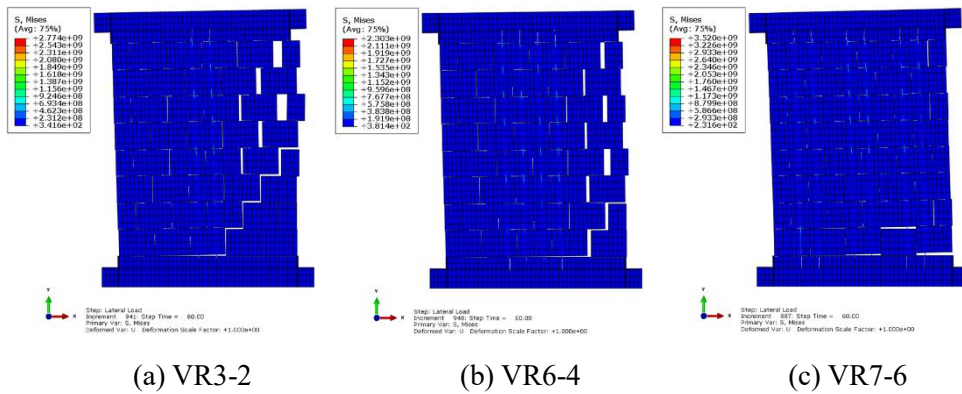


Figure 7-29 Failure mechanism of walls with vertical CFRP2 rebars,  $\sigma = 0.5$  MPa

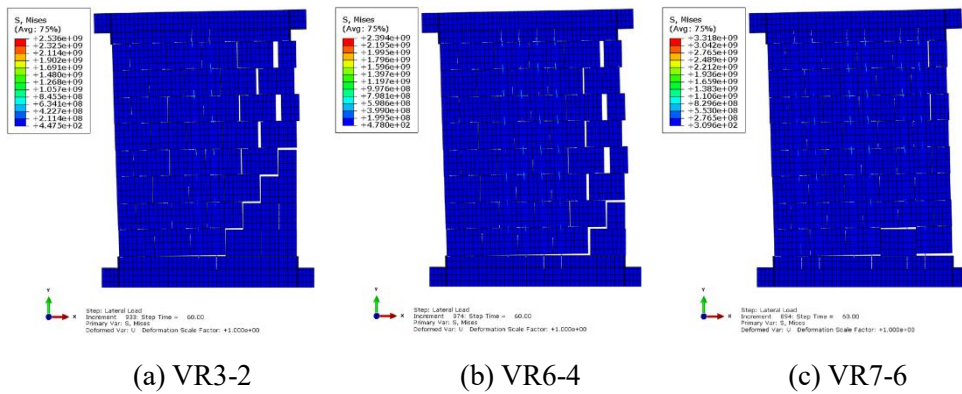


Figure 7-30 Failure mechanism of walls with vertical CFRP2 rebars,  $\sigma = 0.875$  MPa

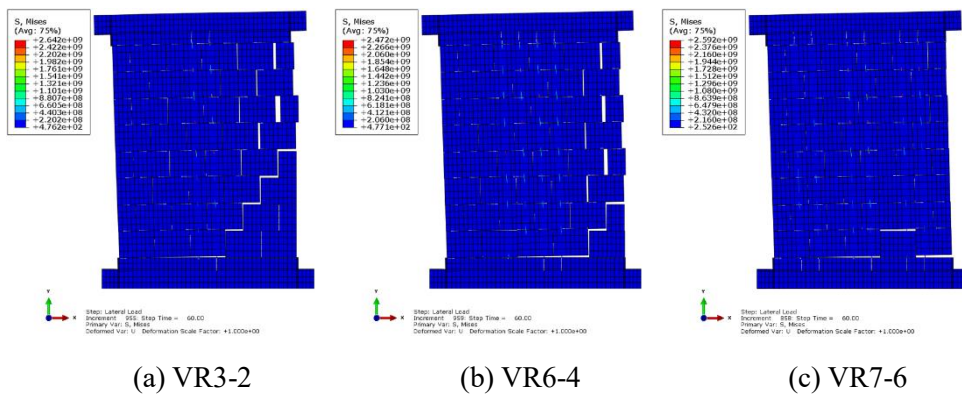


Figure 7-31 Failure mechanism of walls with vertical CFRP2 rebars,  $\sigma = 1.25$  MPa

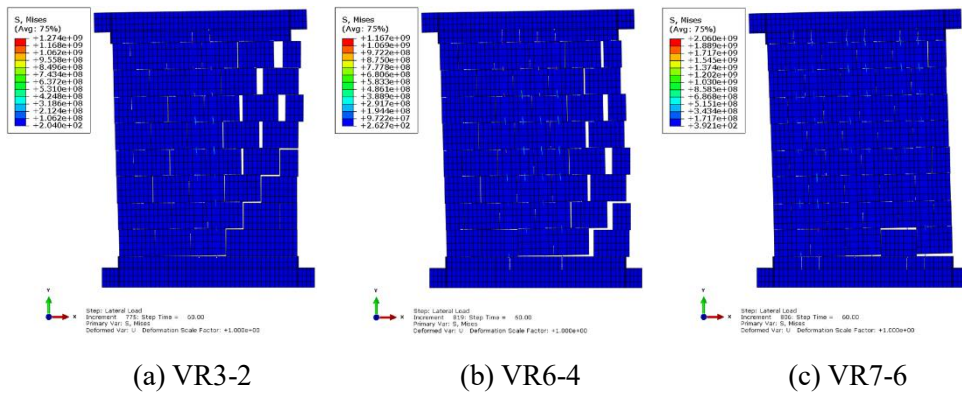


Figure 7-32 Failure mechanism of walls with vertical EGFRP rebars,  $\sigma = 0.2$  MPa

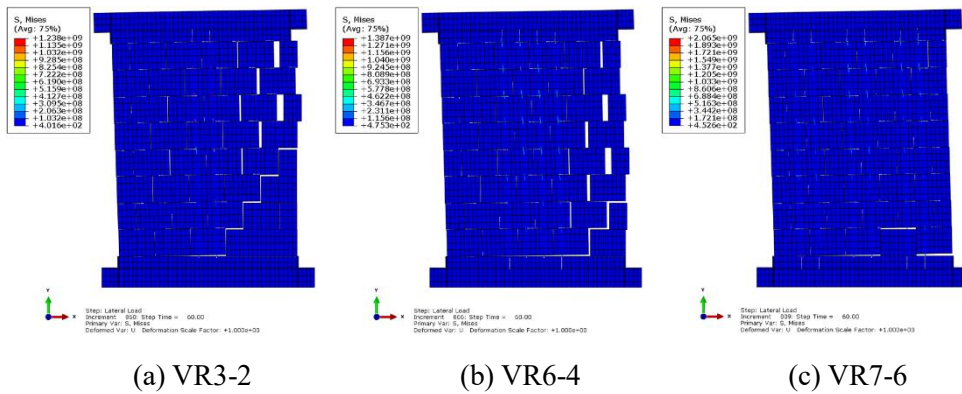


Figure 7-33 Failure mechanism of walls with vertical EGFRP rebars,  $\sigma = 0.5$  MPa

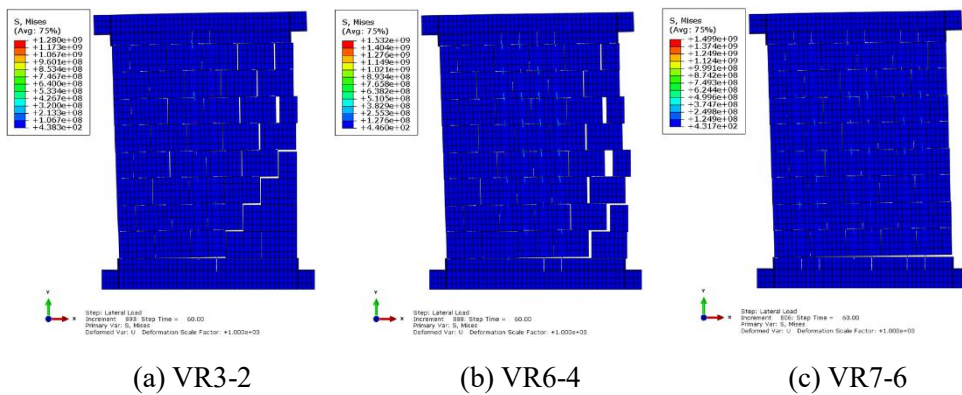


Figure 7-34 Failure mechanism of walls with vertical EGFRP rebars,  $\sigma = 0.875$  MPa

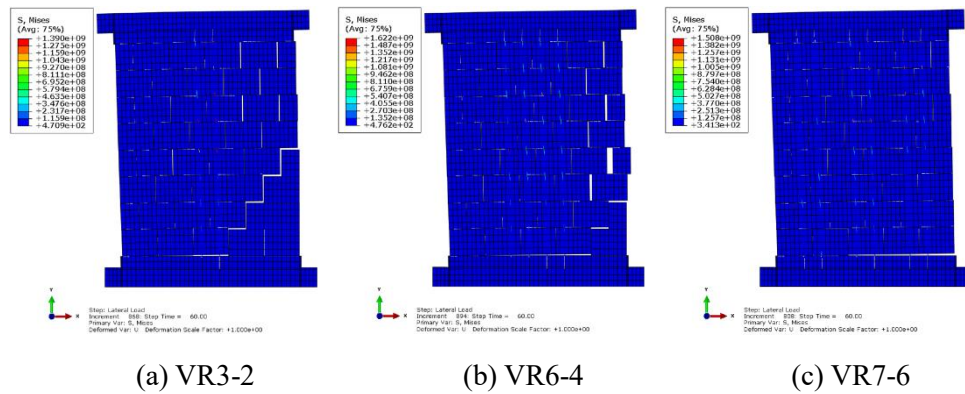


Figure 7-35 Failure mechanism of walls with vertical EGFRP rebars,  $\sigma = 1.25$  MPa

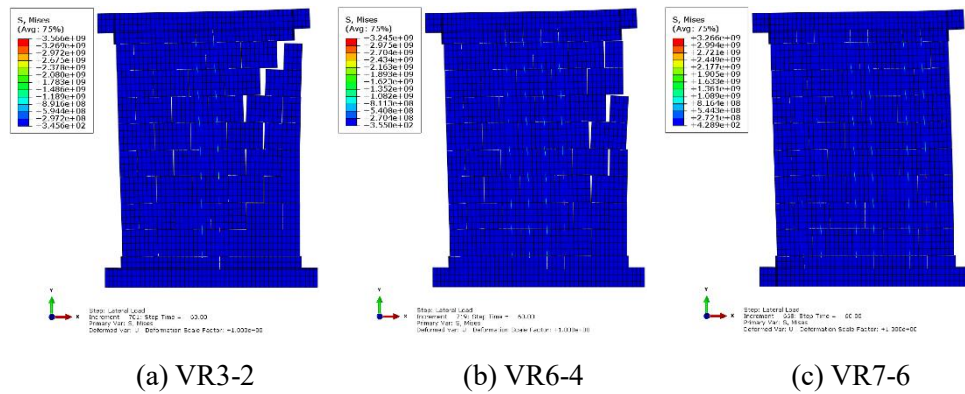


Figure 7-36 Failure mechanism of walls with vertical SGFRP rebars,  $\sigma = 0.2$  MPa

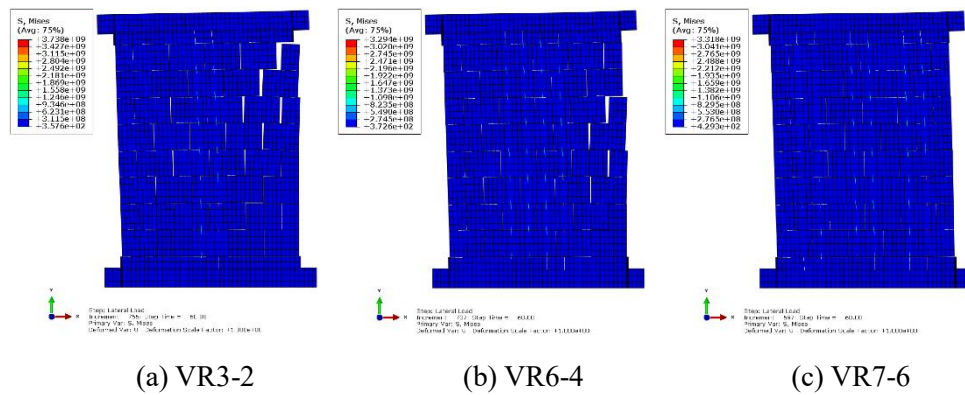


Figure 7-37 Failure mechanism of walls with vertical SGFRP rebars,  $\sigma = 0.5$  MPa

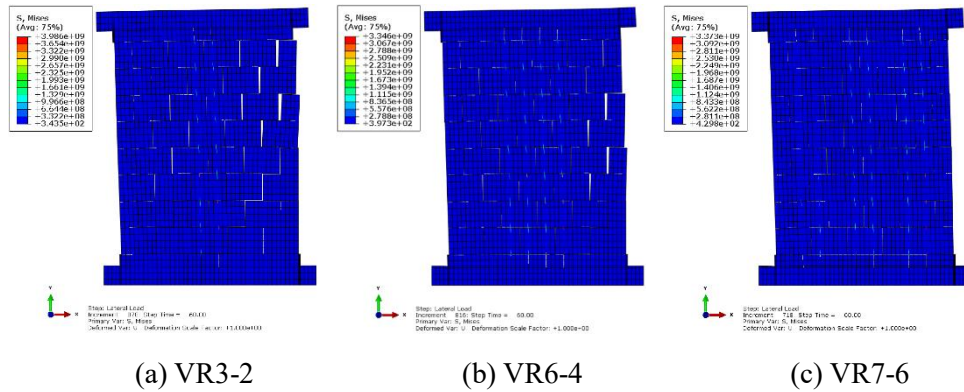


Figure 7-38 Failure mechanism of walls with vertical SGFRP rebars,  $\sigma = 0.875$  MPa

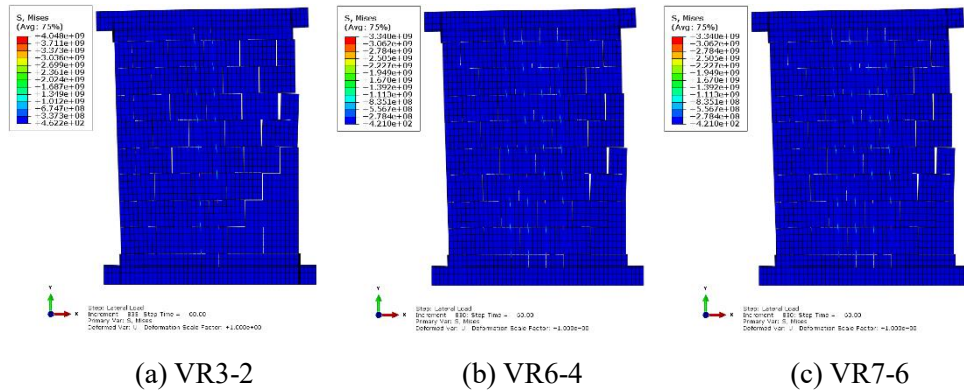


Figure 7-39 Failure mechanism of walls with vertical SGFRP rebars,  $\sigma = 1.25$  MPa

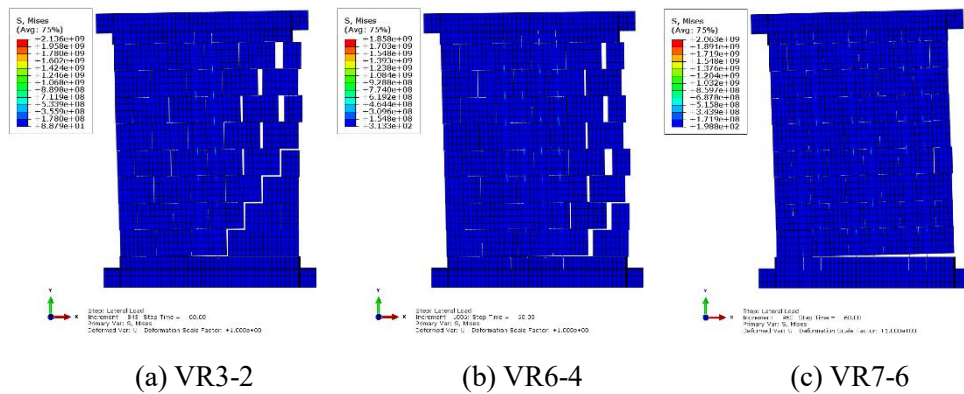


Figure 7-40 Failure mechanism of walls with vertical AFRP rebars,  $\sigma = 0.2$  MPa

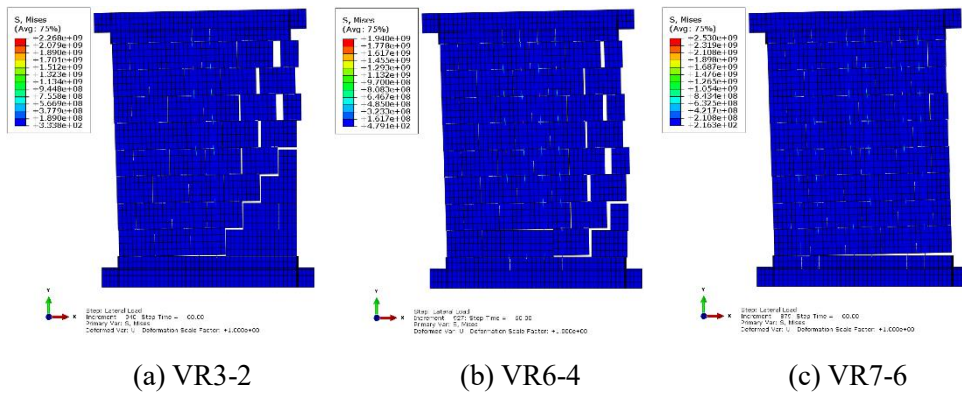


Figure 7-41 Failure mechanism of walls with vertical AFRP rebars,  $\sigma = 0.5$  MPa

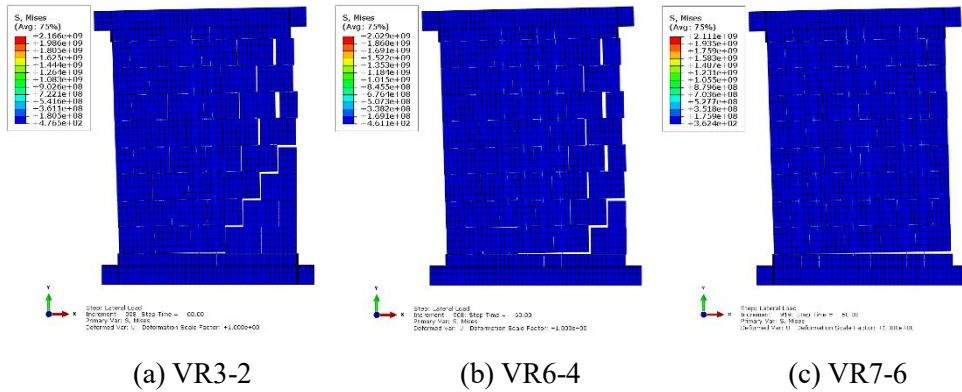


Figure 7-42 Failure mechanism of walls with vertical AFRP rebars,  $\sigma = 0.875$  MPa

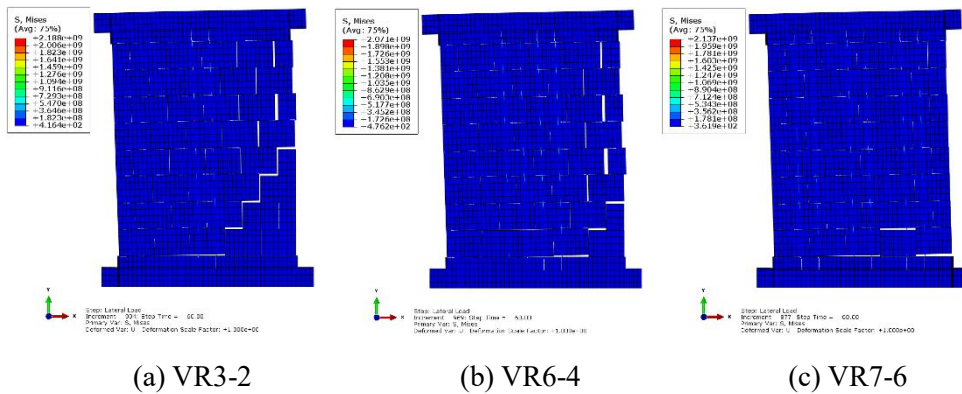


Figure 7-43 Failure mechanism of walls with vertical AFRP rebars,  $\sigma = 1.25$  MPa

### 7.4.3 Diagonal rebar models

In the third type of arrangement, rebars were placed diagonally in the stone wall in different positions and rebars had different lengths depending on their location. Different arrangements were examined by changing the number and position of rebars as shown in **Figure 7-44**, and values of specified spacing in the figure are reported in **Table 7-9**.

As shown in the table, a specific name was assigned to each model based on the number of rebars. For instance, DR1-2 model is diagonal arrangement type 1 with 2 embedded rebars.

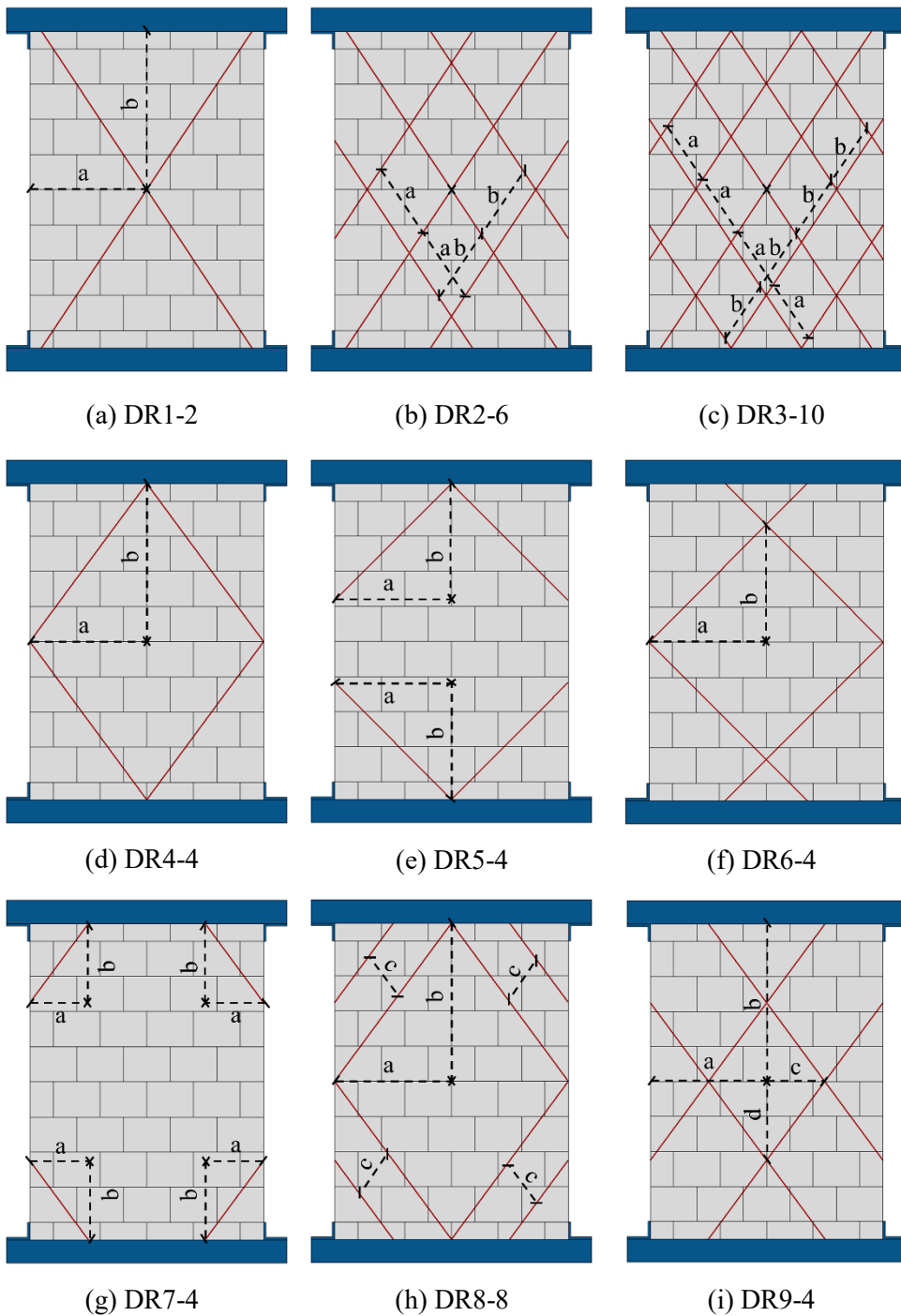


Figure 7-44 Diagonal arrangement of rebars in the stone masonry wall

**Table 7-9** Details of finite element models strengthened with diagonal rebars

Type	Model	No. of bars	Space
1	DR1-2	2	$a = 50 \text{ cm}, b = 67.5 \text{ cm}$
2	DR2-6	6	$a = 30 \text{ cm}, b = 30 \text{ cm}$
3	DR3-10	10	$a = 25 \text{ cm}, b = 25 \text{ cm}$
4	DR4-4	4	$a = 50 \text{ cm}, b = 67.5 \text{ cm}$
5	DR5-4	4	$a = 50 \text{ cm}, b = 50 \text{ cm}$
6	DR6-4	4	$a = 50 \text{ cm}, b = 50 \text{ cm}$
7	DR7-4	4	$a = 25 \text{ cm}, b = 35 \text{ cm}$
8	DR8-8	8	$a = 50 \text{ cm}, b = 67.5 \text{ cm}, c = 20 \text{ cm}$
9	DR9-4	4	$a = 50 \text{ cm}, b = 67.5 \text{ cm}, c = 25 \text{ cm}, d = 33.75 \text{ cm}$

#### a) Stainless steel and titanium

The force-displacement curves of walls retrofitted by stainless steel diagonal rebars are shown in **Figure 7-45**. It can be seen that force-displacement curves of DR5-4 and DR7-4 models are very similar and have the lowest efficiency in terms of the overstrength and hardening stiffness.

On the other hand, DR2-6 and DR3-10 models showed the highest overstrength and hardening stiffness. However, these models under low pre-compression load showed considerable softening behavior after the peak strength. The softening slope is reduced and the behavior is changed to perfect plastic behavior by increasing the pre-compression load. Force-displacement curves of other models are quite similar

to each other and among them, DR4-4 and DR8-8 models have the highest overstrength and hardening stiffness.

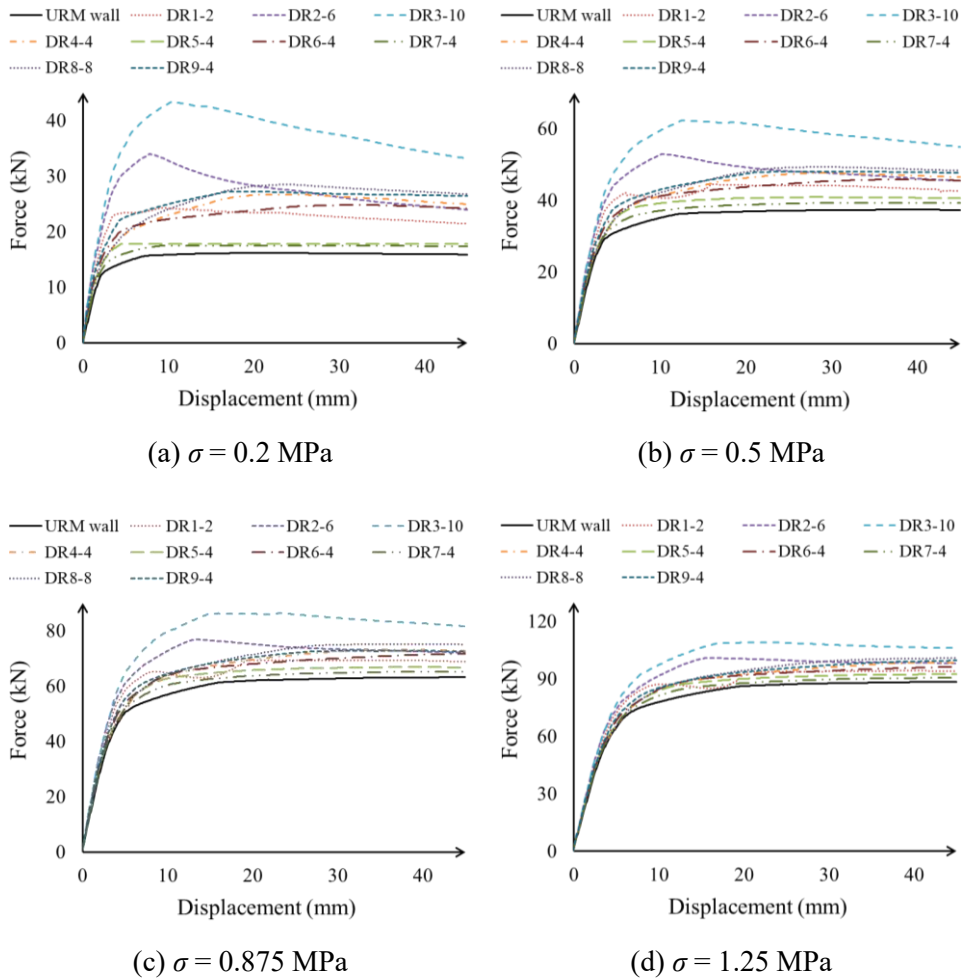


**Figure 7-45** Force-displacement curve of walls with diagonal stainless steel rebars under different levels of pre-compression load ( $\sigma$ )

Based on the results, DR2-6, DR4-4, and DR8-8 models were selected within the proposed arrangements as efficient and practical cases. The failure mechanisms

of these walls at target displacement (45 mm) are shown in **Figures 7-46 to 7-49** for different levels of pre-compression load.

The failure mechanism of both DR4-4 and VR8-8 was quite similar to each other and was in form of stair-stepped cracks under low pre-compression load. However, joints were not opened as much as in the original walls due to the action of rebars. By increasing the pre-compression load, the stair-stepped crack was changed to a flexural (horizontal) crack form at the middle height of the side and continued by a stair-stepped crack start at the middle of width. On the other hand, the failure mechanism of VR2-6 was mainly flexural failure, and joints were opened close to the baseline rather than stair-stepped pattern.

Similar observations were obtained for the walls retrofitted by diagonal titanium rebars, as shown in **Figures 7-50 to 7-54**.

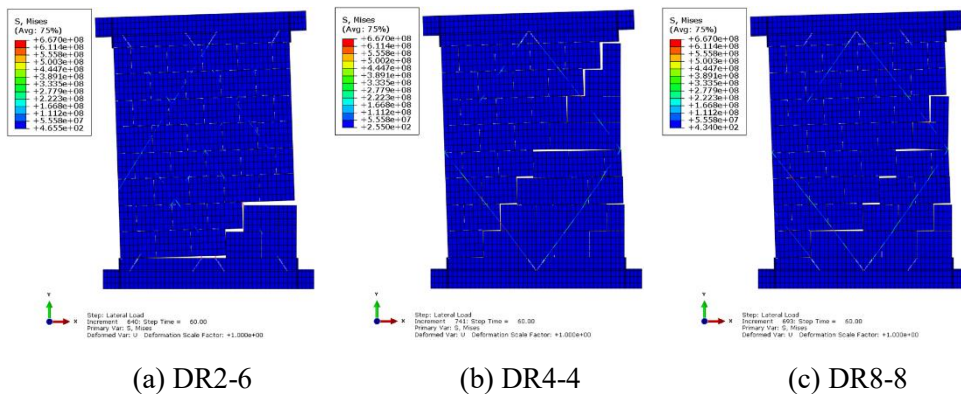


**Figure 7-46** Failure mechanism of walls with diagonal stainless steel rebars,  $\sigma = 0.2$  MPa

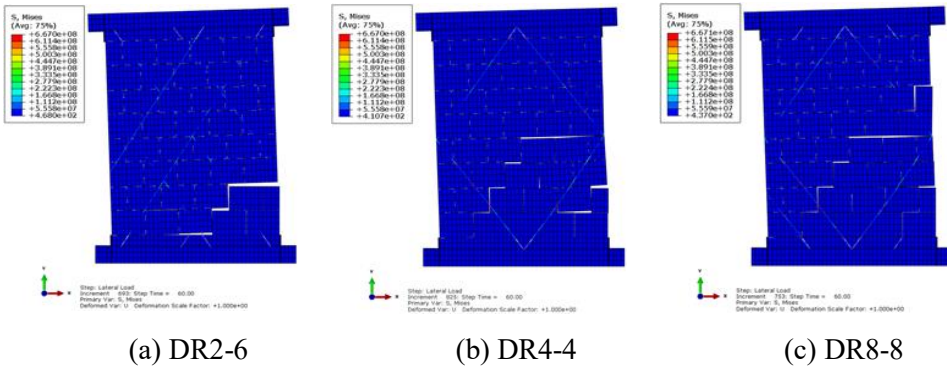


Figure 7-47 Failure mechanism of walls with diagonal stainless steel rebars,  $\sigma = 0.5$  MPa

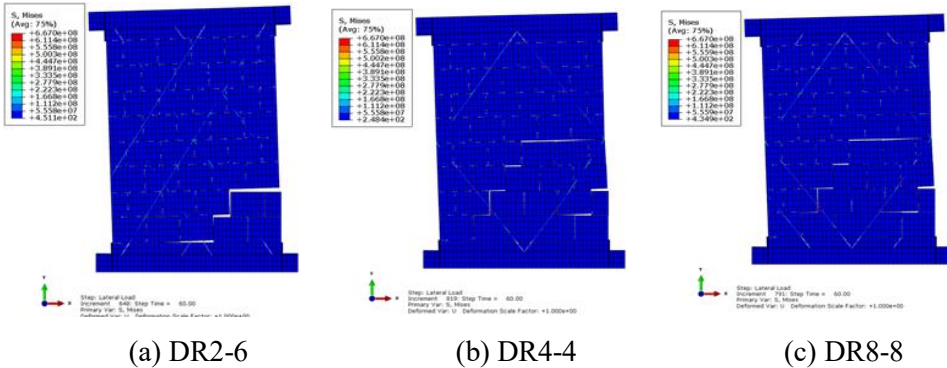


Figure 7-48 Failure mechanism of walls with diagonal stainless steel rebars,  $\sigma = 0.875$  MPa

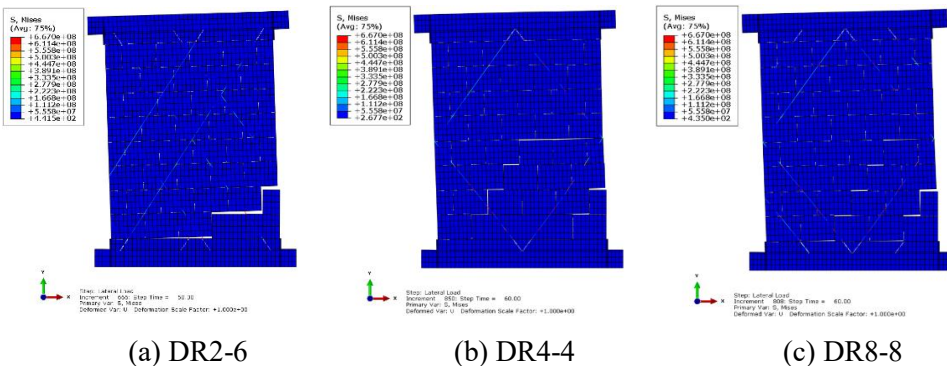
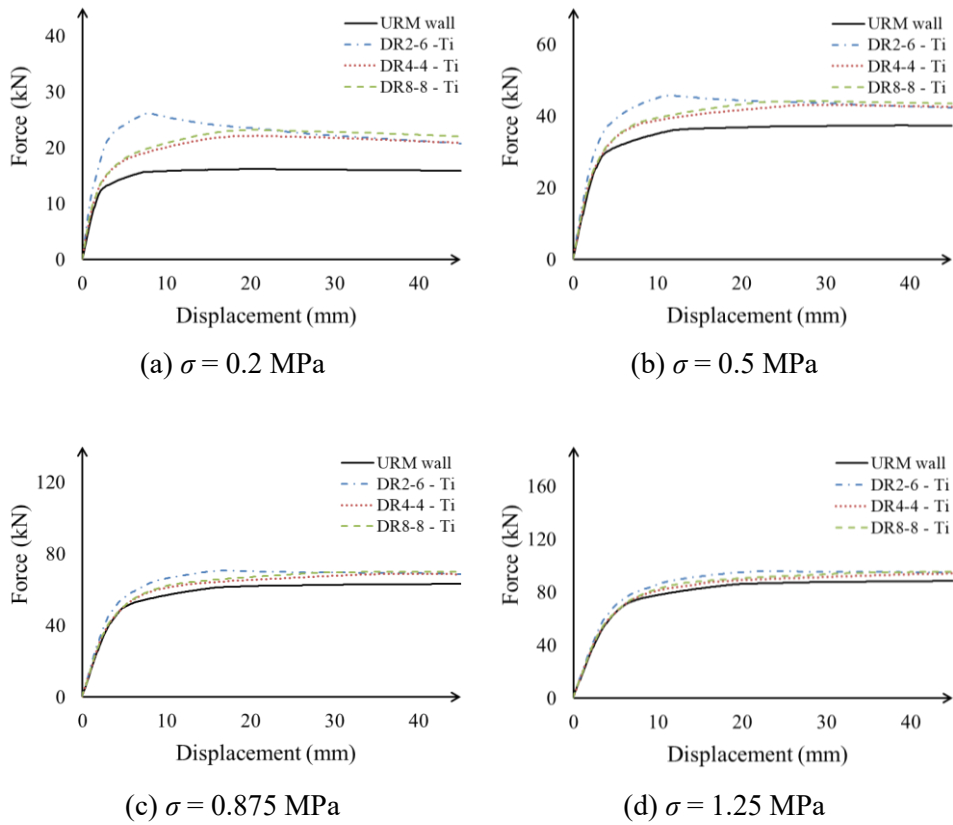
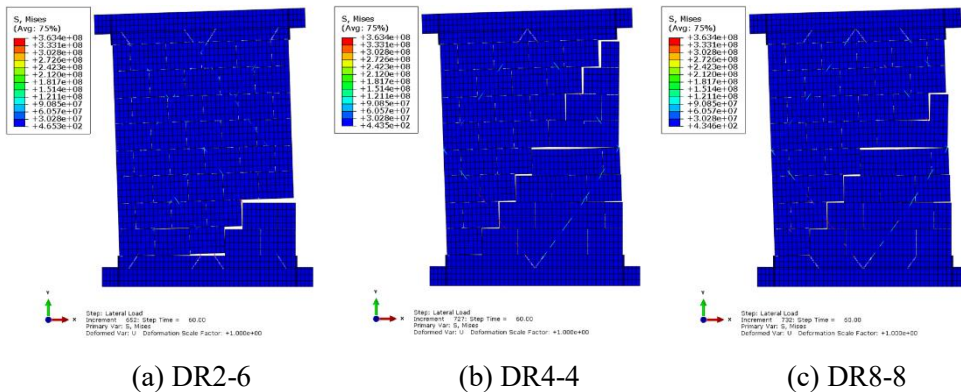


Figure 7-49 Failure mechanism of walls with diagonal stainless steel rebars,  $\sigma = 1.25$  MPa



**Figure 7-50** Force-displacement curve of walls with diagonal titanium rebars under different levels of pre-compression load ( $\sigma$ )



**Figure 7-51** Failure mechanism of walls with diagonal titanium rebars,  $\sigma = 0.2$  MPa

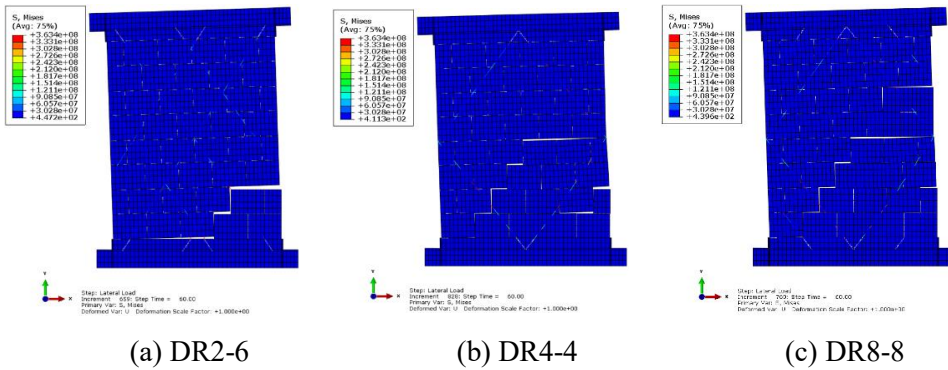


Figure 7-52 Failure mechanism of walls with diagonal titanium rebars,  $\sigma = 0.5$  MPa

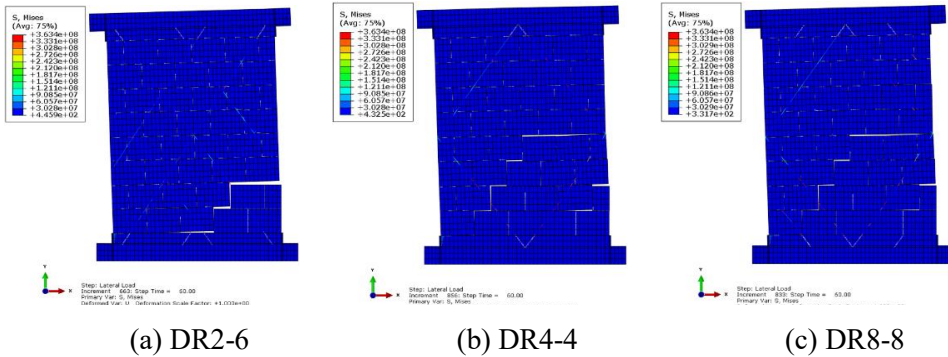


Figure 7-53 Failure mechanism of walls with diagonal titanium rebars,  $\sigma = 0.875$  MPa

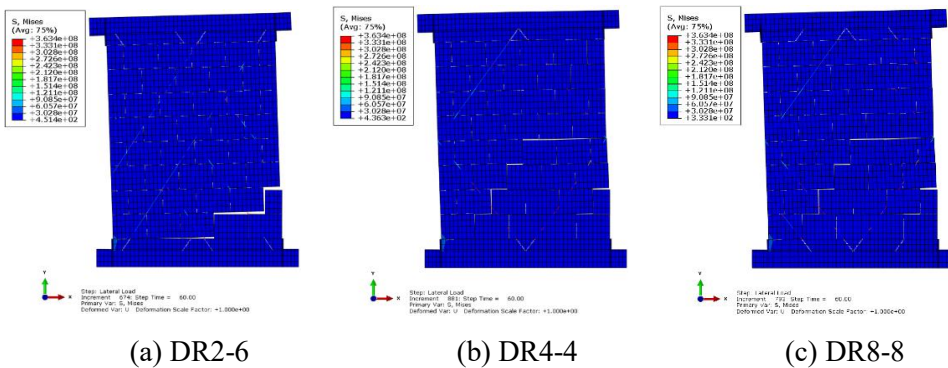


Figure 7-54 Failure mechanism of walls with diagonal titanium rebars,  $\sigma = 1.25$  MPa

The ratios of ultimate strength of the retrofitted wall,  $F_{ur}$ , and the original wall,  $F_{uURM}$ , for the models with stainless steel and titanium diagonal rebars are reported in **Table 7-10**. It can be seen that for all levels of pre-compression load, DR8-8 and DR2-6 had a higher strength. However, the strength ratio was less under higher pre-compression loads.

**Table 7-10** The strength of retrofitted wall with diagonal rebars ( $F_{ur}/F_{uURM}$ )

$\sigma$ (MPa)	Material	Type		
		DR2-6	DR4-4	DR8-8
0.2	SS	2.10	1.65	1.76
	Ti	1.62	1.37	1.43
0.5	SS	1.41	1.27	1.32
	Ti	1.22	1.15	1.18
0.875	SS	1.22	1.16	1.19
	Ti	1.12	1.09	1.11
1.25	SS	1.14	1.11	1.14
	Ti	1.08	1.06	1.08

#### b) FRP

The force-displacement curves of walls retrofitted by diagonal rebars with different FRP materials are shown in **Figures 7-55 to 7-58**. All cases exhibit adding significant hardening stiffness and overstrength to the behavior of the original walls, similar to the observation on the same arrangements with stainless steel and titanium materials. In all cases, by increasing the pre-compression load the effect is getting larger, and retrofitted walls exhibit elastic-hardening plastic behavior. Although the

amount of overstrength by using FRPs is much larger than that obtained for stainless steel and titanium material, the strength is suddenly dropped to the strength of the original wall after peak strength due to the brittle behavior of FRP materials. Among the proposed arrangements, DR2-6 results in the largest overstrength and hardening stiffness with the lowest ductility. The behavior of DR4-4 and DR8-8 was quite similar in terms of overstrength and hardening stiffness, but DR8-8 provides larger ductility (and largest among three cases). Based on the force-displacement curves that the displacement at yielding,  $\delta_y$ , for models with different types of FRP are almost the same with the value of 2.1, 3.0, 4.5, and 6.2 mm under pre-compression of 0.2, 0.5, 0.875, and 1.25 MPa, respectively. The values of ductility,  $(K_{hs} / K_{URM})$ , and  $(F_{uR} / F_{uURM})$  were calculated (as explained for the case with vertical rebars) and are reported in **Tables 7-11 to 7-14**.

Among the FRP material examined for all three arrangement cases (i.e. DR2-6, VR4-4, and VR8-8 models), CFRP2 and SGFRP provide the largest overstrength with relatively close values (in range of 1.35 to 6.95 for CFRP2 and 1.37 to 6.53 for SGFRP under different levels of pre-compression load). However, CFRP2 has larger hardening stiffness (in range of 0.16 to 0.95 under different levels of pre-compression load) and SGFRP exhibit larger ductility (in range of 2.16 to 20.43 under different levels of pre-compression load). Therefore, use of CFRP2 and SGFRP can be considered as the most efficient case.

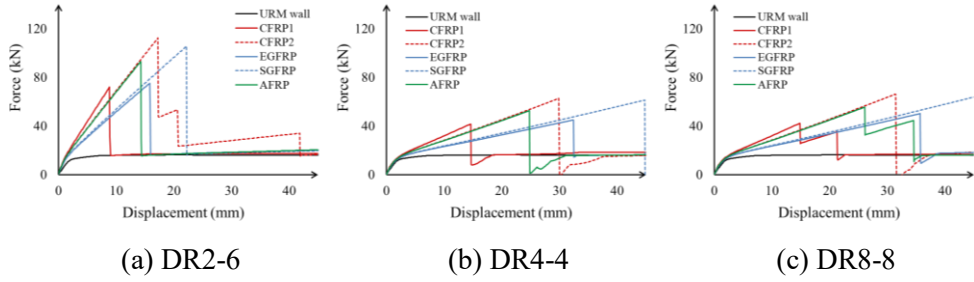


**Figure 7-55** Force-displacement curve of walls with diagonal FRP rebars,  $\sigma = 0.2$  MPa

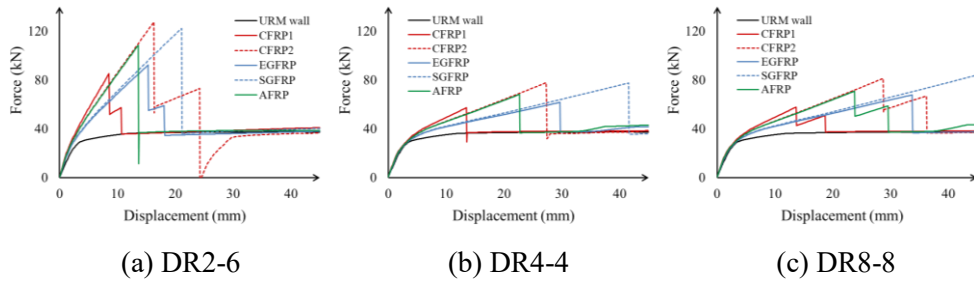


**Figure 7-56** Force-displacement curve of walls with diagonal FRP rebars,  $\sigma = 0.5$  MPa

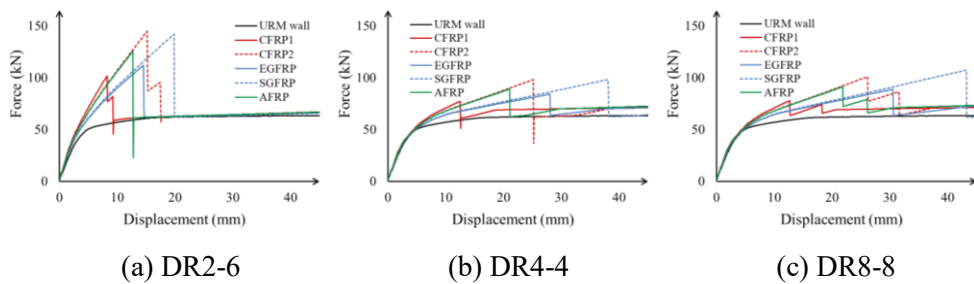


**Figure 7-57** Force-displacement curve of walls with diagonal FRP rebars,  $\sigma = 0.875$  MPa

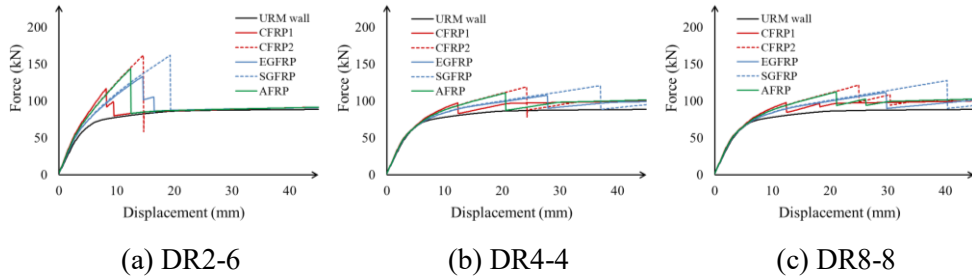


**Figure 7-58** Force-displacement curve of walls with diagonal FRP rebars,  $\sigma = 1.25$  MPa

**Table 7-11** Ductility, hardening stiffness, and strength of retrofitted walls with diagonal rebars,  $\sigma = 0.2$  MPa

Type	Ductility			$K_{hs} / K_{URM}$			$F_{uR} / F_{uURM}$		
	DR2-6	DR4-4	DR8-8	DR2-6	DR4-4	DR8-8	DR2-6	DR4-4	DR8-8
CFRP1	3.21	5.96	6.07	1.26	0.32	0.33	4.45	2.58	2.61
CFRP2	7.21	13.25	13.93	0.95	0.26	0.26	6.95	3.88	4.09
EGFRP	6.21	14.43	16.04	0.66	0.15	0.16	4.65	2.77	3.10
SGFRP	9.57	20.32	20.43	0.67	0.16	0.17	6.53	3.79	3.94
AFRP	5.75	10.82	11.43	0.96	0.25	0.25	5.75	3.25	3.43

**Table 7-12** Ductility, hardening stiffness, and strength of retrofitted walls with diagonal rebars,  $\sigma = 0.5$  MPa

Type	Ductility			$K_{hs} / K_{URM}$			$F_{uR} / F_{uURM}$		
	DR2-6	DR4-4	DR8-8	DR2-6	DR4-4	DR8-8	DR2-6	DR4-4	DR8-8
CFRP1	1.83	3.48	3.55	0.91	0.23	0.23	2.28	1.53	1.54
CFRP2	4.43	8.10	8.58	0.67	0.18	0.18	3.41	2.08	2.17
EGFRP	3.90	8.80	10.00	0.47	0.11	0.11	2.47	1.65	1.81
SGFRP	6.03	12.85	14.00	0.47	0.11	0.12	3.27	2.07	2.25
AFRP	3.53	6.55	6.93	0.68	0.18	0.18	2.90	1.82	1.89

**Table 7-13** Ductility, hardening stiffness, and strength of retrofitted walls with diagonal rebars,  $\sigma = 0.875$  MPa

Type	Ductility			$K_{hs} / K_{URM}$			$F_{uR} / F_{uURM}$		
	DR2-6	DR4-4	DR8-8	DR2-6	DR4-4	DR8-8	DR2-6	DR4-4	DR8-8
CFRP1	0.80	1.73	1.88	1.02	0.25	0.12	1.61	1.22	1.23
CFRP2	2.33	4.58	4.80	0.64	0.17	0.17	2.29	1.55	1.60
EGFRP	2.17	5.13	5.80	0.45	0.11	0.04	1.77	1.33	1.41
SGFRP	3.40	7.47	8.60	0.43	0.10	0.11	2.25	1.56	1.70
AFRP	1.80	3.68	3.85	0.67	0.17	0.17	1.98	1.41	1.44

**Table 7-14** Ductility, hardening stiffness, and strength of retrofitted walls with diagonal rebars,  $\sigma = 1.25$  MPa

Type	Ductility			$K_{hs} / K_{URM}$			$F_{uR} / F_{uURM}$		
	DR2-6	DR4-4	DR8-8	DR2-6	DR4-4	DR8-8	DR2-6	DR4-4	DR8-8
CFRP1	0.41	1.04	1.05	0.55	0.11	0.12	1.32	1.13	1.13
CFRP2	1.37	2.97	3.09	0.66	0.16	0.16	1.83	1.35	1.37
EGFRP	1.36	3.59	3.87	0.45	0.05	0.10	1.51	1.22	1.26
SGFRP	2.16	5.07	5.59	0.42	0.10	0.10	1.83	1.37	1.44
AFRP	1.03	2.36	2.95	0.71	0.17	0.14	1.63	1.25	1.27

Failure mechanisms of walls retrofitted by diagonal rebars with different types of FRP materials at the target displacement are shown in **Figures 7-59 to 7-78**. Generally, the failure mechanisms were very similar to those obtained for stainless steel and titanium material with diagonal rebars. However, it was not the same because in most cases the FRP rebars reached their ultimate strength at a smaller lateral displacement than the target. Therefore, corresponding observed failure mechanisms at target displacements, which are shown in the figures, were a

combination of failure mechanisms observed for stainless steel and titanium material with some local sliding near the broken FRP rebars.

In those cases that FRP rebars were not broken or broken close to target displacements, smaller local sliding occurred and the failure mechanism was more similar to the corresponding case with stainless steel and titanium material.

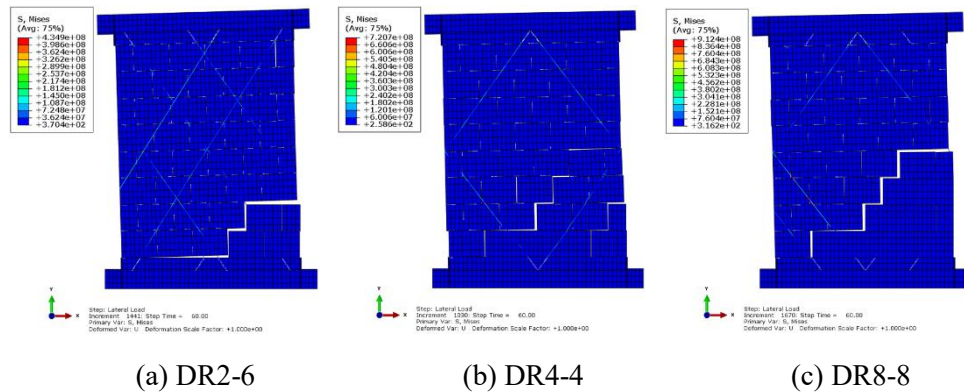


Figure 7-59 Failure mechanism of walls with diagonal CFRP1 rebars,  $\sigma = 0.2$  MPa

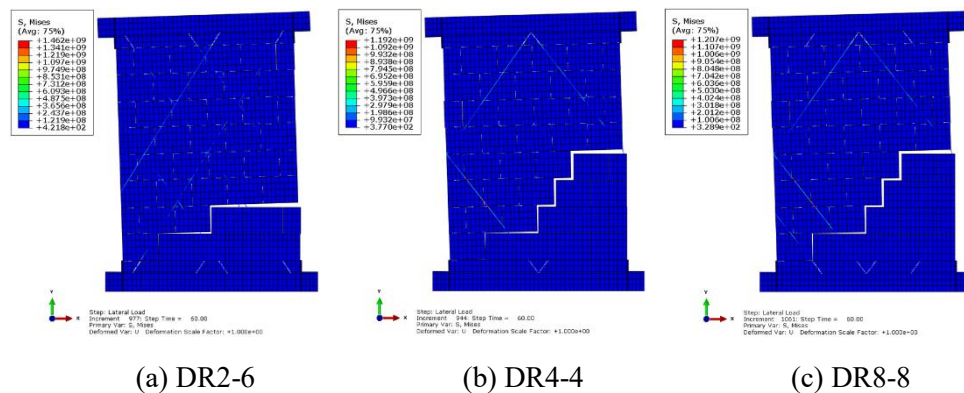
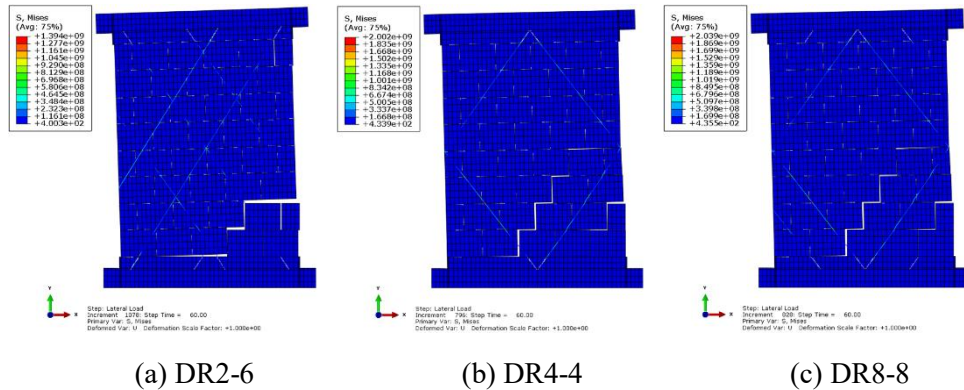
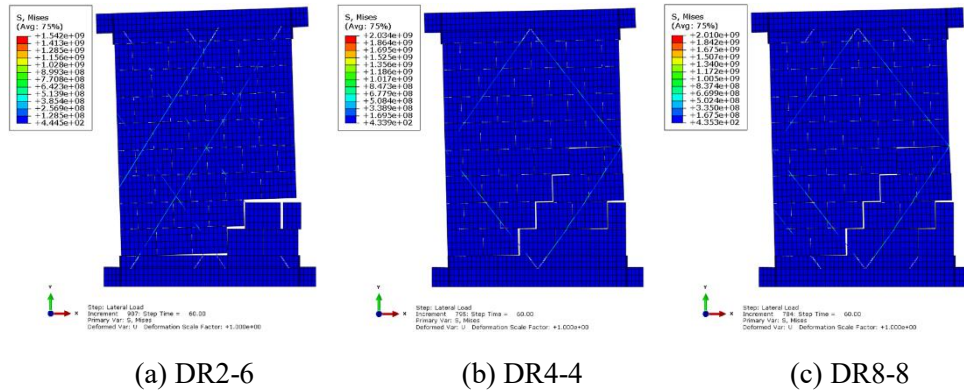


Figure 7-60 Failure mechanism of walls with diagonal CFRP1 rebars,  $\sigma = 0.5$  MPa



**Figure 7-61** Failure mechanism of walls with diagonal CFRP1 rebars,  $\sigma = 0.875$  MPa



**Figure 7-62** Failure mechanism of walls with diagonal CFRP1 rebars,  $\sigma = 1.25$  MPa

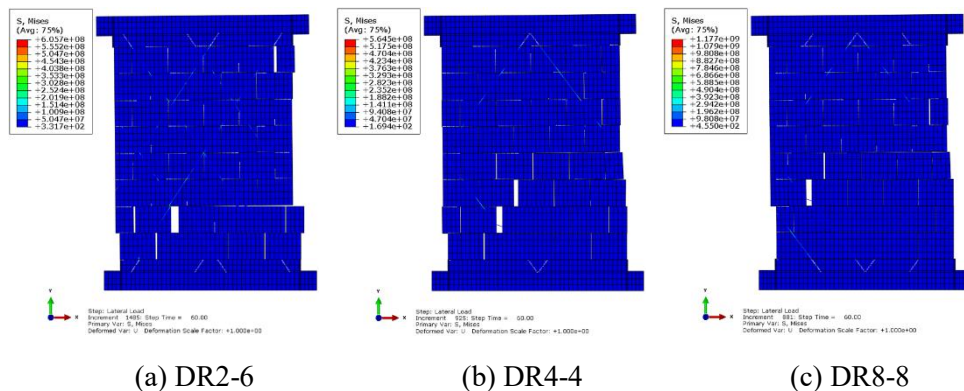


**Figure 7-63** Failure mechanism of walls with diagonal CFRP2 rebars,  $\sigma = 0.2$  MPa

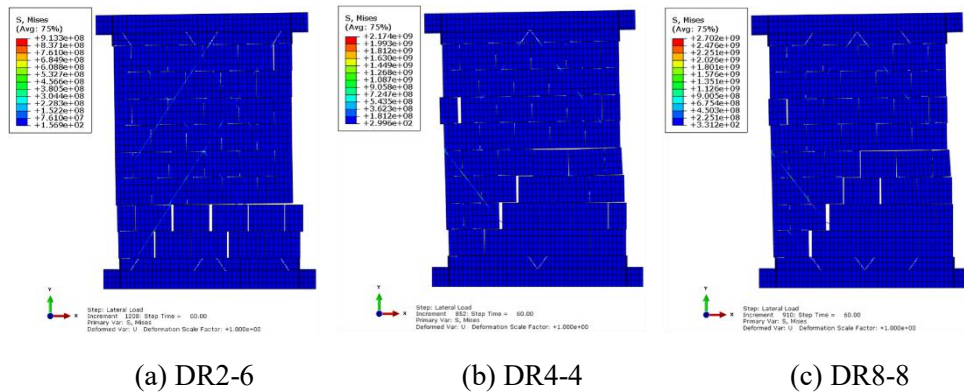


Figure 7-64 Failure mechanism of walls with diagonal CFRP2 rebars,  $\sigma = 0.5$  MPa

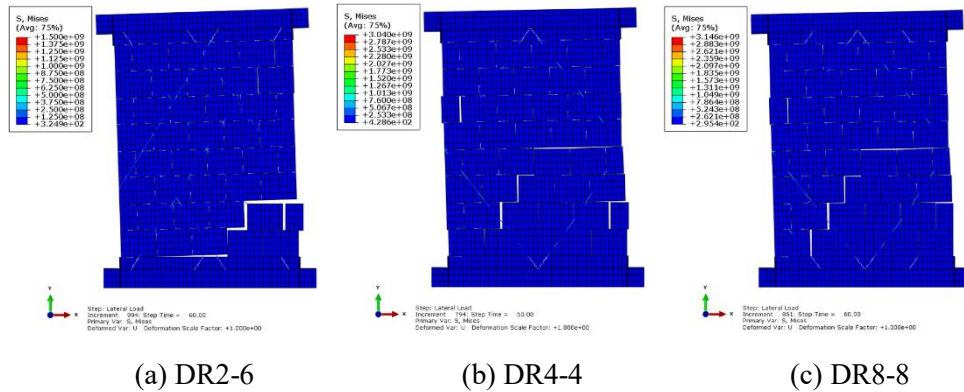


Figure 7-65 Failure mechanism of walls with diagonal CFRP2 rebars,  $\sigma = 0.875$  MPa

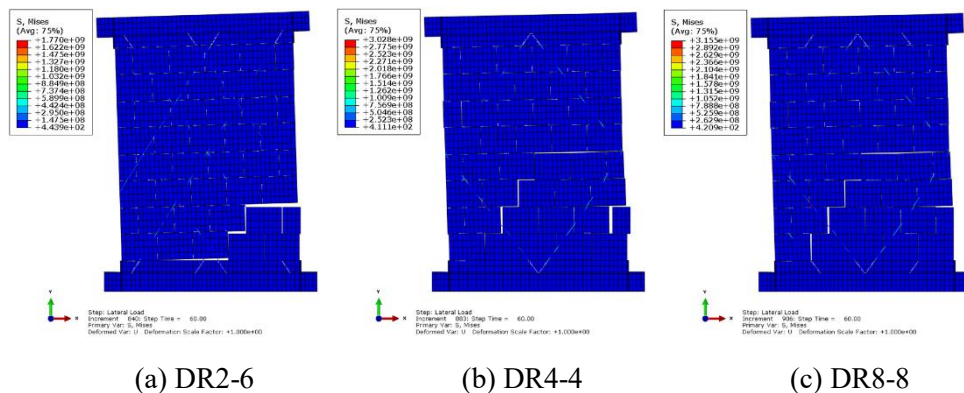


Figure 7-66 Failure mechanism of walls with diagonal CFRP2 rebars,  $\sigma = 1.25$  MPa

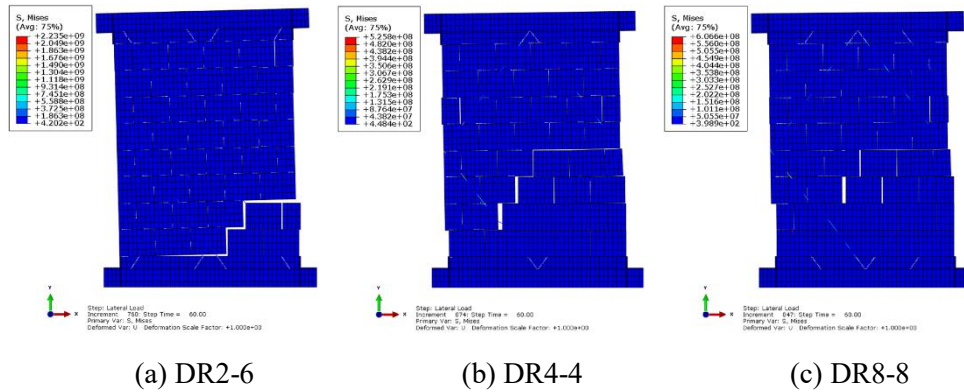


Figure 7-67 Failure mechanism of walls with diagonal EGFRP rebars,  $\sigma = 0.2$  MPa

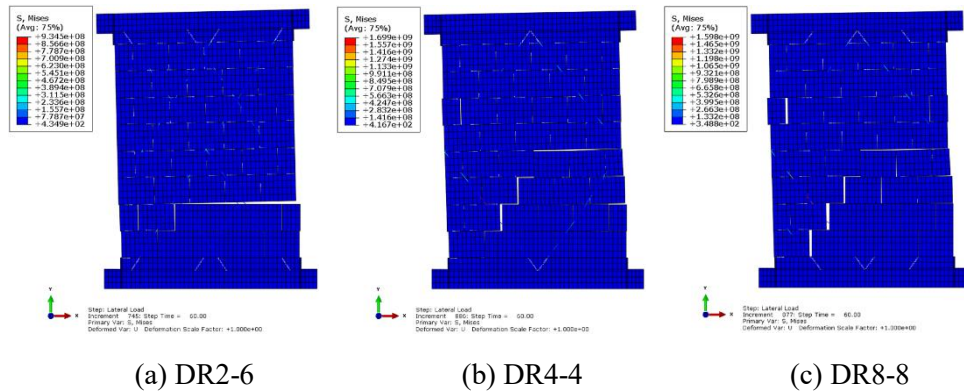


Figure 7-68 Failure mechanism of walls with diagonal EGFRP rebars,  $\sigma = 0.5$  MPa

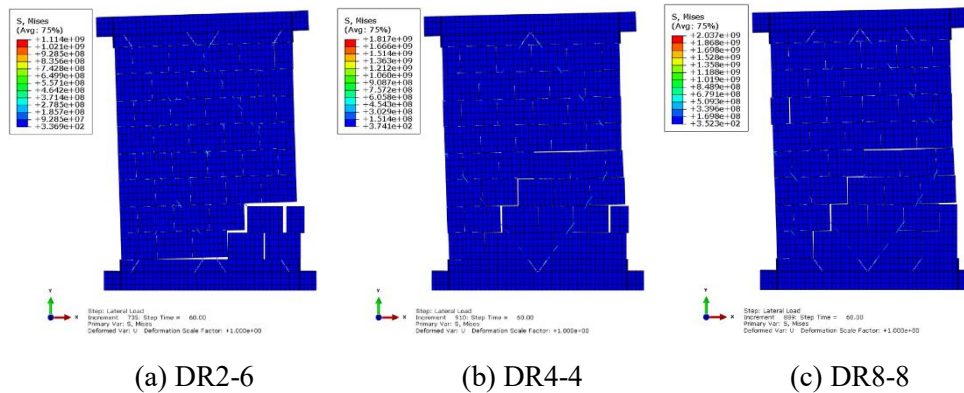


Figure 7-69 Failure mechanism of walls with diagonal EGFRP rebars,  $\sigma = 0.875$  MPa

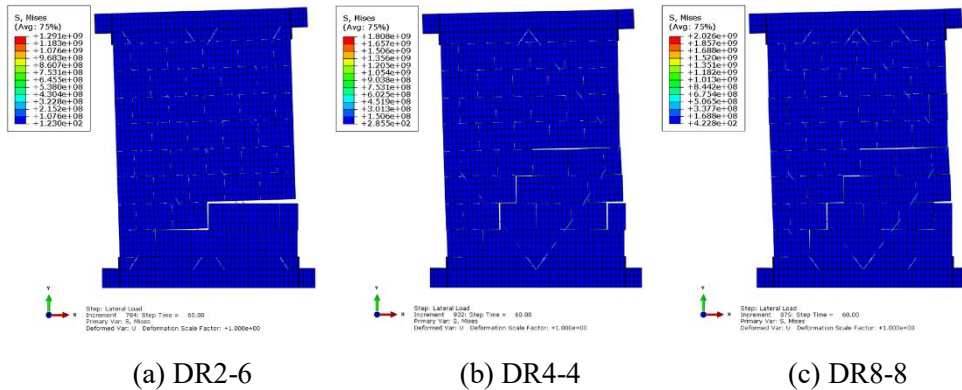


Figure 7-70 Failure mechanism of walls with diagonal EGFRP rebars,  $\sigma = 1.25$  MPa

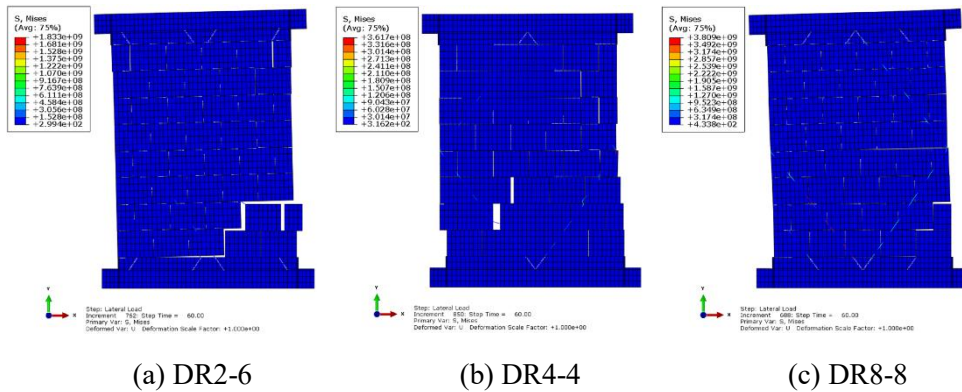


Figure 7-71 Failure mechanism of walls with diagonal SGFRP rebars,  $\sigma = 0.2$  MPa

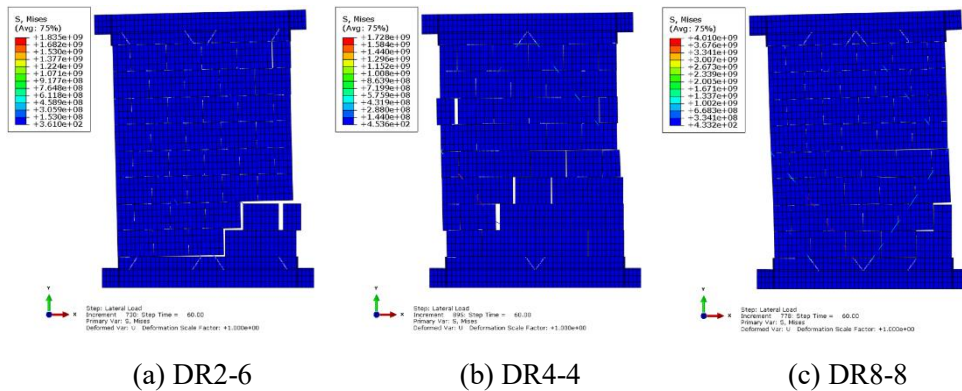
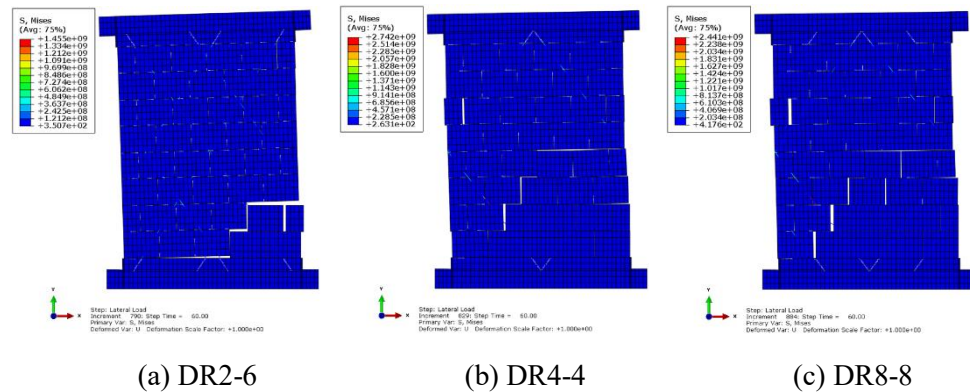
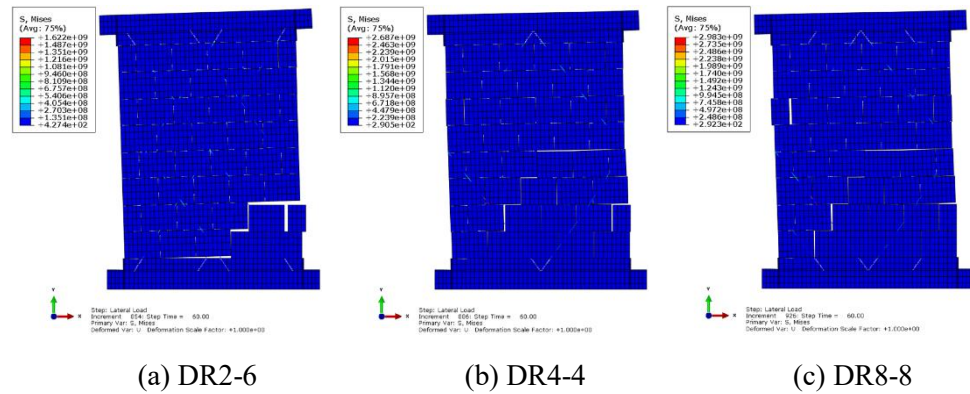


Figure 7-72 Failure mechanism of walls with diagonal SGFRP rebars,  $\sigma = 0.5$  MPa



**Figure 7-73** Failure mechanism of walls with diagonal SGFRP rebars,  $\sigma = 0.875$  MPa



**Figure 7-74** Failure mechanism of walls with diagonal SGFRP rebars,  $\sigma = 1.25$  MPa

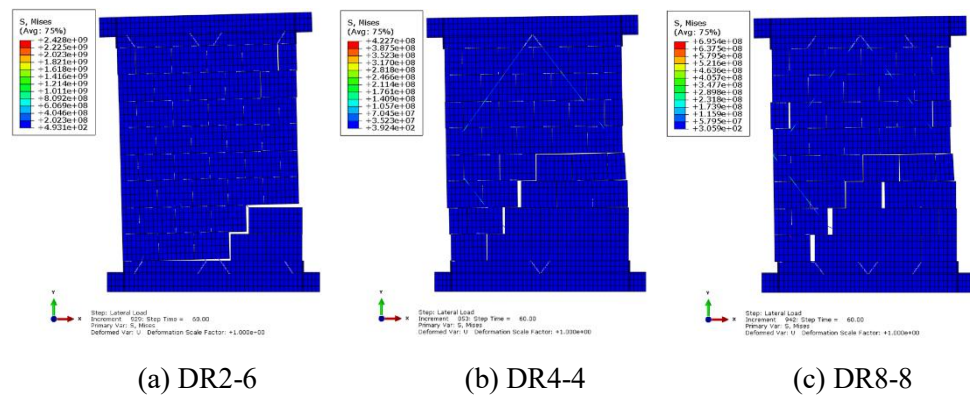


**Figure 7-75** Failure mechanism of walls with diagonal AFRP rebars,  $\sigma = 0.2$  MPa

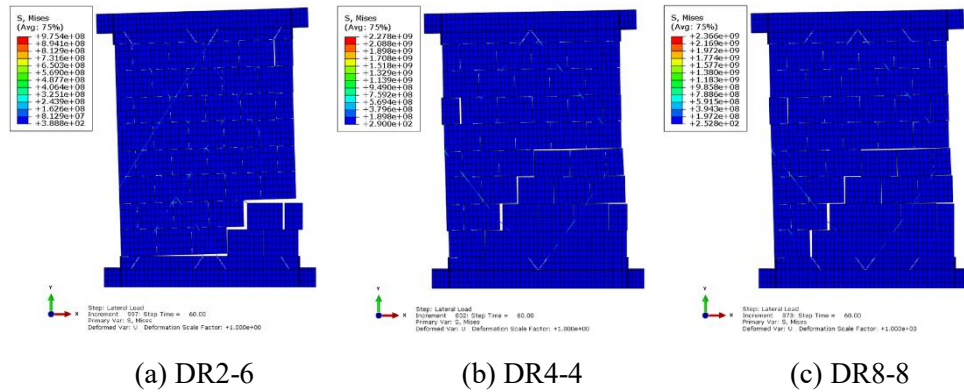


Figure 7-76 Failure mechanism of walls with diagonal AFRP rebars,  $\sigma = 0.5$  MPa

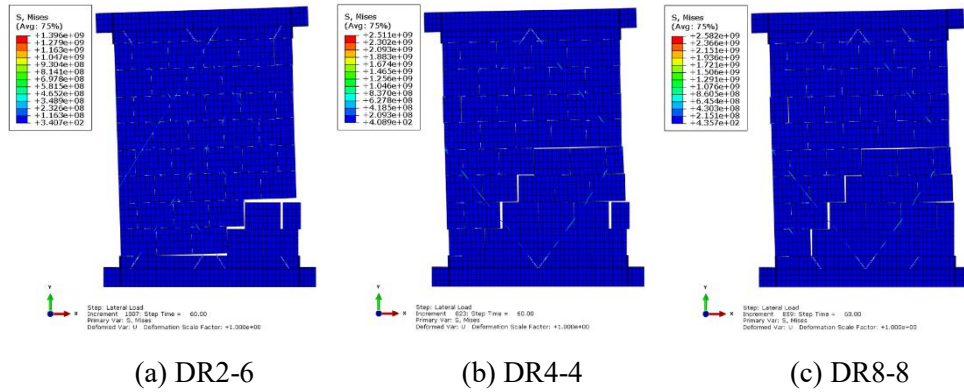


Figure 7-77 Failure mechanism of walls with diagonal AFRP rebars,  $\sigma = 0.875$  MPa

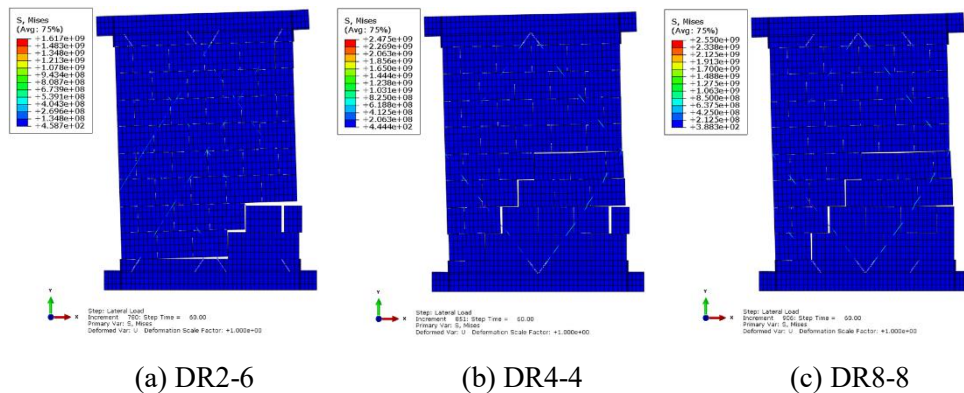
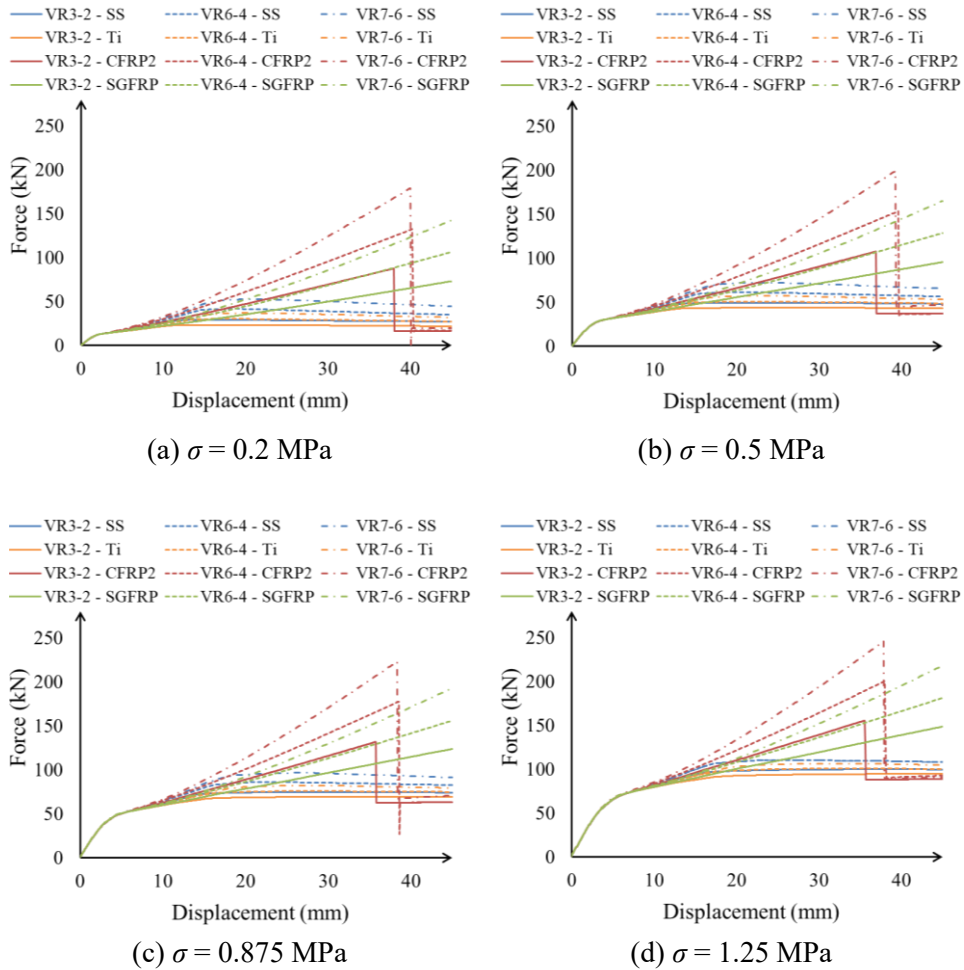


Figure 7-78 Failure mechanism of walls with diagonal AFRP rebars,  $\sigma = 1.25$  MPa

## 7.5 Comparative Studies

Based on the results of retrofitted models reported in **Section 7.4**, horizontal arrangements of rebar are not effective on the seismic behavior of the wall. While vertical and diagonal rebars improve the seismic behavior significantly by providing considerable overstrength and hardening. Within examined cases, VR3-2, VR6-4, and VR7-6 models of vertical arrangements and DR2-6, DR4-4, and DR8-8 models of diagonal arrangements show better performance within the other corresponding cases. According to the results of models with FRP rebars, CFRP2 has higher strength in comparison with other types of FRPs. On the other hand, SGFRP has more ductility with quite similar strength than CFRP2. Therefore, CFRP2 and SGFRP were selected as well as stainless steel and titanium for comparative studies. In this section, the results of these models were compared to find the most efficient retrofit case in terms of material and arrangements. The results of selected vertical arrangements for the selected materials are shown in **Figure 7-79**. Based on the results it can be seen that VR7-6 models have the highest efficiency in terms of over strength and hardening stiffness under all levels of pre-compression load. Both stainless steel and titanium rebars provide large ductility, but stainless steel results in a larger overstrength and hardening slope than titanium. However, CFRP2 and SGFRP provide significantly larger overstrength and hardening stiffness than that of stainless steel under all levels of pre-compression load. Although CFRP2 provides larger overstrength and hardening stiffness than SGFRP, it was not able to sustain the target displacement and broke. While SGFRP did not reach the ultimate strength

at target displacements. Therefore, it can be said that using SGFRP with VR7-6 arrangement can be considered as the most effective vertical case.



**Figure 7-79** Comparison of material properties for vertical arrangements under different levels of pre-compression load ( $\sigma$ )

The results of selected diagonal arrangements for the selected materials are shown in **Figure 7-80**. Similar to results for vertical models, stainless steel and

titanium rebars provide large ductility in all three cases and stainless steel results in larger overstrength and hardening stiffness than titanium rebars. Also in all cases, SGFRP and CFRP2 provide much larger overstrength and hardening than stainless steel.

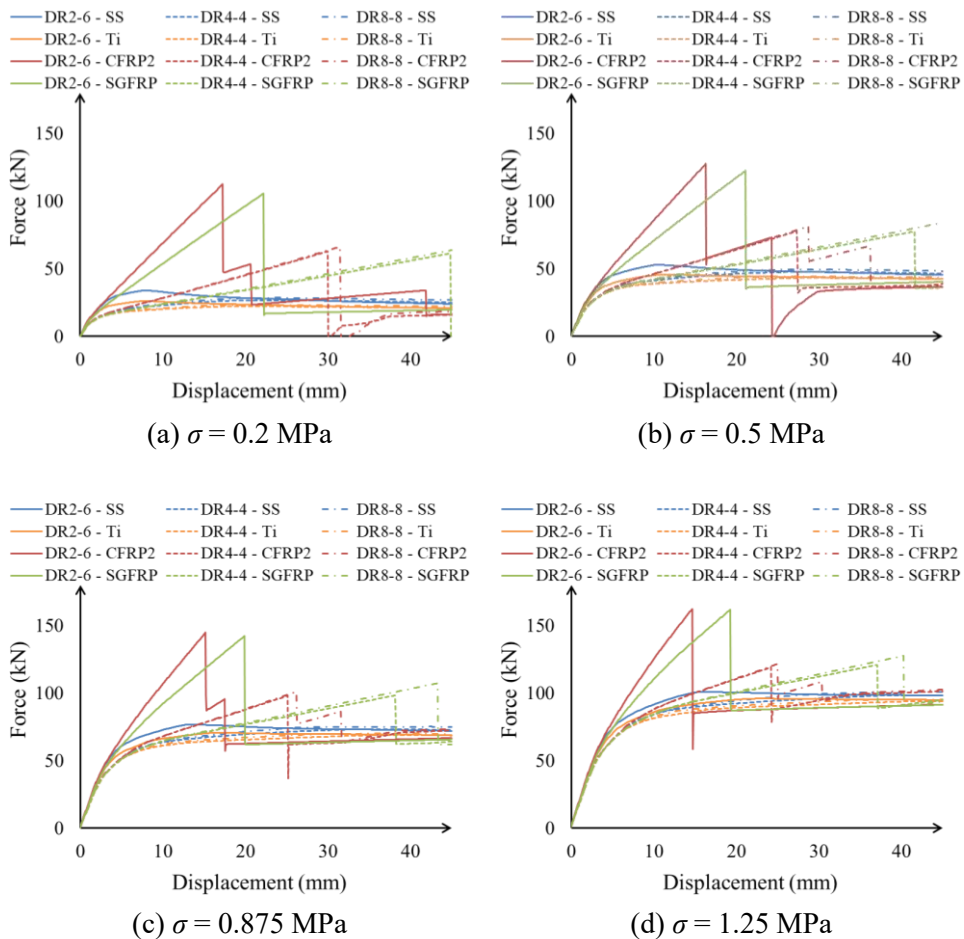


**Figure 7-80** Comparison of material properties for diagonal arrangements under different levels of pre-compression load ( $\sigma$ )

Within the three selected arrangements, DR2-6 model with CFRP2 results in the largest overstrength and hardening stiffness, and DR8-8 with SGFRP results in the largest ductility. In the case of DR8-8 model under low pre-compression loads ( $\sigma = 0.2$  and  $0.5$  MPa), SGFRP could sustain target displacement before failure, but it failed before the target displacement. Therefore, it can be said that using SGFRP with DR8-8 arrangement can be considered as the most effective diagonal case.

Finally, in order to obtain the most efficient case considering rebar materials and arrangements, force-displacement curves of vertical and diagonal arrangements were compared as shown in **Figure 7-81**. It can be seen that vertical arrangements provide a larger overstrength and hardening stiffness than diagonal arrangements. Therefore, VR7-6 with SGFRP material is proposed as the most efficient case for the retrofit of the dry-stack walls. Since SGFRP was not broken by target displacement, it can provide a significant stiffness during cyclic loading.

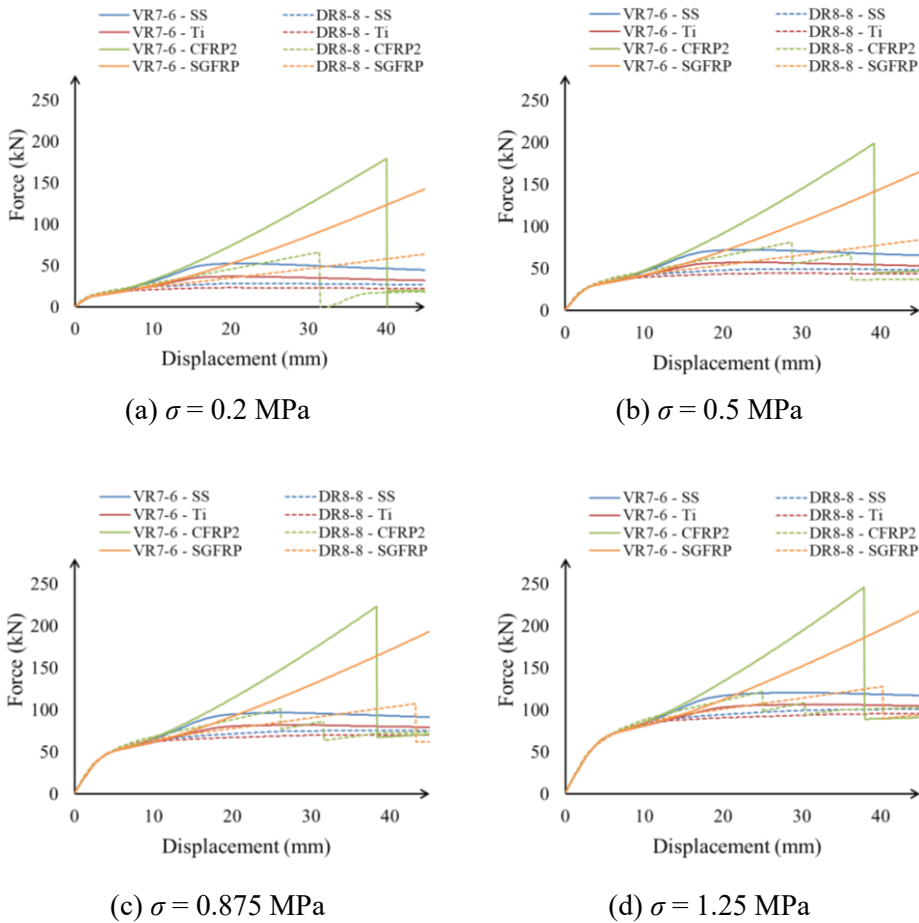


**Figure 7-81** Comparison of the most efficient models of vertical and diagonal arrangements under different levels of pre-compression load ( $\sigma$ )

## 7.6 Cyclic Analysis

In **Section 7.5** it was shown that VR7-6 among the models with vertical rebars and DR8-8 among models with diagonal rebars have the best performance. Besides, it was found that VR7-6 can provide considerably larger overstrength and hardening stiffness than DR8-8. The compression was made based on the results of the pushover analysis. In order to have a more comprehensive comparison, the results of

cyclic analyses for VR7-6 and DR8-8 with the most efficient material are investigated in this section. Hysteresis loops of original walls and retrofitted walls are shown in **Figures 7-82 to 7-85** for VR7-6 and **Figures 7-86 to 7-89** for DR8-8 under different levels of pre-compression load.

One of the observations that can be seen for all cases is that hysteresis loops were more stable by increasing the level of pre-compression load, especially for VR7-6. Also, hysteresis loops of DR8-8 were considerably narrower than that of VR7-6, regardless of material type, which can be considered as a significant defect of DR8-8 model in comparison with VR7-6 model.

The behavior of retrofitted walls with either stainless steel or titanium was quite similar. In the case of VR7-6 with stainless steel or titanium rebars, the cycles were quite symmetric under low pre-compression load.

The biased form of loops (similar to the original wall) can be observed under higher pre-compression load and overall hysteresis behavior was more similar to the original walls. Nonetheless, the free sliding at the unloading stage was improved relatively. On the other hand, observations for DR8-8 with stainless steel or titanium rebars were quite different. First of all, hysteresis loops were symmetric under all levels of pre-compression load and there was no improvement in free sliding at unloading stages.

In the case of models with CFRP2 and SGFRP (either VR7-6 or DR8-8 model), the amount of the biasing of hysteresis loops was considerably less than models with

stainless steel and titanium material. Because FRP materials remained mainly in the elastic range before failure. Also, free sliding at the unloading stage is similar to the results of pushover analysis for VR7-6 and DR8-8 models.

Results of the cyclic analysis showed that CFRP2 rebars significantly improve strength and hardening stiffness of the wall but it failed under smaller deformation than target displacement. Although SGFRP rebars in DR8-8 model did not fail under low pre-compression load, they failed under high pre-compression load. VR7-6 model with SGFRP failed at the last cycle (target displacement of 45 mm), except for  $\sigma = 1.25$  MPa which failed at a cycle before the last one (displacement of 40 mm).

It should be noted that in both pushover and cyclic analyses, the load was applied as displacement-control and it was gradually increased. Therefore, the possible shock that can be imposed on the system at the moment of FRP failure cannot be detected. This issue requires further study by investigating the behavior of the wall under seismic load through dynamic analysis, which is out of the scope of this study.

Among all models, it can be seen that VR7-6 model with SGFRP rebars showed the best performance. First of all, rebars failed at the target displacement in most cases. It improved the behavior of the wall by adding significant overstrength and hardening stiffness to the system, as it was also shown by pushover analysis. Furthermore, it effectively enhanced hysteresis behavior in several aspects. Based

on these results, it not only restrained the biasing of the loops, it minimized the values of free sliding which results in a larger hysteresis area (absorbed energy).

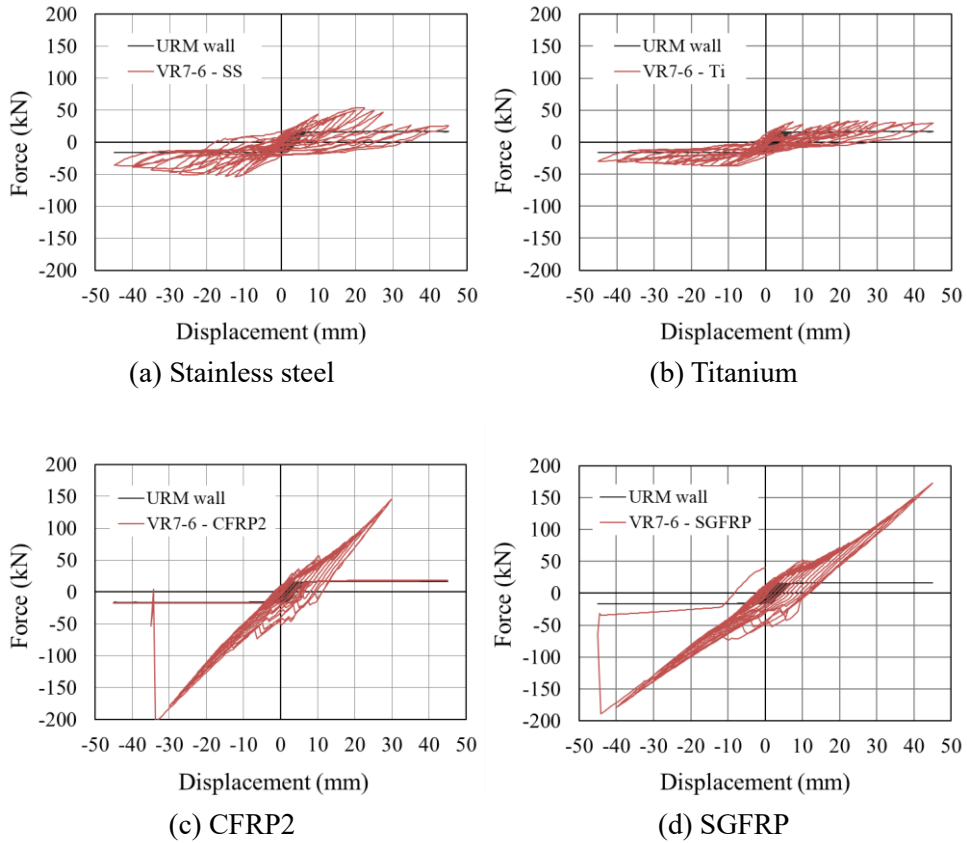


**Figure 7-82** Cyclic behavior of VR7-6 model,  $\sigma = 0.2$  MPa

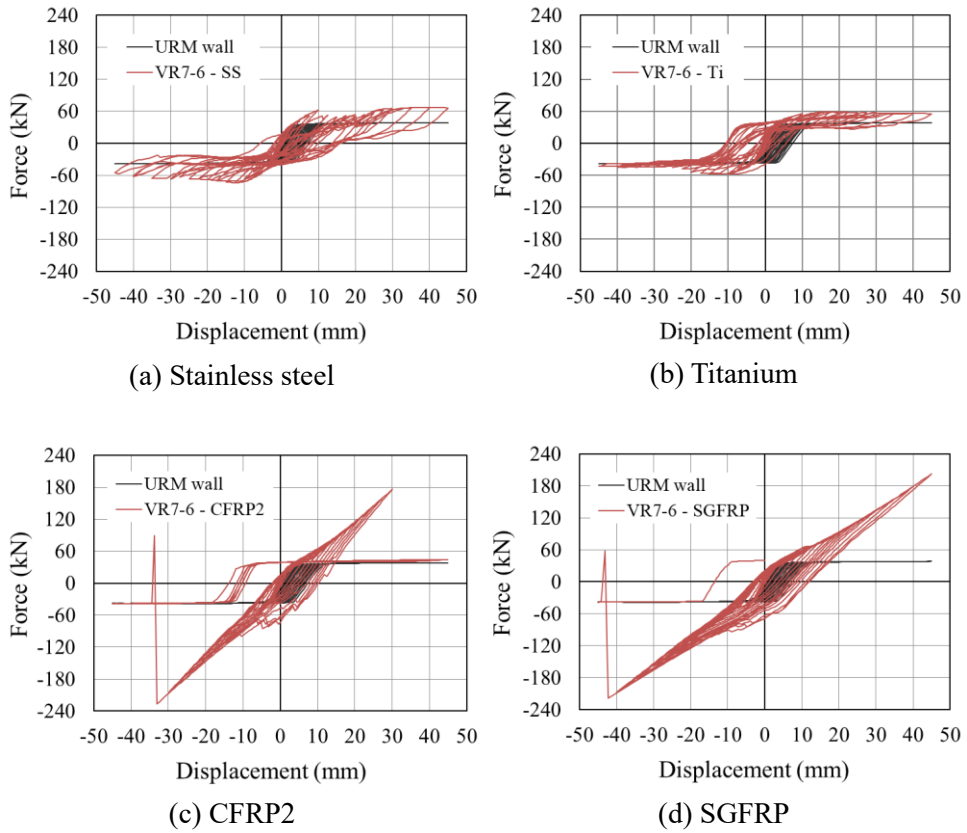
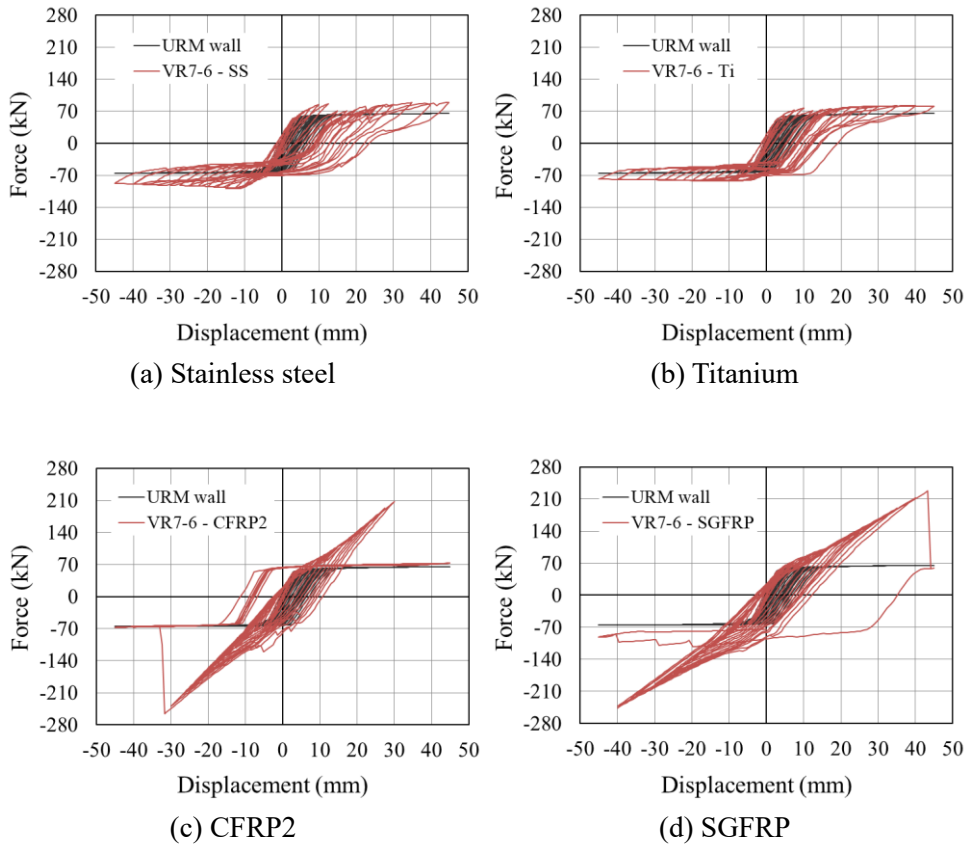
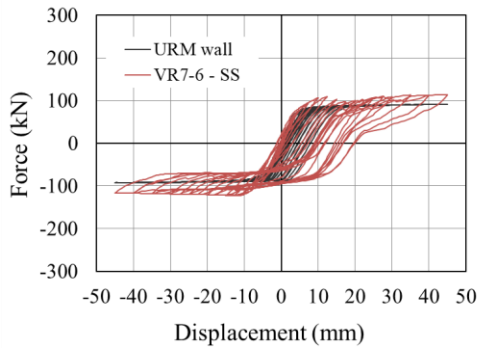


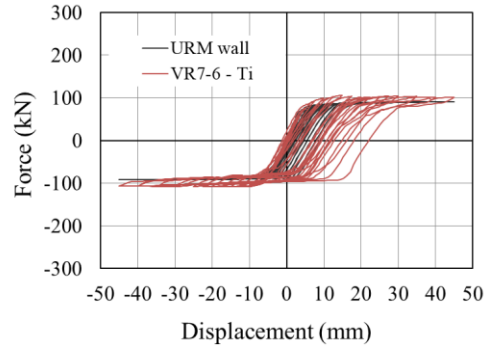
Figure 7-83 Cyclic behavior of VR7-6 model,  $\sigma = 0.5$  MPa



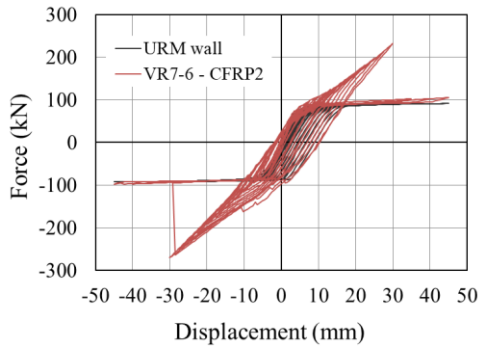
**Figure 7-84** Cyclic behavior of VR7-6 model,  $\sigma = 0.875$  MPa



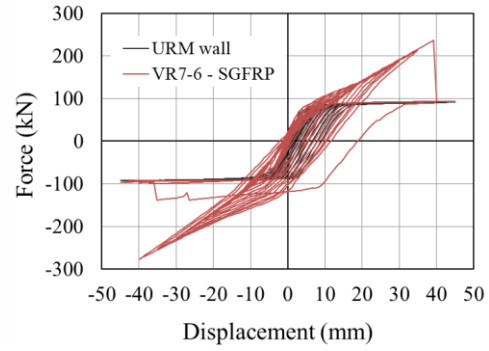
(a) Stainless steel



(b) Titanium



(c) CFRP2



(d) SGFRP

**Figure 7-85** Cyclic behavior of VR7-6 model,  $\sigma = 1.25$  MPa

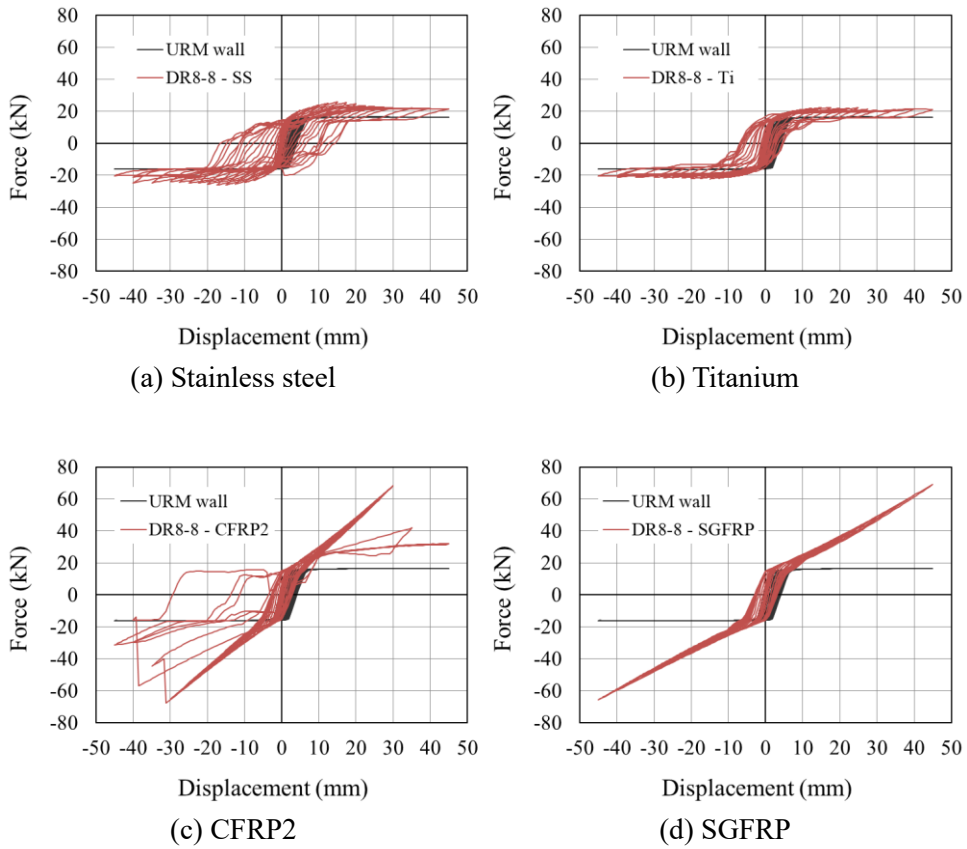


**Figure 7-86** Cyclic behavior of DR8-8 model,  $\sigma = 0.2$  MPa

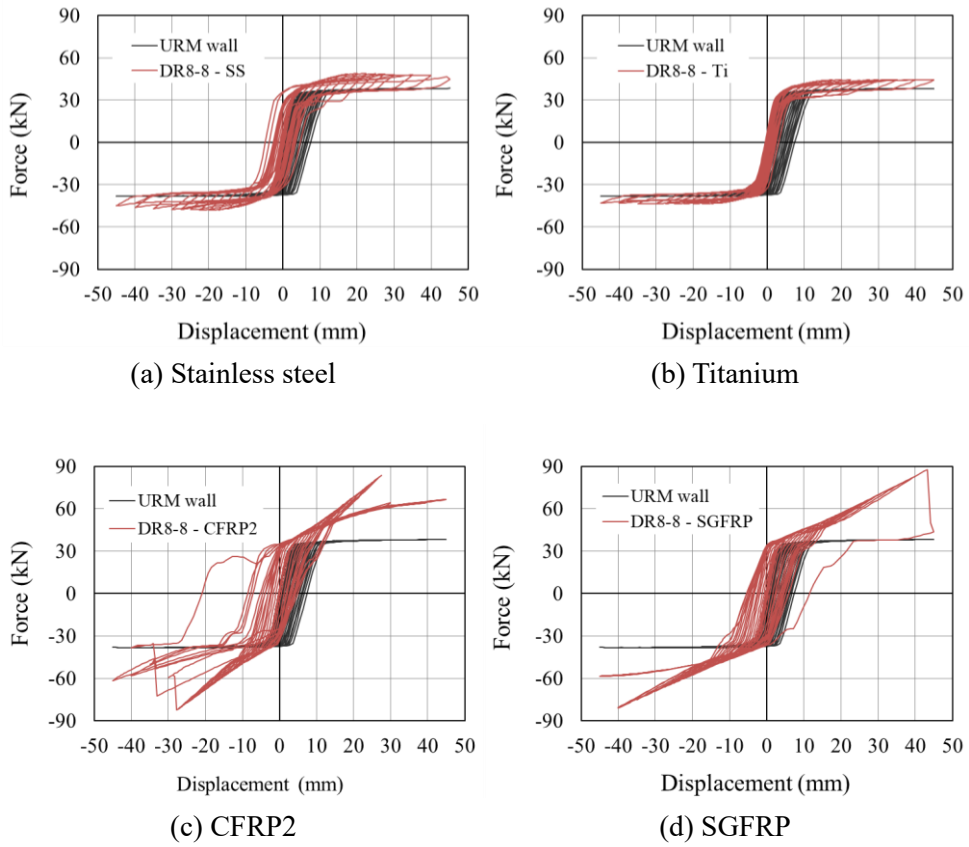


**Figure 7-87** Cyclic behavior of DR8-8 model,  $\sigma = 0.5$  MPa

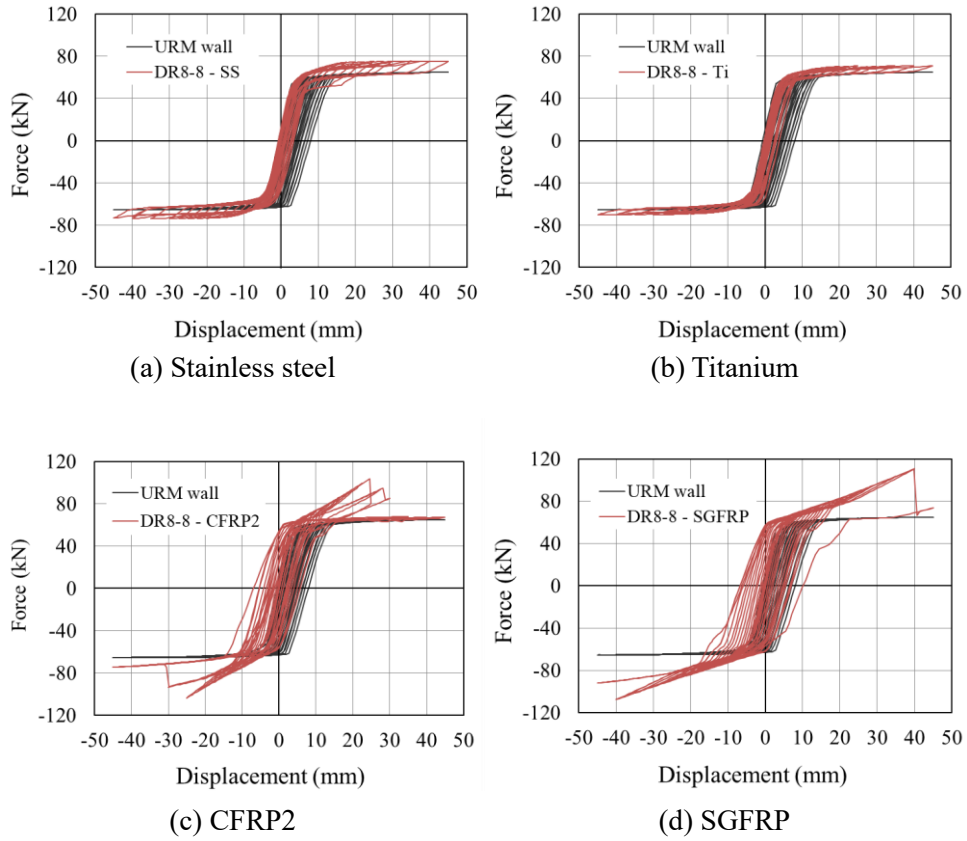


**Figure 7-88** Cyclic behavior of DR8-8 model,  $\sigma = 0.875$  MPa

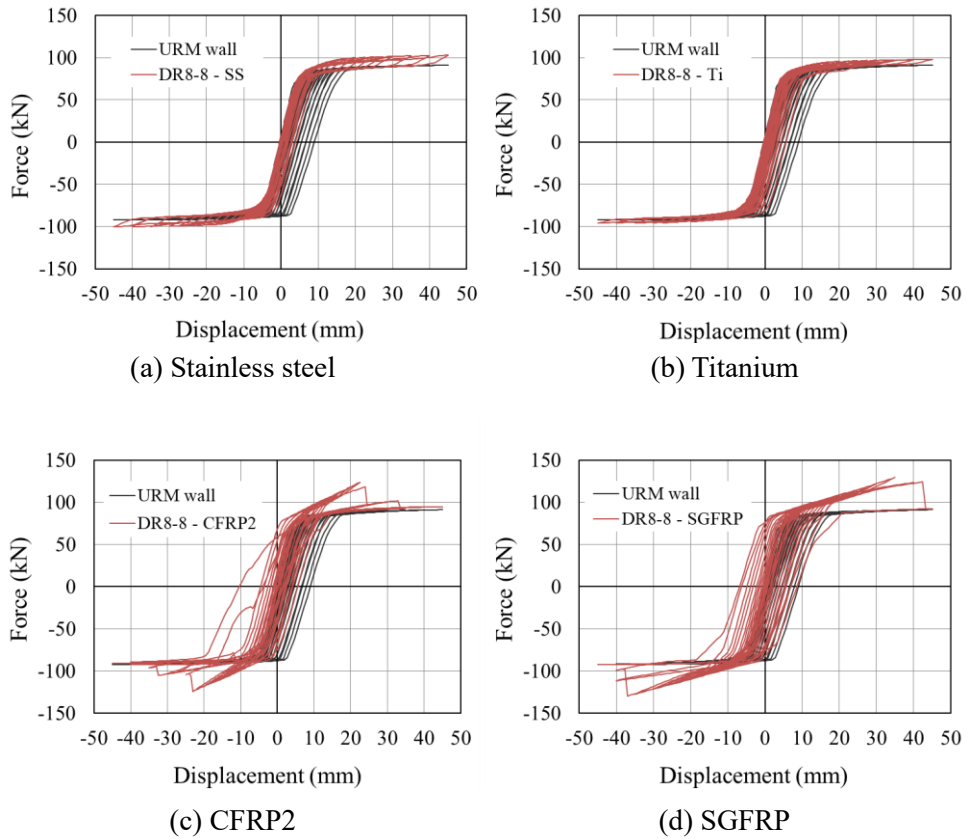


**Figure 7-89** Cyclic behavior of DR8-8 model,  $\sigma = 1.25$  MPa

The normalized dissipated energy of the models with respect to results of URM wall (Table 6-18) are reported in Table 7-15. It can be seen that, in all cases, the normalized dissipated energy was reduced by increasing pre-compression load. Also, values for VR7-6 were considerably larger than DR8-8 which is another superiority of VR7-6 model. For DR8-8 model, CFRP2 has a larger value than SGFRP for lower pre-compression loads and a smaller value under higher pre-compression loads. However, CFRP2 bars failed at smaller lateral displacement than SGFRP, which reduced its efficiency. For VR7-6 model, SGFRP has larger value than CFRP2 for

all pre-compression loads. Titanium and stainless steel also provided comparable dissipated energy with SGFRP (especially at higher pre-compression load). Nonetheless, SGFRP is more effective because of providing significant hardening stiffness and overstrength.

**Table 7-15** Normalized value of cyclic dissipated energy of retrofitted walls

Type	Material	Pre-compression load (MPa)			
		$\sigma = 0.2$	$\sigma = 0.5$	$\sigma = 0.875$	$\sigma = 1.25$
VR7-6	Ti	35.86	10.53	8.57	4.49
	SS	40.86	15.71	10.60	7.51
	CFRP2	52.94	17.23	10.25	6.88
	SGFRP	77.59	26.39	16.19	8.91
DR8-8	Ti	24.62	4.78	2.27	1.53
	SS	36.04	9.10	3.62	2.08
	CFRP2	28.79	12.41	5.73	3.75
	SGFRP	17.92	11.66	5.73	5.37

## 7.7 Summary

In this chapter, the seismic behavior of dry-stack walls retrofitted by inserting rebars was investigated. Three groups of arrangements based on horizontal, vertical, and diagonal rebars were considered. Each case was investigated for several material properties including stainless steel, titanium, and common types of FRP materials. Based on the results, horizontal arrangement of rebars is not an effective method for improving the mechanical behavior of the wall. On the other hand, vertical and diagonal arrangements considerably enhance the behavior of the wall in terms of overstrength and hardening stiffness. The most efficient cases of vertical and diagonal arrangements were selected and results were compared. The results showed that vertical models were more efficient and VR7-6 was the most efficient case, which includes 6 rebars positioned at sides and center. In addition, it was found that using FRP materials results in larger overstrength and hardening stiffness than steel and titanium. However, due to the brittle behavior of FRPs, SGFRP was selected as the most efficient case due to its large deformation capacity. Finally, a set of cyclic analyses has been done for a more comprehensive investigation. The results of cyclic analyses also confirmed that VR7-6 model with SGFRP rebars has the best performance among the proposed models.

## **Chapter 8. Summary and Conclusion**

In this study, different types of Historical Unreinforced Masonry (HURM) structures were investigated and classified in terms of material, configuration, and geometry. The most common failure mechanism and damage modes of a structure subjected to seismic loads were identified based on the observations of previous earthquakes. FEM analyses were conducted to assess the seismic performance of stone masonry walls under lateral loads. Based on the numerical analysis, the appropriate retrofitting method was suggested for stone masonry structures and examined for different conditions.

## 8.1 Summary

Unreinforced masonry (URM) structure is the most common construction that has been used generally from ancient times so far all over the world. This type of structure can be defined as the assemblage of units (stone, brick, or adobe) at the joints (frictional or mortar-based joints).

Heritage buildings are of great importance in the history of nations. Therefore, understanding the performance of historical masonry structures and their relevant characteristics is essential in the maintenance and preservation works. In this study, an in-depth investigation of typology, geometry, materials, configuration, structural and construction weaknesses, etc. was done. The main structural and non-structural components, which can be observed mostly in historical structures, were identified and their important role in the structural behavior of historical buildings was investigated. Generally, walls are the main structural element in historical URM buildings subjected to seismic load. The damage of this component may lead to the collapse of the whole structure. Therefore, wall behavior under compressive, tensile, and shear loads was discussed in detail based on the previous research works. Typical damage was classified into two main categories as damage because of seismic events or destructive activities and damage because of erosion. Both types of damage and their influence on the performance of HURM buildings were discussed in detail. The information and explanation provided in this dissertation can assist in detecting and

predicting the type and location of critical damage in elements that can accelerate the process of preservation works.

Preservation as a young science is an important scientific field to protect the value and authenticity of historical constructions. Maintaining these values, mostly the beautiful appearance of the building, is a substantial factor to select a proper technique. There are various types of retrofitting methods to improve the mechanical behavior of masonry structures. In this study, a list of the most common retrofit methods was introduced and classified based on their action. These methods can be divided into three main categories as (I) improving the structural integrity; (II) reducing the seismic demands; and (III) upgrading the structural system of the existing building. The implementation, advantages, and drawbacks of each method, and also the applicability of the method for HURM structures were discussed in detail. This information can be used as a practical reference in the primary stage of the retrofitting project for selecting more suitable methods.

In this study, the behavior of the wall and the efficiency of the retrofit method were investigated by using numerical models. To obtain reliable results from numerical simulation, it should be properly calibrated with experimental or theoretical results. Also, a correct understanding of the philosophy of the numerical method as well as its advantages and limitation is an essential step before performing analyses. Additionally, some of the most common experimental and numerical methods for masonry structures were introduced. The current methods of existing numerical techniques, with emphasis on applicable methods for masonry structure,

were discussed. Among the different types of walls used in historical structures, walls with dry-stack joints were selected in this study for investigation as one of the most vulnerable elements, and also due to lack of research on this type of walls in comparison with irregular or rubble masonry types. Numerical models were created based on finite elements by using ABAQUS software and seismic behavior under lateral load was investigated by conducting pushover analysis. The results of experimental tests conducted by Vasconcelos (2005) were selected and used for the calibration of numerical models. A framework was proposed to check the validity of numerical results based on calibration of the model by selecting the most uncertain parameters. After calibration, a set of sensitivity and parametric studies were performed to have a better understanding of wall behavior. To enhance the seismic behavior of the wall and taking into account the importance of preserving the wall appearance, retrofit by inserting rebars inside the wall was proposed. The efficiency of the retrofit method was examined with different materials (stainless steel, titanium, and common types of FRP materials) and arrangements of rebars (horizontal, vertical, diagonal).

### **8.2 Conclusion**

The following main conclusions were derived from the results of numerical simulation of in-plane behavior of dry-stack stone masonry walls and the retrofitted walls under lateral load:

1. Utilizing a micro-modeling approach and performing pushover analysis could precisely measure the stiffness and strength of dry-stack walls under in-plane lateral load. Also, the observed failure mechanism was the same as the experiment.

2. The overall behavior of the dry-stack wall under pushover load was in form of elastic-perfect plastic behavior. Also, the behavior of dry-stack walls was highly influenced by the level of pre-compression load. Both stiffness and strength of the wall were considerably larger under higher pre-compression loads. These results are the same as those reported by Vasconcelos (2005).

3. Based on the sensitivity analysis, it was found that the main influential parameter on strength of the wall was the friction coefficient. However, the relation between the friction coefficient and the strength was not linear.

4. The results showed that for the friction coefficient equal to or less than 0.35, the failure mechanism was horizontal sliding. Whereas, for the case with the value of 0.4 and larger the failure mechanism was in form of diagonal stair-stepped cracks (joint opening). The strength of the wall with stair-stepped cracks was larger than horizontal sliding under all levels of pre-compression load. For the values larger than 0.4, the increase in strength was not considerable. Besides, the effect of the friction coefficient was not significant on the stiffness of the wall.

5. The main influential numerical parameters on the stiffness of the wall were mesh size and slip tolerance factor. Both parameters change the penalty stiffness such that smaller mesh size and friction tolerance factor reduce the penalty stiffness, and

larger values increase the penalty stiffness. Note that a larger penalty stiffness increases the wall stiffness and vice versa. Even so, the computational cost is increased by reducing mesh size (more number of elements), while changing slip tolerance factor does not require more elements, and computational cost is not changed. Based on the sensitivity analysis, the default value of the software (0.005) for slip tolerance factor resulted in the best fit of the numerical model and experimental results. Although the value of 0.005 was suitable here, it may not be appropriate for all other cases in general and sensitivity analysis may be required.

6. By comparing the results of 3D and 2D models, it was found that there was no significant difference between results in terms of the force-displacement curves, stress distributions, and failure mechanisms.

7. Although it was found that friction coefficient  $\mu = 0.4$  and larger results in a similar response in monotonic test, the results of cyclic test showed a significant influence of  $\mu$  on hysteresis behavior. Based on the results, hysteresis energy was considerably overestimated for small  $\mu$  (e.g. 0.4). By increasing  $\mu$ , this error was significantly reduced. However, for very large  $\mu$ , direction of the biasing was inverted. Considering all characteristics,  $\mu = 0.55$  was found to have a best fit with experimental results.

8. Results of the cyclic analysis showed a well matching with experimental results. Although overall results were consistent with the experiment, it had one main defect. Based on experimental results, there is a delay (free displacement) at the start

of the unloading stage before the wall recovers its stiffness. The effect was detected by the model, but with a smaller delay that resulted in larger bias and hysteresis energy. However, this error could be observed only at large displacements and for small displacement was negligible. Also, the pushover curves were matched with the backbone of cyclic analysis.

9. The parametric study on the effect of stone unit size showed that increasing the unit size resulted in larger stiffness and strength of the wall, but the effect was not significant, and also the failure mechanism was the same. Nevertheless, further study is required to generalize the conclusion.

10. Parametric study on the wall width showed that the failure mode of the wall was not changed by increasing the width and remained as stair-stepped mechanism. The main difference was that for walls with a width larger than the original wall the cracks did not reach the top corner. So, it can be expected that the joint in these walls under cyclic load will be open in form of an eccentric inverted V-shape (“/ \”) instead of X-shape stair-stepped. The results showed that strength and stiffness were considerably increased by increasing the width.

11. Parametric study on the height of the wall showed that by increasing the height the failure mode was somehow similar to the effect of changing the width. The main difference was that crack reached the tensile face rather than the top corner. The results showed that the strength and strength were considerably decreased by increasing the height.

12. It was also found that keeping the aspect ratio constant and increasing the wall size, the behavior was similar to the original wall. In this case, the stiffness remained almost constant, while strength is almost linearly increased by the ratio of the wall size.

13. Based on the results of retrofitting programs, inserting horizontal rebars was not an effective method and did not change the stiffness and strength of the wall.

14. Inserting vertical or diagonal rebars added overstrength and hardening stiffness to the behavior of the original wall. By using FRP rebars, larger overstrength and hardening stiffness were achieved in comparison with stainless steel or titanium rebars. However, due to the brittle behavior of FRP material, rebars were broken before the target displacement in many cases. Whereas, stainless steel and titanium sustained a large lateral deformation through their plastic deformation.

15. Among FRP materials, CFRP2 provided the largest overstrength and hardening stiffness. On the other hand, SGFRP sustained the target displacement without failure and with a pretty similar overstrength obtained by CFRP2. In the case of vertical rebars, SGFRP did not fail at target displacement under all four examined levels of pre-compression load. Just that under high pre-compression load it failed in diagonal arrangements which reduced its efficiency.

16. In the comparison of models with diagonal and vertical rebars, it was found that vertical rebars have more efficiency in terms of overstrength, hardening stiffness, (and ductility for FRP materials).

17. Based on the results on the efficiency of the retrofit methods by inserting different arrangements of rebars, VR7-6 model (with 6 rebars arranged at both sides and the center) was proposed as the most efficient case.

18. Along with VR7-6 model of the arrangement, SGFRP rebars provided significant overstrength ratio (8.81 ( $\sigma = 0.2$  MPa) and 2.44 ( $\sigma = 1.25$  MPa)) and hardening stiffness ratio (0.44 ( $\sigma = 0.2$  MPa) and 0.32 ( $\sigma = 1.25$  MPa)). Also, it could sustain large lateral deformation. Therefore, it was proposed as the most efficient material.

19. Results of cyclic analysis also confirmed that VR7-6 model with SGFRP material has better performance than the other proposed models. Hysteresis loops were stable and improved by increasing the pre-compression load. Since SGFRP rebars in VR7-6 model remained in the elastic range, except for the last or last several cycles, two main defects in hysteresis loops of the original wall, i.e. biasing the loops to one side and free sliding at the start of the unloading stage were almost removed.

20. Since the stiffness was recovered immediately, the hysteresis loops were larger and improved the energy absorption of the wall. The amount of ratio of energy dissipation of the model and URM wall was 77.59 ( $\sigma = 0.2$  MPa) or 8.91 ( $\sigma = 0.2$  MPa), which is significant values.

21. If it is not possible to use SGFRP rebars (regardless of unavailability, cost issue, etc.), stainless steel rebars and titanium rebars can be considered as a better substitute than other types of FRP material. Although stainless steel and titanium

rebars did not increase overstrength and hardening stiffness as much as other types of FRP material (such as CFRP2), they provided a ductile behavior. While other FRPs had a small lateral deformation capacity, which is a critical aspect of seismic behavior.

### **8.3 Future Work**

Although it was attempted to comprehensively investigate the seismic behavior of HURM structures, many aspects have been left for future study. In the following, some issues that can be improved or extended further and also a group of interesting studies that are worth for future works are listed:

1. Evaluating other possible arrangements of inserted rebars including a combination of vertical and diagonal rebars;
2. Improving the modeling technique to obtain more accurate results from the cyclic analysis;
3. Evaluating the seismic performance of dry-stack walls by performing time history dynamic analysis;
4. Out-of-plane behavior of dry-stack walls and practical retrofit techniques;
5. Investigation of box-type behavior by including wall-roof and perpendicular walls;
6. Developing a homogenized model for dry-stack walls;
7. Investigation of masonry walls with mortar-based joint with rubble stones;
8. Investigation of masonry walls with mortar-based joint with irregular stones for different arrangements and unit sizes.

## References

ABAQUS (2020). “ABAQUS Documentation”, Dassault Systèmes Simulia Corporation, Providence, RI.

Abdulsalam, B., and Ali, A. H. (2014). “The Preservation of Historical Masonry Heritage Structures Using Advanced Composite Materials”, *International Journal of Engineering Sciences and Research Technology*, 4(8), 14-24.

Abrams, D. P., and Lynch, J. M. (2001). “Flexural Behavior of Retrofitted Masonry Piers”, *In KEERC-MAE Joint Seminar on Risk Mitigation for Regions of Moderate Seismicity*, 234-243.

ACI 549R-18. (2018). “Report on Ferrocement”, *American Concrete Institute*, Reported by ACI Committee 549.

Aguilar, A. (2016). “The Seismic Rehabilitation of Historic Buildings”, *Government Printing Office, National Park Service*, ISSN: 0885-701641, 1–20.

AIJ. (2015). “Recommendations for Loads on Buildings (AIJ-RLB-2015)”, *Architectural Institute of Japan*, (English version, 2018).

Akcay, C., Bozkurt, T. S., Sayin, B., and Yildizlar, B. (2016). “Seismic Retrofitting of the Historical Masonry Structures Using Numerical Approach”, *Construction and Building Materials*, 113, 752-763.

Akcay, C., Sayin, B., and Yildizlar, B. (2017). “The Conservation and Repair of Historical Masonry Ruins Based on Laboratory Analyses”, *Construction and Building Materials*, 132, 383-394.

Al-Jaberi, Z., Myers, J. J., and ElGawady, M. (2015). “Influence of Near-Surface Mounted (NSM) FRP on the out-of-Plane Behavior of Reinforced Masonry Walls”, *In 12th North American Masonry Conference, I*, 1107-1119.

Amiraslanzadeh, R., Ikemoto, T., Miyajima, M., and Fallahi, A. (2012). “A Comparative Study on Seismic Retrofitting Methods for Unreinforced Masonry Brick Walls”, *In 15th World Conf. on Earthquake Engineering, International Association for Earthquake Engineering*, 2-10, Tokyo.

Anthoine, A., Magonette, G., and Magenes, G. (1995, August). “Shear-Compression Testing and Analysis of Brick Masonry Walls”, *In Proceedings of the 10th European Conference on Earthquake Engineering*, 3, 1657-1662.

Apostolopoulou, M., Aggelakopoulou, E., Siouta, L., Bakolas, A., Douvika, M., Asteris, P. G., and Moropoulou, A. (2017). “A Methodological Approach for the Selection of Compatible and Performable Restoration Mortars in Seismic Hazard Areas”, *Construction and Building Materials*, 155, 1-14.

Applied Technology Council (ATC) (1999). "Evaluation of Earthquake Damaged Concrete and Masonry Wall Buildings", Technical Resources, 307, *Federal Emergency Management Agency*, Washington, D.C., (FEMA-307).

ASCE. (2017). "Minimum Design Loads and Associated Criteria for Buildings and Other Structures (ASCE 7-16)", *American Society of Civil Engineers*, Reston, VA.

Asteris, P. G., Tzamtzis, A. D., Vouthouni, P. P., and Sophianopoulos, D. S. (2005). "Earthquake Resistant Design and Rehabilitation of Masonry Historical Structures", *Practice Periodical on Structural Design and Construction*, 10(1), 49-55.

ASTM C270-12. (2012). "Standard Specification for Mortar for Unit Masonry", *American Society for Testing and Materials (ASTM)*, West Conshohocken, PA.

ASTM E518/E518M-15. (2015). "Standard Test Methods for Flexural Bond Strength of Masonry", *American Society for Testing and Materials (ASTM)*, West Conshohocken, PA.

ATC-24. (1992). "Guidelines for Cyclic Seismic Testing of Components of Steel Structures for Buildings", Report No. ATC-24, *Applied Technology Council*, Redwood City, CA.

Atkinson, R. H., Amadei, B. P., Saeb, S., and Sture, S. (1989). "Response of Masonry Bed Joints in Direct Shear", *Journal of Structural Engineering*, 115(9), 2276-2296.

- Augenti, N., and Parisi, F. (2009). “Non-linear Static Analysis of Masonry Structures”, *In Proceedings of the 13th Italian National Conference on Earthquake Engineering, 1*, paper no. S4.
- Azevedo, J. O., Sincaian, G., and Lemos, J. V. (2000). “Seismic Behavior of Blocky Masonry Structures”, *Earthquake Spectra, 16*(2), 337-365.
- Badoux, M., Elgwady, M. A., and Lestuzzi, P. (2002). “Earthquake Simulator Tests on Unreinforced Masonry Walls Before and After Upgrading with Composites”, *In 12th European Conference on Earthquake Engineering*, 9-13.
- Baggio, C., and Trovalusci, P. (1995). “Stone Assemblies under in-Plane Actions, Comparison between Nonlinear Discrete Approaches”, *Comput Methods Struct Mason, 3*, 184-193.
- Baird, A., and Ferner, H. (2017). “Damage to Non-structural Elements in the 2016 Kaikōura Earthquake”, *Bulletin of the New Zealand Society for Earthquake Engineering, 50*(2), 187-193.
- Bazant Z.P., Oh B. (1983). “Crack Band Theory for Fracture of Concrete”, *RILEM Materials and Structures, 16*, 155–177.
- Belytschko, T., and Black, T. (1999). “Elastic Crack Growth in Finite Elements with Minimal Remeshing”, *International Journal for Numerical Methods in Engineering, 45*(5), 601-620.

- Bhattacharya, S., Nayak, S., and Dutta, S. C. (2014). "A Critical Review of Retrofitting Methods for Unreinforced Masonry Structures", *International Journal of Disaster Risk Reduction*, 7, 51-67.
- Block P. (2005). "Equilibrium Systems. Studies in Masonry Structure", MS Dissertation, *Department of Architecture, Massachusetts Institute of Technology, Cambridge, MA*.
- Block P., Ciblac T., and Ochsendorf J.A. (2006). "Real-time Limit Analysis of Vaulted Masonry Buildings", *Computers and Structures*, 84, 1841-1852.
- Blondet, M., Vargas, J., Torrealva, D., Tarque, N., and Velázquez, J. (2006). "Seismic Reinforcement of Adobe Houses Using External Polymer Mesh", *In First European Conference on Earthquake Engineering and Seismology*, Geneva, Switzerland.
- Borri, A., Castori, G., Corradi, M., and Speranzini, E. (2011). "Shear Behavior of Unreinforced and Reinforced Masonry Panels Subjected to in Situ Diagonal Compression Tests", *Construction and Building Materials*, 25(12), 4403-4414.
- Borri, A., Castori, G., and Grazini, A. (2009). "Retrofitting of Masonry Building with Reinforced Masonry Ring-Beam", *Construction and Building Materials*, 23(5), 1892-1901.
- Bosiljkov, V., Page, A., and Bokan, B. V. (2003). "Performance Based Studies of in-Plane Loaded Unreinforced Masonry Walls".

- Boussabah, L. and M. Bruneau (1992). “Review of the Seismic Performance of Unreinforced Masonry Walls”, *10th World Conference on Earthquake Engineering*, Rotterdam, Netherlands, 4537-4540.
- Branco, M., and Guerreiro, L. M. (2011). “Seismic Rehabilitation of Historical Masonry Buildings”, *Engineering Structures*, 33(5), 1626-1634.
- Brasile, S., Casciaro, R., and Formica, G. (2007). “Multilevel Approach for Brick Masonry Walls–Part I: A Numerical Strategy for the Nonlinear Analysis”, *Computer Methods in Applied Mechanics and Engineering*, 196(49-52), 4934-4951.
- Bruneau, M. (1994). “Seismic Evaluation of Unreinforced Masonry Buildings-A State-of-the-Art Report”, *Canadian Journal of Civil Engineering*, 21(3), 512-539.
- Calvi, G. M., Kingsley, G. R., and Magenes, G. (1996). “Testing of Masonry Structures for Seismic Assessment”, *Earthquake Spectra*, 12(1), 145-162.
- Candeias, P. (2008). “Seismic Vulnerability Assessment of Ancient Buildings”, Doctoral Dissertation, University of Minho, Guimarães, Portugal. (in Portuguese)
- Casapulla, C., and Argiento, L. U. (2018). “In-plane Frictional Resistances in Dry Block Masonry Walls and Rocking-Sliding Failure Modes Revisited and Experimentally Validated”, *Composites Part B: Engineering*, 132, 197-213.

Cervera, M., and Chiumenti, M. (2006). “Smearred Crack Approach: Back to the Original Track”, *International Journal for Numerical and Analytical Methods in Geomechanics*, 30(12), 1173-1199.

CEN, “EN 1052-3. (2002). “Methods of Test for Masonry - Part 3: Determination of Initial Shear Strength”, (European Standard).

Chambers, J., and Kelly, T. (2004). “Nonlinear Dynamic Analysis—the Only Option for Irregular Structures”, *In 13th World Conference on Earthquake Engineering*, Vancouver, Canada.

Clark, P., Frank, K., Krawinkler, H., and Shaw, R., 1997. “Protocol for Fabrication, Inspection, Testing, and Documentation of Beam-Column Connection Tests and Other Experimental Specimens”, *SAC Steel Project Background Document*. October, Report No. SAC/BD-97/02.

Clemente R., Roca P., Cervera M. (2006). “Damage Model with Crack Localization-Application to Historical Buildings”, *Structural V International Seminar on Structural Analysis of Historical Constructions - SAHC06*, New Delhi, India, 1125-1135.

Corsanego A. and Gavarini C. (1993). “Ten Years of Research into the Seismic Vulnerability of Constructions in Italy”, 149-156.

Croci, G., (1998). “The Conservation and Structural Restoration of Architectural Heritage”, Advances in Architecture Series, *Computational Mechanics Publications*, Southampton, UK, *WIT Press*, 1.

Corradi, M., Borri, A., Castori, G., and Sisti, R. (2016). “The Reticulatus Method for Shear Strengthening of Fair-Faced Masonry”, *Bulletin of Earthquake Engineering*, 14(12), 3547-3571.

Csikai, B., Ramos, L. F., Bastos, P., Moreira, S. M. T., and Lourenço, P. B. (2014). “Flexural out-of-Plane Retrofitting Technique for Masonry Walls in Historical Constructions”, In *SAHC2014–9th International Conference on Structural Analysis of Historical Constructions*, Mexico City, Mexico.

Cundall P.A., Hart P. (1971). “A Computer Model for Simulating Progressive Large Scale Movements in Blocky Rock Systems”, *Symposium on Rock Fracture -ISRM*, Nancy, France, 1, No. II-8.

Dalkılıç, N., and Nabikoğlu, A. (2017). “Traditional Manufacturing of Clay Brick Used in the Historical Buildings of Diyarbakir (Turkey)”, *Frontiers of Architectural Research*, 6(3), 346-359.

Da Porto, F., Guidi, G., Dalla Benetta, M., and Verlato, N. (2013). “Combined in-Plane/out-of-Plane Experimental Behaviour of Reinforced and Strengthened Infill Masonry Walls”, In *Proceedings of the 12th Canadian Masonry Symposium*, 2-5, Vancouver, Canada.

- Darbhanzi, A., Marefat, M. S., and Khanmohammadi, M. (2014). "Investigation of in-Plane Seismic Retrofit of Unreinforced Masonry Walls by Means of Vertical Steel Ties", *Construction and Building Materials*, 52, 122-129.
- Dazio, A., and Beyer, K. (2010). "Seismic Behaviour of Different Types of Masonry Spandrels", *In Proceedings of the 14th European Conference on Earthquake Engineering* (No. CONF), Ohrid, Macedonia.
- D'Ayala, D., Paganoni, S. (2011). "Assessment and Analysis of Damage in L'Aquila Historic City Centre After 6th April 2009", *Bulletin of Earthquake Engineering*, 9(1), 81-104.
- D'Ayala, D., and Speranza, E. (2003). "Definition of Collapse Mechanisms and Seismic Vulnerability of Historic Masonry Buildings", *Earthquake Spectra*, 19(3), 479-509.
- De Borst, R., Remmers, J. J., Needleman, A. y Abellan, M. A. (2004), "Discrete vs Smeared Crack Models for Concrete Fracture: Bridging the Gap", *International Journal for Numerical and Analytical Methods in Geomechanics*, 28, 583-607.
- Dejong, M. J. (2009). "Seismic Assessment Strategies for Masonry Structures", Doctoral Dissertation, *Massachusetts Institute of Technology*, Cambridge, MA.
- De Lorenzis, L., and Teng, J. G. (2007). "Near-Surface Mounted FRP Reinforcement: An Emerging Technique for Strengthening Structures", *Composites Part B: Engineering*, 38(2), 119-143.

De Luca A., Giordano A., Mele E. (2004). “A Simplified Procedure for Assessing the Seismic Capacity of Masonry Arches”, *Engineering Structures*, 26, 1915-1929.

Deppe, K. (1988). “The Whittier Narrows, California Earthquake of October 1, 1987-Evaluation of Strengthened and Unstrengthened Unreinforced Masonry in Los Angeles City”, *Earthquake Spectra*, 4(1), 157-180.

De Santis, S. (2017). “Bond Behaviour of Steel Reinforced Grout for the Extrados Strengthening of Masonry Vaults”, *Construction and Building Materials*, 150, 367-382.

Dhakal, R. P. (2010). “Damage to Non-structural Components and Contents in 2010 Darfield Earthquake”, *Bulletin of the New Zealand Society for Earthquake Engineering*, 43(4), 404-411.

Dizhur, D., Griffith, M., and Ingham, J. (2014). “Out-of-Plane Strengthening of Unreinforced Masonry Walls Using Near Surface Mounted Fibre Reinforced Polymer Strips”, *Engineering Structures*, 59, 330-343.

Doebling, S. W., Farrar, C. R., Prime, M. B., and Shevitz, D. W. (1996). “Damage Identification and Health Monitoring of Structural and Mechanical Systems from Changes in their Vibration Characteristics: A Literature Review (No. LA-13070-MS)”, *Los Alamos National Lab.*, NM, United States.

Dowling, D., Samali, B., and Li, J. (2005). "An Improved Means of Reinforcing Adobe Walls-External Vertical Reinforcement", *University of Technology*, Sydney, Australia.

Dutta, S. C., Mukhopadhyay, P., and Goswami, K. (2013). "Augmenting Strength of Collapsed Unreinforced Masonry Junctions: Principal Damage Feature of Walls Damaged by Moderate Indian Earthquakes", *Natural Hazards Review*, 14(4), 281-285.

Ehsani, M. R., Saadatmanesh, H., and Velazquez-Dimas, J. I. (1999). "Behavior of Retrofitted URM Walls under Simulated Earthquake Loading", *Journal of Composites for Construction*, 3(3), 134-142.

ElGawady, M. A., Lestuzzi, P., and Badoux, M. (2007). "Static Cyclic Response of Masonry Walls Retrofitted with Fiber-Reinforced Polymers", *Journal of Composites for Construction*, 11(1), 50-61.

ElGawady, M., Lestuzzi, P., and Badoux, M. (2004a). "A Review of Conventional Seismic Retrofitting Techniques for URM", *In 13th International Brick and Block Masonry Conference*, 1-10.

ElGawady, M., Lestuzzi, P., and Badoux, M. (2004b). "A review of Retrofitting of Unreinforced Masonry Walls Using Composites", *In Proc., 4th International Conf. on Advanced Composite Materials in Bridges and Structures*. CSCE.

ElGawady, M. A., Lestuzzi, P., and Badoux, M. (2006). "Retrofitting of Masonry Walls Using Shotcrete", *In 2006 NZSEE Conference*, 45.

Elvin, A., and Uzoegbo, H. C. (2011). "Response of a Full-Scale Dry-Stack Masonry Structure Subject to Experimentally Applied Earthquake Loading", *Journal of the South African Institution of Civil Engineering*, 53(1), 22-32.

Fajfar, P., and Fishinger, M. (1988). "N2-A Method for Nonlinear Analysis of Regular Buildings", *Proceedings of the 9th WCEE, Tokyo and Kyoto*, 5, 111-116.

Fanelli, M., and Pavese, A. (1993). "Diagnosis of Masonry Towers by Dynamic Identification," *IABSE REPORTS*, 131-131.

FEMA-356. (2000). "Prestandard and Commentary for the Seismic Rehabilitation of Buildings", *American Society of Civil Engineers, ASCE*.

FEMA-440. (2005). "Improvement of Nonlinear Static Seismic Analysis Procedures", *Federal Emergency Management Agency, Washington, D.C.*

FEMA-461. (2007). "Interim Protocols for Determining Seismic Performance Characteristics of Structural and Nonstructural Components through Laboratory Testing", Draft document, *Federal Emergency Management Agency*.

Felice, G. D., and Giannini, R. (2001). "Out-of-Plane Seismic Resistance of Masonry Walls", *Journal of Earthquake Engineering*, 5(02), 253-271.

- 
- Fonti, R., Borri, A., Barthel, R., Candela, M., and Formisano, A. (2017). "Rubble Masonry Response under Cyclic Actions: Experimental Tests and Theoretical Models", *International Journal of Masonry Research and Innovation*, 2(1), 30-60.
- Gambarotta, L., and Lagomarsino, S. (1997a). Damage Models for the Seismic Response of Brick Masonry Shear Walls Part I: The Mortar Joint Model and Its Applications", *Earthquake Eng. Struct. Dyn.*, 26(4), 423-439.
- Gambarotta, L., Lagomarsino, S. (1997b). Damage Models for the Seismic Response of Brick Masonry Shear Walls. Part II: The Continuum Model and Its Applications", *Earthquake Eng. Struct. Dyn.*, 26, 441-462.
- Giovinazzi S. (2005). "The vulnerability Assessment and the Damage Scenario in Seismic Risk Analysis", Doctoral Dissertation, Technical University Carolo-Wilhelmina, Braunschweig, and University of Florence, Italy.
- Griffith, M. C., Kashyap, J., and Ali, M. M. (2013). "Flexural Displacement Response of NSM FRP Retrofitted Masonry Walls", *Construction and Building Materials*, 49, 1032-1040.
- Hamid, A. A., Mahmoud, A., and El Magd, S. A. (1994). "Strengthening and Repair of Unreinforced Masonry Structures: State-of-the-Art", *In Proc., 10th Int. Brick and Block Masonry Conf*, 2, 485-497.

Hillerborg, A., Modeer, M., and Petersson, P. E. (1976). “Analysis of Crack Formation and Crack Growth in Concrete by Means of Fracture Mechanics and Finite Elements”, *Cement and Concrete Research*, 6, 773–782.

IMI. (2011). “Masonry Detailing Series”, *International Masonry Institute*, Retrieved from <https://www.imiweb.org/02-410-0132-high-lift-grouting-procedures/>.

Islam, R. (2008). “Inventory of FRP Strengthening Methods in Masonry Structures”, Master Thesis, Universitat Politècnica de Catalunya.

Jefferson, A. D., and Mills, N. R. (1998). “Fracture and Shear Properties of Concrete Construction Joints from Core Samples”, *Materials and Structures*, 31(9), 595-601.

Jiménez, B., Pelà, L., and Hurtado, M. (2018). “Building Survey Forms for Heterogeneous Urban Areas in Seismically Hazardous Zones. Application to the Historical Center of Valparaíso, Chile”, *International Journal of Architectural Heritage*, 12(7-8), 1076-1111.

Juhásová, E., Sofronie, R., and Bairrão, R. (2008). “Stone Masonry in Historical Buildings-Ways to Increase their Resistance and Durability”, *Engineering Structures*, 30 (8), 2194-2205.

Jukes, P., and Riddington, J. R. (1997). “Review of Masonry Joint Shear Strength Test Methods”, *Masonry International*, 11(2), 37-43.

Jukes, P., and Riddington, J. R. (1998). "Review of Masonry Tensile Bond Strength Test Methods", *Masonry International*, 12(2), 51-57.

KBC (Korean Building Code) (2016). *Ministry of Land, Infrastructure and Transport of Korea*, Seoul, Korea. (both in Korean and English)

Kadam, S. B., Singh, Y., and Li, B. (2015). "Out-of-Plane Behaviour of Unreinforced Masonry Strengthened Using Ferrocement Overlay", *Materials and Structures*, 48(10), 3187-3203.

Karantoni, F. V., and Fardis, M. N. (1992). "Effectiveness of Seismic Strengthening Techniques for Masonry Buildings", *Journal of Structural Engineering*, 118(7), 1884-1902.

Kappos, A.J., Penelis, G.G. and Drakopoulos, C.G. (2002). "Evaluation of Simplified Models for Lateral Load Analysis of Unreinforced Masonry Buildings", *ASCE Journal of Structural Engineering*, 128(7), 890-897.

Lagomarsino S. (2006). "On The Vulnerability Assessment of Monumental Buildings", *Earthquake Engineering*, 4, 445-463. European Commission, Brussels.

Langenbach, R. (2008). "Understanding What Works: Learning from Earthquake Resistant Traditional Construction", *Heritage at Risk*, 87-98.

Lat, I. (2020). "Lat Works Construction", Retrieved from <https://www.Lat-works.com>.

- Lee, J., and Fenves, G. L. (1998). "Plastic-Damage Model for Cyclic Loading of Concrete Structures", *Journal of Engineering Mechanics*, 124(8), 892-900.
- Lin, K., Liu, H., Wei, C., and Huang, Q. (2017). "Effects of Shear Rate on Cyclic Behavior of Dry Stack Masonry Joint", *Construction and Building Materials*, 157, 809-817.
- Liu, H., Ban, L., Lan, C., and Yang, X. (2015). "Quasi-Static Test of Unreinforced Brick Walls Retrofitted with Post-Tensioning Tendons", *Journal of Building Structures*, 36, 142-149.
- Lourenço, P. B. (1996). "Computational Strategies for Masonry Structures", Doctoral Dissertation, Delft University of Technology, Netherlands.
- Lourenço, P. B., and Rots, J. G. (1997). "Multisurface Interface Model for Analysis of Masonry Structures", *Journal of engineering mechanics*, 123(7), 660-668.
- Lourenço, P. B., Rots, J. G., and Blaauwendraad, J. (1998). "Continuum Model for Masonry: Parameter Estimation and Validation", *Journal of Structural Engineering*, 124(6), 642-652.
- Lourenço, P. B. (2002). "Computations on Historic Masonry Structures", *Progress in Structural Engineering and Materials*, 4(3), 301-319.

Lourenço, P. B., Oliveira, D. V., Roca, P., and Orduña, A. (2005). “Dry Joint Stone Masonry Walls Subjected to in-Plane Combined Loading”, *Journal of Structural Engineering*, 131(11), 1665-1673.

Lourenço, P. B., Mendes, N., Ramos, L. F. and Oliveira, D. V (2011). “Analysis of Masonry Structures without Box Behavior”, *International Journal of Architectural Heritage*, 5, 369–382.

Macabuag, J. (2007). “An Introduction to Modelling and Retrofitting of Non-Engineered Masonry Buildings under Seismic Loading”.

Macabuag, J., Guragain, R., and Bhattacharya, S. (2012). “Seismic Retrofitting of Non-engineered Masonry in Rural Nepal”, *Proceedings of the Institution of Civil Engineers-Structures and Buildings*, 165(6), 273-286.

Macchi, G., (1992). “Structural diagnosis and Rehabilitation of Historical Buildings”, *Cuadernos INTEMAC*.

Macchi, G., (1997). “General Methodology. The Combined Use of Experimental and Numerical Techniques inside a Single Study”, P. Roca *et al.* (eds): *Structural Analysis of Historical Constructions*. CIMNE, Barcelona, 10-23.

Magenes, G. and Della Fontana, A. (1998). “Simplified Non-Linear Seismic Analysis of Masonry Buildings”, In *H.W.H. West (Ed.), Proceedings of the British Masonry Society*, 8, 190-195.

Mahdi, T. (2016). “Seismic Vulnerability of Arches, Vaults and Domes in Historical Buildings”, *In Civil and Environmental Engineering: Concepts, Methodologies, Tools, and Applications*, 101-144.

Mahmood, H., and Ingham, J. M. (2011). “Diagonal Compression Testing of FRP-Retrofitted Unreinforced Clay Brick Masonry Wallettes”, *Journal of Composites for Construction*, 15(5), 810-820.

Malena, M., Portioli, F., Gagliardo, R., Tomaselli, G., Cascini, L., and de Felice, G. (2019). “Collapse Mechanism Analysis of Historic Masonry Structures Subjected to Lateral Loads: A Comparison between Continuous and Discrete Models”, *Computers and Structures*, 220, 14-31.

Martins, A., Vasconcelos, G., Fangueiro, R., and Cunha, F. (2015). “Experimental Assessment of an Innovative Strengthening Material for Brick Masonry Infills”, *Composites Part B: Engineering*, 80, 328-342.

Meguro, K., Mayorca, P., Sathiparan, N., Guragain, R., and Nasrollahzadeh Nesheli, K. (2005). “PP-Band Retrofitting Technique: Affordable, Acceptable and Feasible Method for Developing Countries”, *Institute of Industrial Science, University of Tokyo*.

Mehta, P. K., and Monteiro, P. I. M. (1993). “Concrete: Structure, Properties, and Materials”, 2nd Ed., *Prentice-Hall, Inc.*, Englewood Cliffs, N.J.

- Meli, R. (1998). “Structural Engineering of the Historical Buildings (in Spanish).” *Civil Engineers Association (ICA) Foundation, A. C., Mexico.*
- Mendes, N. (2012). “Seismic Assessment of Ancient Masonry Buildings: Shaking Table Tests and Numerical Analysis”, Doctoral Dissertation.
- Milani, G., Lourenço, P.B. and Tralli, A. (2006a). “Homogenised Limit Analysis of Masonry Walls, Part I: Failure Surfaces”, *Computers and Structures*, 84, 166-180.
- Milani, G., Lourenço, P.B. and Tralli, A. (2006b). “Homogenised Limit Analysis of Masonry Walls, Part II: Structural Examples”, *Computers and Structures*, 84, 181-195.
- Milani, G., Lourenço, P.B. and Tralli, A. (2007). “3D Homogenized Limit Analysis of Masonry Buildings under Horizontal Loads”, *Engineering Structures*, 29, 3134-3148.
- Meireles, H., and Bento, R. (2013). “Rehabilitation and Strengthening of Old Masonry Buildings”, *Technical Report ICIST DTC n°02/13, ICIST-IST, Lisbon*, 1-25.
- Mistler, M. (2006). “Deformation-Based Seismic Measure Concept for Masonry Constructions”, Doctoral Dissertation, University of Aachen, Germany. (in German)
- Moës, N., Dolbow, J., and Belytschko, T. (1999). “A Finite Element Method for Crack Growth without Remeshing”, *International Journal for Numerical Methods in Engineering*, 46(1), 131-150.

Mojsilović, N. (2011). “Tensile Strength of Clay Blocks: An Experimental Study”, *Construction and Building Materials*, 25(11), 4156-4164.

Moon, F. L. (2003). “Seismic Strengthening of Low-Rise Unreinforced Masonry Structures with Flexible Diaphragms”, Doctoral Dissertation, Georgia Institute of Technology.

Ngo D, Scordelis AC. (1967). “Finite Element Analysis of Reinforced Concrete Beams”, *Journal of the American Concrete Institute*, 64, 152–163.

Novelli, V. I., and D’Ayala, D. (2019). “Use of the Knowledge-Based System LOG-IDEAH to Assess Failure Modes of Masonry Buildings, Damaged by L’Aquila Earthquake in 2009”, *Frontiers in Built Environment*, 5, 95.

Ochsendorf J. A. (2002). “Collapse of Masonry Structures”, University of Cambridge, Doctoral Dissertation.

Okail, H., Abdelrahman, A., Abdelkhalik, A., and Metwaly, M. (2016). “Experimental and Analytical Investigation of the Lateral Load Response of Confined Masonry Walls”, *HBRC Journal*, 12(1), 33-46.

Oliveira, D. V. (2003). “Experimental and Numerical Analysis of Blocky Masonry Structures under Cyclic Loading”, Doctoral Dissertation, doktorski rad, Universidade do Minho.

Orduña A., Lourenço P.B. (2003). “Cap Model for Limit Analysis and Strengthening of Masonry Structures”. *Journal of Structural Engineering*, 129(10), 1287-1430.

Orduña A., Lourenço P.B., (2005a). “Three-Dimensional Limit Analysis of Rigid Blocks Assemblages. Part I: Torsion Failure on Frictional Joints and Limit Analysis Formulation”, *International Journal of Solids and Structures*, 42, (18-19), 5140-5160.

Orduña A., Lourenço P.B., (2005b). “Three-Dimensional Limit Analysis of Rigid Blocks Assemblages. Part II: Load-Path Following Solution Procedure and Validation”, *International Journal of Solids and Structures*, 42(18- 19), 5161-5180.

Oskouei, A. V., Jafari, A., Bazli, M., and Ghahri, R. (2018). “Effect of Different Retrofitting Techniques on in-Plane Behavior of Masonry Wallettes”, *Construction and Building Materials*, 169, 578-590.

Ötes, A., and Löring, S. (2006). “Bearing Behavior of Masonry Constructions under Earthquake Loading”, *Published in Bautechnik*, 83.

Page, A. W. (1978). “Finite Element Model for Masonry”, *Journal of the Structural Division*, 104(8), 1267-1285.

Page, A. W. (1981). “The Biaxial Compressive Strength of Brick Masonry”, *Proceedings of the Institution of Civil Engineers*, 71(3), 893-906.

Paganoni, S., and D' Ayala, D. (2015). "Dissipative Anchor Devices for The Seismic Retrofit of Heritage Buildings", Doctoral Dissertation, University of Bath.

Paikara, S., and Rai, D. C. (2006). "Confining Masonry Using Pre-Cast RC Element for Enhanced Earthquake Resistance", *In Proceedings of the 8th US National Conference on Earthquake Engineering*, San Francisco, California, USA.

Palacios S. (2004). "State of the Art in Seismic Vulnerability", *Institutional Repository of Alicante University*.

Palmer, R. (2017). "Traditional Anchorage Used for HURM Buildings", Retrieved from <https://www.blsurveyors.com/2366-2/>.

Papastamatiou, D., and Psycharis, L. (1993). "Seismic Response of Classical Monuments-A Numerical Perspective Developed at the Temple of Apollo in Bassae", Greece. *Terra Nova*, 5(6), 591-601.

Pappas, A. (2012). "Calibration of the Numerical Material Behaviour of Multi-Leaf Stone Masonry Walls Based on Experimental Results", Doctoral Dissertation.

Paret, T. F., Freeman, S. A., Searer, G. R., Hachem, M., and Gilmartin, U. M. (2008). "Using Traditional and Innovative Approaches in the Seismic Evaluation and Strengthening of a Historic Unreinforced Masonry Synagogue", *Engineering Structures*, 30(8), 2114-2126.

---

PCM, Presidenza del Consiglio dei Ministri (2005). “Ulteriori Modifiche Ed Integrazioni All'ordinanza N .3274 Del 20/3/2003, Recante “Primi Elementi in Materia Di Criteri Generali Per La Classificazione Sismica Del Territorio Nazionale E Di Normative Tecniche Per Le Costruzioni in Zona Sismica”, *OPCM*, n. 3431, 3 May 2005. *Official Bulletin*, (107), 10 May 2005. (in Italian)

Porter, M.L., 1987. “Sequential Phased Displacement (SPD) Procedure for TCCMAR Testing”, *Proceedings, 3rd Meeting of the Joint Technical Coordinating Committee on Masonry Research, US-Japan Coordinated Research Program*.

Przewłócki, I., Dardzińska, I., and Świniański, J. (2005). “Review of Historical Buildings, Foundations”, *Geotechnique*, 55(5), 363-372.

Psycharis, I. N., Lemos, J. V., Papastamatiou, D. Y., Zambas, C., and Papantonopoulos, C. (2003). “Numerical Study of the Seismic Behaviour of A Part of the Parthenon Pronaos”, *Earthquake Engineering and Structural Dynamics*, 32(13), 2063-2084.

Ötes, A. and Löring, S. (2006). “Bearing Behavior of Masonry Constructions under Earthquake Loading”, *Published in Bautechnik* 83, Heft 2. (in German)

Quiroz, A. P. (2011). “Seismic Vulnerability Reduction of Historical Masonry Towers by External Prestressing Devices”, Doctoral Dissertation, Technische Universität Braunschweig.

Rashid, Y. R. (1968). "Ultimate Strength Analysis of Prestressed Concrete Pressure Vessels", *Nuclear Engineering and Design*, 7(4), 334-344.

Redgwick (2017). "Traditional Wall Tie Patress Plates", Retrieved from <https://www.redgwick.co.uk/>.

Remseth, S. N. (1979). "Nonlinear Static and Dynamic Analysis of Framed Structures", *Computers and Structures*, 10(6), 879-897.

Roca P., López-Almansa F., Miquel J, Hanganu A. (2007). "Limit Analysis of Reinforced Masonry Vaults", *Engineering Structures*, 29(3), 431-439.

Roca, P., Lourenço, P. B., and Gaetani, A. (2019). "Historic Construction and Conservation: Materials, Systems and Damage", *Routledge*.

Rots, J. G. (1991). "Numerical Simulation of Cracking in Structural Masonry", *Heron*, 36(2), 49-63.

Rots, J. G. (1997). "Structural Masonry: An Experimental/Numerical Basis for Practical Design Rules", *Published by Balkema, ISBN 90 5410 680 8*, Rotterdam, Netherlands.

Saetta A., Scotta R., Vitaliani R. (2000). "An Orthotropic Fourth-Rank Damage Model for Masonry Structures", *European Congress on Computational Methods in Applied Sciences an Engineering - ECOMAS 2000*, Barcelona, Spain.

Salonikios, T., Karakostas, C., Lekidis, V. and Anthoine A. (2003). “Comparative Inelastic Pushover Analysis of Masonry Frames”, *Engineering Structures*, 25, 1515-1523.

Samarasinghe, W., AW, P., and AW, H. (1981). “Behaviour of Brick Masonry Shear Walls”.

Sar, D. (2014). “Seismic Evaluation of Un-Reinforced Masonry Structures”, Doctoral Dissertation.

Sathiparan, N., Mayorca, P., Nesheli, K. N., Guragain, R., and Meguro, K. (2005). “Experimental Study on in-Plane and out-of-Plane Behavior of Masonry Wallettes Retrofitted by PP-Band Meshes”, *Seisan Kenkyu*, 57(6), 530-533.

Sayin, B., Yildizlar, B., Akcay, C., and Gunes, B. (2019). “The Retrofitting of Historical Masonry Buildings with Insufficient Seismic Resistance Using Conventional and Non-conventional Techniques”, *Engineering Failure Analysis*, 97, 454-463.

Schultz, A., Cheok, G., and Magana, R. (1998). “Performance of Precast Concrete Shear Walls”, *In 6th US National Conference on Earthquake Engineering*.

Schuller, M. P., Atkinson, R. H., and Borgsmiller, J. T. (1994). “Injection Grouting for Repair and Retrofit of Unreinforced Masonry”, *In Proceedings of the 10th International Brick and Block Masonry Conference*.

Senthivel, R., and Lourenço, P. B. (2009). “Finite Element Modelling of Deformation Characteristics of Historical Stone Masonry Shear Walls”, *Engineering Structures*, 31(9), 1930-1943.

Shad, S. (2015). “The Choice of Interventions for Strengthening of Historical Adobe Structures and Remains in Bam Citadel “Arg-e Bam””, Doctoral Dissertation, *Technische Universität Dresden*.

Shrestha, K. C., Nagae, T., and Araki, Y. (2011). “Finite Element Modeling of Cyclic out-of-Plane Response of Masonry Walls Retrofitted by Inserting Inclined Stainless Steel Bars”, *Journal of Disaster Research*, 6(1), 36-43.

Silva B., (2008a). “Aplicação de um modelo de dano contínuo na modelação de estruturas de alvenaria de pedra. igreja de gondar - um caso de estudo”, Master Thesis, Faculdade de Engenharia da Universidade do Porto, Porto, Portugal. (in Portuguse)

Simões, A. (2018). “Evaluation of the Seismic Vulnerability of the Unreinforced Masonry Buildings Constructed in the Transition between the 19th and 20th Centuries in Lisbon, Portugal”, Doctoral Dissertation, *Instituto Superior Técnico, Universidade de Lisboa*, Lisboa.

Soltanzadeh, G., Osman, H. B., Vafaei, M., and Vahed, Y. K. (2018). “Seismic Retrofit of Masonry Wall Infilled RC Frames Through External Post-Tensioning”, *Bulletin of Earthquake Engineering*, 16(3), 1487-1510.

Soudki, K., And Alkhrdaji, T. (2005). “Guide for the Design and Construction of Externally Bonded FRP Systems for Strengthening Concrete Structures (ACI 440.2 R-02)”, *In Structures Congress, Metropolis and Beyond*, 1-8.

Sperbeck, S. (2008). “Seismic Risk Assessment of Masonry Walls and Risk Reduction by Means of Prestressing”, Doctoral Dissertation.

Spina, G., Ramundo, F., and Mandara, A. (2004). “Masonry Strengthening by Metal Tie-Bars, a Case Study”, *In Structural Analysis of Historical Constructions. In Proceedings of the Fourth International Seminar on Structural Analysis of Historical Constructions*, Padova, Italy, 10-13.

Sukumar, N., Moës, N., Moran, B., and Belytschko, T. (2000). “Extended Finite Element Method for Three-Dimensional Crack Modelling” *International Journal for Numerical Methods in Engineering*, 48(11), 1549-1570.

Taghdi, M., Bruneau, M., and Saatcioglu, M. (2000). “Seismic Retrofitting of Low-Rise Masonry and Concrete Walls Using Steel Strips”, *Journal of Structural Engineering*, 126(9), 1017-1025.

Tanner, J. E., and Klingner, R. E. (2017). “Masonry Structural Design”, *McGraw Hill Professional*.

Tehrani, P., and Maalek, S. (2006). “Comparison of Nonlinear Static and Nonlinear Dynamic Analyses in the Estimation of the Maximum Displacement for Structures

Equipped with Various Damping Devices”, *In 4th International Conference on Earthquake Engineering*, Taipei, Taiwan.

Tinazzi, D., Arduini, M., Modena, C., and Nanni, A. (2000). “FRP-Structural Repointing of Masonry Assemblages”, *In Proc., 3rd Int. Conf. on Advanced Composite Materials in Bridges and Structures, ACMBS, 3*, 585-592.

Tomažević, M., and Klemenc, I. (1997). “Seismic Behaviour of Confined Masonry Walls”, *Earthquake Engineering and Structural Dynamics*, 26(10), 1059-1071.

Tomažević, M. (1999). “Earthquake-Resistance Design of Masonry Buildings”, *Series on Innovation in Structures and Construction, 1*, Imperial College Press.

Toranzo-Dianderas, L. A., Restrepo, J. I., Carr, A. J., and Mander, J. B. (2004). “Rocking Confined Masonry Walls with Hysteretic Energy Dissipators and Shake-Table Validation”, *In Proc., 13th World Conf. on Earthquake Engineering (CD-ROM)*.

Turco, V., Secondin, S., Morbin, A., Valluzzi, M. R., and Modena, C. (2006). “Flexural and Shear Strengthening of Un-Reinforced Masonry with FRP Bars”, *Composites Science and Technology*, 66(2), 289-296.

Turer, A., Korkmaz, S. Z., and Korkmaz, H. H. (2007). “Performance Improvement Studies of Masonry Houses Using Elastic Post-Tensioning Straps”, *Earthquake Engineering and Structural Dynamics*, 36(5), 683-705.

Uzoegbo, H. C., and Ngowi, J. V. (2003). "Structural Behaviour of Dry-stack Interlocking Block Walling Systems Subject to in-Plane Loading", *Concr. Bet.*, 103, 9-13.

Valente, G. (2003). "Fracture Mechanics for the Reconstruction of Noto Cathedral", *Construction and Building Materials*, 17, 579-593.

Van der Pluijm, R. (1993). "Shear Behaviour of Bed Joints", A.A. Hamid and H.G. Harris (eds): *Proc. 6th North American Masonry Conference*, 1, 125-136.

Van der Pluijm, R. (1997). "Non-linear Behaviour of Masonry under Tension", *Heron-English Edition*, 42, 25-54.

Vasconcelos, G. (2005). "Experimental Investigations on the Mechanics of Stone Masonry: Characterization of Granites and Behavior of Ancient Masonry Shear Walls".

Vermeltfoort, A. T. (1997). "Effects of the Width and Boundary Conditions on the Mechanical Properties of Masonry Prisms under Compression", *In Proc. 11th Int. Brick/Block Masonry Conference*, Shanghai, 181-190.

Voto, S. (2009). "Seismic Retrofitting and Restoration of Historical Buildings Using Innovative Materials: the Case of Carmine's Bell Tower in Naples", Doctoral Dissertation, University of Naples Federico II.

Wang, C., Sarhosis, V., and Nikitas, N. (2018). “Strengthening/Retrofitting Techniques on Unreinforced Masonry Structure/Element Subjected to Seismic Loads: A Literature Review”, *The Open Construction and Building Technology Journal*, 12(1).

Wood, C., and Burns, C. (2019). “Grouting Solid Masonry Walls”, Retrieved from <https://www.buildingconservation.com/articles/grouting/grouting.htm>.

Yavartanoo, F., Kang, T. H. K., Ha, T. U., Lim, W. Y., and Hong, S. G. (2020). “Restoration of Mireuksaji Stone Pagoda: Evaluation of Reinforced Granite Members with Titanium Bars”, *Journal of Performance of Constructed Facilities*, 34(4), 04020046.

Yi, T., Moon, F.L., Leon, R.T. and Kahn, L.F. (2006). “Analyses of a Two-Story Unreinforced Masonry Building”, *ASCE Journal of Structural Engineering*, 132(5), 653-662.

Zamani Ahari, G. (2013). “Structural in-Plane Behavior of Masonry Walls Externally Retrofitted with Fiber Reinforced Materials”, Doctoral Dissertation, 九州大学, *Kyushu University*.

Zhuge, Y., Thambiratnam, D., and Corderoy, J. (1998). “Nonlinear Dynamic Analysis of Unreinforced Masonry”, *Journal of structural engineering*, 124(3), 270-277.

## **Acknowledgment**

It is acknowledged that the academic advisor of this doctoral dissertation is Prof. Thomas Kang in the Department of Architecture & Architectural Engineering at Seoul National University.

## Abstract in Korean

역사적 구조물은 인류의 문화적, 건축적, 역사적 가치를 지니며, 동시에 이러한 가치를 미래 세대에게 전달하는 데 있어 중요한 역할을 한다. 그러나, 많은 문화 유산들은 오랜 세월 지진이나 기타 자연재해로 심각한 피해를 입어왔다. 구조적인 측면에서 볼 때, 높은 질량, 낮은 인장강도, 낮은 전단강도 및 낮은 연성 등이 불리하게 작용하였으며, 조적조 구조물의 경우 재료의 특성, 형상, 구성, 요소 배치, 연결부, 기초의 강도 등 여러 변수가 해당 구조물의 내진거동에 영향을 끼쳤다. 이는 구조물의 부분 및 전체 붕괴로 이어질 수 있기에 역사적인 조적조 구조물의 보존과 보강은 계속적으로 연구가 필요한 주제이다. 본 논문에서는, 가장 중요한 구조적 요소인 비보강 조적조 벽체의 건축적, 구조적 특성을 분석하였고, 지진하중에 의해 야기되는 전형적인 손상에 대해 서술하였다. 그 후, 분석적 연구에 적합한 방법을 선택하기 위해 몇 가지 보강 방법에 대한 장단점을 조사하였다. 본 연구에서는 여러 유형의 비보강 조적조 벽체 중 건식 석조 벽체에 특히 집중하여 분석이 진행되었다. 유한요소해석을 통해 단조 및 반복 가력에서의 벽체 거동이 평가되었고, 수치해석 결과를 검증하기 위해 기존 연구자들의 실험결과가 사용되었다. 또한, 요소와 벽체의 배열 및 규모에 따라 매개변수적 연구가 수행되었다. 최종적으로 모델의 수치해석 결과와 파괴 양상을 고려하여 해당 구조물에 적합한 보강 방법이 선정되었다. 이 때, 기존의 역사적 구조물의 보

강에 있어 가장 효율적이고 실용적인 방법 중 하나로 평가 받고 있는 철근 삽입 공법이 심층 분석되었다. 가장 효율적인 재료와 철근 배치를 탐구하기 위해 매개변수적 연구가 추가적으로 수행되었다. 본 논문의 연구를 통하여 궁극적으로 비보강 조적조 벽체의 내진거동과 적절한 보강 방법, 그리고 이를 어떻게 향상시킬 수 있는 지에 대한 해법을 도출할 수 있었다.